

TECHNISCHE UNIVERSITÄT MÜNCHEN

Max-Planck-Institut für Biochemie

Abteilung Strukturforschung

Biologische NMR-Arbeitsgruppe

Molecular basis for the inhibition of p53

by Mdmx and Mdm2

Anna Czarna

Vollständiger Abdruck der von der Fakultät für Chemie der Technischen Universität München zur Erlangung des akademischen Grades eines

Doktors der Naturwissenschaften

genehmigten Dissertation.

Vorsitzender: Univ.-Prof. Dr. M. Groll

Prüfer der Dissertation: 1. Priv.-Doz. Dr. N. Budisa

2. Univ.-Prof. Dr. Chr. F. W. Becker

Die Dissertation wurde am 25.09.2009 bei der Technischen Universität München eingereicht und durch die Fakultät für Chemie am 03.11.2009 angenommen.

*I sought in mine heart to give myself unto wine, yet
Acquainting mine heart with wisdom; and to lay hold on folly,
Till I might see what was that good for the sons of men, which
They should do under the heaven all the days of their life.*

The Old Testament – Ecclesiastes 2:3

Acknowledgements

I am indebted to number of people related to the Department of Structural Research at the Max Planck Institute for Biochemistry, that were integral to the completion of this thesis.

First I would like to thank Dr. Tad A. Holak for being my supervisor, to whom I am foremost indebted for his great intellectual and moral support, scientific guidance and care.

I am grateful to PD Dr. Nediljko Budisa for being my Doctorvater.

I would like to thank all co-workers and colleagues from Max Planck Institute and the Erasmus students for their nice company and many random conversations.

Special thanks to colleagues who with great commitment introduced me to the scientific world: Grzegorz Popowicz, Ulli Rothweiler and Tomasz Sitar.

To Ulli Rothweiler, Ola Mikolajka and Arkadiusz Sikora for their friendship and great support during bad time.

To Prof. Alexander Dömling for great and fruitful collaboration.

To Prof. Adam Dubin and Grzegorz Dubin for their continuous help, support, and nice collaboration.

Last but same wholeheartedly thanks to my parents and Radek for all love, care and being always with me.

Publications

Popowicz GM, Dubin G, Stec-Niemczyk J, **Czarna A**, Dubin A, Potempa A, Holak TA. Functional and Structural Characterization of Spl Proteases from Staphylococcus aureus. J Mol Biol 2006; 358: 270–279.

Dubin G, Stec-Niemczyk J, Kisielewska M, Popowicz GM, Bista M, Pustelny K, Boulware KT, Stennicke HR, Kantyka T, Phopaisarn M, Daugherty PS, **Czarna A**, Enghild JJ, Thornberry N, Thogersen IB, Potempa J, Dubin A. Enzymatic Activity of the Staphylococcus aureus SplB Serine Protease is Induced by Substrates Containing the Sequence Trp-Glu-Leu-Gln. J Mol Biol 2008; 379: 343–356.

Rothweiler U, **Czarna A**, Weber L, Popowicz GM, Brongel K, Kowalska K, Orth M, Stemmann O, Holak TA. NMR screening for lead compounds using tryptophan-mutated proteins. J Med Chem 2008; 51: 5035-5042.

Rothweiler U, **Czarna A**, Krajewski M, Ciombor J, Kalinski C, Khazak V, Ross G, Skobeleva N, Weber L, Holak TA. Isoquinolin-1-one inhibitors of the Mdm2-p53 interaction. ChemMedChem 2008; 3: 1118-1128.

Popowicz GM, **Czarna A**, Rothweiler U, Szwagierczak A, Krajewski M, Weber L, Holak TA. Molecular basis for the inhibition of p53 by mdmx. Cell Cycle 2007; 6: 2386-2392.

Popowicz GM, **Czarna A**, Holak TA. Structure of the human Mdmx protein bound to the p53 tumor suppressor transactivation domain. Cell Cycle 2008; 7: 2441-2443.

Czarna A, Popowicz GM, Pecak A, Wolf S, Dubin G, Holak TA. High affinity interaction of the p53 peptide-analogue with human Mdm2 and Mdmx. Cell Cycle 2009; 8: 1-9.

Srivastava S, Beck B, Wang W, **Czarna A**, Holak TA, Dömling A. Rapid and efficient hydrophilicity tuning of p53/mdm2 antagonists. J Comb Chem 2009; 11: 631-639.

Czarna A, Beck B, Srivastava S, Popowicz GM, Balachandran R, Day B, Holak TA, Dömling A. Multiple small molecular weight scaffolds inhibiting the protein-protein interaction Hdm2-p53.
Submitted.

Beck B, Balachandran R, Yanamala N, **Czarna A**, Dudgeon DD, Johnston P, Day B, Klein-Seetharaman J, Holak TA, Herdtweck E, Dömling A. Imidazole p53-Hdm2 antagonists with cellular anticancer activity.
Submitted.

Popowicz GM, **Czarna A**, Wolf S, Wang K, Wang W, Dömling A, and Holak TA. Structures of low molecular weight inhibitors bound to MDMX and MDM2 reveal new approaches for p53-MDMX/MDM2 antagonist drug discovery.
Submitted.

Bista M, Kowalska K, **Czarna A**, Krajewski M, Cichon P, Holak TA. NMR characterization of the Mdmx-p53 interaction.
Manuscript under preparation.

Table of contents

1 Background and significance	1
1.1 The p53 tumor suppressor pathway	1
1.2 The p53 and Mdm2/x system	3
1.2.1 Inhibitors of Mdm2/x-p53 interaction	10
1.3 Fragment-based drug discovery and the role of NMR in fragment screening	15
2 Goals of the study	21
3 Materials and laboratory methods	22
3.1 Materials	22
3.1.1 E. coli strains and plasmids	22
3.1.2 Cell growth media and stocks	23
3.1.2.1 Media	23
3.1.2.2 Stock solutions	24
3.1.3 Solutions for making chemically competent E. coli cells	25
3.1.4 Protein purification – buffers	25
3.1.5 Buffer for DNA agarose gel electrophoresis	28
3.1.6 Reagents and buffers for the SDS-PAGE	29
3.1.6.1 SDS-PAGE gel preparation	29
3.1.6.2 Protein visualization	30
3.1.8 Reagents and buffers for electroblotting for N-terminal sequencing	30
3.1.9 Enzymes and other proteins	31
3.1.10 Kits and reagents	32
3.1.11 Protein and nucleic acids markers	32
3.1.12 Chromatography equipment, columns and media	32
3.2 Laboratory methods and principles	33
3.2.1 General remarks on construct design and choice of the expression system	33
3.2.2 DNA techniques	34
3.2.2.1 Preparation of plasmid DNA	34
3.2.2.2 PCR	34
3.2.2.3 Digestion with restriction enzymes	40
3.2.2.4 Purification of PCR and restriction digestion products	40
3.2.2.5 Ligation	40
3.2.2.6 Ligation independent cloning	41
3.2.2.7 Mutagenesis	41
3.2.2.8 Agarose gel electrophoresis of DNA	43
3.2.3 Transformation of E. coli	43

3.2.3.1	Making chemically competent cells	43
3.2.3.2	Transformation of chemically competent cells	44
3.2.4	Protein chemistry methods & techniques	44
3.2.4.1	The general strategy of the protein expression in Escherichia coli.	44
3.2.4.2	E.coli expression in minimal medium	46
3.2.4.3	Sonication	46
3.2.4.4	General remarks on protein purification strategies	47
3.2.4.4.1	Protein purification under native conditions	48
3.2.4.4.2	Protein purification under denaturing conditions	49
3.2.4.5	SDS polyacrylamide gel electrophoresis (SDS-PAGE)	50
3.2.4.6	Visualization of separated proteins	50
3.2.4.7	Western blot	50
3.2.4.8	Determination of protein concentration	51
3.2.5	NMR spectroscopy	51
3.2.6	X-ray crystallography	52
3.2.6.1	Protein crystallization	52
3.2.6.2	Data collection and structure analysis	53
3.2.7	Isothermal titration calorimetry	54
3.2.8	Fluorescence polarization binding assays	55
3.2.9	General experimental methods for synthesis of small molecular weight inhibitors	56
3.2.10	Computational library generation and docking	56
3.2.11	Cell based assay	57
4	Results and discussion	59
4.1	Molecular basis for the inhibition of p53 by Mdmx and Mdm2 proteins and structural studies of these interactions	59
4.1.1	Cloning and constructs used for the study	59
4.1.1.1	Constructs of Mdm2 and Mdmx prepared for the study	59
4.1.1.2	Zebrafish (Danio rerio) Mdmx and the humanized clone	61
4.1.1.3	Constructs of the p53 protein	62
4.1.2	Protein expression and purification strategies	64
4.1.2.1	Results of the expression and classical purification profiles of Mdm2 and Mdmx	65
4.1.2.2	Exemplary expression and purification of p53 constructs used for this part of work	66
4.1.3	Structural studies of Mdm2 and Mdmx proteins with p53 and derived peptides	71

4.1.3.1	Preparing the crystallization conditions	71
4.1.3.2	Structure of the wild type and humanized Zebrafish Mdmx-p53 complex	71
4.1.3.2.1	Crystallization and data collection	71
4.1.3.2.2	Features of the structure of the zebrafish Mdmx-p53 complex	75
4.1.3.3	Structure of human Mdmx protein bound to the p53 tumor suppressor transactivation domain	78
4.1.3.3.1	Crystallization and data collection	79
4.1.3.3.2	Structural properties of the p53 binding pocket of human Mdmx	81
4.1.3.4	Structural base for nanomolar simultaneous inhibitors of Mdmx and Mdm2 interactions with p53	82
4.1.3.4.1	Crystallization and data collection	83
4.1.3.4.2	Structure of the complex between the N-terminal domain of Mdmx and the P4 peptide	85
4.1.3.4.3	Structure of the complex between the N-terminal domain of Mdm2 and the P4 peptide and comparison to the Mdmx-P4 structure	87
4.1.3.4.4	Conclusions	88
4.1.4	Functional studies of the interaction between Mdm2 and Mdmx proteins with p53	89
4.1.4.1	Binding of various peptides and small molecule binding partners of Mdm2, Mdmx and zebrafish Mdmx	89
4.1.4.1.1	ITC	89
4.1.4.1.2	The inhibitory activity of known Mdm2-p53 competitors on the Mdmx-p53 binding using NMR techniques	93
4.1.4.1.3	Fluorescence polarization (FP) assay	99
4.2.	Multiple Small Molecular Weight Scaffolds Inhibiting the Protein-Protein Interaction p53-Mdm2	105
4.2.1	Results and discussion	106
4.2.1.1	Anchor generation, docking and MCR chemistry	107
4.2.1.2	Exemplary reactions of the antagonist synthesis	113
4.2.1.3	High content NMR-based affinity screening	116
4.2.1.4	Antagonist induced dissociation assay (AIDA)	122
4.2.1.5	Cell based studies	124
4.2.2	Conclusions	126

5 Summary	130
6 Zusammenfassung	132
7 Appendix	134
8 Abbreviations	147
9 Literature references	149

1 Background and significance

1.1 The p53 tumor suppressor pathway

The tumor suppressor p53 protein, "the guardian of the genome", has an overarching role in protecting the organisms from cancer. p53 protein was first identified in 1979 (Lane and Crawford, 1979; DeLeo et al., 1979; Linzer and Levine, 1979) in virologic and serologic studies, and subsequently its gene *TP53* was cloned in 1983 (Oren and Levine, 1983). p53 was initially thought to be a proto-oncogene. It was found that p53 could immortalize normal cells and sensitize them for transformation in response to Ras oncogene (Eliyahu et al., 1984; Jenkis et al., 1984). Examination of all the available murine p53 cDNA clones revealed sequence differences not linked to the polymorphism, important for both: the conformation and biological activity of the protein (Finlay et al., 1988; Eliyahu et al., 1989). These observations were supported by study of Laviguer et al. (1989) who showed that transgenic mice carrying a mutant *TP53* develop many types of tumor with high frequency of sarcomas. In early 1990 the p53 gene was implicated in most cases of the Li-Fraumeni syndrome, a rare inherited condition which is associated with high occurrence of different types of cancers. In all cases, there was a strict correlation between transmission of the p53 mutated allele and development of cancer. However, it took more than 10 years to realise that in most cases the cDNA clones used in transfection experiments contained point mutations, which actively participated in cellular transformation. To date, p53 is recognized as in the cell's major tumor suppressor and the most frequently inactivated gene in human cancers (Vousden and Lu, 2002).

Human p53 contains 393 amino acids and can be divided into five functional domains that are connected by flexible linkers (Figure 1). The transactivation domain (TAD, residues: 1-61) comprises two subdomains: TAD1 (residues 1-40) and TAD2 (residues 40-61). The NMR study, as well as the circular dichroism of TAD, showed that it is natively unfolded, with no tertiary and secondary structure elements at physiological conditions. The DNA binding domain (residues: 94-292) is the most affected region by mutations in cancer cells (Vousden and Lane 2007). This domain is naturally unstable, with melting temperature of 40-42°C; this could explain its high susceptibility to oncogenic mutations (Canadillas et al., 2006). The oligomerization domain, residues 325-356, has crucial role in the tetramer formation *in vivo*, while the last C-terminus regulatory domain takes part in binding to single stranded DNA and RNA (Tidow et al., 2007). The quaternary structure model of the full p53 and different domains constructs in their free form and bound to a specific DNA sequences was recently obtained from NMR, X-ray scattering (SAXS) in solution, and electron microscopy (EM) of

p53 adsorbed to a carbon support layer (Tidow et al., 2007). This issue was fully reviewed by Jorger and Fersht (2008).

p53 architecture



Figure 1: The human p53 protein consists of 5 regions: the N-terminal intrinsically unstructured transactivation domain (TAD), which interacts with Mdm2, the regulatory proline-rich domain (PRD), a well-structured DNA binding core domain (DBD), the tetramerization domain (4D) and the C-terminal region.

The main function of p53 is to organize cell defence against cancerous transformation by coordinating the signal transduction network (Vassilev et al., 2007; Harris and Levine 2005; Oren, 2003). p53 can be activated by many types of signals, such as cell stress, or DNA damage which can trigger several cellular responses that suppress tumor formation. It is so-called Upstream (cellular stress) and Downstream (cellular responses) Regulation (Figure 1). p53 is stabilized by posttranslational modifications mechanism and accumulates in the cell nuclei; therefore activates or inhibits its target genes inducing cell cycle arrest or apoptosis.

In addition, transcription-independent activities of p53 (Moll et al., 2005) can further enhance and/or differentiate cellular responses to stress, which are precisely controlled by p53 to assure that individual cells choose the irreversible path of self-destruction only as a last resort (Vousden and Lu, 2002).

In order to escape the "safeguard" system mediated by p53 nearly all human cancers have either mutated the p53 (50% all cancers) or compromised the effectiveness of the p53 pathway (Vogelstein et al., 2000; Vousden and Lane, 2007; Toledo and Wahl, 2006). Many mutants of p53 are more stable than wild-type p53 protein and could accumulate in cells. Since the impact of activated p53 is detrimental for cancer, the restitution of p53 function has become the one of the most promising strategy in cancer therapeutics. The implication of p53 in effective cancer therapy is also proven by radiotherapy that induces various proteins which recognize damage and transfer this information to p53 that in turn induces cell death.

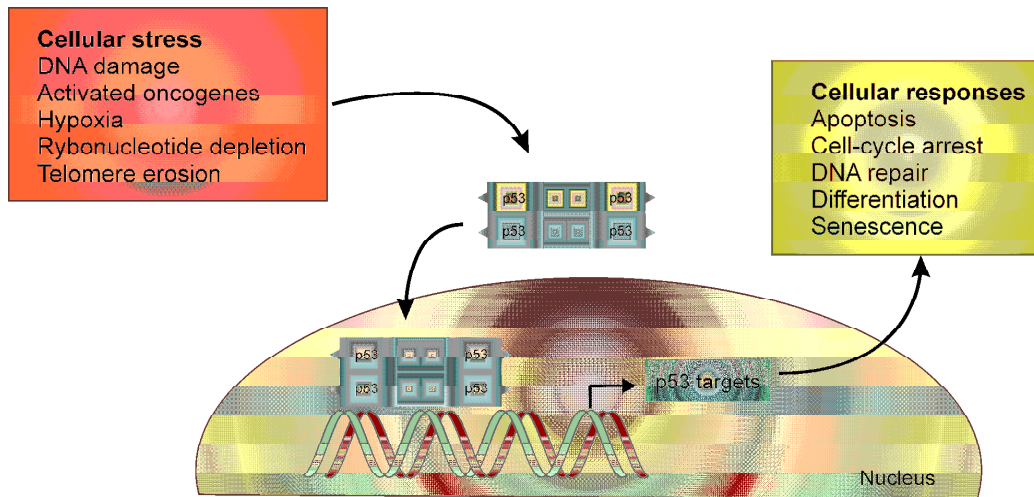


Figure 2. The p53 mediated response. p53 exists in nonstressed cells at a very low concentration. Under stress conditions, the p53 protein accumulates in the cell, binds in its tetrameric form to p53-response elements and induces the transcription of various genes that are involved in cell-cycle control, apoptosis, DNA repair, differentiation and senescence.

The malignant cell transformation is less likely to occur in cells that maintain a functional p53 pathway since mutations are rather found in the cells which perform the genomic instability (during division) that generates the advisable environment for tumor initiation.

1.2 The p53 and Mdm2/x system

The p53 pathway is mostly inactivated by its negative regulators: Mdm2 (Murine double minute 2, Hdm2 in humans) and its relative the Mdmx protein (Vogelstein et al., 2000; Toledo and Wahl, 2006; Vousden and Lane, 2007). Mdm2 is the first to gain the distinction of a principal cellular antagonist of p53. This protein was first identified in 1987 as one of the three genes being amplified in a transformed mouse cell line 3T3DM (Cahilly-Snyder et al., 1987). The Mdm2 gene was found as overexpressed in 30% of osteosarcomas and soft tissue tumor (Oliner et al., 1992). This finding was correlated with discovery that Mdm2 gene product co-precipitate with p53 (Momand et al., 1992; Barak and Oren 1992).

Mdm2 acts as an ubiquitin ligase (it is a member of the RING E3 ubiquitin ligase family), promoting ubiquitination of p53 for the proteasome degradation will follow (Haupt et al., 1997; Kubbutat et al., 1997). As Mdm2 gene is regulated by p53 pathway, the level of

p53 is maintained by autoregulatory feedback loop (Momand et al., 1992; Ringshausen et al., 2006). This allows for mutual controlling the cellular levels of both proteins (Figure 3). After p53 is bound to the promoter, and regulates the expression of Mdm2 (one of its transcription target), rising amounts of Mdm2 triggers inactivation of p53, via direct blocking of the transactivation domain of p53 and by targeting the p53 protein to the proteasome.

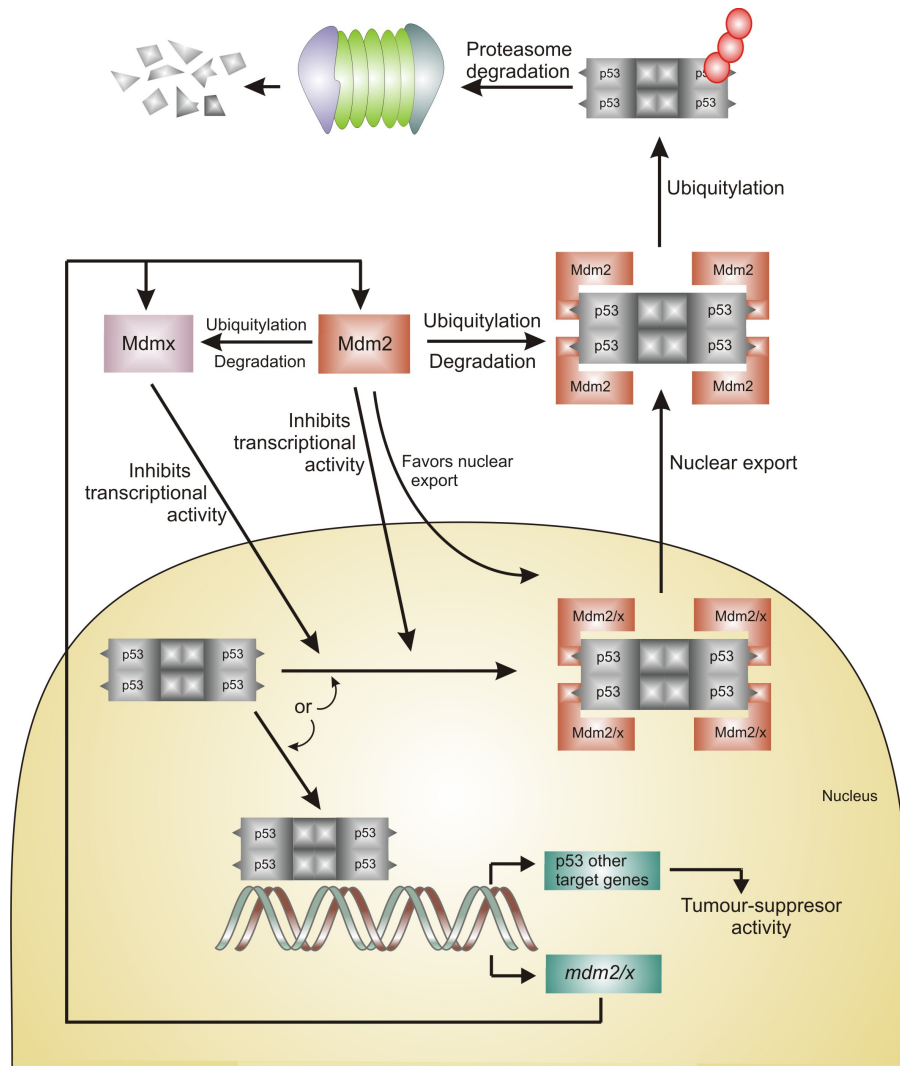


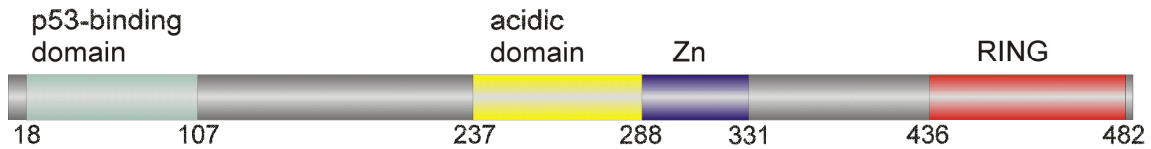
Figure 3. Regulation of p53 by Mdm2 and Mdmx through the autoregulatory feedback loop. p53 is a potent growth suppressive and proapoptotic protein that would harm normal proliferating cells if left uncontrolled. The level of p53 protein in a cell is low and its concentration and activity are subjected to tight control both under normal physiological conditions and during stress. The activity of p53 in a cell is regulated at the level of protein degradation, not at the level of expression of the p53 gene. In an unstressed cell, this is accomplished by Mdm2-mediated degradation via the ubiquitin-proteasome pathway (regulation of p53 stability), and by inactivation of p53 transcriptional activity due to primarily the Mdmx-mediated occlusion of the p53 transactivation domain (inhibition of p53 activity). In addition

Mdm2 and Mdmx modify the activity of p53 by transporting p53 into cytoplasm, away from nuclear DNA. Thus the activity of p53 as a transcription factor is out of reach. After stress, Mdm2 degrades itself and Mdmx, leading to the accumulation and activation of p53; thus a transcriptional response of p53 is mounting. Mdm2 and Mdmx are one of the p53 target genes, and increased nuclear levels of p53 activate Mdm2/x gene transcription, leading to elevated levels of Mdm2 and Mdmx. As activated p53 transactivates Mdm2, the increasingly abundant Mdm2 degrades Mdmx more efficiently, enabling full p53 activation: the transcriptional stress response is at its peak. Following stress relief, the accumulated Mdm2 preferentially targets p53 again; p53 levels decrease, and Mdmx levels increase, p53 activity also decreases. Small amounts of p53 will reduce the amount of Mdm2 protein and this will result in an increase of p53 activity, thus completing the loop. The switch that makes Mdm2 preferentially target p53 for degradation in unstressed cells, then target itself and Mdmx after stress relief, is not precisely understood.

The model described above and in figure 3 assumes that Mdm2 and Mdmx work independently to inhibit p53 activity (Toledo and Wahl, 2006; Marine et al., 2007). In addition, an alternative model suggests that Mdm2 and Mdmx form a heterodimer that is more effective at inhibiting p53 transactivation or enhancing p53 turnover. This model is supported by *in vitro* experiments which show that the Mdm2/Mdmx heterodimers are more effective p53 ubiquitin ligases than individual Mdm2 homodimers (Linke et al., 2008).

Human Mdm2 is a 491 amino acid protein composed of functional domains connected by unstructured regions. Mdm2 interacts primarily through its 100 residue N-terminal domain with the N-terminal transactivation domain of p53 (Kussie et al., 1996; Dawson et al., 2003; Yu et al, 2006). The domain structure Mdm2 is shown in Figure 4. The RING domain is the primary binding site for E2s. The Mdm2 RING domain also mediates Mdm2 homodimerization and heterodimerization with the structurally related Mdmx. The Mdm2 binding site on p53 partially overlaps its transactivation domain, thereby Mdm2 effectively inhibits the p53 transcriptional activity (Momand et al., 1992). The p53 binding domain is followed by a region containing nuclear localization and export signals. The central acidic domain is rich in negatively charged residues (Figure 4).

A Mdm2 architecture



B Mdmx architecture

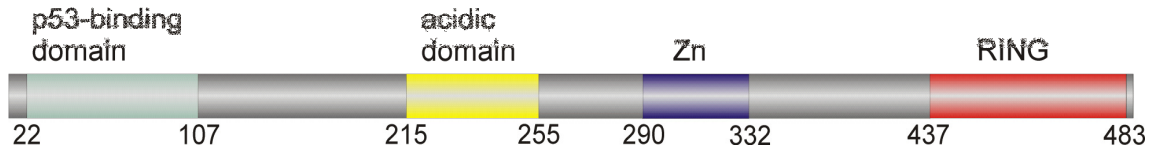


Figure 4. A: The Mdm2 protein comprises 4 domains: the N-terminal p53-binding domain, the acidic domain of yet unknown function, the zinc finger domain similar to RNA-binding protein motifs and the C-terminal RING domain responsible for the ubiquitin ligase activity of the protein.

B: The Mdmx protein comprises 4 similar domains as observed in Mdm2, the acidic domain is relatively shorter than of Mdm2. The human MDMX protein; the RING domain of MDMX does not have the ubiquitin ligase activity.

The high resolution crystal structure of the N-terminal domain of Mdm2 with short peptides derived from p53 provided insights into the atomic details of the p53-Mdm2 interaction (Kussie and Pavletich et al., 1996 (1YCR); Grasberger et al., 2005 (1T4E)). In the crystal structure shown in the Figure 5*, Mdm2 is composed of two major repeats of the secondary structure arranged along a dyad axis. The deep, hydrophobic cleft, lined along these repeats on the Mdm2 surface, forms the p53 pocket binding. the pocket is built by two long and two short α -helices and β -sheets, which seal the sides of the pocket. Surprisingly, the cleft is asymmetric and can be derived into three subpockets occupied by p53 side-chains.

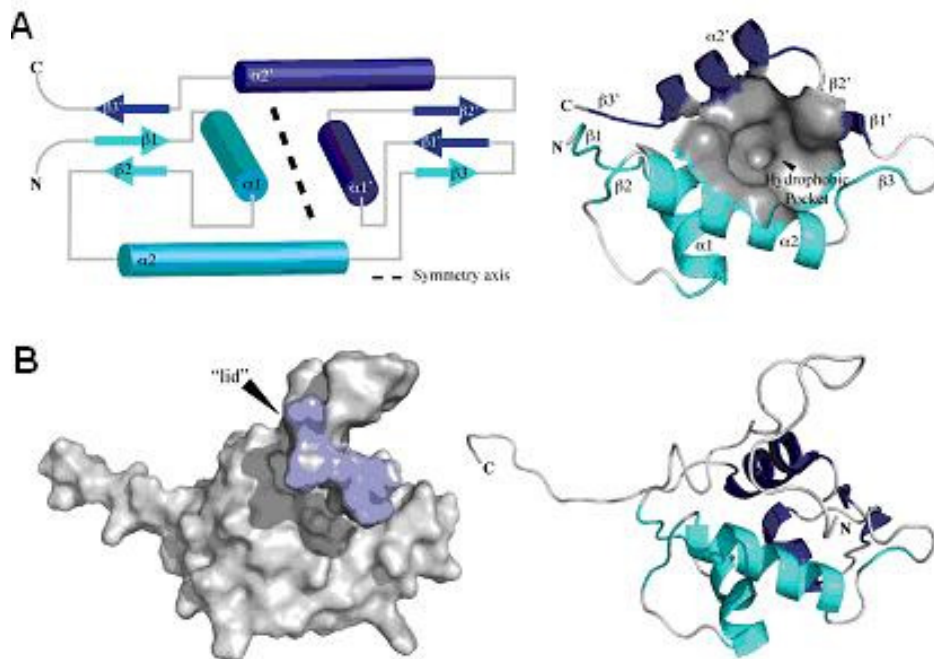


Figure 5*. The structure of Mdm2. A: Holo-Mdm2 (1YCR), Mdm2 is composed of two repeats of the secondary structure that are arranged along an approximate dyad axis of symmetry. Repeat one (cyan), repeat two (blue). The interface of the two monomers is lined with hydrophobic residues that form the cleft for p53 interaction. B: Apo-Mdm2 (1Z1M). The elements of the secondary structure are shorter in the unbound form and the hydrophobic pocket smaller. The N-terminal region folds over the binding pocket and forms a protective "lid".

Upon binding to Mdm2, the p53 peptide forms an amphipathic helix highly complementary to the hydrophobic pocket at the Mdm2 surface. Main contacts for the interaction are hydrophobic and are driven by three p53 amino acids (Phe¹⁹, Trp²³, Leu²⁶). The interface between Mdm2 and p53 consists mainly of van der Waals contacts. In addition, one hydrogen bond is formed between the NH-group of the Trp²³-sidechain of p53 and the carbonyl group of Leu⁵⁴ of Mdm2. The second hydrogen bond is formed between the backbone amide of p53's Phe¹⁹ and side-chain amide of Gln⁷² of Mdm2 (Kussie et al., 1996). Figure 5 shows structural details of the Mdm2- p53 interaction.

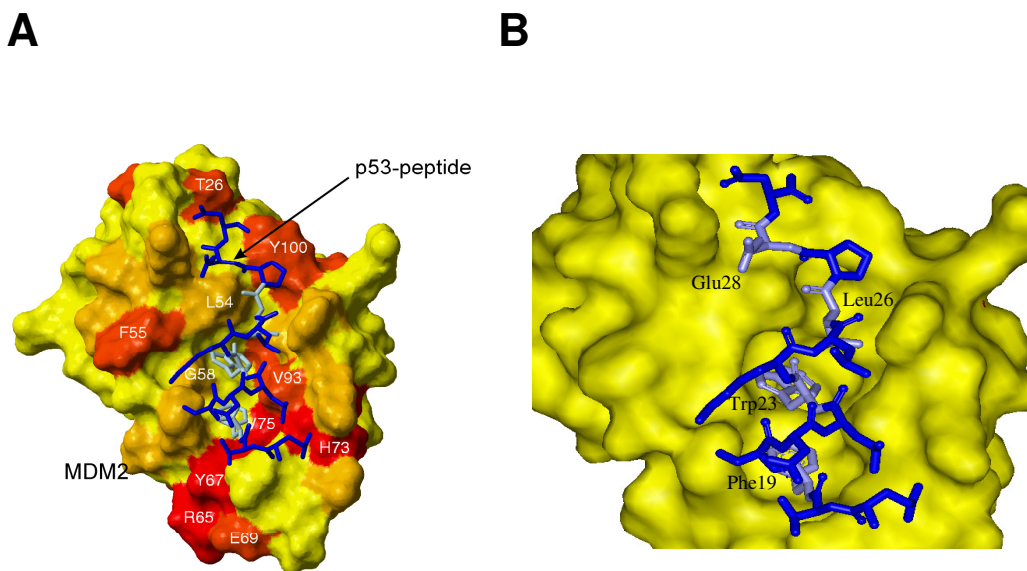


Figure 5. A: Human Mdm2 (surface representation, residues 25-109; PDB: 1YCR) in complex with the p53 peptide (shown in blue sticks with residues Phe¹⁹, Trp²³, and Leu²⁶ colored in gray). Residues of Mdm2 that show significant induced NMR chemical shifts upon complexation with the p53 peptide are highlighted. These residues are shown in brown and red for observed NMR vectorial shifts 0.12-0.2 ppm and greater than 0.2 ppm, respectively. B: Details of the p53-Mdm2 interaction. The interface of p53/Hdm2 relies on the steric complementarity between the Hdm2 cleft and the hydrophobic face of the p53 (-helix and, in particular, on a triad of p53 amino acids Phe¹⁹, Trp²³, and Leu²⁶, which insert deep into the Hdm2 cleft. Thus the p53 amino acid triad comprises the “hot spot” of the p53/Hdm2 interaction. Noteworthy is the cross section dimension of the p53 binding site in Hdm2 of 18 Å (from C(-Tyr67 to C(-Tyr100), which is the size of small organic molecules thus indicating the possibility of small molecule interference.

Mdmx, also known as Mdm4, has only recently emerged as a critical, non-redundant regulator of p53 activation (Toledo and Wahl, 2006; Laurie et al., 2006; Marine et al., 2007). The protein composed of 490 residues was first isolated from the mouse cDNA library (Shvarts et al., 1996). The same group in 1997 identified the human analogue. Independently, Tanimura et al. (1999) showed that Mdmx is associated with Mdm2 in hybrid yeast. Sequence alignment shows that the wild type human Mdmx is highly homologous to human Mdm2 (identity 31.3%, similarity 50.1% for the full length proteins and identity 51.5%, similarity 69.2% in the N-terminal region comprising p53 binding domain). Another highly conserved region-common for both proteins is located at the C terminus (the RING domain, with 42.9% identity and 66.1% of similarity) and enables heterodimerization with Mdm2. In

contrast to Mdm2, the RING domain of Mdmx does not possess the ubiquitin ligase function. The heterodimers of Mdmx-Mdm2 seem to have higher affinity to each other than homodimers of Mdm2 and presumably act as a more efficient ubiquitin ligase (Tanimura et al., 1999). The homodimeric forms of Mdmx were not found in any study, suggesting that free Mdmx may be monomeric.

Aberrant expression of Mdm2 and Mdmx proteins, as well as elevated levels of their mRNA was found in many tumor formations (Table 1).

Table 1. Examples of percentage of tumors with increased mRNA or protein level of Mdmx.

Tumor type	% of cases
Retinoblastoma	60
Glioblastoma	4
Colon	19
Lung	18
Breast	19
Melanoama	14
Hepatocellular carcinoma	50
Head and neck	50
Sarcoma	22
Bladder cancer	25
All cell lines	40

1.2.1 Inhibitors of Mdm2/x-p53 interaction

As already stated in section 1.1, the rescue of the impaired p53 function by disrupting the Mdm2-p53/Mdmx-p53 interaction offers a fundamentally new principle for anticancer therapeutics (Figure 6), (Chene, 2003; Vassilev, 2006; Toledo and Wahl, 2006; Vousden and Lane, 2007; Marx, 2007).

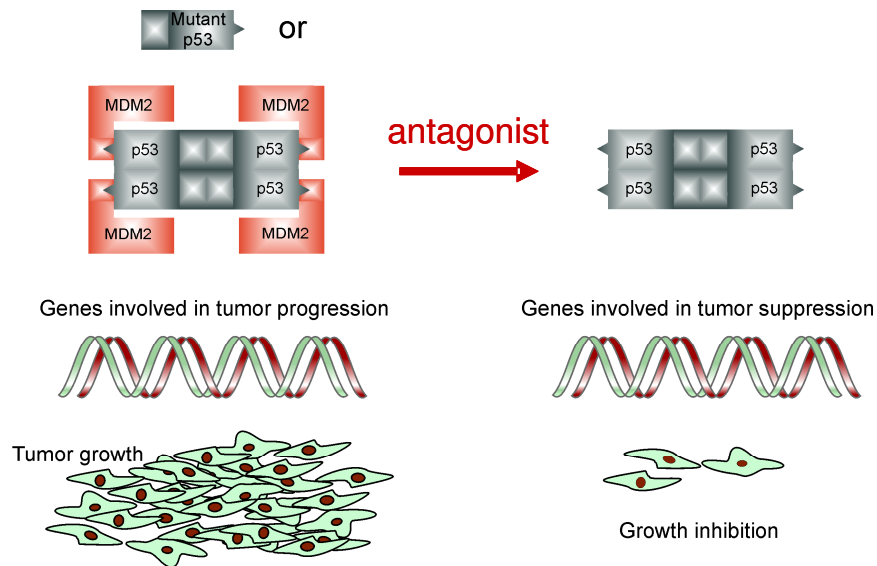


Figure 6. Inactivation of the p53: by p53 mutation (which occurs in 50% of human cancers), and (for the remainder half of all cancers) by inhibition of the wildtype p53 by Mdm2 (shown here) and Mdmx. The rescue of the impaired p53 function by disrupting the Mdm2-p53 should lead to growth inhibition of tumors.

Three independent teams have very recently verified that restoring the antitumor activity of p53 can indeed eliminate cancers in mice (Figure 7) (Marx, 2007; Martins et al., 2006; Ventura et al., 2007; Xue et al., 2007).

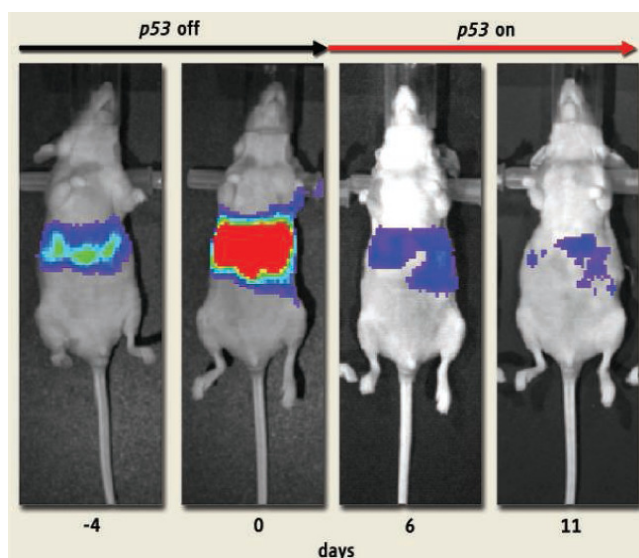


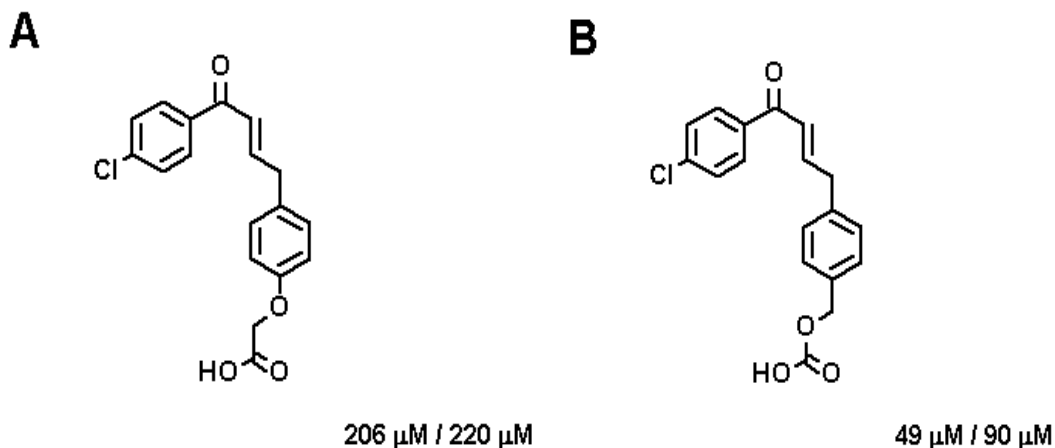
Figure 7. Reactivation of p53 leads to rapid tumor regression (adapted from Xue et al., 2007).

Crystal structures of Mdm2-p53 complexes revealed structural details of the Mdm2-p53 interaction and in fact raised the expectation that high affinity small molecular weight compounds for this interaction could be designed. Mdm2 possesses a well-defined binding site for p53. For most protein-protein interactions the binding energy is mostly concentrated into “hotspots”, such as for example, the triad of Mdm2-binding amino acids of p53 (Phe¹⁹, Trp²³, Leu²⁶). The p53 derived peptides were the starting points for designing of inhibitors for Mdm2-p53. It is known that the p53 native peptide is unstructured in solution and adopts a helical structure only after binding to Mdm2 (Botuyan et al., 1997; Bernal et al., 2007). Recently, more potent p53-mutant peptide inhibitors were discovered using phage display peptide libraries (Bottger et al., 1996). Garcia-Echeverria et al. (2000) found peptides with the 28-fold increased affinity for Mdm2 compared to the native p53 peptide. These authors also found that the chloro- substituent in Trp²³ increased the binding around 1800-fold compared to the wild type peptide. Thus, the small molecule Mdm2-p53 inhibitors should aim at mimicking the interaction of p53 with Mdm2 and ideally mimic at least one of the hydrogen bonds involved in this binding.

The first reported low-molecular weight inhibitors of the p53-Mdm2 interaction (Stoll et al., 2001) were chalcones (Scheme 1). These compounds, derived from 1,3-diphenyl-2-propen-1-one, are known to have broad tumor suppressing activities (Dore and Viel, 1974). The binding of chalcones to Mdm2 is in the double-digit μM range. The strongest binding to Mdm2 was seen for the chalcones that contained a chlorophenyl group and it subsequently

turned out that this substituent is crucial for the binding to Mdm2. All the known, more potent inhibitors of Mdm2 possess this group (Vassilev et al., 2004; Grasberger et al., 2005).

Scheme 1. Representative chalcone skeletons. Inhibition of Mdm2 binding to p53 measured by ELISA (IC_{50} values given on the left side of the slash) and by NMR titration experiments (K_D values given on the right side of the slash).



More recently, several lead compounds have recently been reported to inhibit the Mdm2-p53 interaction (see Table 2) (Vassilev et al., 2004; Vassilev, 2006; Grasberger et al., 2005; Shangary et al., 2008). Through extensive high throughput screening of large chemical libraries potent small molecular inhibitors, termed nutlins were obtained by Vassiliev and colleagues (Vassiliev et al., 2004). Nutlins were the first nanomolar drug-like compounds developed for Mdm2-p53 interaction. They induce apoptosis in p53 wild-type cells and show *in vivo* efficacy in mice xenograft models, however, this effect is shown only at high non-physiological concentrations (Vassilev et al., 2004).

The second potent class of inhibitors are benzodiazepinediones obtained also through high-throughput screening (Parks et al., 2005; Grasberger et al., 2006). However, further studies showed the low cellular activity of these compounds. After increasing solubility, as well as the cellular permeability of the compounds, the optimal final compound restored the functions of p53 transcriptional targets, and inhibited the proliferation of cells with wild-type p53 (Koblish et al., 2006).

The most recently discovered Mdm2 antagonists are spiro-oxindole (“Mi” compounds) obtained using structure-based de novo design strategy (Ding et al., 2008; Shangary et al.,

2008). The best product Mi-219, showed high potency and selectivity in cancer cells with wild type p53 (Shangary et al., 2008; Ding et al., 2006). The *in vivo* antitumor activity of nutlin-3 and Mi-219 was checked for several xenograft mice models of cancer and reach the stage of early-phase clinical trials. The inhibitors showed little toxicity in animals at therapeutic dosages. Another class of most recent nm inhibitors of the Mdm2-p53 interaction are derivatives of 3-imidazozy-indiles, patented by novartis. No “cellular” data is available for this class of compounds (Table 2).

The model of *cis*-imidazoline analog nutlin-3 and the predicted binding model of spiro-oxindole analog Mi-219 to Mdm2 are displayed in Figure 8. The most recent nanomolar inhibitors of the Mdm2-p53 interaction are derivatives of 3-imidazozy-indoles, patented by Novartis. No “cellular” data is available for this class of compounds (Table 2).

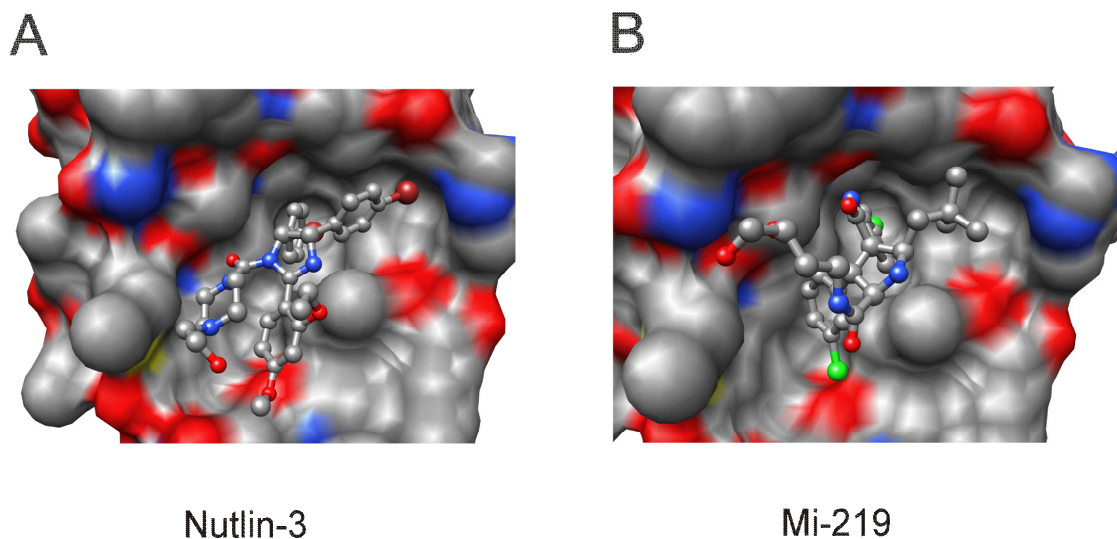
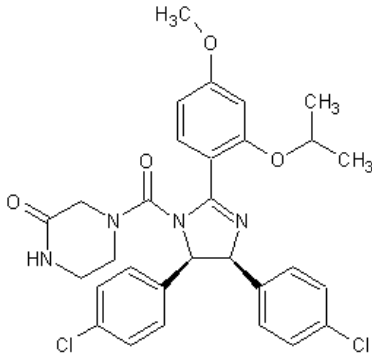
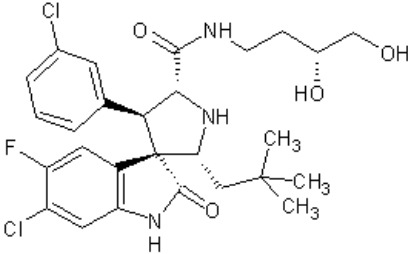
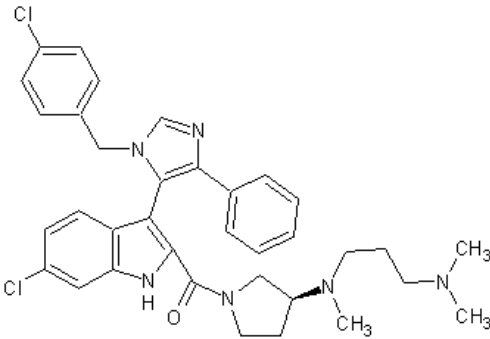


Figure 8. A: Binding model of the *cis*-imidazoline analog nutlin-3. B: The predicted binding model of spiro-oxindole analog Mi-219 to Mdm2. Side chains of nutlin-3 and Mi-219 are shown in ball and stick representation. Nutlin-3 is shown with carbons in cyan, nitrogen in blue, oxygen in red, and bromine in brown. The predicted binding of Mi-219 to Mdm2 is shown with carbons in grey, nitrogen in blue, oxygen in red, fluorine in light blue, and chlorine in green. The surface representation of Mdm2 in each case is shown with carbons in grey, nitrogen in blue, oxygen in red, and sulfur in yellow. Hydrogen and hydrogen atoms are excluded for clarity. The Chimera program was used to generate figures.

Table 2. Nonpeptidic small-molecule inhibitors currently in the development for the Mdm2-p53 interaction

Chemical class compound	Development status (refs.)
<p data-bbox="256 333 412 361">Cis-imidazoline</p>  <p data-bbox="480 747 561 772">Nutlin-3</p>	<p data-bbox="946 333 1341 449">Preclinical models of human cancer retaining wildtype p53 (Vassilev et al., 2004; Vassilev, 2007).</p>
<p data-bbox="256 808 402 835">Spiro-oxindole</p>  <p data-bbox="480 1113 561 1136">Mi-219</p>	<p data-bbox="946 808 1341 924">Preclinical models of human cancer retaining wildtype p53 (Shangary et al., 2008).</p>
<p data-bbox="256 1167 456 1194">3-imidazolyl-indoles</p>  <p data-bbox="448 1556 586 1583">Novartis 101</p>	<p data-bbox="946 1167 1341 1283">Preclinical models of human cancer retaining wildtype p53 (Patent WO 2008/119741).</p>

Regarding Mdmx, several recent studies concluded that nutlin-3 does not disrupt Mdmx-p53 complexes (Hu et al., 2006; Toledo et al., 2006; Wade et al., 2006; Popowicz et al., 2007) whereas one report (Laurie et al., 2006) provides evidence that the potency of nutlin-3 is sufficient to disrupt the Mdmx-p53 interaction and to efficiently kill retinoblastoma cancer cells (Laurie et al., 2006; Marine et al., 2007). Our own NMR and ITC binding data clearly show that Mdm2/p53 antagonists are not effective in the inhibition of the Mdmx/p53 interaction (Popowicz et al., 2007). The retinoblastoma tumor cell killing effect of nutlin-3 observed by Laurie et al. (2006) could be explained by an indirect action of nutlin in which extremely high, “rancid” concentrations of the compound would effect Mdmx protein levels (Vassilev, 2006) or activate E2F1 (Ambrosini et al., 2007).

In general, it has been confirmed in several binding assays that the lead compounds reported so far bind stronger to Mdm2 than to Mdmx (Laurie et al., 2006; Shangary et al., 2008). A recent NMR study as well as amino acid sequence analysis of the p53 binding regions in Mdm2 and Mdmx suggested a possible explanation (Rallapalli et al., 2008). These authors proposed that the Mdmx region that constitutes the Pro⁹⁵-Ser⁹⁶-Pro⁹⁷ motif, not present in Mdm2, could be responsible for the difference in binding affinity.

There are no potent small molecular weight Mdmx antagonists available up to date. However, several groups discovered peptides showing similar and potent nM affinity to both Mdm2 and Mdmx, like for example, the recently solved crystal structures of Mdmx with phage displayed derived p53 peptide (Czarna et al., 2009) and the peptides described by Kallen et al. (2009). Based on these studies there is a hope that also nonpeptidic small dual action Mdm2/Mdmx inhibitors can be discovered. If the cooperative model of p53 by Mdm2 and Mdmx is correct, such inhibitors may be a promising tool for a wide range of cancer research.

Mdm2/x antagonists may have also important utility in protecting normal proliferating tissues during anti-mitotic chemotherapy of tumors expressing mutant p53. Normal cells possess wildtype functional p53, and pretreatment with Mdm2/x antagonists will arrest their proliferation and may protect them from the toxicity of chemotherapy. The proliferation may be restored after drug removal. Cancer cells with mutant p53 would be insensitive to Mdm2/x antagonists and thus be selectively vulnerable to the drug (Vassilev, 2006).

1.3 Fragment-based drug discovery and the role of NMR in fragment screening

Fragment-based drug design has become an important and powerful approach in structure-based lead discovery (reviewed in: Rees et al., 2004; Schade and Oschkinat, 2005; Jahnke and Erlanson, 2006; Erlanson, 2006; Hajduk and Greer, 2007; Hubbard et al., 2007). Compared with traditional screening hits, the starting fragments have considerably lower

molecular mass, and although the binding interactions of these fragments with a target protein are weak, they are structurally understood through X-ray crystallography or NMR, and they exhibit high “ligand efficiency”. Synthetic linking or merging of the fragments should generate chemical series with high-affinity lead-like properties. In its essence, fragment-based drug design attempts to describe high-affinity ligands in terms of the molecular pieces that comprise a composite inhibitor. Much has been discussed about the proper physicochemical properties (e.g., molecular weight, hydrophobicity, etc.) that should be considered when utilizing fragment leads in drug design. However, only recently the emphasis was placed on the potency of the resulting fragment leads. A recent retrospective analysis of 18 highly optimized inhibitors, in which the compounds were systematically deconstructed until the minimal binding elements could be identified, showed that a nearly linear relationship exists between molecular weight and binding affinity over the entire range of sizes and potencies represented in the dataset (Hajduk, 2006). Based on these observations, prediction maps can be constructed that enable critical and quantitative assessments of the process of lead identification and optimization. These data place well-defined limits on the ideal size and potency of fragment leads that are being considered for use in fragment-based drug design.

NMR-based drug screening methods, like for example, the NMR chemical shift perturbation method (Shuker et al., 1996), are powerful techniques used for the identification and characterization of ligand-protein interactions (reviewed in: Diercks et al., 2001; Stockman and Dalvi, 2002; Coles et al., 2003; Meyer and Peters, 2003; Jahnke and Widmer, 2004; Lepre et al., 2004; Peng et al., 2004; Schade and Oschkinat, 2005; Klages et al., 2007). In comparison with other screening technologies, a unique feature of NMR is its robust ability to detect weak intermolecular interactions. This ability makes NMR ideal for fragment-based screening for which detection of binding between low-affinity fragments and target proteins is required (Babaoglu and Shoichet, 2006; reviews: Rees et al., 2004; Schade and Oschkinat, 2005; Klages et al., 2007).

The recently described NMR-based assay for studying the effect of antagonists on protein-protein interactions (D’Silva et al., 2005; Krajewski et al., 2005; Krajewski et al., 2007; Rothweiler et al., 2008a), named AIDA (for the Antagonist Induced Dissociation Assay) NMR, provides unambiguous information on whether an antagonist of a protein-protein interaction is strong enough to dissociate the complex and whether its action is through denaturation, precipitation, or release of a protein in its functional folded state. This method was checked for several lead compounds that have been reported in the literature to inhibit the p53-Mdm2 interaction, only one of them, nutlin-3, turned out to be a potent inhibitor of this interaction *in vitro* (D’Silva et al., 2005; Krajewski et al., 2005; Popowicz et al., 2007).

AIDA NMR requires the protein complex of interest to be formed between proteins with considerably varying molecular weights. For a two-protein interaction complex, the size of one component (the NMR reporter protein) should be small enough (less than ca. 15 kDa) to provide a good quality ^{15}N (^{13}C) HSQC spectrum after ^{15}N (^{13}C) labelling. The size of the second, unlabeled component should be large enough so that the molecular weight of the preformed complex is larger than ca. 40 kDa. Formation of the complex should result in higher NMR transverse relaxation rates R_2 of the reporter protein, which causes a decrease in its NMR intensities to a point that they may completely disappear. The spectrum of the protein-protein complex changes dramatically, if an inhibitor that breaks the complex is added. Two outcomes are possible in the case of the complex dissociation: either the reporter spectrum is recovered unchanged, when the inhibitor binds to the larger protein, or the recovered spectrum displays modifications caused by the inhibitor binding. It is noteworthy to point out that the dissociation is detected irrespectively of the protein the compound acts on. Thus, there are two targets checked simultaneously and the selection of the right binding site and the inhibition strength is obtained in principle without any prior knowledge of these parameters. The AIDA approach therefore targets protein-protein interactions and not a single protein. A schematic representation of the 2D NMR version of AIDA, (D´Silva et al., 2005; Krajewski et al., 2005; Krajewski et al., 2007; Rothweiler et al., 2008) is shown in Figure 9 and of the 1D proton NMR version (Rothweiler et al., 2008) in Figure 10.

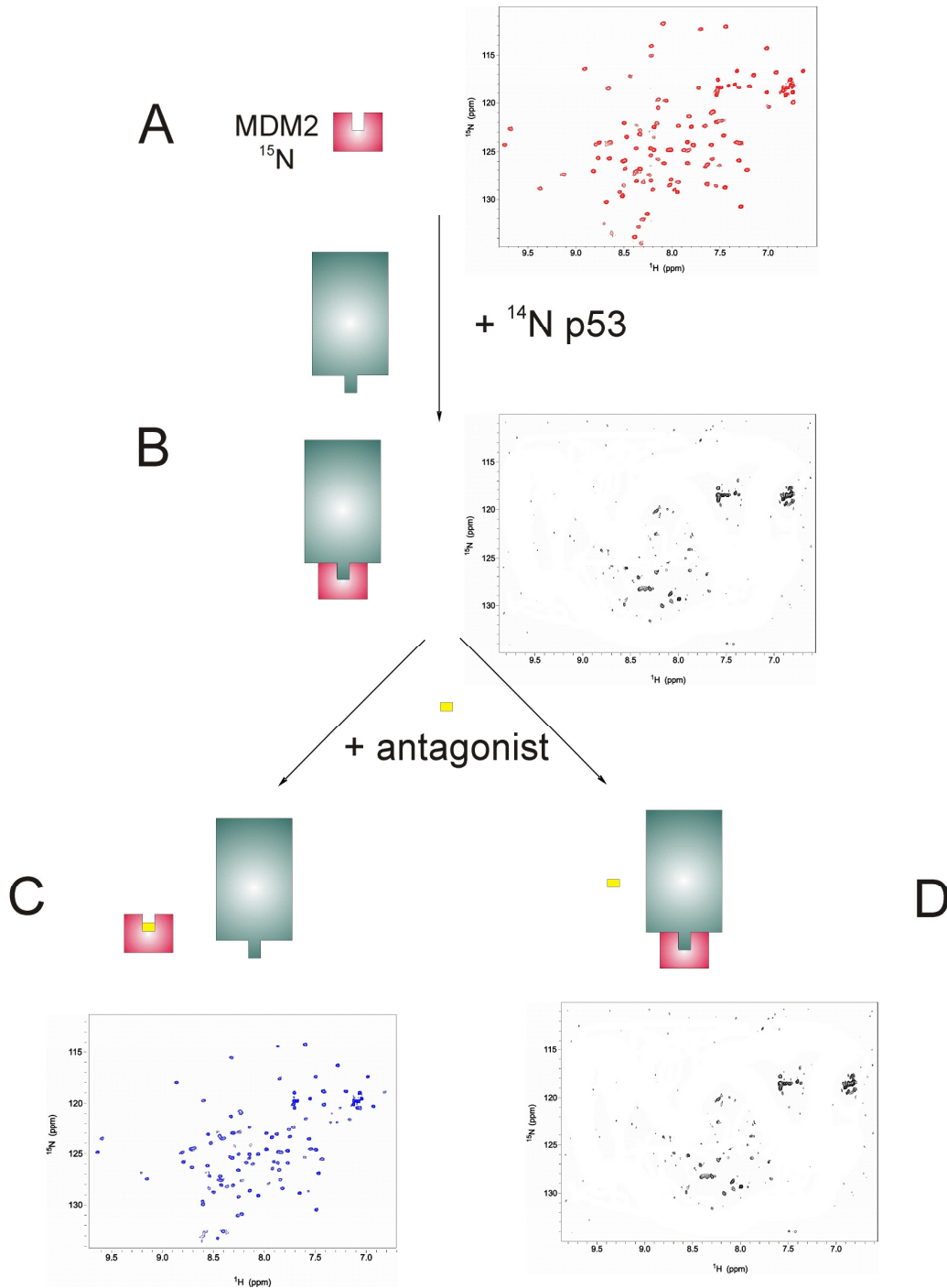


Figure 9. The 2D version of the AIDA (Antagonist-Induced Dissociation Assay) requires a small reporter ^{15}N -labeled protein that gives a good quality ^1H - ^{15}N -HSQC spectrum and a large (unlabeled) interaction partner protein (e.g. p53). A: ^{15}N HSQC spectrum of a ca. 12 kDa uniformly ^{15}N labeled Mdm2 (each amino acid gives a cross peak for the N-H pair, the side chain N-H resonances are observed at around 7 ppm ^1H and at 120 ppm ^{15}N chemical shifts). B: The cross-peaks disappear on addition of a large fragment of the p53 protein (ca. 35 kDa) that forms a complex with the smaller one.

Due to increase in the rotational correlation time of the protein-protein complex, the HSQC signals get broadened and fall into the noise level. C: Addition of an effective antagonist of the protein-protein interaction results in release of the small ^{15}N -labeled protein from the complex and the HSQC signal recovery. D: A weak inhibitor does not dissociate the complex.

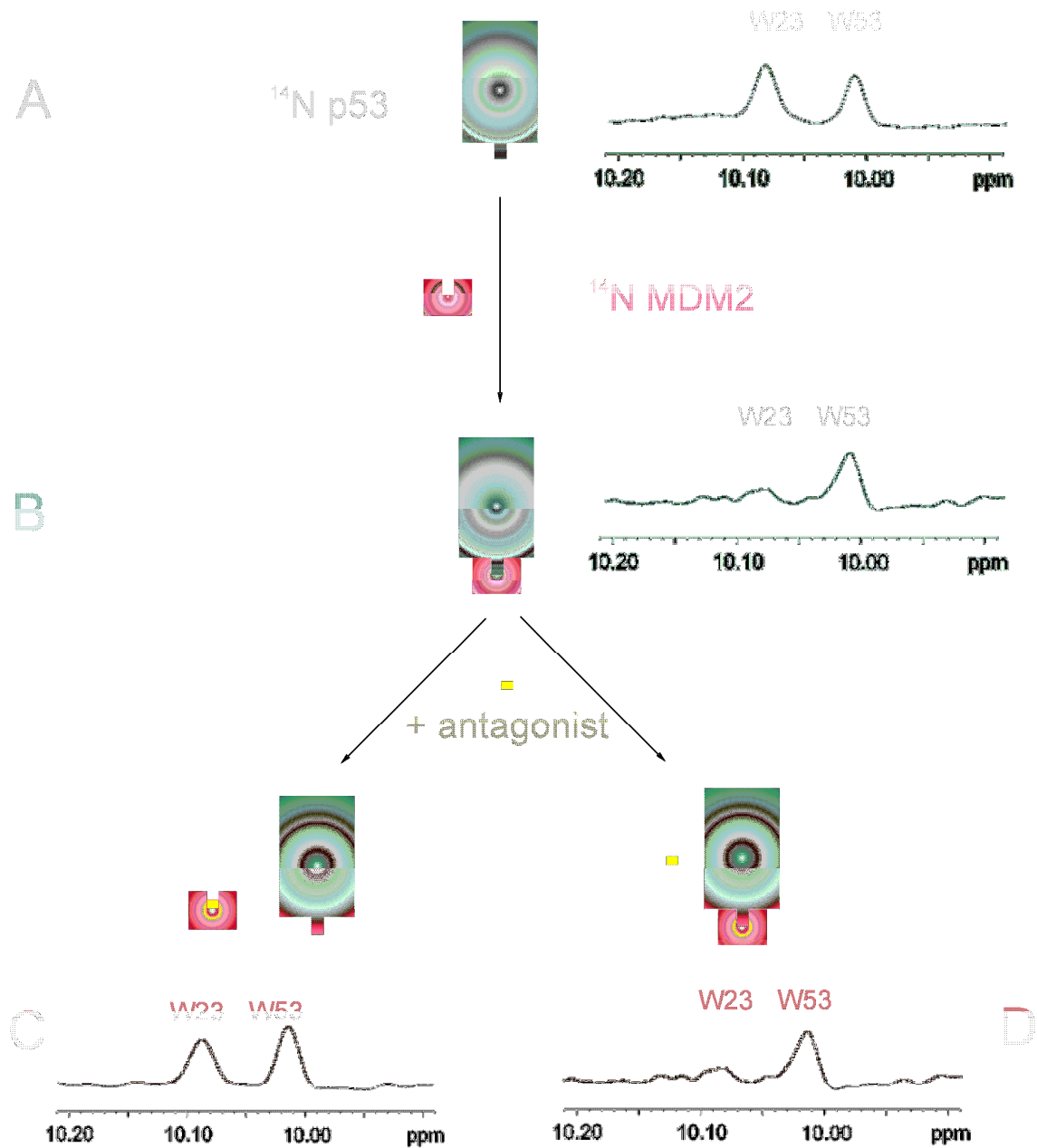


Figure 10. 1D NMR version of the AIDA assay. A: The 1D proton NMR spectrum of the side chains of tryptophans (W) of free p53 (residues 1-321). The N-terminal domain of p53 has three tryptophan residues: W23, W53, and W91 (the N-terminal domain encompasses residues 1-94; the p53 domain

structure is shown in Figure 3). Because of a highly flexible nature of the very N-terminal segment of p53 between residues 1-73, the side chains of W23 and W53 give rise to sharp lines. B: On forming the complex with Mdm2, the signal of W23 disappears. This is because W23, together with the p53 residues 17 to 26 comprise the primary binding site for Mdm2. Upon binding, these residues participate in a well-defined structure of a large p53-Mdm2 complex, whereas W53 is still not structured when p53 is bound to Mdm2 (D'Silva et al, 2005; Krajewski et al., 2007; Rothweiler et al., 2008a). The observed $1/T_2$ transverse relaxation rate of the bound W23 in the complexes increases thus significantly and broadening of NMR resonances results in the disappearance of this signal in the spectra. C: Disruption of the Mdm2-p53 interaction results in the release of free p53 and the recovery of the W23 p53 ^1H signal. The height of W23 peak corresponds to the fraction of free p53 and thus, when total concentrations of the complex and the antagonist are known, the K_D of the Mdm2-antagonist interaction can be determined from a single competition experiment. D: A weak inhibitor does not dissociate the complex.

2 Goals of the study

In the past few years, new drugs have been developed that can improve cancer patient survival. But oncogenes are only one part of the tumorigenic driven system. It is believed that all human cancers also have defects in tumor suppressor genes that would normally contain cancer development. The tumor suppressor genes are thus increasingly targeted for possible therapies that work by restoring their activity.

I have undertaken the project to develop specific, potent inhibitors for both the Mdmx-p53 and Mdm2-p53 interactions using nuclear magnetic resonance (NMR) and structure based approaches to search for agents that induce the activity of the tumor suppressor protein p53. Within this research, we have determined the structure of Mdmx bound to several p53 peptides, thus establishing the structural basis for the inhibition of p53 by Mdmx.

3 Materials and laboratory methods

3.1 Materials

3.1.1 *E. coli* strains and plasmids

Table 3.1. *E. coli* strains used in the study

Strain	Usage	Company
XL1-Blue	Cloning	Stratagene (USA)
One Shot TOP10	Cloning	Novagen (Canada)
DH5 α	Cloning	Novagen (Canada)
GigaSingles	Cloning	Stratagene (USA)
BL21 Star	Expression	Invitrogen (Holland)
BL21 Star(DE3) pLysS	Expression	Invitrogen (Holland)
BL21 Star(DE3) RIL	Expression	Invitrogen (Holland)
Rosetta (DE3)	Expression	Novagen (Canada)
RosettaBlue(DE3)	Expression	Novagen (Canada)
Arctic	Expression	Novagen (Canada)
BL21 Prar	Expression	Novagen (Canada)

Table 3.2. Vectors used in the study

Vector	Antibiotic	Tag	Company
pET 28a(+)	Kanamycin	C-terminal 6-His	Novagen (Canada)
pET 20b(+)	Ampicillin	no tag	Novagen (Canada)
pET 41 Ek/LIC	Kanamycin	6-His/GST	Novagen (Canada)
pET 46 Ek/LIC	Ampicillin	N-terminal 6-His	Novagen (Canada)
pEt 28 SUMO-3	Kanamycin	His/GFP/SUMO	Novagen (Canada)
pGEX 4T1	Ampicillin	N-terminal GST	Amersham–Pharmacia (Sweden)

3.1.2 Cell growth media and stocks

3.1.2.1 Media

For 1 liter LB medium

10 g peptone
5 g bacto yeast extract
10 g sodium chloride

pH was adjusted to 7.0. For the preparation of agar plates the medium was supplemented with 15 g agar.

For 1 liter TB medium

1 g bacto tryptone
24 g bacto yeast extract
10 g sodium chloride
4 ml glycerol
900 ml deionized water

The medium was autoclaved, cooled; 100 ml sterile K phosphate and glucose were added. The final concentration of glucose was 0.5%

For 1 liter K-phosphate, pH 7.1

23.1 g KH_2PO_4
125.4 g K_2HPO_4

Minimal medium (MM) for uniform enrichment with ^{15}N

For 1 liter MM

0.5 g NaCl
1.3 ml trace elements solution
1 g citric acid monohydrate
36 mg ferrous citrate
4.02 g KH_2PO_4
7.82 g $\text{K}_2\text{HPO}_4 \times 3\text{H}_2\text{O}$
1 ml Zn-EDTA solution
1 g NH_4Cl or $^{15}\text{NH}_4\text{Cl}$

pH was adjusted to 7.0 with NaOH, the mixture was autoclaved, upon cooling, separately sterilized solutions were added: 25 ml glucose, 560 μl thiamine, antibiotics, 2 ml MgSO_4 stock.

Defined medium for selective ^{15}N labeling of proteins

For 1 liter of medium

400 mg Ala, Gln, Glu, Arg, Gly
 255 mg Asp, Met
 125 mg cytosine, guanosine, uracil
 100 mg Asn, Leu, His, Lys, Pro, Thr
 100 mg Try
 400 mg Ile, Val
 50 mg Phe, thymine, thymidine
 1.6 g Ser
 10 mg CaCl₂
 2 g NaAc
 10 g K₂HPO₄
 1 g citric acid
 1.3 ml trace element solution
 36 mg ferrous citrate
 1 ml Zn-EDTA solution
 1g NH₄Cl

pH was adjusted to 7.0 with NaOH, the mixture was autoclaved. To the cooled medium, separately sterilized solutions were added: 25 ml glucose, 560 µl thiamine, antibiotics, 2 ml 1 M MgSO₄, sterile filtered

50 mg Cys, Trp, nicotinic acid
 0.1 mg biotin
 X mg ¹⁵N-amino acid

Another portion of the ¹⁵N-amino acid is added at the time of induction as well (same amount as added before, 0.22 µm filtered).

3.1.2.2 Stock solutions

Ampicillin: 100 mg/ml of ampicillin in deionized H₂O, sterilized by filtration, stored in aliquots at -20°C until used. Working concentration: 150 µg/ml.

Chloramphenicol: was dissolved in ethanol (0.34 g/10 ml) to the end concentration of 34 mg/ml. Working concentration: 34 µg/ml.

Kanamycin: 100 mg/ml of kanamycin in deionized H₂O, sterile filtrated and stored in aliquots at -20°C until used. Final concentration: 100 µg/ml.

Gentamycin: 50 mg/ml industrially prepared stock solution, 8 µg/ml of the working concentration.

Streptomycin: 60 mg/ml water stock solution, final concentration 60 µg/ml.

IPTG: A sterile filtered 1 M stock of IPTG in distilled water was prepared and stored in aliquots at -20°C until used.

Glucose: 20% (w/v) in deionized H₂O, autoclaved.

Thiamine, 1%, in deionized H₂O, sterilized by filtration.

MgSO₄, 1 M, in deionized H₂O, sterilized by filtration.

Zn-EDTA solution	5 mg/ml EDTA
	8.4 mg/ml Zn(Ac) ₂
Trace elements solution:	2.5 g/l H ₃ BO ₃
	2.0 g/l CoCl ₂ x H ₂ O
	1.13 g/l CuCl ₂ x H ₂ O
	9.8 g/l MnCl ₂ x 2H ₂ O
	2.0 g/l Na ₂ MoO ₄ x 2H ₂ O
	pH lowered with citric acid or HCl.

3.1.3 Solutions for making chemically competent *E. coli* cells

Solutions for making competent cells

Buffer A	100 mM MgCl ₂ x 6H ₂ O
Buffer B	100 mM CaCl ₂ –15% glycerol

3.1.4 Protein purification – buffers

Heparin sepharose affinity chromatography buffers

P(0)	50 mM KCl
	50 mM TRIS-HCl
	5 mM DTT
	10% Glycerol
	pH 7.5

P(1)	50 mM KCl 50 mM TRIS-HCl 1M KCl 5 mM DTT pH 7.5
PBS	140 mM NaCl 2.7 mM KCl 10 mM Na ₂ HPO ₄ 1.8 mM KH ₂ PO ₄ 0.05% NaN ₃ pH 7.3
Crystallization buffer	5 mM TRIS-HCl 50 mM NaCl 10 mM Betamercaptoetanol pH 8.0
Buffer for gel filtration	50 mM Na ₂ HPO ₄ 50 mM KH ₂ PO ₄ 5 mM DTT pH 7.5
Affinity chromatography buffers - Sepharose glutathione	
Binding buffer	PBS
Wash buffer	PBS
Elution buffer	50 mM Tris-HCl 150 mM NaCl 10-30 mM glutathione reduced pH 8.0
Buffers for immobilized metal-chelate chromatography (IMAC) under native conditions	
Binding buffer	50 mM NaH ₂ PO ₄ 300 mM NaCl 10 mM imidazole pH 8.0
Wash buffer	50 mM NaH ₂ PO ₄ 300 mM NaCl

Elution buffer	20 mM imidazole pH 8.0 50 mM NaH ₂ PO ₄ 300 mM NaCl 250 mM imidazole pH 8.0
Buffers for IMAC under denaturing conditions	
Buffer A (binding buffer)	6 M guanidinium chloride 100 mM NaH ₂ PO ₄ x H ₂ O 10 mM Tris 10 mM β-mercaptoethanol pH 8.0
Buffer B (wash buffer)	6 M guanidinium chloride 100 mM NaH ₂ PO ₄ x H ₂ O 10 mM Tris 10 mM β-mercaptoethanol pH 6.5
Buffer C (elution buffer)	6 M guanidinium chloride 100 mM NaAc x 3H ₂ O 10 mM β-mercaptoethanol pH 4.0
Buffer D (dialysis buffer)	6 M guanidinium chloride pH 3.0
Buffer E (refolding buffer)	1 mM arginine HCl 1 mM EDTA 100 mM Tris 5 mM DTT 8.8% (v/v) glycerol 0.05% NaN ₃ pH 8.4
Buffers for refolding and hydrophobic interaction	
Dialysis buffer	4M GuHCl 5 mM DTT

	pH 3.5
Solubilization buffer	6 M GuHCl 100 mM TRIS 10 mM DTT
	pH 8.0
Elution buffer	100 mM Tris 10 mM DTT
	pH 7.0
Refolding buffer	10 mM TRIS-HCl 4 mM EDTA 10 mM DTT
	pH 7.0
Buffer EK (Enterokinase cleavage buffer)	20 mM Tris 100 mM NaCl 2 mM CaCl ₂ 0.01% NaN ₃
	pH 7.5
Buffer PP (PreScission Protease cleavage buffer)	50 mM Tris 150 mM NaCl 1 mM EDTA 1 mM DTT pH 7.0

3.1.5 Buffer for DNA agarose gel electrophoresis

50X TAE buffer (for 1 l)

40 mM Tris-acetate

1 mM EDTA

Glacial acetic acid

242 g of Tris base

100 ml of 0.5 M EDTA (pH 8.0)

57.1 ml

3.1.6 Reagents and buffers for the SDS-PAGE and protein visualization

3.1.6.1 SDS-PAGE gel preparation

Anode buffer (+)	200 mM Tris pH 8.9
Cathode buffer (-)	100 mM Tris pH 8.25 100 mM tricine 0.1% SDS
Separation buffer	1 M Tris pH 8.8 0.3% SDS
Stacking buffer	1 M Tris pH 6.8 0.3% SDS
Separation acrylamide	48% acrylamide 1.5% bis-acrylamide
Stacking acrylamide	30% acrylamide 0.8% bis-acrylamide
Pouring polyacrylamide gels	
Separation gel	1.675 ml H ₂ O 2.5 ml separation buffer 2.5 ml separation acrylamide 0.8 ml glycerol 25 µl APS 2.5 µl TEMED
Intermediate gel	1.725 ml H ₂ O 1.25 ml separation buffer 0.75 ml separation acrylamide 12.5 µl APS 1.25 µl TEMED
Stacking gel	2.575 ml H ₂ O 0.475 ml stacking buffer 0.625 ml stacking acrylamide 12.5 µl 0.5 M EDTA, pH 8.0 37.5 µl APS 1.9 µl TEMED

3.1.6.2 Protein visualization

Coomassie-blue solution	450 ml ethanol 100 acetic acid 450 ml water 2.5 g Coomassie Blue R-250
Destaining solution	400 ml ethanol 100 ml acetic acid 500 ml water

3.1.7 Reagents and buffers for Western blots

Transfer buffer	25 mM Tris 192 mM glycine pH 8.3
To make the final working solution mix 80 ml of the transfer buffer with 20 ml of methanol	
Alkaline phosphatase buffer	100 mM Tris 100 mM NaCl 5 mM MgCl ₂ pH 9.5
Wash buffer	10 mM Tris 150 mM NaCl 0.05% Tween20 pH 8.0
1 st antibody solution	1:2000 diluted in the wash buffer
2 nd antibody solution (linked to alkaline phosphatase)	1:2000 diluted in alkaline phosphatase buffer
Substrate for alkaline phosphatase	BCIP (Sigma); dissolve 1 tablet in 10 ml of water

3.1.8 Reagents and buffers for electroblotting for N-terminal sequencing

CAPS buffer (10x, 100mM)	22.13 g CAPS 90 ml deionized water pH 11
Electroblotting solution	10 mM CAPS in 10% MeOH

Tris-Glycine buffer	25 mM Tris base 192 mM Glycine 10% (v/v) MeOH pH 8.3
PVDF membrane	
Filter paper	

3.1.9 Enzymes and other proteins

BSA	New England BioLabs (USA)
CIP	New England BioLabs (USA)
BamH I	New England BioLabs (USA)
EcoR I	New England BioLabs (USA)
Nco I	New England BioLabs (USA)
Not I	New England BioLabs (USA)
Sal I	New England BioLabs (USA)
Xho I	New England BioLabs (USA)
SenP2	Core Facility MPI (Martinsried)
Pfu turbo DNA Polymerase	Stratagene (USA)
Pfu DNA Polymerase	Fermentas (Lithuania)
Phusion HF DNA Polymerase	BioCat (Germany)
Vent ^R polymerase	New England BioLabs (USA)
Platinum Polimease	Invitrogene
T4 DNA Ligase	New England BioLabs (USA)
Dpn I	Fermentas (USA)
Xa Factor	Novagen (Canada)
Enterokinase	Novagen (Canada)
PreScissionProtease	Amersham Biosciences(Sweden)
Thrombin	Sigma (USA)
Anti His antibodies (mouse)	Santa Cruz biotech (USA)
Goat anti mouse antibodies	Santa Cruz biotech (USA)

3.1.10 Kits and reagents

QIAquick PCR Purification Kit	Qiagen (Germany)
QIAprep Spin Miniprep Kit	Qiagen (Germany)
QIAGEN Plasmid Maxi Kit	Qiagen (Germany)
QuikChange Site-Directed Mutagenesis Kit	Stratagene (USA)
Pre-Crystallization Test (PCT)	Hampton Research (USA)
Rapid Ligation Kit	Roche (Germany)
Complete Protease Inhibitor Cocktail	Roche (Germany)
pET LIC cloning Kits	Novagen (Canada)

3.1.11 Protein and nucleic acids markers

Prestained Protein Marker	New England BioLabs (USA)
100 BP DNA marker	New England BioLabs (USA)
1Kb DNA marker	New England BioLabs (USA)
Broad Range (6-175 kDa) 1 kb DNA-Leiter	Peqlab (Germany)

3.1.12 Chromatography equipment, columns and media

ÄKTA explorer 10	Amersham Pharmacia (Sweden)
Peristaltic pump P-1	Amersham Pharmacia (Sweden)
Fraction collector RediFrac	Amersham Pharmacia (Sweden)
Recorder REC-1	Amersham Pharmacia (Sweden)
UV flow through detector UV-1	Amersham Pharmacia (Sweden)
BioLogic LP System	Biorad (USA)
HiLoad 26/60 Superdex S75pg	Amersham Pharmacia (Sweden)
HiLoad 16/60 Superdex S75pg	Amersham Pharmacia (Sweden)
HiLoad 16/60 Superdex S200pg	Amersham Pharmacia (Sweden)
HiLoad 10/30 Superdex S75pg	Amersham Pharmacia (Sweden)
HiLoad 10/30 Superdex S200pg	Amersham Pharmacia (Sweden)
Mono Q HR 5/5, 10/10	Amersham Pharmacia (Sweden)
Mono S HR 5/5, 10/10	Amersham Pharmacia (Sweden)
NiNTA-agarose	Qiagen (Germany)
GST Sepharose FF	Amersham Pharmacia (Sweden)

3.2 Laboratory methods and principles

3.2.1 General remarks on construct design and choice of the expressions system

Optimization of protein constructs is essential for X-ray crystallography and NMR studies. Unstructured and flexible fragments of proteins or loop regions usually inhibit crystallization or result in crystals of low quality. The idea behind designing the protein constructs is to have well defined, folded and stable domains and at the same time to have them biologically active. Determination of stable and folded constructs requires employing various techniques like for example: limited proteolysis, protein sequencing, mass spectrometry, and NMR spectroscopy (Rehm et al., 2004). In some cases designing of the constructs may be based on previously published literature and secondary structure prediction with the help of bioinformatics tools.

Successful expression of heterologous proteins requires proper expression systems (Makrides, 1996). In this work pET or pGEX series of vectors were used for the expression of proteins in *E. coli* (pET system manual, Novagen, 2003; Amersham Pharmacia, 2003). Large fusion tags, such as glutathione S-transferase, thioredoxin or maltose binding protein often increase solubility and promote proper folding of recombinant fusion partners. For proteins directed into inclusion bodies, presence of a 6-histidine fusion peptide (His-Tag) makes use of immobilized metal chromatography (IMAC) possible under strong denaturing/reducing conditions, enabling rapid purification.

Removal of the fusion tag is often required for functional studies of a recombinant protein and for crystallization. This is usually achieved with an aid of a specific restriction protease. The enzymes most commonly used are: 1) factor Xa - cleaves after R in an IEGRX sequence; 2) thrombin - cleaves after R in a LVPRGS sequence; 3) enterokinase - cleaves after K in a DDDDK sequence; 4) PreScission Protease - cleaves after Q in a LEVLFQGP sequence; 5) exopeptidases (dipeptidase) - cleave dipeptides from the N-terminus of a fusion protein, and stops before Arg, Lys or 1 or 2 residues before Pro. The enzyme is active in the presence of PMSF and EDTA, making it ideal for work with degradation susceptible proteins. However, this enzyme is used for removal of only short N-terminal His-tags.

Vectors with specific protease sites are commercially available otherwise they could be inserted using PCR. All constructs of Mdm2 and Mdmx and a few constructs of p53 were designed as a His-tag fusion protein using LIC system. Few of p53 constructs were designed as fusion proteins with GST tag (pGEX4T1). The Mdm2/Mdmx construct designated for crystallization were cloned into pET 20, pET 15b, without tag and with the C-terminal His-tag (pET 28) using the classical cloning.

3.2.2 DNA techniques

3.2.2.1 Preparation of plasmid DNA

The isolation of plasmid DNA from *E. coli* was carried out using dedicated plasmid purification kits from Qiagen. The kits employ a standard alkalic lysis of the precipitated bacteria in the presence of RNase and a strong ionic detergent, SDS, followed by neutralization/DNA renaturation with acetate. For purification, a crude cell lysate is loaded onto a silica gel column, washed with an ethanol-containing buffer, and eluted in a small volume, yielding up to 20 µg of the plasmid DNA.

3.2.2.2 PCR

A polymerase chain reaction was employed to amplify desired DNA fragments and genes, introduce restriction sites, STOP codons and sequences encoding restriction protease cleavage sites. The primers were prepared according to standardized principles regarding the length, GC-content, melting temperature and occurrence of secondary structures of the hairpin type. All primers used for cloning and mutagenesis are listed in Table 3.3. Three different kinds of recombinant thermostable DNA polymerases were used, each operating at slightly different conditions:

	Melting temp.	Annealing temp.	Synthesis temp.
Phusion HF	98°C	55°C	72°C
<i>Pfu</i> Turbo	95°C	55°C	68°C, 72°C
Vent ^R	95°C	55°C	72°C

The stock solution of the primer was always 0.1 nM. The working solution was 0.01 nM. Usually 2 µl of the working solution was used per PCR reaction for each primer

Table 3.3. Primers used in this work.

NAME	SEQUENCE	enzy	
		me	aa
LIC PRIMER FÜR P53			
UR 65	GAC GAC GAC AAG ATG GGA GAA TAT TTC ACC CTT CAG ATC CG		325 →
UR 66	GAG GAG AAG CCC GGT TCA CTT CAG GTG GCT GGA GTG AGC		370 ←
UR 69	GAC GAC GAC AAG ATG GAG GAG CCG CAG TCA GAT CC		1 →
UR 70	GAG GAG AAG CCC GGT TCA GTT GGG CAG TGC TCG CTT AGT GC		310 ←
UR 85	GAG GAG AAG CCC GGT CTA GTC TGA GTC AGG CCC TTC		393 ←
UR 94	GAG GAG AAG CCC GGT TCA CAC GGG GGG AGC AGC CTC TG GAC GAC GAC AAG ATG		73 ←
UR 129	AGTCAGGAAACATTTTCAGACCTATGGAACTACTTCC GAG GAG AAG CCC GGT CTA		15 →
UR 130	TTTCTTCTTTGGCTGGGGAGAGGAGCTGGTGTGTTGGGC		321 ←
MUTATIONSPRIMER FÜR P53			
	CCGTGGGCGTGAGCGCTTCGAGATGTTCCGAGAGTCGAATGAGGCCTT	L344	
AC139	GGAACTCAGGATGCCC	S	→
	GGGCATCCTTGAGTTCCAAGGCCTCATTGACTCTCGGAACATCTCGAA	L344	
AC140	GCGCTCACGCCAGG	S	←
	CCGTGGGCGTGAGCGCTTCGAGATGTTCCGAGAGTAGAATGAGGCCTT	L344	
AC141	GGAACTCAGGATGCCC	Y	→
	GGGCATCCTTGAGTTCCAAGGCCTCATTGACTCTCGGAACATCTCGAA	L344	
AC142	GCGCTCACGCCAGG	Y	←
		L344	
AC143	CTTCGAGATGTTCCGAGAGCAGAATGAGGCCTTGGAACTC	Q	→
		L344	
AC144	GAGTTCCAAGGCCTCATTCTGCTCTCGGAACATCTCGAAG	Q	←
		L344	
AC145	GCTTCGAGATGTTCCGAGAGAAAAATGAGGCCTTGGAACTC	K	→
		L344	
AC146	GAGTTCCAAGGCCTCATTTTTCTCTCGGAACATCTCGAAGC	K	←
PRIMERS FOR MDM2			
UR 79	AAA ACC ATG G GAA CAA GAG ACC CTG GTT AGA CC	Nco1	23 →
	A AAA GGA TCC TCA ATT GAC TAC TAC CAA GTT CCT GTA GAT CAT	BamH	
UR 80	GG	1	111 ←
UR 81	AAA ACC ATG GAA CAA GAG ACC CTG GTT AGA CC	Nco1	23 →
UR 126	AG GCA TTC CAT ATG TGC AAT ACC AAC ATG TCT G	Nde1	1 →
UR 127	AG GCA TTC CAT ATG CAG ATT CCA GCT TCG GAA C	Nde1	17 →

		BamH	
UR 128	CAT GGA TCC CTA GTT CTC ACT CAC AGA TGT ACC TG	1	125 ←
stop	GGA ACTTGGTAGTAGTCAATTAGCAGGAATCATCGGACTCAGG	Nde1	17 →
		BamH	
stop	CCTGAGTCCGATGATTCCTGCTAATTGACTACTACCAAGTTC	1	111

LIC PRIMER FOR MDM2

UR 71	GAC GAC GAC AAG ATG TGC AAT ACC AAC ATG TCT GTA CC		1 →
UR 72	GAG GAG AAG CCC GGT TCA TGA GTC CGA TGA TTC CTG CTG		118 ←
UR 73	GAC GAC GAC AAG ATG GAA CAA GAG ACC CTG GTT AGA CC		23 →
	GAG GAG AAG CCC GGT TCA TAC TAC CAA GTT CCT GTA GAT CAT		
UR 74	GG		109 ←
UR 77	GAC GAC GAC AAG ATG AAA GAG TTT GAA AGG GAA GAA ACC		412 →
UR 78	GAG GAG AAG CCC GGT TCA AGG TTC AAT GGC ATT AAG GGG C		437 ←
	GAG GAG AAG CCC GGT CTA GGG GAA ATA AGT TAG CAC AAT CAT		
UR 115	TTG AAT TGG		491 ←
UR 103	GAC GAC GAC AAG ATG TCA CAG ATT CCA GCT TCG GAA C		17 →
UR 104	GAG GAG AAG CCC GGT TCA GTT CTC ACT CAC AGA TGT ACC TG		125 ←
UR 105	GAC GAC GAC AAG ATG TCA CAG ATT CCA GCT TCG G	J&J	17 →
UR 106	GAG GAG AAG CCC GGT TTA GTT CTC ACT CAC CGA TGT GC	J&J	125 ←
	GAG GAG AAG CCC GGT TCA AAT GAC TAC TAC CAA GTT CCT GTA		
revLIC	GAT CATG		111 ←

MUTATIONSPRIMER FOR MDM2 HUMANIZED

	GGCTGTAAGTCAGCAA GAG TCC TCC		
UR 95	GACTCTGGCACATCGCTGAGTGAGAGC	LOOP ESS	→
	GCGATGTGCCAGAGTC GGA GGA CTC		
UR 96	TTGCTGACTTACAGCCACTAAATTTCTGTAG	LOOP ESS	←
UR 97	GAC TCT GGC ACA TCG <u>GTG</u> AGT GAG <u>AAC</u> TAA GGA TCC G	L→V S→N	→
UR 98	C GGA TCC TTA GTT CTC ACT CAC CGA TGT GCC AGA GTC	L→V S→N	←
		A108	
AC7	CAGAAATTTAGTGGTTGTAATCAGCAAGAGTCCTCCGACTCTGGC	V	→
		A108	
AC8	CGGAGGACTCTTGCTGATTTACAACCACTAAATTTCTGTAGATCATGG	V	←
	GGCTGTAAGTCAGCAAGAGTCCTCCGACTCTGGCACATCGGTGAGTGA		
AC5	GAAC	LOOP ESS	→
	CCGATGTGCCAGAGTCGGAGGACTCTTGCTGACTTACAGCCACTAAATT		
AC6	TCTGTAG	LOOP ESS	←
			→

MUTATIONPRIMERS FOR TRYPTOPHAN MUTANTS OF HDM2

UR 99	G AAA GAG GTT CTT TGG TAT CTT GGC CAG TAT ATT ATG	F55W	→
-------	---	------	---

UR 100	G GCC AAG ATA CCA AAG AAC CTC TTT CAT AGT ATA AGT GTC	F55W	←
UR 107	GGC CAG TAT ATT ATG TGG AAA CGA TTA TAT GAT GAG AAG C	T63W	→
UR 108	G CTT CTC ATC ATA TAA TCG TTT CCA CAT AAT ATA CTG GCC	T63W	←
	CT GTT GGT GCA CAA AAA GAC TGG TAT ACT ATG AAA GAG GTT CTT		
UR 109	TTT TAT CTT GG	T47W	→
	CC AAG ATA AAA AAG AAC CTC TTT CAT AGT ATA CCA GTC TTT TTG		
UR 110	TGC ACC AAC AG	T47W	←
	C TTC TCT GTG AAA GAG CAC AGG TGG ATA TAT ACC ATG ATC TAC		
UR 111	AGG AAC TTG G	K98W	→
	C CAA GTT CCT GTA GAT CAT GGT ATA TAT CCA CCT GTG CTC TTT		
UR 112	CAC AGA GAA G	K98W	←
AC1	TCTTGGCTGGTATATTATGACTAAACGATTATATGATGAGAAGCAACAC	Q59W	→
	AGTCATAATATACCAGCCAAGATAAAAAAGAACCTCTTTCATAGTATAAG		
AC2	TGTC	Q59W	←
	GCACAGGAAAATATATTGGATGATCTACAGGAACTTGGTAGTAGTCAATC	T101	
AC3	AGCAGGA	W	→
		T101	
AC4	CCTGTAGATCATCCAATATATTTTCTGTGCTCTTTCACAGAGAAG	W	←
AC11md	GACACTTATACTATGTGGGAGGTTCTTTTTTATCTTGGCCAGTATATTAT		
m2	GAC	K51W	→
	CTGGCCAAGATAAAAAAGAACCTCCCACATAGTATAAGTGTCTTTTTGTG		
AC12	CACC	K51W	←
	CTGTGAAAGAGCACTGGAAAATATATACCATGATCTACAGGAACTTGGTA		
AC13	GTAGTC	R97W	→
AC14	CATGGTATATATTTCCAGTGCTCTTTCACAGAGAAGCTTGGCACG	R97W	←
	CC CTG GTT AGA CCA AAG CCA TTG TTT TTG AAG TTA TTA AAG TCT		
UR 116	GTT GGT GC	L34F	→
	GC ACC AAC AGA CTT TAA TAA CTT CAA AAA CAA TGG CTT TGG TCT		
UR 117	AAC CAG GG	L34F	←
	G GTT AGA CCA AAG CCA TTG CTT TTG AAG TTT TTA AAG TCT GTT		
UR 118	GGT GCA CAA AAA GAC AC	L37F	→
	GT GTC TTT TTG TGC ACC AAC AGA CTT TAA AAA CTT CAA AAG CAA		
UR 119	TGG CTT TGG TCT AAC C	L37F	←
	CAT ATT GTA TAT TGT TCA AAT GAT CTT TTT		
UR 120	GGAGATTTGTTTGGCGTGCCAAGC	L82F	→
	GCT TGG CAC GCC AAA CAA ATC TCC AAA AAG ATC ATT TGA ACA		
UR 121	ATA TAC AAT ATG	L82F	←
	GT TCA AAT GAT CTT CTA GGA GAT TTT TTT GGC GTG CCA AGC TTC		
UR 122	TCT GTG AAA GAG C	L85F	→
	G CTC TTT CAC AGA GAA GCT TGG CAC GCC AAA AAA ATC TCC TAG		
UR 123	AAG ATC ATT TGA AC	L85F	←

	G AAA GAG CAC AGG AAA ATA TAT ACC TTT ATC TAC AGG AAC TTG	M102	
UR 124	GTA GTA GTC AAT C	F	→
	G ATT GAC TAC TAC CAA GTT CCT GTA GAT AAA GGT ATA TAT TTT	M102	
UR 125	CCT GTG CTC TTT C	F	←

PRIMERS FOR HDMX TO MIMIC TO HDM2

AC15		I24E	→
AC16		I24E	←
	GGTCAGTACATAATGGTGAAGCGTCTTTATGATCAGCAGGAGCAGCATA		
AC17	TG	Q64R	→
	CCTGCTGATCATAAAGACGCTTCACCATTATGAACTGACCTAAATAGTGC		
AC18	ATGACC	Q64R	←
AC19	GCGTCTTTATGATCAGAAGGAGCAGCATATGGTATATTGTGGTGG	Q64K	→
AC20	CCATATGCTGCTCCTTCTGATCATAAAGACGCTTCACCATTATGAAC	Q64K	←
AC21	GGTGAACGTACTTTATGATCAGAAGCAGCATATGGTATATTGTGG	E70Q	→
AC22	CCACAATATACCATATGCTGCTGCTTCTGATAAAGTACGTTCCACC	E70Q	←
AC23	CCGTGAAAGACCCACGTCCTCTCTATGATATGCTAAGAAAAG	S96R	→
AC24	GCATATCATAGAGAGGACGTGGGTCTTTCACGGAGAAGCTCTG	S96R	←
AC25	CTATGATATGCTATATAAGAATCTTGTCACTTTAGCCACTGCTACTACAG	R103Y	→
AC26	GACAATCTTATATAGCATATCATAGAGAGGACGTGGGTCTTTCACGG	R103Y	←
AC27	GCTATATAAGAATCTTGTCACTTTAAACTGCTACTACAGATGCTGC	A110N	→
AC28	GCAGCATCTGTAGTAGCAGTGTAAAGTGACAAGATTCTTATATAGC	A110N	←
	TAATGGTGAAGCGTCTTTATGATCAGAAGCAGCAGCATATGGTATATTGT		
ACk1a	GG	QQE	→
ACk1b	CCATCTGCTCTGCTAATCATAAAGACGCTTCACCATTATGTAAGTACC	QQE	←
	GACCCACGTCCTCTCTATGATATGCTATATAAGAATCTTGTCACTTTAAA		
ACk2a	CACTGCTAC	SRA	→
	GTSGCTGSGTTTTAAAGTGACAAGAGGCTTATATAGCATATCATAGAGAG		
ACk2b	GACGTGGGTC	SRA	←

MUTATIONPRIMERS FOR HDMX TO RELEASE BINDING SITE

M53V			→
M53V			←
	GCTTCTCCGTGAAAGACCCAAGCCCTCTCGCTGATATGCTAAGAAAGAA		
Y99A	TCTTGTCACTTTAGC		→
	GGCTAAAGTGACAAGATTCTTTCTTAGCATATCAGCGAGAGGGCTTGGG		
Y99A	T		←
	GCTTCTCCGTGAAAGACCCAAGCCCTCTCACCGATATGCTAAGAAAGAA		
Y99T	TCTTGTCACTTTAGC		→
	GGCTAAAGTGACAAGATTCTTTCTTAGCATATCGGTGAGAGGGCTTGGG		
Y99T	T		←
DLYF	GCT TCT CCG TGA ACC CAA GCC CTA TGG CTG ATA TGC TAA GAA		→

AGA ATC TTG TCA CTT TAGC

GGC TAA AGA GAC AAG ATT CTT TCT TAG CAT ATC AGC CAT AGG

ACT TGG GTC TTT CAC GGA GAA G

DLYR

←

LIC FOR HDMX

	GAC GAC GAC AAG ATG AGG		
AC18F	ATCTCTCTGGACAAATCAATCAGGTACGACC	18	→
AC28F	GACGACGACAAGATGCGACCAAACTGCCGCTTTTGAAGATTTTG	28	→
AC1F	GACGACGACAAGATAGACATCATTTTCCACCTCTGCTCAGTGTC		→
	GAGGAGGAGAAGCCCGTTAGTGGCTAAAGTGGCTAAAGTGACAAGAT		
AC111R	TCTTTCTTAGC		←
	GAGGAGGAGAAGCCCGTTAGTAAGTAGCAGTGGCTAAAGTGGCTAAA		
AC113R	GTGACAAGATTCTTTCTTAGC		←
	GAGGAGGAGAAGCCCGTTATAGTAAGTAGCAGTGGCTAAAGTGGCTA		
AC114R	AAGTGACAAGATTC		←
ACF271			
12	GACGACGACAAGATGCGACCAAACTGCCGCTTTTGAAGATTTTG		→

PRIMERS FOR HDMX

F112NT	AAAAACCATGGCATCTTCCACCTCTGCTCAGTGTTCAACATCTG	Nco1	p15b	
	TTTTGGATCCCTAAGGTAGCAGTGGCTAAAGTGACAAGATTCTTTCTTAG			
R112NT	CATAT	BamH1	112	
AC151	AAACCATGGCTTGCAGGATCTCTCCTGGAC	Nco1	16	→
AC156	AAACCATGGGCAGGATCTCTCCTGGACAAATCATC	Nco1	18	→
AC157	TTTGGATCCCTAAGTAGCAGTGGCTAAAGTGACAAGATTC	BamH1	112	←
AC158	AAACCATGGGCAGGATCTCTCCTGGACAAATCATCAATCAGGTA	Nco1	18	←
	TTCGGATCCCTAATGATGATGATGATGATGATGAGTAGCAGTGGCTAAA			
AC159	GTGACAAGATTC	BamH1	112	←
				p2
AC160	AAACCATGGGCAGGATCTCTCCTGGACAAATCAATCAGG	Nco1	18	8
AC161	TTTCTCGAGAGTAGCAGTGGCTAAAGTGACAAGATTCTTTCTTAGC	Xho1	112	←
AC162	AAACCATGGGCCAGGATCTCTCCTGG	Nco1	18	→
AC163	GCGCTCGAGAGTAGCAGTGGCTAAAGTG	Xho1	112	←
AC164	AAACCATGGTA CGACCAAACTGCCGCTTTTG	Nco1	28	→

ANOTHER

		Mdm		
		CAG	2	
AC149	GGAACCTGGTAGTAGTCAATTAGCAGGAATCATCGGACTCAGG	TAG	Stop	→
AC150	CCTGAGTCCGATGATTCTGCTAATTGACTACTACCAAGTTC			←

UR 59 GGG CTG GCA AGC CAC GTT TGG TG GST FORWARD PRIMER



→Primer Forward

← Primer Reverse

3.2.2.3 Digestion with restriction enzymes

Usually, 1-2 units of each restriction enzyme were used per 1 µg of plasmid DNA to be digested. The digestion was performed in a buffer specified by the manufacturer at the optimal temperature (37°C) for 5-16 h. The fragments ends that occurred after digestion were cohesive. To eliminate possibility of plasmid recirculation (possible when double-digestion does not occur with 100% efficiency), 5'-ends of a vector were dephosphorylated using calf intestine phosphatase (CIP). CIP treatment was performed with 1 unit of enzyme per 3 µg of plasmid DNA, at 37°C for 1 h.

3.2.2.4 Purification of PCR and restriction digestion products

DNA obtained from restriction digestion, phosphatase treatment or PCR was purified from primers, nucleotides, enzymes, buffering substances, mineral oil, salts, agarose, ethidium bromide, and other impurities, using a silica-gel column (QIAquick PCR Purification Kit, Qiagen). The QIAquick system uses a simple bind-wash-elute procedure. A binding buffer was added directly to the PCR sample or other enzymatic reaction, and the mixture was applied to the spin column. Nucleic acids adsorbed to the silica-gel membrane in the high-salt conditions provided by the buffer. Impurities and short fragments of single or double-stranded DNAs were washed away and pure DNA was eluted with a small volume of 10 mM Tris pH 8.0 or water.

3.2.2.5 Ligation

The ligation of digested and purified inserts and vectors was performed according to the protocol described in the T4 DNA Ligase instruction (New England BioLabs).

The ligation mixture contained (20 µl):

insert	6 µl (0.15 µM)
10 x T4 DNA ligase reaction buffer	2 µl
vector	3 µl
T4 DNA Ligase	1.5 µl

3.2.2.6 Ligation Independent Cloning (LIC)

The ligation independent cloning requires the PCR amplification of the gene of interest with the compatible overhang at both ends (LIC cloning kit). Following are the sequences of the overhangs:

For pET41 and 46 LIC/Ek

Forward primer 5' – **GACGACGACAAGAT** – 3'

Reverse primer 5' – **GAGGAGAAGCCCGGT** – 3'

Rest of the procedure was followed as per the instructions of the manufacturer (pET system: manual, Novagen, 2003).

3.2.2.7 Mutagenesis

Site directed mutagenesis of Mdmx and Mdm2 proteins were performed with PCR, using enzymes and instructions supplied in the QuikChange Site-Directed Mutagenesis Kit (Stratagene). The mutagenic oligonucleotide primers were designed according to suggestions provided by the manufacturer. The desired mutation was in the middle of the primer with ~ 10-15 bases of a correct sequence on both sides (Table 3.3, primers:). Vectors pET 20b and pEt 46/LIC, containing copies of a gene encoding Mdm2 and Mdmx, respectively, were used as DNA templates. The high melting temperatures of the designed , oligonucleotides, high concentration of the template DNA and low number of PCR cycles, combined with high accuracy and fidelity of highly processive DNA polymerase *Pfu* Turbo, minimizes the occurrence of unwanted mutations.

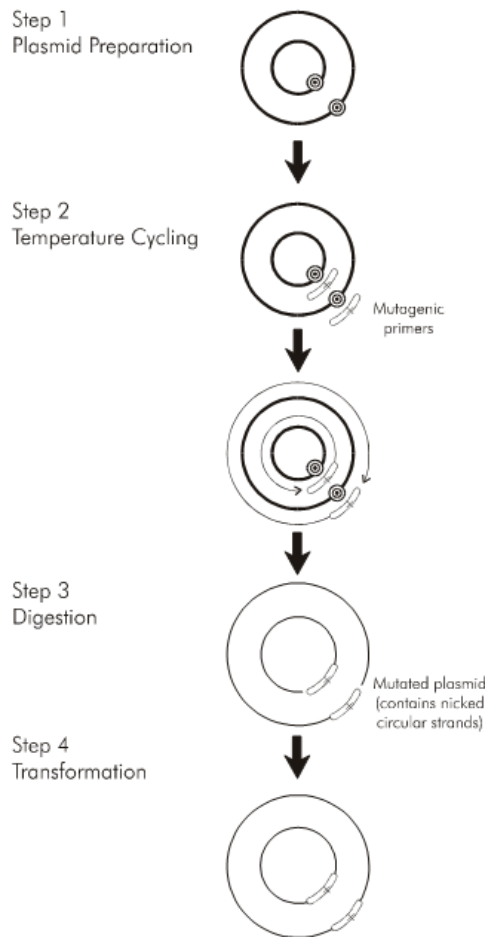


Figure 3.1. Overview of the Quik-change Site-directed Mutagenesis experiment.

(Figure adopted from the Manual for the Site –directed Mutagenesis Kit, Stratagene)

The mutagenic PCR reaction mixture contained:

10 × reaction buffer	5 μl
dNTP mix	1 μl
plasmid (5 ng/μl)	1 μl (10 ng)
oligonucleotide primer F	2 μl (125 ng)
oligonucleotide control primer F	2 μl (125 ng)
<i>PfuTurbo</i> DNA polymerase (2.5 U/μl)	1 μl
milli-Q to a final volume of 50 μl	38 μl

PCR cycling parameters:

denaturation	95°C, 1'
denaturation	95°C, 30''
annealing	55°C, 1'
synthesis (1 min per 1000 base pairs)	72°C, 13'

Following the temperature cycling, the product was treated with Dpn I (10 U, 37°C, for 2 h). The Dpn I endonuclease (target sequence: 5'-Gm⁶ATC-3') is specific for methylated and hemimethylated DNA and is used to digest the parental DNA template and to select for mutation-containing synthesized DNA. 2 µl of the mixture were used to transform XL1-Blue or Top10 chemically competent cells. Plasmid DNA was isolated using QIAprep Spin Miniprep Kit (Qiagen) and was subjected to verification by automated sequencing.

3.2.2.8 Agarose gel electrophoresis of DNA

For verification of the presence and length of PCR or restriction digestion products, agarose gel electrophoresis was performed. For this purpose 1% agarose in a TAE buffer supplemented with Sybr green was prepared. The DNA samples were mixed with the 6x sample buffer prior to loading. DNA samples were run along with the 100 bp and/or 1 kb DNA ladder (NEB or pEQ lab) at 100-120 V DC. Results were visualized using UV illumination.

3.2.3 Transformation of *E. coli*

3.2.3.1 Making chemically competent cells

A single colony of overnight grown bacteria from a LB agar plate was inoculated into 100 ml of LB media in a 500 ml flask. Culture was incubated at 37°C with vigorous agitation, monitoring the growth of cells. Cells were grown till the OD₆₀₀ reach ~0.6. The bacterial culture was transferred to sterile, disposable, ice-cold 50 ml polypropylene tubes and cooled down to 4°C on ice for 10 min. Cells were recovered by centrifugation at 3000 g for 10 min at 4°C. Supernatant media was decanted and tubes were kept in an inverted position on a pad of paper towel for 1 min to allow the last traces of media to drain away. Pellets were resuspended by gentle vortexing in 30 ml of the ice-cold MgCl₂ solution. Again, cells were recovered by centrifugation at 3000 g for 10 min at 4°C. Supernatant solution was decanted and tubes were kept in an inverted position on a pad of a paper towel for 1 min to allow the last traces of solution to drain away.

Pellet of the cells was recovered by gentle stirring in 2 ml of ice-cold 0.1 M CaCl₂ containing 15% glycerol, for each 50 ml of original culture. After this cells were dispensed into aliquots of 50 µl, flash frozen in liquid nitrogen and stored at -70°C.

3.2.3.2 Transformation of chemically competent cells

3 µl of a ligation mix or ca. 50 µg of plasmid DNA was added to 50 µl of chemically competent cells. The mixture was incubated on ice for 30 min followed by a heat shock of 45 s at 42°C, 2 min cooling on ice, and the addition of a 250 µl of glucose and magnesium containing medium. After 1 h of incubation at 37°C, 20-50 µl of the mixture was spread out on LB agar plates (supplemented with selective antibiotic) and incubated overnight at 37°C. A number of factors have been elucidated that produced an increase in transformation efficiency. Such factors include: prolonged incubation of bacteria with CaCl₂, addition of multiple cations, such as Mg²⁺ or Cs²⁺ into the transformation mixture and treatment of bacteria with dimethyl sulfoxide (DMSO), polyethylene glycol, hexaminocobalt, and dithiothreitol in the presence of both monovalent and divalent cations (Chung et al., 1989). After incubation with DNA, in order to make the cells retain the plasmid and to be certain that they survive, the cells were heat shocked for several seconds to induce heat shock genes, which aid in survival and recovery. The cells were then incubated at 37°C without selective pressure; sufficient time was given for expression of antibiotic resistance genes. Plating on selective media enabled recovery of those cells that actually received the DNA.

3.2.4 Protein chemistry methods and techniques

3.2.4.1 The general strategy of the protein expression in *Escherichia coli*.

To speed up protein production, we have adopted a strategy of parallel expression of a protein from a variety of vectors containing different tags and/or fusion partners, and a variety of *E. coli* host strains. This approach should not only gain us a lot of time but also result in a larger number of successfully expressed proteins. The expression strategy consists of the following two sets of experiments: A): the expression of a protein in a basic *E. coli* host strain from a variety of vectors with different tags and/or fusion partners. B): The expression of a protein from a standard vector in a number of different *E. coli* host strains. The choice of the host strains depends more on the nature of the heterologous protein.

If the protein contains a high number of rare *E. coli* codons, it is worthwhile trying to express it in a strain that co-expresses the tRNAs for these rare codons. There are several strains commercially available:

BL21 (DE3) CodonPlus-RIL	AGG/AGA (arginine), AUA (isoleucine) and CUA (leucine)	Stratagene
BL21 (DE3) CodonPlus-RP	AGG/AGA (arginine) and CCC (proline)	Stratagene
Rosetta or Rosetta (DE3)	AGG/AGA (arginine), CGG (arginine), AUA (isoleucine) CUA (leucine) CCC (proline), and GGA (glycine)	Novagen

If the protein contains one or more disulfide bonds, proper folding is stimulated in host strain with a more oxidizing cytoplasmic environment. Two strains are commercially available from Novagen: AD494 and Origami. If the protein is toxic to the cell, expression in a strain containing the pLysS or pLysE vector tightens regulation of expression systems using the *T7* promoter. These vectors express lysozyme, which binds to and inactivates *T7* RNA polymerase. Strains are commercially available from different manufacturers. A typical expression experiment consists of the following steps: A) picking of a single colony from a freshly streaked plate of the expression host containing the recombinant vector. When the heterologous protein is toxic for the cells, higher expression levels are obtained by using the so-called "plating" method. B) growing of a starter culture. Inoculate with the picked colony up to 50 ml of rich medium (such as LB or 2xYT) containing the appropriate antibiotic. When a larger starter culture is required, inoculate 4 ml of rich media with the single colony; grow for 4-8 hours at 37°C; and use this to inoculate the starter culture. Inoculation of the main culture and incubation until OD₆₀₀ reaches 0.4-1. The optimal OD value depends on the culture method and the medium. For flask cultures using LB-medium an OD₆₀₀ of 0.6 is recommended. To increase the growth rate, we carry out the cultures at 37°C until the OD for induction is reached. Then the cultures are cooled to the induction temperature in ice-water. For good aeration, not more medium than 20% of the total flask volume is used. Protein expression is induced by the addition of the proper inducer or by changing the growth conditions. From this point on the cells will use most of their resources for the production of the target protein and will not grow much further. For the most used promoters induction conditions are listed in Table 3.4. After induction the cultures are incubated from 3 hours to overnight depending on the induction temperature.

Table 3.4. The optimal temperature and duration of the protein expression in E.coli

Incubation temperature	Incubation time
15°C	overnight
20°C	overnigh
25°C	overnigh
30°C	5-6 h
37°C	3-4 h

Harvesting of the cell pellet by the centrifugation (20 min at 6000 g). Cell pellets are stored at -20°C.

3.2.4.2 *E.coli* expression in minimal medium.

- A 5 ml LB were inoculated with a single colony and shaken (200 rpm) overday in a 15 ml falcon tube at 37°C.
- B 100 ml MM were inoculated with 100 µl of the overday culture and shaken (150 rpm) overnight in a 250 ml flask at 37°C.
- C 1 l MM was inoculated with 100 ml of the overnight culture and shaken (150 rpm) in a 3 l flask.
- D Cells were induced with IPTG (final concentration 0.2 -1.0 mM) at OD600 of 0.7- 0.9.
- E After an overnight incubation with shaking, the cells were pelleted by centrifugation at 4000 rpm at 4°C in a Beckman centrifuge for 20 min.
- F The cell pellet (after the expression) was used directly for the protein purification or was stored at -80°C for longer time or -20°C if to be used in 1-2 days.

3.2.4.3 Sonication

Pulsed mode of operation was applied (output control 8, 60% duty cycle) and sonication was carried out on ice, in 5 steps of 2 min each, with 3 min intervals between steps, to avoid overheating of the sample.

3.2.4.4 General remarks on protein purification strategies

Most purification protocols require more than one step to achieve the desired level of product purity. This includes any conditioning steps necessary to transfer the product from one technique into conditions suitable to perform the next technique. Each step in the process will cause some loss of product. Consequently, to reach the targets for yield and purity with the minimum number of steps and the simplest possible design, it is not efficient to add one step to another until purity requirements have been fulfilled. Occasionally when a sample is readily available purity can be achieved by simply adding or repeating steps. However, experience shows that, even for the most challenging applications, high purity and yield can be achieved efficiently in fewer than four well-chosen and optimized purification steps (Figure 3.2). Techniques should be organized in a logical sequence to avoid the need for conditioning steps and the chromatographic techniques selected appropriately to use as few purification steps as possible.

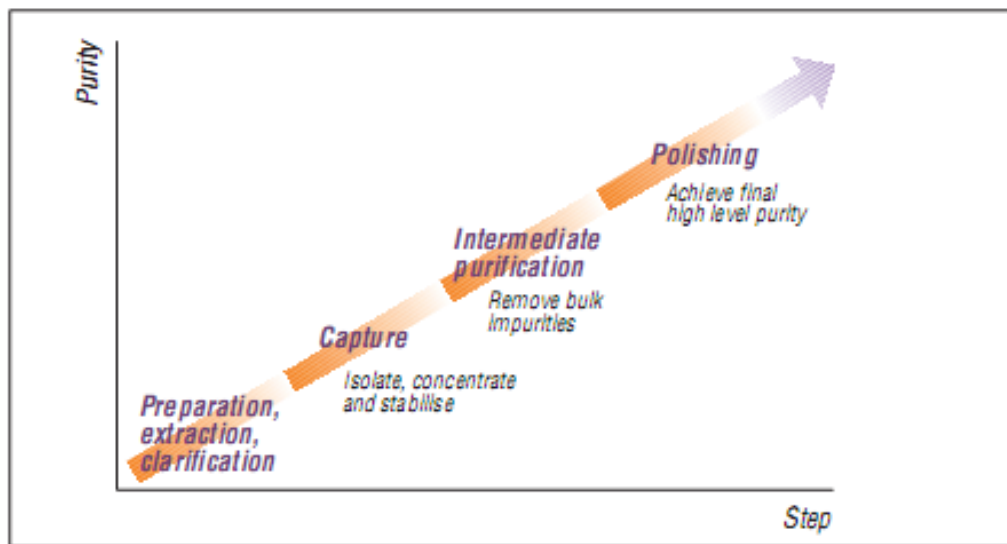


Figure 3.2. Preparation and the Three Phase Purification strategy. (Figure adopted from the Amersham Biosciences Handbook).

Every technique offers a balance between resolution, speed, capacity and recovery and should be selected to meet the objectives for each purification step. In general, optimisation of any one of these four parameters can only be achieved at the expense of the others and a purification step will be a compromise. The importance of each parameter will vary depending on whether a purification step is used for capture, intermediate purification or polishing. This will steer the

optimization of the critical parameters, as well as the selection of the most suitable media for the step. Proteins are purified using chromatographic purification techniques which separate according to differences in specific properties, as shown in Table 3.5

Table 3.5. Protein properties used during purification.

Protein property	Technique
Charge	Ion exchange (IEX)
Size	Gel filtration (GF)
Hydrophobicity	Hydrophobic interaction (HIC), Reversed phase (RPC)
Biorecognition (ligand specificity)	Affinity (AC)
Charge, ligand specificity, hydrophobicity	Expanded bed adsorption (EBA) follows the principles of AC, IEX or HIC

3.2.4.4.1 Protein purification under native conditions.

The recombinant human Mdmx (residues 18-111) was obtained from an *E. coli* BL21(DE3) RIL expression system, using the pET-46Ek/LIC vector (Novagen). Cells were grown at 37°C and induced with 0.5 mM IPTG at an OD_{600nm} of 0.6 and were expressed for 12 h at 20°C. The protein was first purified under native condition using Ni-NTA Agarose (Qiagen) using solutions described in section:Materials. Further the solution was dialyzed to the enterokinase buffer and His-tag was cleaved with enterokinase at 4°C for a period of 3-4 days.

Two of the selected constructs of p53 were purified under native conditions. The construct comprising the transactivation domain (1-73) in fusion with GST tag and second, composed of residues (1-321) with 6-His tag. The proteins were expressed in LB medium with 100mg/ml of ampicillin and 34mg/ml of chloramphenicol and induced overnight in 20°C. The recombinant human p53 protein (residues 1-73) was overexpressed at 37°C for 3h in *E. coli* BL21 using a pGEX vector. The protein was purified under native conditions via GST-Sepharose FF (Pharmacia), (Materials). The analogous construct with 6-His tag was overexpressed overnight in 20°C. The purification was carried out in room temperature using the Ni-NTA Agarose (Qiagen) purification system. Gel filtration was investigated as the natural first choice for a final polishing step to remove trace contaminants and transfer the sample to a suitable

storage conditions. It was carried out with a HiLoad 16/60 Superdex75 or a HiLoad 10/30 Superdex S200pg gel filtration column.

3.2.4.4.2 Protein purification under denaturing conditions.

In the case of insoluble proteins accumulated in inclusion bodies (IBs), the following protocol has been developed for Mdm2 and Mdmx. The recombinant human Mdm2 and Mdmx constructs were obtained from an *E. coli* BL21 (DE3)codonplusRIL expression system using various the pET vectors (Novagen). Cells were grown at 37°C and to be adjusted to produce the insoluble protein induced with 1 mM IPTG at an OD_{600nm} of 0.9, afterwards they were expressed for 4.5 h at 37°C and purified from inclusion bodies. After washing with PBS with 0.05% Triton X100 with subsequent low-speed centrifugation (12000G), the inclusion bodies were solubilized in 6 M GuHCl in 100 mM Tris-HCl, pH 8.0 including 1 mM EDTA and 10 mM DTT. The dialysis against 4M Gu-HCl pH 3.5 was carried overnight out to decrease amount of GuHCl and keep the reducing conditions. For renaturation the protein was diluted (1:100) into 10 mM Tris-HCl, pH 7.0, including 1 mM EDTA and 10 mM DTT by adding the protein in several pulses to the refolding buffer.

Refolding was performed overnight at 4°C then ammonium sulphate was added to the final concentration of 2 M. After few hours the prep was mixed with 10 ml of the Butyl Sepharose 4 Fast Flow (Pharmacia, FRG). The protein was eluted with 100 mM Tris-HCl, pH 7.2, supplied with 5 mM DTT. The purification was carried out without any affinity column. The final purification of both proteins was by the HiLoad 16/60 Superdex75 pg gel filtration (Amersham Biosciences). The purity and folding of proteins were confirmed by SDS-gel electrophoresis, mass spectrometry, and NMR measurements.

One of p53 constructs comprising residues 1-312 was also purified from inclusion bodies. The recombinant human p53 protein (residues 1-312) was overexpressed at 37°C overnight in *E. coli* BL21(DE3) RIL using the pET-46Ek/LIC vector. The protein was purified under denaturing conditions using a Ni-NTA (Qiagen) column (Materials), refolded in the arginine buffer (Materials) by dialysis, and further purified using a Heparin Sepharose 6 Fast Flow (Amersham) column. Before the affinity chromatography was carried out, the arginine was removed from the protein solution by gradient dialysis. Final purification was carried out via a HiLoad 10/30 Superdex S200pg gel filtration column.

3.2.4.5 SDS polyacrylamide gel electrophoresis (SDS-PAGE)

The SDS polyacrylamide gel electrophoresis was performed at various stages of purification to check the purity and identity of the eluted proteins. For all expressed proteins, tricine gels were applied (Schagger and von Jagow, 1987). The protein samples were prepared by mixing 20 μ l of protein solution with 5 μ l of sample buffer (SB) followed by 5 min incubation at 100°C. Due to rapid precipitation of SDS in contact with guanidine, the samples (after Ni-NTA chromatography under denaturing conditions) were prepared as follows: 20 μ l of the protein solution in a denaturing buffer was diluted with 400 μ l 20% trichloroacetic acid (TCA). The sample was incubated for 5 min on ice followed by centrifugation for 5 min at 20 000 x g. Supernatant was discarded by suction, the precipitated protein pellet was washed once by vortexing with 400 μ l ethanol. After centrifugation and ethanol removal, the protein pellet was resuspended in 20 μ l of 2x SB and the sample was boiled for 5 min.

3.2.4.6 Visualization of separated proteins

For visualization of the protein bands, the gels were stained in a Coomassie-blue solution. Background was cleared by incubation of the gel in a destaining solution. Both processes were greatly accelerated by brief heating with microwaves of the gel submerged in an appropriate solution.

3.2.4.7 Western blot

Western blot is a functional assay to check the identity of proteins or identify the protein out of a number of proteins. The semi-dry Western blot was applied. The Western blot assay starts with running the desired sample on the SDS-PAGE. The nitrocellulose membrane and six Watmann paper of the size of the SDS-PAGE gel were cut and soaked in the transfer buffer. Watmann paper, SDS-PAGE (gel), and nitrocellulose membrane were arranged in the following order over the electroblot: three wet Watmann paper, wet nitrocellulose paper, and SDS-PAGE gel followed by three Watmann wet papers. The apparatus was closed and run (transfer) at constant voltage of 100 V for 1-1:30 h. After the transfer, the nitrocellulose membrane is taken and kept in the blocking solution for 2 h with constant shaking. The SDS-PAGE is stained by Commassie blue solution to check the success of transfer. After blocking, the membrane is washed three times with the wash buffer and incubated for 1.5 h at room temperature with the 1st antibody solution (the procedure can be stopped at this point by keeping the blot in the 1st antibody solution at

4°C for overnight). The membrane was washed with the wash buffer and incubated in the 2nd antibody solution for 1.5 h at room temperature. After this the membrane was washed three times with the wash buffer and the blot was developed by incubating it in the substrate (BCIP) solution for 10 min.

3.2.4.8 Determination of protein concentration

The concentration of proteins in solution was estimated by means of the Bradford colorimetric assay. 5 µl of the protein sample was added to 1 ml (10 x diluted stock) of Bradford reagent (BioRad) in a plastic cuvette. After gentle mixing, A_{595} was measured and converted to the protein concentration on the basis of a calibration curve prepared for known concentrations of BSA.

Determination of protein concentration was performed spectrophotometrically. Absorption at 280 nm was measured and converted to a protein concentration on the basis of theoretical extinction coefficients. It has been shown that it is possible to estimate the molar extinction coefficient $E_{\lambda}(\text{Prot})$ of a protein from knowledge of its amino acid composition (Gill and Hippel, 1989). From the molar extinction coefficient of tyrosine, tryptophan and cystine (cysteine residues do not absorb appreciably at wavelengths >260 nm, while cystine does) at a given wavelength λ the extinction coefficient of a protein can be computed using the equation:

$$E_{\lambda}(\text{Prot}) = \text{Numb}(Y) \times \text{Ext}_{\lambda}(Y) + \text{Numb}(W) \times \text{Ext}_{\lambda}(W) + \text{Numb}(C) \times \text{Ext}_{\lambda}(C)$$

Protein concentration (C_p) can be calculated using the following formula:

$$A_{\lambda}(\text{Prot}) = E_{\lambda}(\text{Prot}) \times C_p(\text{Prot}) \times (\text{cuvette path length in cm})$$

3.2.5 NMR spectroscopy

All NMR spectra were acquired at 300 K on a Bruker DRX 600 MHz spectrometer equipped with a cryoprobe except for the MAD2 titration, which was carried out on a Bruker DRX 500 MHz spectrometer. Typically, NMR samples contained up to 0.1 mM of protein in 50 mM KH₂PO₄, 50 mM Na₂HPO₄, 150 mM NaCl, 5 mM DTT, pH 7.4. Water suppression was carried out using the WATERGATE sequence. NMR data were processed using the Bruker program Xwin-NMR version 3.5.

NMR ligand binding experiments were carried out in an analogous way to those previously described (Stoll et al., 2001). 500 µl of the protein sample containing 10% D₂O, at a

concentration of about 0.1 mM, and a 20 mM stock solution of nutin-3 (purchased from Cayman Chemical, MI) or 20 mM NXN-6 (NexusPharma) in DMSO-d₆ were used in all of the experiments. The maximum concentration of DMSO at the end of titration experiments was less than 1%. The pH was maintained constant during the entire titration. The method was performed by use two proteins, one N15 labeled with low molecular weight, and second bigger.

The AIDA (antagonist induced dissociation assay) was performed for the monitoring of the inhibitory activity of several compounds with the Mdm2/Mdmx-p53 complex. The N-terminal domain of p53 (residues 1-321) has three tryptophan residues and we have used 1D proton spectra of the ¹H^ε side chains of these tryptophan residues for monitoring the state of p53 in Mdm2/ -p53 (res. 1-321) complexes upon treatment with various ligands. On forming the complex with wt-Mdm2, the signal of W23 disappears. This is because W23, together with the p53 residues 17 to 26, comprise the primary binding site for Mdm2. Upon binding, these residues participate in well-defined structures of large p53-Mdm2 complexes, whereas W53 is still not structured when p53 is bound to Mdm2 (Dawson et al., 2003; D'Silva et al., 2005). The observed 1/T₂ transverse relaxation rate of the bound W23 in the complexes increases thus significantly and broadening of NMR resonances results in the disappearance of this signal in the spectra.

3.2.6 X-ray crystallography

3.2.6.1 Protein crystallization

The protein buffer used for crystallization contained 5 mM Tris/HCl pH 8.0 and 50 mM NaCl. Crystallization of the protein was carried out with the sitting drop vapor diffusion method. The protein buffer used for crystallization contained 5 mM Tris/HCl pH 8.0 and 50 mM NaCl. After addition of the peptide, Mdmx and/or Mdm2 proteins were concentrated to about 20 mg/ml. Crystallization of the proteins was carried out with the sitting drop vapor diffusion method in 4 °C and in the room temperature. Zebrafish Mdmx with the p53 peptide P1 (SQETFSDLWKLLPEN) crystallized in the form of very thin plates from a crystallization solution containing 30% PEG 300, 0.1 M MES pH 6.5. They appeared in several days and grew to a final size of ca. 0.3 x 0.1 x 0.01 mm. Crystals were directly plunged frozen.

The human Mdmx with the p53-wildtype peptide (P1) crystallized in 25% PEG3350 and MES buffer pH 6.5 - 6.75 for and the zebrafish variant of Mdmx with p53 derived peptide P3 (ETFSDLWKLLPENNVLSPLPS) in 30% PEG300 0.1 M MES pH6.5. Crystals appeared after several days and grew to a final size of ca. 0.3 x 0.3 x 0.01 mm. Crystals were plunged frozen

after few second in mother liquor containing additionally 20% glycerol. Crystallization of the human Mdm2 with the P4 (LTFEHYWAQLTS) peptide was also carried out with the sitting drop vapor diffusion method at room temperature. The crystals appeared in 0.1 M TRIS-HCl, 0.2 M ammonium sulphate, pH 7.5 and 28% PEG 5000 MME after several days forming thick plates. The P4-Mdmx complex was obtained from the hanging drop in the cold-room. The crystallization solution contained 0.1 M HEPES pH 7.5 4.3 M NaCl. The cubical and regular crystals appeared after several days and grew to a final size of ca. 0.4 x 0.2 x 0.1 mm. A few seconds before the crystals were plunged frozen, 20% glycerol was added to the mother liquor.

3.2.6.2 Data collection and structure analysis

The crystals of the humanized and wildtype zebrafish Mdmx complexes with P1 peptide belong to the space group P21 and contained three complexes per an asymmetric unit. The crystals of human Mdmx with P1 p53 peptide and human-mimic Mdmx with P3 p53 derived peptide belong to the space group P21 and contained four complexes per an asymmetric unit for a human protein and two of human mimic zebrafish. An acceptable quality dataset up to 2.3 Å was collected for human mimic zebrafish Mdmx with P1 and 1.9 Å for the human Mdmx with the P1 peptide. The P4-Mdmx crystals belong to the space group C2 and the P4-Mdm2 ones to P212121 and contained four complexes per an asymmetric unit. High quality datasets up to 1.8 Å (Mdm2) and 1.4 Å (Mdmx) were collected. The high-resolution datasets were collected on the MPG/GBF beamline BW6 at DESY, Hamburg, Germany and SLS beamline PXII at Paul Scherrer Institut, Villigen, Switzerland. Collected data were integrated, scaled and merged by XDS and XSCALE programs (Kabsch, 1993). The structure was determined by molecular replacement using the Molrep program from the CCP4 suite (CCP4, 1994). The models were then refined by Refmac5 (Collaborative Computational Project, 1994) and rebuilt by XtalView/Xfit (McRee, 1999) and by a subsequent Refmac5 refinement. Water molecules were added by Arp/Warp (Murshudov et al., 1997). The features and factors for certain crystal structures are described in the appropriate paragraphs.

The final R crystallographic factor was 0.21 and Rfree 0.27 and 0.25/0.31 for the "human-mimicking" and native Mdmx structures, respectively. The final R crystallographic factor was 19.6 and Rfree 25.7 for a human complex with the P1 peptide and 20.5 and 24.2 for the "human-mimicking" with the P3 peptide, respectively. For the complexes of Mdm2/X with P4 mutant-p53 peptide the final R crystallographic factor was 0.18 and Rfree 0.24 for the Mdmx complex and 21.2 and 26.8 for Mdm2. Relatively high R factors arise from significant radiation damage during measurement. Most of the Mdm2 complexes had a clear interpretable electron

density between Glu25 and Asn111 for one Mdm2 molecule, and Thr26 and Val108 for the second. Most of the Human Mdmx had clear interpretable electron density between Gln23 and Leu109. Zebrafish crystals electron density was interpretable from Ala22 to Leu106. The Mdm2 complexes had a clear interpretable electron density between Glu25 and Asn111 for one Mdm2 molecule, and Thr26 and Val108 for the second. Certain solvent exposed side-chains without clear electron density were omitted in the models.

3.2.7 Isothermal titration calorimetry

Isothermal titration calorimetry (ITC) is a thermodynamic technique for monitoring any chemical reaction initiated by the addition of a binding component, and has become the method of choice for characterizing biomolecular interactions. When substances bind, heat is either generated or absorbed. Measurement of this heat allows accurate determination of dissociation constants (K_D), reaction stoichiometry (n), enthalpy (ΔH) and entropy (ΔS), thereby providing a complete thermodynamic profile of the molecular interaction in a single experiment. All ITC experiments were carried out according to references provided by the manufacturer. Proteins (p53) or p53 derived peptides (P1, P2 P3, P_ZF) were used at 0.3-0.4 mM in PBS and titrated with 2mM TCEP (Sigma-Aldrich) from a 300 μ l syringe into a sample chamber holding 1.43 ml of 0.03-0.04 mM of a respective binding partner. All solutions were degassed prior to measurements. Heat generated by protein dilution was determined in separate experiments by injecting a protein solution into PBS filled sample chamber. All data were corrected for the heat of protein dilution. Data were fitted using χ^2 minimization for a model assuming a single set of binding sites, to calculate the binding affinity K_D . All steps of the data analysis were performed using ORIGIN (V5.0) software provided by the manufacturer. The details of the experimental and injection parameters for two different equipments are described below.

Parameters of the experiments:

total number of injections	58/20
volume of a single injection [μ l]	5/1.5
duration of an injection [s]	10/3
intervals between injections [s]	400/300
filter period [s]	2/2
equilibrium cell temperature [$^{\circ}$ C]	20/25
initial delay [s]	60/40
reference power [μ Cal/s]	15/15
stirring speed [RPM]	270/600

3.2.8 Fluorescence polarization assay

Fluorescence polarization experiments were read on an Ultra Evolution 384-well plate reader (Tecan) with the 485 nm excitation and 535nm emission filters. The fluorescence intensities parallel (Intparallel) and perpendicular (Intperpendicular) to the plane of excitation were measured in black 384-well NBS assay plates (Corning) at room temperature ($\sim 20^{\circ}$ C). The background fluorescence intensities of blank samples containing the references buffer were subtracted and steady-state fluorescence polarization was calculated using the equation: $P = (Intparallel - GIntperpendicular)/(Intparallel + GIntperpendicular)$, and correction factor G ($G = 0.998$ determined empirically) was introduced to eliminate differences in transmission of vertically and horizontally polarized light. All fluorescence polarization values were expressed in millipolarization units (mP). The binding affinities of the fluorescent P4 peptide towards Mdm2 and Mdmx proteins were determined in the buffer, which contain 50 mM NaCl, 10 mM Tris pH 8.0, 1 mM EDTA, 10% DMSO. Each sample contained 10 nM of the fluorescent P4 peptide and Mdm2 (the Mdm2 concentration used, from 0 to 1 μ M and Mdmx, from 0 to 10 μ M) in a final volume of 50 μ l. The binding experiment was analyzed at initial time points: 0 h, 4 h, 8 h and 24 h, to test for temporal stability of Mdm2/Mdmx interactions with the fluorescent labeled P4 peptide. To determine the effect of different salt concentrations (50 mM, 100 mM, and 200 mM NaCl) and DMSO concentrations (0%, 5%, 10%, and 15%) in the assay, the experiments were carried out under similar condition to those described above except that the concentrations of NaCl or DMSO were varied.

Competition binding assays were performed using the 10 nM fluorescent P4 peptide, 15 nM Mdm2 or 120 nM Mdmx, and compound Mi219, the unlabeled P4 peptide (both used at concentration from 0 to 10 μ M) and the P1 peptide (0-100 μ M). Unlabeled peptides, compounds,

and stock solutions of the fluorescent-labeled peptides were dissolved in 100% DMSO. Plates were read at 30 min after mixing of all assay components. Binding constant and inhibition curves were fitted using the SigmaPlot (SPSS Science Software). The suitability of the presented assay for HTS applications was assessed by calculation of the Z' value from the following equation: $Z' = 1 - (3 \text{ SD}_{\text{bound}} + 3 \text{ SD}_{\text{free}}) / (m\text{P}_{\text{bound}} - m\text{P}_{\text{free}})$. Z' was calculated from 96 points measured separately.

3.2.9 General experimental methods for synthesis of small molecular weight inhibitors

Standard syringe techniques were applied for transfer of air sensitive reagents. Dry solvents and all purchased chemicals were purchased from Aldrich, Fisher Scientific, Acros Organics or Alfa Aesar and used as received. ^1H - and ^{13}C -NMR spectra were recorded on 600MHz Bruker spectrometer. Chemical shift values are in ppm relative to external TMS. Flash chromatography was performed with the indicated solvent mixture on Silica gel, MP Silitech 32-63 D, 60 Å, Bodman. Chromatotron chromatography was performed on Harrison Research Chromatotron, Ser. no. 65F with the indicated solvent mixture using Silica gel, Merck, TLC grade 7749, with gypsum binder and fluorescent indicator, Sigma Aldrich. Thin Layer Chromatography was performed using Whatmann flexible-backed TLC plates on aluminum with fluorescence indicator. Compounds on TLC were visualized by UV-detection. HPLC-MS measurements were done on a Shimadzu prominence UFLC (HPLC) and API 2000 LC/MS/MS System, Applied Biosystems MDS SCIEX, (MS) using a Dionex Acclaim 120 column (C18, 3µm, 120 Å, 2.1 x 150mm), mobile phase: water with 0.1% acetic acid and acetonitrile, gradient: 5-90% acetonitrile in 7 min, injection volume: 5 µl, detection wavelength 254 nm. HRMS measurements were performed at the Department of Chemistry, University of Pittsburgh with a Q-ToF spectrometer, ionization mode: ESI. Microwave reactions were performed on the Emrys Optimizer system from Personal Chemistry.

3.2.10 Computational library generation and docking

A database of several hundred scaffolds amenable to MCR chemistry in one or two synthetic transformations served as the underlying chemical space (Levine, 1997). The virtual libraries were generated using the REACTOR software including rule based scope and limitations as apparent from the literature (Pirok et al., 2006). The fragment indol or 4-chlorophenyl was included in each scaffold in the different variable positions. The other positions of each scaffold were complemented by commercially available substituents covering a broad physicochemical

property space, e.g. aliphatic, aromatic, small, bulky substituents. All possible stereoisomers to a particular compound were created. The created SMILES libraries were converted into 3D coordinates using the OMEGA software. The constrained docking including energy minimization, was performed using the MOLOC software using the template matching routine (Gerber and Müller, 1995, Gerber, 1998). The resulting docking poses of the virtual MCR molecules were visually inspected and ranked. A molecule was ranked high if besides the anchor residue sitting in the Trp23 also the Leu26 and Phe19 binding site was occupied by hydrophobic substituents (electrostatic complementarity), if no sterical clashes with the Hdm2 receptor occurred and if the starting materials were commercially available or easy to synthesize. In addition, we preferred to use the chemistry for which we had prior knowledge and experience.

3.2.11 Cell based assays

Modified p53^(-/-) knock out HCT116 cancer cells and the human ovarian cancer-derived A2780 cisplatin-resistant CP70 clone cell lines were gratefully donated by Vogelstein (Howard Hughes Medical Institute) and Hamilton (Fox Chase Cancer Institute). Cells were cultured in RPMI 1640 medium without phenol red (Invitrogen) containing 10% fetal bovine serum (Gemini Bioproducts) at 37°C in a humidified 5% carbon dioxide humidified incubator. Cells were plated in 96 well tissue culture plates (Costar) for 48 hours and the compounds (prepared in 100% DMSO as a stock solution) were added in quadruplicate. At least 5 different concentrations were tested for each compound. In each experiment, one plate consisted entirely of cells and medium used for time zero cell number determination, at the time/day of addition of compounds. After four days 20ul of Promega Cell Titer reagent was added into each well and plates were incubated in the tissue culture incubator. Approximately, 2 hours later the plates were read in a Biorad Ultra Mark Imaging system plate reader at 490 nm minus 630 nm absorbance /wavelengths. The data was then analyzed using an Excel Spread sheet grid. Resulting average values ranging from < 50 or >50 for two different concentrations was used to calculate the GI50.

For the Western Blotting cells were washed in cold Hanks balanced salt solution (HBSS) and lysed in Chaps Cell extraction buffer (Cell Signaling). After centrifugation at 4°C, an aliquot of the supernatant was diluted 1:100 and protein was estimated using Biorad DC protein assay. Equal amounts of protein was loaded into the wells of 12% polyacrylamide gels and separated by electrophoresis. Protein was transferred to nitrocellulose membranes (Biorad) using a Biorad Trans-Blot Semi-Dry transfer system. Membranes were washed in 50 mM Tris buffer (pH 7.4) containing 0.5 M NaCl, 0.1% Tween 20 (Biorad), and then blocked using Amersham membrane blocking reagent. Antibodies were purchased from Calbiochem or Cell Signalling. After

incubating with appropriate primary antibodies and peroxidase conjugated secondary antibodies the membranes were washed three times. ECL chemiluminescence sytem (GE Healthcare) and Kodak film was used to detect the protein bands. Films were scanned and protein bands were quantified with Biorad Multifluor –S and multianalyst /PC Image analysis system.

4 Results and discussions

4.1 Molecular basis for the inhibition of p53 by Mdmx and Mdm2 proteins and structural studies of these interactions

4.1.1 Cloning and constructs used for the study

4.1.1.1 Constructs of Mdm2 and Mdmx prepared for the study

The length of given constructs was chosen based on the structural and functional studies (Kussie et al., 1996; Grasberger et al., 2005). The Mdm2 full length DNA clone was obtained from Roche as a construct in the pET 20b vector. The residues of interest comprise the p53 binding domain. Purification strategy for Mdm2 constructs revealed that no tag is required for this step. However, the further crystallization trials required the number of different constructs.

Two point mutations using the Site Directed Mutagenesis Kit (Materials and Methods) were introduced to one of the human Mdmx construct, to release the binding site and make it more accessible for p53. The idea was taken up from the Mdm2-p53 interaction, because of high homology between Mdm2 and Mdmx in the N-terminal region of these two proteins.

Table 4.1. List of constructs of Mdm2 and Mdmx proteins and characteristics of the clones.

Constructs of Mdm2	Range of residues	Plasmid	Presence of tag
M2_2FL (Full length)	1-492	pET 46 LIC/E	N-terminal his tag
M2_A	1-118	pET46/LIC	N-terminal his tag
M2_JJ	1-125	pET 21	no tag
M2_B	23-109	pET46/LIC	N-terminal his tag
M2_C	18-111	pET 20	no tag
M2_D	18-125	pET 20	no tag
Constructs of human Mdmx (Hdmx)			
MX_FL (Full length)	1-490	pET 46/LIC	N-terminal his tag
MX_LM	1-134	pET 46/LIC	N-terminal his tag
MX_LM_M53V	1-134	pET 46/LIC	N-terminal his tag
MX_LM_Y99T	1-134	pET 46/LIC	N-terminal his tag
MX_LM1	1-147	pET 46/LIC	N-terminal his tag
MX_LL	1-210	pET 46/LIC	N-terminal his tag
MX_M	18-134	pET 46/LIC	N-terminal his tag
MX_A	18-113	pET 46/LIC	N-terminal his tag
MX_B	1-113	pET 46/LIC	N-terminal his tag

MX_C	1-112	pET 46/LIC	N-terminal his tag
MX_D	18-112	pET 46/LIC	N-terminal his tag
MX_E	18-114	pET 46/LIC	N-terminal his tag
MX_F	1-114	pET 46/LIC	N-terminal his tag
MX_T	23-111	pET 46/LIC	N-terminal his tag
MX_ST1	28-111	pET 46/LIC	N-terminal his tag
MX_ST2	28-111	pET 28b	C-terminal his tag
Mdmx mutants (human construct)			
LM_Mut1	Ile24>Glu	pET 46/LIC	N-terminal his tag
LM_Mut125	LM_Mut1 plus Gln64>Arg, Ser96>Arg	pET 46/LIC	N-terminal his tag
LM_Mut7	LM_Mut125 plus Glu70 > Gln Ser96 > Arg Arg103 > Tyr Ala110 > Asn	pET 46/LIC	N-terminal his tag

4.1.1.2 The Zebrafish (*Danio rerio*) Mdmx and its humanized clone

Initial attempts to crystallize human Mdmx in complex with p53 were unsuccessful, therefore as a starting point for our study the Mdmx zebrafish variant was used for cloning. The conserve Mdmx protein in eukaryotic organisms is expected to perform similar interaction as human one. After the proper sequence alignment two amino acids were found to differ between these clones and thereby they were mutated to mimic the human protein. The length of constructs and mutations are shown in Table 4.2 below. The Mdmx clones used for the study were taken from the genom of zebrafish (*Danio rerio*) and human.

Table 4.2. Results of cloning of the zebrafish Mdmx constructs.

Constructs of Mdmx Zebrafish	Range of residues	Plasmid	Presence of tag
ZF_FL (Full length)	1-491	pET 46 LIC/E	N-terminal his tag
ZF_M	15-129	pET46/LIC	N-terminal his tag
ZF_M_Humanized	15-129, mutations: L46>V, V95>L	pET 21b	no tag

4.1.1.3 Constructs of the p53 protein

Several constructs of p53 were cloned using the standard ligation procedure (described in the section Materials and Methods) and the LIC cloning method. The aim was to obtain the optimal construct expressed under native conditions. All constructs that have been successfully obtained are included in Table 4.3. Various other constructs were further cloned taking into consideration the full-length protein as a template. The constructs were designed based on the functional domains of p53. The graphical representation below gives an overview of the prepared constructs.

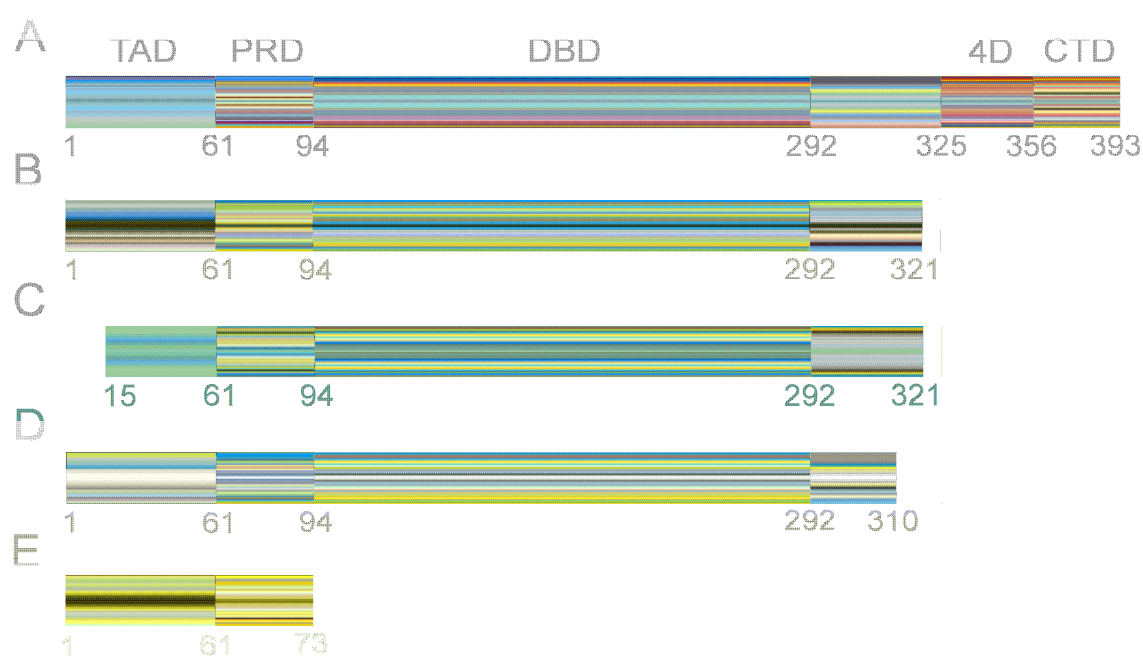


Figure 4.1 Graphical representation of various p53 constructs cloned and used in this study. The constructs are compared with the full-length protein.

Table 4.3. Results of cloning of various p53 constructs and characteristics of the clones.

Construct's name	Range of residues	Plasmid	Presence of tag
p53FL (Full length)	1-492	pGEX 4T1	N-terminal GST
p53TD1	1-73	pET46/LIC	N-terminal his tag
p53TD2	1-73	pGEX 4T1	N-terminal GST
p53TD3	1-73	pET 41/LIC	HIS, GST
p53TPD1	1-312	pET 46/LIC	N-terminal his tag
p53TPD2	1-321	pET 46/LIC	N-terminal his tag
p53TPD2	15-321	pET 46/LIC	N-terminal his tag

4.1.2 Protein expression and purification strategies

4.1.2.1 Results of the expression and classical purification profiles of Mdm2 and Mdmx

The *E. coli* expression system was successfully used for all proteins, in particular for Mdm2 and allowed to obtain high yield of the protein from refolding. The competent cells (Materials and Methods) BL21 (DE3) RIL with additional codons for human amino acids were used. The Mdm2 construct comprising residues 1-118 was cloned into the pET 46 LIC vector but did not express the protein in the native fraction under various conditions. For the NMR techniques this construct was the most commonly used in our study. The 6 His-tag was not cleaved off, after it was shown that it does not perturb the protein NMR spectrum. For further crystallization purposes the protein was cloned into the not-tagged vector to obtain a variety of constructs for cases that the tag could influence crystallization. For those purposes the pET 20b was used as a vector.

For the large scale expression of all of Mdm2 clones, 10 ml of the overnight pre-culture, enriched with antibiotics, was inoculated to 1 l of the LB medium. Cells were induced with 1 mM IPTG at induction temperature of 37°C and continuously growing for next 4-5 hours and purified from inclusion bodies. The induction at OD₆₀₀ 0.8 guaranteed the highest yield of the expression. Subsequently, the cells were centrifuged and were ready for the first purification step. Presence of the His-tag enabled the first step of purification using reagents for denaturing conditions for the Ni-NTA Agarose (buffers in Materials and Methods). However, omitting this step resulted in the same purity of the protein and simplified the purification (by removing the tag at the cloning step). After washing with PBS, the inclusion bodies were resuspended in the solubilization buffer (Materials and Methods). Dialysis enabled to decrease pH to 3-4. For renaturation, the protein was added in several pulses to the refolding buffer (fast dilution refolding). The graphical representation of the purification strategy is shown in the form of a flow-chart (Figure 4.2)

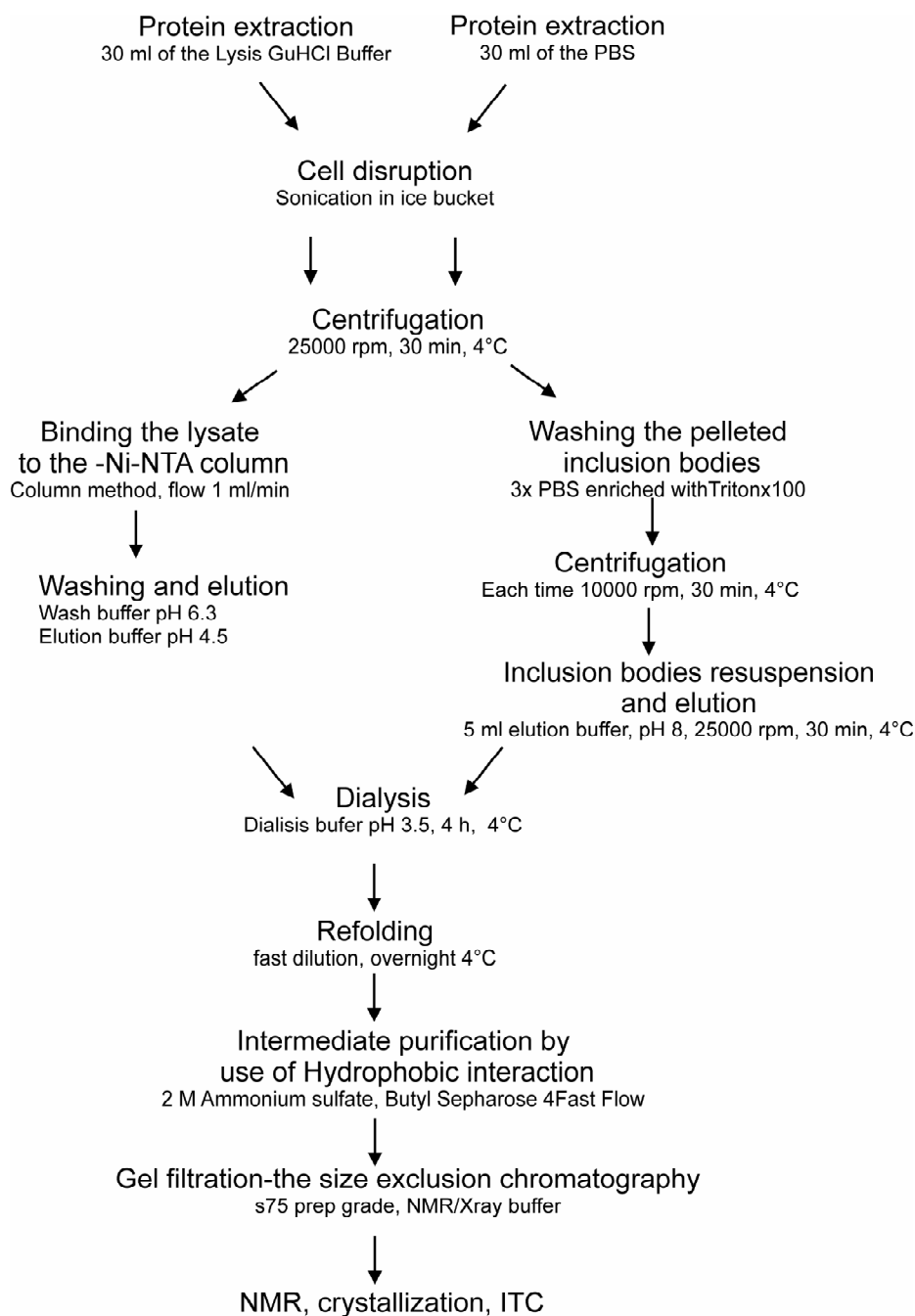


Figure 4.2. Flow chart of the purification of Mdm2 and Mdmx proteins.

Refolding was performed overnight at 4°C then ammonium sulphate was added to the final concentration of 2 M and, after couple of hours, the prep was mixed with 10 ml of the Butyl Sepharose 4 Fast Flow (Pharmacia, FRG). The protein was refolded, salted out with ammonium sulphate and further purified by Buthyl-Sepharose FF (Amersham). This purification was carried out without any affinity column.

The recombinant human Mdmx (residues 18-111) was obtained from an *E. coli* BL21 (DE3)RIL expression system, using the pET46Ek/LIC vector (Novagen). Cells were grown at 37°C and induced with 0.5 mM IPTG at an OD_{600nm} of 0.6 and were expressed for 12 h at 20°C. The protein was first purified under native condition using Ni-NTA Agarose (Qiagen), dialyzed to the enterokinase buffer and the His-tag was cleaved with enterokinase at 4°C for a period of 3-4 days.

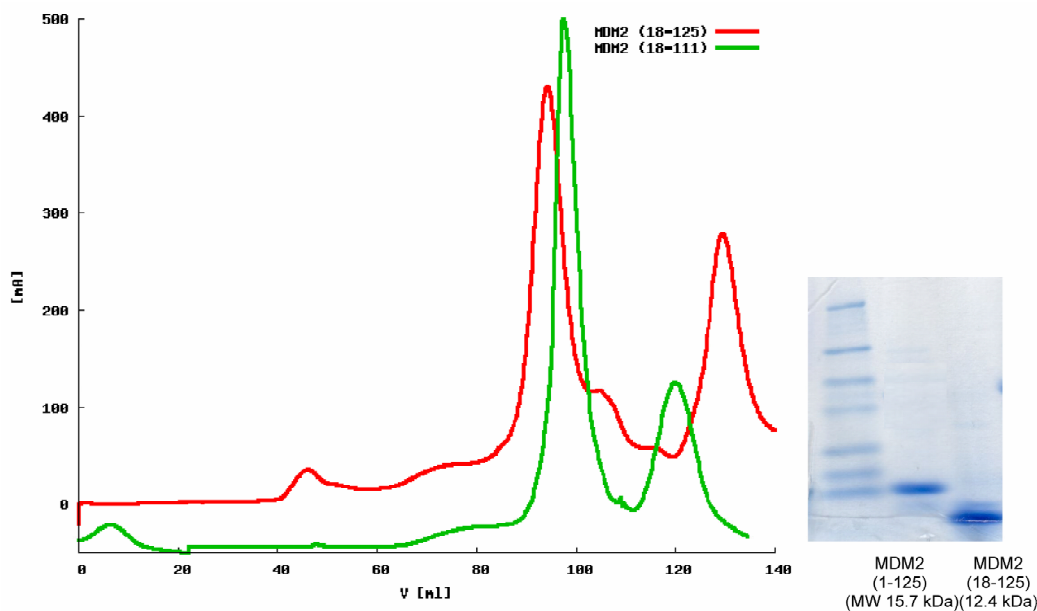


Figure 4.3. Typical chromatogram and SDS-PAGE of the two different constructs of Mdm2. The Mdm2 construct, comprising residues 1-125 was cloned into the pET 46/LIC vector. SDS-PAGE shows the purified protein.

The expression of the zebrafish Mdmx protein was carried on in pET 46/LIC vector with ampicillin and chloramphenicol. The human variant of Mdmx was cloned into pET 46/LIC, pET 15b, and pET 28b. The recombinant human Mdmx (residues 1-134), Mdmx mutants of the human clone: M53V and Y99T, the p53-binding domains of zebrafish Mdmx (residues 15-129) and the "human mimic" Mdmx (residues 15-129, mutations L46V and V95L) were also obtained from an *E. coli* BL21(DE3) RIL expression system using the pET-46Ek/LIC vector. After the large scale culture was inoculated, cells were grown at 37°C and induced with 1 mM IPTG at an OD_{600nm} of 0.7. The proteins were expressed for 12 h at 20°C. The proteins were first purified under native condition using Ni-NTA Agarose (Qiagen) and finally by the HiLoad 16/60 Superdex75 gel filtration (Pharmacia). The uniformly ¹⁵N-isotopically enriched protein

samples were prepared by growing the bacteria in minimal media containing $^{15}\text{NH}_4\text{Cl}$ (Materials and Methods).

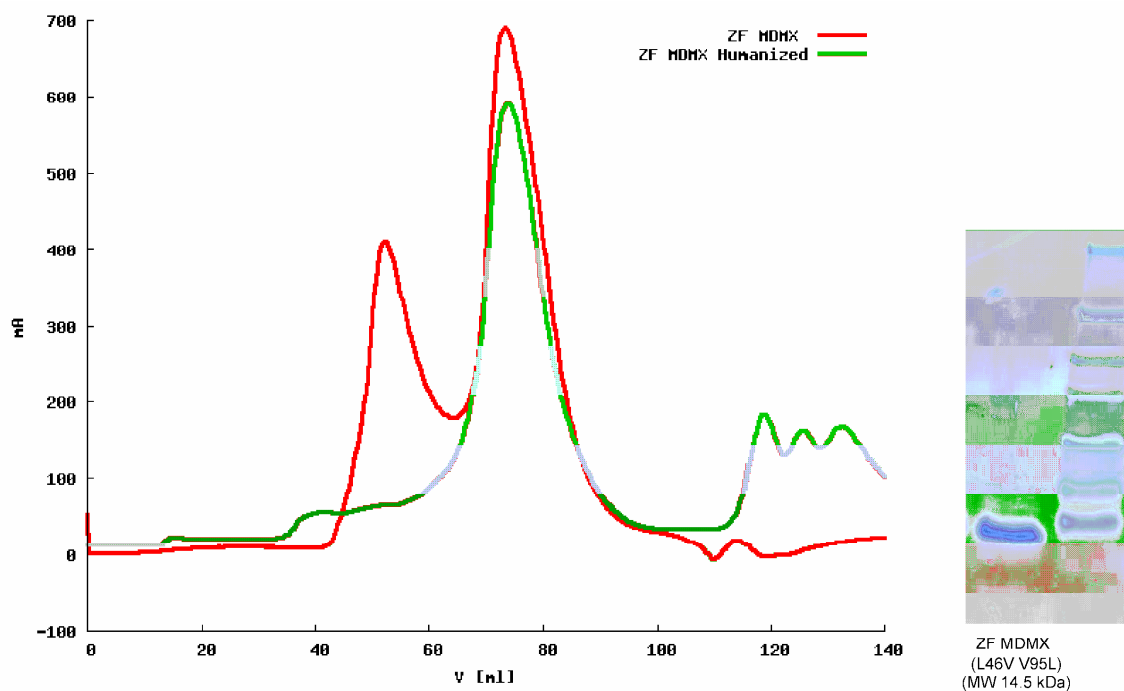


Figure 4.4. Purification profile for the Mdmx zebrafish constructs (native in red, humanized in green) and the SDS-PAGE of the middle fraction from the peak of the purified humanized Mdmx (green).

The final purification for both Mdm2 and Mdmx was with the HiLoad 16/60 Superdex75 gel filtration (Amersham Biosciences). The p53 constructs as well as complexes with Mdm2 and Mdmx were purified by the HiLoad Superdex 200 prep grade gel filtration. The complexes between Mdm2 and p53 as well as Mdmx and p53 were formed by mixing the protein with with the 3-fold excess of the smaller component (Mdm2/Mdmx), concentrating with stirring (>20 mg/ml for Mdm2, >10 mg/ml for Mdmx) and spinning before setting the crystal plates. The purity and folding of proteins were confirmed by SDS-gel electrophoresis, mass spectrometry, and NMR measurements. Examples of 1D proton spectra of various constructs of Mdmx are shown in Figure 4.5.

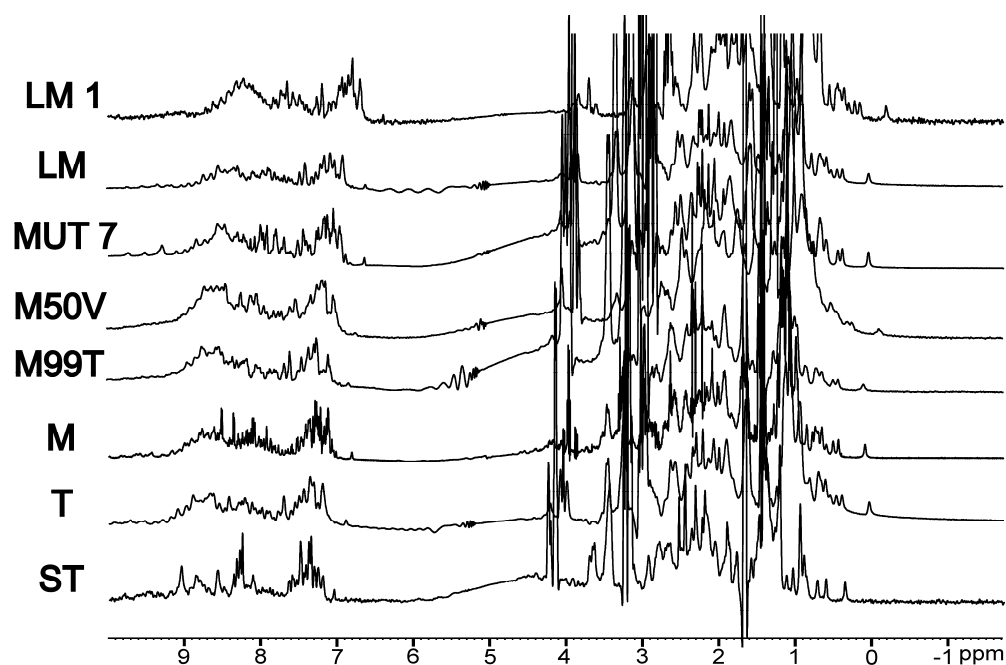


Figure 4.5. 1D-¹H spectra of various human Mdmx constructs showing their folding characteristics.

Large NMR signal dispersion at approximately 8.5-11 ppm in the 1D proton spectrum indicates the protein to be folded. A second diagnostic region for folding is the aliphatic region between 1.0 and 1.0 ppm a large signal dispersion versus a steep flank of the dominant peaks at approximately 1 ppm separates an unstructured protein from the folded one (Zhang and Forman-Kay, 1995; Rehm et al., 2002).

Table 4.4. Final list of constructs of Mdm2 and Mdmx/Hdmx used in this study.

Constructs of Mdm2	MW (Da)	Expression level	NMR	Results of the crystallization
1-118	1444.1	Inclusion bodies, very high	Folded, AIDA	-
1-125	1578.3	Very high	Folded, AIDA	-
18-125	1245.6	High	Folded	crystals with P1, P4 peptides and Mi-63
18-111	1098.0	High in BL21prar	Folded	crystals with Mi-63
Constructs of Mdmx	MW (Da)	Expression level	NMR	Results of the crystallization
ZF_M	14536.4	High	Folded	crystals with the P1 peptide

ZF_M_Mut	14536.4	Moderate	Folded	crystals with P1 and P3 peptides
MX_LM	16351.5	High, IB	Folded	-
MDMX_C	13968.9	High, IB	Folded	-
MX_D	10659.5	High, native and IB	Folded	crystals with the P4 peptide
MX_T	10321.1	Very high	Folded	crystals with the P1 peptide
MX_ST1	9738.4	Very high	Folded	crystals with the P3 peptide

AIDA: Antagonist Induced dissociation assay, constructs were used to carry out this assay

IB: inclusion bodies

-: no crystallization trials

4.1.2.2 Expression and purification of p53 constructs

Two constructs of p53 (Table 4.5) were prepared for NMR study: one comprising the transactivation domain (1-73) in fusion with GST tag and second, composed of residues (1-321) with 6-His tag. The proteins were expressed in the LB medium with 100 mg/ml of ampicillin and 34 mg/ml of chloramphenicol and induced overnight in 20°C. The GST tag was not cleaved as we wanted to obtain the p53 protein of high molecular weight for AIDA experiment. To decrease the number of non-p53 amino acids, the expression of the longer clone of p53 was optimized. The recombinant human p53 protein (residues 1-312) was overexpressed at 37°C overnight in *E. coli* BL21(DE3) RIL using the pET-46Ek/LIC vector. The protein was purified under denaturing conditions using Ni-NTA (Materials and Methods), refolded, and further purified using a Heparin Sepharose 6 Fast Flow (Amersham) column. Final purification was carried out via a HiLoad 10/30 Superdex S200pg gel filtration.

The p53-GST was overexpressed at 37°C for 3 h in *E. coli* BL21 using a pGEX vector. The protein was purified under native conditions via GST-Sepharose FF (Materials and Methods). Final purification was carried out with the HiLoad 16/60 Superdex S75 or a HiLoad 10/30 Superdex S200pg gel filtration column.

The purification strategy for p53 constructs with GST or His-tag is presented in Figure 4.6.

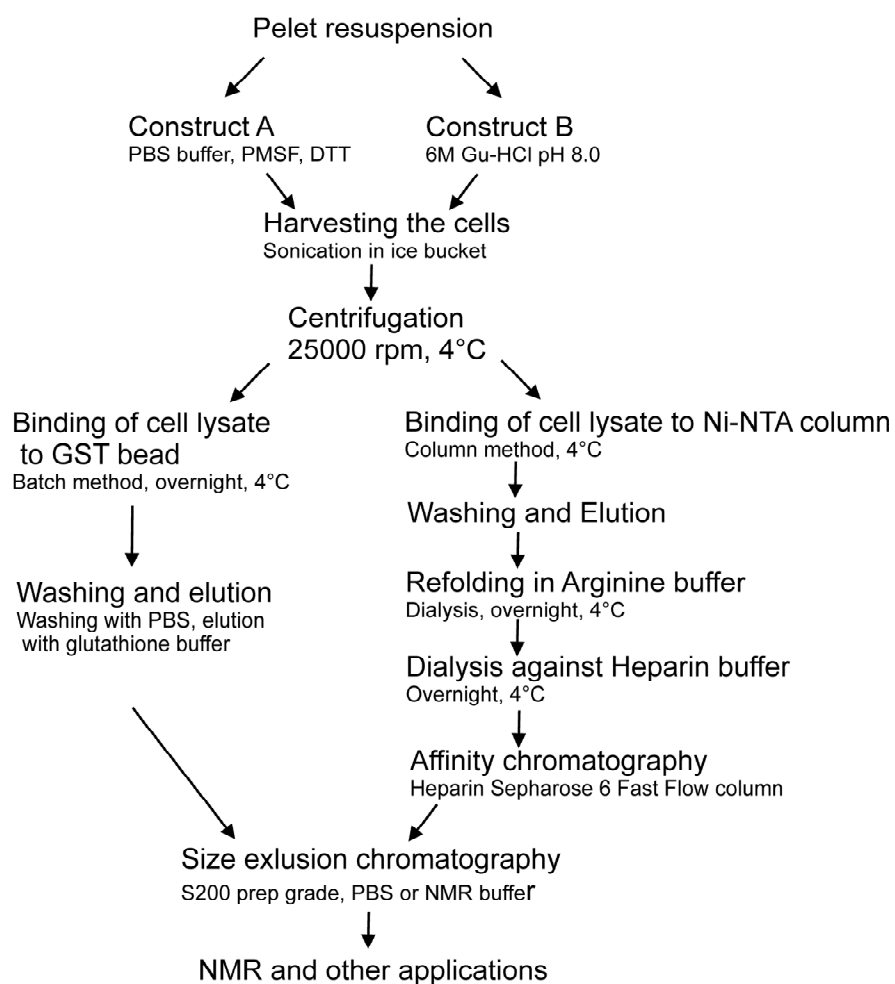


Figure 4.6. Flow chart of purification of the recombinant human p53 protein with different tags.

The heparin affinity column was used for the purification of p53 construct (residues 1-312). This helped to remove the impurities left after the refolding. The final purification of the p53 construct was carried out via the HiLoad Superdex 200 prep grade gel filtration. Figure 4.7 shows the adequate chromatograms for this p53 purification step.

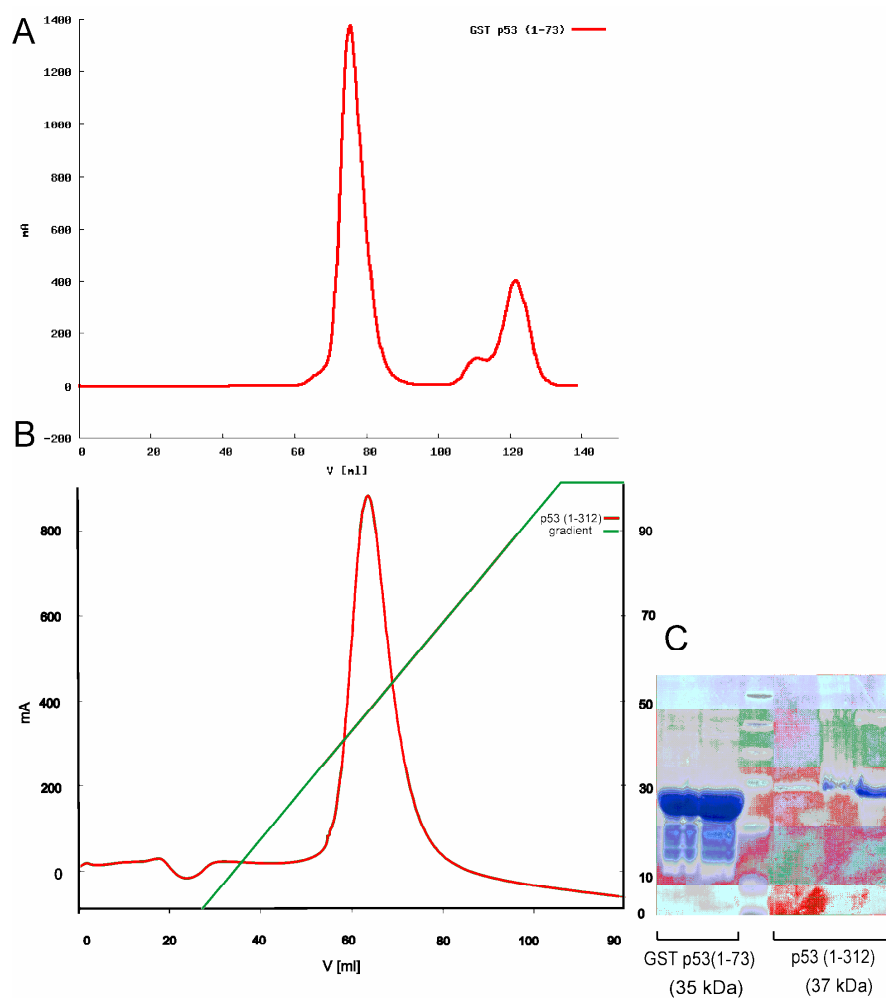


Figure 4.7. A: Profile of gel filtration (S200 Superdex prep grade) for GST-p53 (residues 1-73)
 B: Purification from the heparin affinity column for p53 (residues 1-312).
 C: SDS-PAGE of the finally purified constructs: GST-p53 (residues 1-73) and 6-His tag p53 (residues 1-312)

Table.4.5. Properties of the p53 constructs and the p53-derived peptides used for the study.

Peptide name	Sequence or range of residues	MW (Da)	E280 ($M^{-1}cm^{-1}$)
P1	SQETFSDLWKLLPEN	1806.9	5500
P2	RFMDYWEGL	1216.3	6990
P3	ETFSDLWKLLPENNVLSPLPS	2399.7	5500
P4	LTFEHYWAQLTS	1495.6	6990
(5-FAM) P4	5'FAM-LTFEHYWAQLTS	1735.9	6990
P_ZF	DSQEFAELWEKNLIQ	1963.1	5500

p53 constructs			
p53TD2	GST-(1-73)	35418.7	56840
p53TPD1	1-312	36224.6	33920
p53TPD2	1-321	37192.8	33920

5-FAM: molecular formula: C₂₁H₁₂O₇, molecular weight: 376.32
 ZF: p53 peptide analog for *Danio Rerio* (zebrafish).

p53 peptides were chemically synthesized and were purified by reversed phase chromatography. Coupling of the P4 peptide to 5-carboxyfluorescein (5' FAM) was performed via the N,N'-diisopropylcarbodiimide (DIC)/1-hydroxy-benzotriazole (HOBt) activation in N,N-dimethylformamide (DMF). Peptides were synthesized with an N-terminal amino group and a C-terminal carboxyl group. Peptides were analyzed by HPLC and MS.

4.1.3 Structural studies of Mdm2 and Mdmx proteins with p53 and p53 derived peptides

4.1.3.1 Preparing the crystallization conditions.

The protein buffer used for final step of the purification via gel filtration contained 5 mM Tris/HCl pH 8.0 and 50 mM NaCl and 10 mM β-mercaptoethanol. After addition of the peptide, protein was concentrated to about 15-20 mg/ml in case of Mdmx and 25-30mM for Mdm2. Crystallization of the protein was carried out with the sitting drop vapor diffusion method. Further optimization was carried out with the sitting and hanging drop vapor diffusion at 4 and 18 °C.

4.1.3.2 Structure of the wildtype and humanized zebrafish Mdmx-p53 complex.

4.1.3.2.1 Crystallization and data collection.

Zebrafish Mdmx crystallized in the form of thin plates from a crystallization solution containing 30 % PEG 300, 0.1 M MES pH 6.5. The crystals appeared in several days and grew to a final size of ca. 0.3 x 0.1 x 0.01 mm. They belong to the space group P2₁ and contained three complexes per an asymmetric unit. An acceptable quality dataset up to 2.3 Å was collected on the MPG/GBF beamline BW6 at DESY, Hamburg, Germany. The collected data were integrated, scaled and merged by XDS and XSCALE programs (Kabsh, 1993).

The structures were determined by molecular replacement using the Molrep program from the CCP4 suite (CCP4 Collaborative computational project, 1994). The structure of the Mdm2 taken from the PDB entry 1T4F (Grasberger et al., 2005) was used as a probe. The initial R-factor of the model was 0.46. The models were then refined by Refmac5 (Lamzin et al., 1995) and rebuilt by XtalView/Xfit (McRee, 1999) and by a subsequent Refmac5 refinement. Water molecules were added by Arp/warp (Lamzin et al., 1995). The final R crystallographic factor was 0.21 and R_{free} 0.27 and 0.25/0.31 for the "human-mimicking" and native structures, respectively. Most of the Mdmx models had clear interpretable electron density between Arg15 and Leu106, with M chain having barely interpretable electron density from lysine and isoleucine from the enterokinase cleavage site preceding Arg15 of Mdmx. Certain solvent exposed side-chains without clear electron density were omitted in the model. Data collection and refinement statistics are summarized in Table 4.6.

Table 4.6. Data collection and refinement statistics for native Mdmx–P1 and humanized zebrafish-P3 complexes.

Data collection	Native	Human-mimic
Space group	P2 ₁	P2 ₁
Cell constants (Å)	a=80.52 b=30.44 c=100.85 β =102.47	a=81.08 b=30.54 c=101.1 β =102.94
Resolution range (Å)	30-2.3	30-2.3
Wavelength (Å)	1.05	1.05
Observed reflections	102529	93820
Unique reflections	21546	23555
Whole resolution range		
Completeness (%)	91.6	93.2
R_{merg}	13.5	9.32
$I/\sigma(I)$	8.42	14.0
Last resolution shell:		
Resolution range (Å)	2.3-2.	2.4-2.5
Completeness (%)	82.0	96.3
R_{merg}	30.0	25
$I/\sigma(I)$	4.0	5.25
Refinement		
No. of reflections	20724	18354
Resolution (Å)	20-2.3	20-2.4
R-factor (%)	24.7	21.1

R _{free} (%)	31.0	27.1
Average B (Å ²)	26.25	20.69
R.m.s bond length (Å)	0.009	0.009
R.m.s. angles (°)	1.426	1.2
Content of asymmetric unit		
RMSD of monomers (Å)	0.47	0.5
No. of complexes	3	3
No. of protein residues/atoms	296/2377	310/2516
No. of solvent atoms	147	324

The X-ray structure of a complex between human p53 (residues 15-29) and a variant of zebrafish Mdmx (residues 15-129), in which the p53 binding site has been mutated to that of human Mdmx (Hdmx), was solved by molecular replacement using the structure of Mdm2 1T4F (Grasberger et al., 2005) as a model. We also solved the structure of the wild-type zebrafish Mdmx (residues 15-129) bound to human p53 (residues 15 to 29). The structures are closely similar (rmsd for the mainchain superposition is 0.39 Å) and we will concentrate below on the structure of the human-mimic Mdmx. Initial crystallization of the N-terminal domain of human Mdmx produced crystals that were not suitable for structural analysis, whereas zebrafish Mdmx crystals diffracted up to 2.3-2.4 Å. Sequence alignment shows that the wild-type zebrafish Mdmx is highly homologous both to human Mdmx (identity 48.8% for the full-length proteins, and identity 66%, similarity 85% within the 95 residues included in the structures) and to Mdm2 (identities 33.5%, 50.0%, similarity 74%, respectively), (Figure 4.8).

A

MDM2 human	MCNTNMSVPTDGAVTTS---QIPASEQETLVRPKPLLLKLLKLSVGAQKDYTMKEVLFYFYL	57
MDM2 mouse	MCNTNMSVSTEGAASTS---QIPASEQETLVRPKPLLLKLLKLSVGAQNDYTMKEVLFYI	57
MDM2 hamster	-----STDGAEGTS---QIPASEQETLVRPKPLFLKLLKLSVGAQKDYTMKEVILSW	49
MDM2 cat	MCNTNMSVSTDGAVSTS---QMPASEQETLVRPKPLLLKLLKLSVGAQKDYTMKEVLFYFYL	57
MDM2 dog	MCNTNMSVSTGGAVSTS---QIPASEQETLVRPKPLLLKLLKLSVGAQKDYTMKEVLFYFYL	57
MDM2 frog	M----NLTSTTNCLENN---HISTSDQEKLVQPTPLLLSLLKSAGAQQKETFMTKEVLYHHL	53
MDM2 zebrafish	M-----ATESCLSSS---QISKVDNEKLVVRPKVQLKSLLLEDAGADKDVFTMKEVLFYFYL	50
MDMX human	M----TSFSTSAQCSTSDSACRISPGQINQVRPKLPLLLKILHAAGAQQEMFTVKEVMHYL	56
MDMX mouse	M----TSHSTSAQCSASDSACRISSEQISQVRPKLQLLKILHAAGAQQEVFTMKEVMHYL	56
MDMX zebrafish	M----TSLASSSQLPGS---CRTLPGEQTQVHPRAPLLQILKVAGAQQEEVFTLKEVMHYL	53
	.: . : ** : .:* .*** : :***: :	
MDM2 human	GQYIMTKRLYDEKQQHIVYCSNDLLGDLFGVPSFSVKEHRKIYTMIIYRNLVVVNQQESSD	117
MDM2 mouse	GQYIMTKRLYDEKQQHIVYCSNDLLGDLFGVPSFSVKEHRKIYAMIYRNLVAVSQQ---D	114
MDM2 hamster	-QYIMTKRLYDEKQQHIVYCSNDLLGDLFGVPSFSVKDHRKIYIMIIYRNLVVVSQQETLQ	108
MDM2 cat	GQYIMTKRLYDEKQQHIVYCSNDLLGDLFGVPSFSVKEHRKIYTMIIYRNLVVVNQHEPSD	117
MDM2 dog	GQYIMTKRLYDEKQQHIVYCSNDLLGDLFGVPSFSVKEHRKIYTMIIYRNLVVVNQHEPSD	117
MDM2 frog	GQYIMAKQLYDEKQQHIVHCSNDPLGELFGVQEFVKEPRRLYAMISRNLVSANVKES--	111
MDM2 zebrafish	GKYIMSKEYLQKQQHIVHCGEDPLGAVLGVKSFVKEPRALFALINRNLVTVKNPE---	107

```

MDMX human      GQYIMVKQLYDQQEQHMVYCGGDLLGELLGRQSFVKD PSPLY DMLRKNLVTLATATT-D 115
MDMX mouse      GQYIMVKQLYDQQEQHMVYCGGDLLGDLLGCQSFVKD PSPLY DMLRKNLVTSASNNT-D 115
MDMX zebrafisch GQYIMMKQLYDKRQHIVHCHDDPLGELLEVGSFVKN PSPVY EMLKRNLVILNNS---D 110
              :*** *.***:...*:.*:.* * ** :. .****:  :. :.:.*

MDM2 human      SGTSVSENRC-HLEGGSDQ----KDLVQELQEEKPSSSHLVSRPSTSS---RRRAISETE 169
MDM2 mouse      SGTSLSESRR-QPEGGSDL----KDPLQAPPEEKPSSSDLISRLSTSS---RRRSISETE 166
MDM2 hamster    SGTSVSESRC-QPEGGSEQ----KDPVQEPQEEK-SSSDSVSRPSTSS---RRRTISETE 159
MDM2 cat        SGTSVSENRC-HLEGGSDQ----KDPVQELQEEKPSSSSDLVSRPSTSS---RRRTISETE 169
MDM2 dog        SGTSVSENSC-HREGGSDQ----KDPVQELQEEKPSSSSDLISRPSTSS---RRRTISETE 169
MDM2 frog       SEDIFGNVCC-FPDKQSSQ----KEKLQELPDKLIAPASD-SKPCNLS---QRKSSNETE 163
MDM2 zebrafish  SQSTFSEPRS-----QSEPDRGPGDTSDSRSSTSQQRRRRRSSSDPE 150

MDMX human      AAQTLALAQDHSMDIPSQD--QLKQSAESSTSRKRTTEDDIPTLPTS---EHKCIHSRE 170
MDMX mouse      AAQTLALAQDHTMDFPSQD--RLKHGATEYSNPRKRTEEEDTHTLPTS---RHKCRDSRA 170
MDMX zebrafisch AAKNLSVGKD-SNESPSEDPGVSSGSINSAQPLIAGSSTGTTQSCS---QRRPRDP-- 164
              :  ..  .  . :

```

B

```

Mdmx human      RISPGQINQVRPKLPLLKILHAAGAQGEMFTVKEVMHYLGQYIMVK
human-mimic    RTLPGEGTQVHPRAPLLQILKVAGAQEEVFTVKEVMHYLGQYIMMK

Mdmx human      QLYDQQEQHMVYCGGDLLGELLGRQSFSVKDPSPLYDMLRKNLVTL
human-mimic    QLYDKQRQHIVHCHDDPLGELLEVGSFSVKNPSPLYDEMLKRNLVIL

```

Figure 4.8. Sequence alignment of N-terminal domains of Mdm2 and Mdmx. A: Residues in green constitute the major differences in the sequences between the Mdm2 and Mdmx proteins. B: Structure-based sequence alignment between the p53 binding region of human Mdmx (Hdmx) and the zebrafish Mdmx mutated to mimic human features. Identical residues are highlighted in gray; the red-highlighted residues form directly the p53-binding site. To achieve binding site identical to human, the Mdmx Leu46 and Val95 were mutated to Val46 and Leu95, respectively, those residues are marked by black background.

Considering the residues important for the p53 binding in these proteins, the zebrafish Mdmx is closer to human Mdmx than to human Mdm2. The amino acid sequence of the native zebrafish Mdmx differs from that of human Mdmx only by Leu46 and Val95 in the p53 binding region and thus these residues were mutated to Val46 and Leu95 to achieve the human-featured p53 binding site.

The major difference between amino acid sequences of the first 100 residues of Mdmx and Mdm2 is at a stretch of the Mdm2 residues His96-Arg97-Lys98-Ile98, which are replaced by Pro95-Ser96-Pro97-Leu98 and Pro92-Ser93-Pro94-Val95 in human and zebrafish Mdmx, respectively. The affinities of zebrafish Mdmx's for the largest fragment of p53 (residues 1-312) and for nutlin-3 are analogous to those of human Mdmx. Thus we have concluded that zebrafish Mdmx is an excellent model for its human counterpart.

4.1.3.2.2 Features of the structure of the zebrafish Mdmx-p53 complex

The overall fold of zebrafish Mdmx is similar to that of Mdm2 (rmsd for the heavy atoms superposition between residues 25-109 of Mdm2 and residues 20-106 of zebrafish Mdmx is 1.28 Å) (Figure 4.9 A).

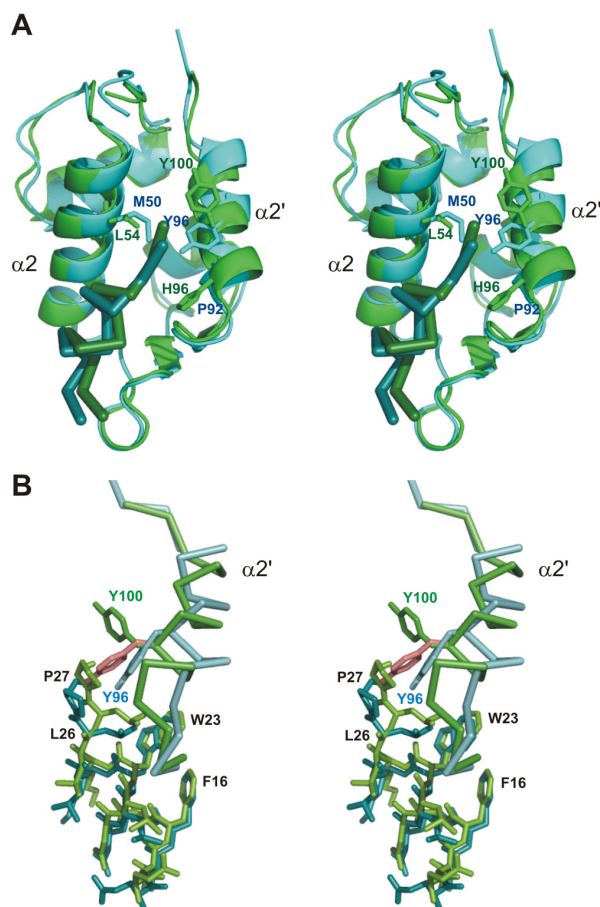


Figure 4.9. The structure of the complex between the variant of Mdmx (residues 15-129, mutations L46V and V95L) and p53 superimposed on the structure of the Mdm2/p53 complex. A: Stereoview of an overlay of Mdmx (blue) and Mdm2 (green). Residues shown, M50, P92 and Y96 for zebrafish Mdmx, and L54, H96 and Y100 for Mdm2, are important for binding to p53. B: The interaction of the p53 peptide 1 (stick plot) with α_2' helix (α -carbon plot) of Mdmx (blue) and Mdm2 (green). Tyr100 of Mdm2 in the structure of the nutlin/Mdm2 complex (26) is shown, in addition, in red.

The fold preserves the principal elements of the structure of Mdm2: a structural repetition into two portions of about 40 residues long, β_1 α_1 β_2 α_2 and β_1' α_1' β_2' α_2' , that

are related by an approximate dyed axis of symmetry (Kussie et al., 1996), and a hydrophobic cleft on one side of the structure formed by the repeat packing across their hydrophobic sides. The leading difference is located in helix $\alpha 2'$. This helix is moved by 2.5 Å in zebrafish Mdmx towards its C-terminus compared to Mdm2. It also starts later, all because of the Pro92-Ser93-Pro94 sequence; however the changes in $\alpha 2'$ start already at the zebrafish Mdmx Asn91 (human Mdm2, Glu95) and the $\alpha 2'$ helices of zebrafish Mdmx and Mdm2 get successively out of the register to each other until Leu103 (Leu107 human Mdm2), without large single differences in $\Phi\Psi$ angles (Figure 4.9 b). It is worth mentioning here that the $\Phi\Psi$ angles of the Pro92-Ser93-Pro94 sequence are still in the α -helical range (Figure 4.10)

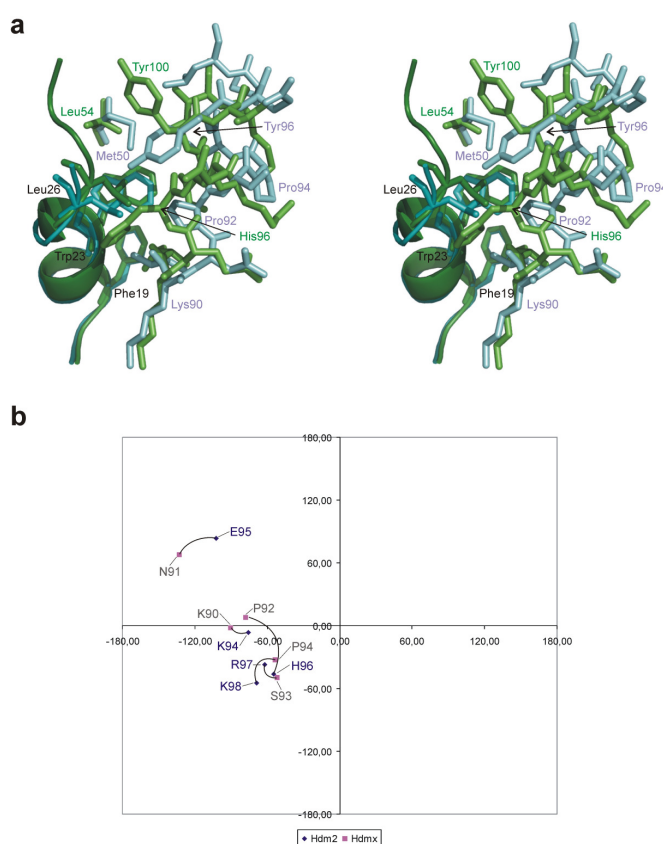


Figure 4.10. a: stereo plot of the fragment of the structure containing Pro92-Ser93-Pro94. In Mdmx (residues 15-129, mutations L46V and V95L) (blue), these residues cause different shape of the p53-binding cleft by a massive main chain shift compared to that of Mdm2 (green) where the corresponding residues are His96-Arg97-Lys98. Tyr96 is buried much deeper into the hydrophobic core and unable to move its sidechain outward as in Mdm2. Tyr96 together with Met50 causes the p53 peptide to exit the binding cleft earlier than in Mdm2 what is visible for Leu26 of the p53 peptide. b: A Ramachandran plot of main chain angles of the Lys90-Ser93 in Mdmx and corresponding Lys94-Arg97 of Mdm2. The angles are almost identical up to Lys90 (Lys94) then starting to diverge with maximal differences at

Asn91 (Gln95) and Pro92 (His96). Ser93 (Arg97) have again similar angles typical for an α -helix but the whole $\alpha 2'$ helix is shifted and have different conformation because of the differences in the Pro92-Pro94 region.

The binding cleft of zebrafish Mdmx is smaller than that of Mdm2 (Figure 4.11). This is because the sidechain of Tyr96 protrudes into the binding pocket, making it shallower (despite that C α is moved by 1 Å to the outside of the cleft, towards helix $\alpha 1'$, e.g away from the center of the p53-binding pocket). The position of the aromatic ring of Tyr96 is identical in all Mdmx molecules present in our structures, but different compared to that of the corresponding Mdm2 Tyr100 seen in all resolved structures of Mdm2 (Figure 4.9 A, B). In those structures Tyr100 participates in a rim around the p53-binding site; which is primarily made up by the sidechain of the Mdm2 His96. Zebrafish Mdmx has Pro92 (Pro97 in human Mdmx) at this position; thus the rim of the Mdm2 structure is effectively absent in zebrafish Mdmx. This makes the binding cleft of Mdmx shallower on the side of $\alpha 2'$.

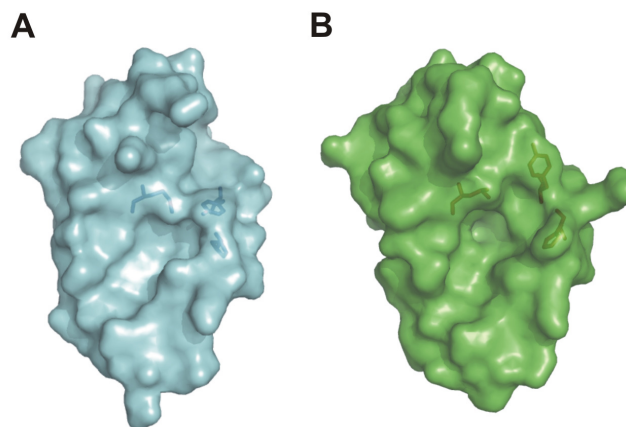


Figure 4.11. Surface representations of: A: Mdmx and B: Mdm2 structures. Residues highlighted are Met50, Tyr96, and Pro92 of Mdmx, and Leu54, His96, and Tyr100 of Mdm2 (see the text).

When the structure is viewed in the standard orientation in the Figure 4.9 A, the apex of the p53-binding cleft is further blocked from the opposite side by the sidechain of Met50 of helix $\alpha 2$ of zebrafish Mdmx (Met53 in human Mdmx). The Met50 sidechain points into the p53-binding pocket (this is the same orientation as the corresponding Leu46 of Mdm2 (Ile50 in *Xenopus laevis* Mdm2) but the larger Met50 sidechain makes the p53-binding cleft smaller (Figures 4.9 A and 4.11). Other distinct differences in amino acid sequences between Mdmx and Mdm2 are the Mdm2 residues 86 and 104. There is Leu82 (Leu85 in human Mdmx)

instead of Phe86 at the bottom of binding site in zebrafish Mdmx and no Tyr104 - instead we have Lys100 (Arg103 in human Mdmx). These substitutions however have small effects on the shape of the p53-binding cleft; for example, the aromatic ring of the Mdm2 Tyr104 is filled with the sidechain of Leu17 in Mdmx.

Determinants of the binding of p53 to Mdm2 found in the p53-Mdm2 interaction remain mostly intact for the p53-Mdmx binding. The primary contacts to Mdmx are made by hydrophobic Phe19, Trp23, and Leu26 of human p53 that form together an interface that is complementary to and fills up a hydrophobic pocket of zebrafish Mdmx (Figure 4.9 B). In the p53 peptide, the sidechains of Phe19 and Trp23, which insert deep into the zebrafish Mdmx cleft, are seen in the same positions in both Mdm2 and zebrafish Mdmx structures. However, the segment of the p53 peptide starting at Leu25, e.g. Leu25-Leu26-Pro27, is ca 1.7 Å shifted to the outside compared to that in Mdm2 (Figure 4.9 B).

4.1.3.3 Structure of human Mdmx protein bound to p53

This section presents structural data for human Mdmx bound to the P1 peptide and the second structure of the humanized zebrafish variant of the protein with a longer version of the p53 peptide (P3). The first structure is between the N-terminal domain of human Mdmx (residues 23-111, construct T) and the p53 peptide (residues 15-29, P1); the second is for the analogous complex involving p53 residues 17-37 (P3), and a variant of zebrafish Mdmx (residues 15-129) in which the p53 binding site has been mutated to that of human Mdmx (L46V and V95L).

4.1.3.3.1 Crystallization and data collection

The crystallization trials were performed for the tagged and not tagged proteins. For an untagged Mdmx, a 15 amino acids His-tag was removed by recombinant enterokinase according to the manufacturer manual.

The NMR spectra 1D-¹H showed that Mdmx was folded after removal of the His-tag, proteins crystallized in 25% PEG3350 and MES buffer, pH 6.5 - 6.75 for human Mdmx protein and 30% PEG300 0.1 M MES pH6.5 for the zebrafish variant of Mdmx. Crystals appeared after several days and grew to a final size of ca. 0.3 x 0.3 x 0.01 mm. The crystals belong to the space group P2₁ and contained four complexes per an asymmetric unit for a human protein and two of human mimic zebrafish. High quality datasets were collected on the SLS beamline PXII at Paul Scherrer Institut, Villigen, Switzerland.

Most of the human Mdmx had clear interpretable electron density between Gln23 and Leu109. For the zebrafish Mdmx, electron density was interpretable from Ala22 to Leu106. Data collection and refinement statistics are summarized in Table 4.7.

Table 4.7 Data collection and refinement summary for human Mdmx with the P1 and the “human-mimic” zebrafish complex with the P3 derived peptide.

Data collection	Human Mdmx-p53	Zebrafish Mdmx-p53
Space group	P2 ₁	P2 ₁
Cell constants (Å)	a=36.73 b=58.87 c=96.11 β=91.99	a=66.43 b=30.81 c=70.09 α=107.43
Resolution range (Å)	40-1.9	30-1.9
Wavelength (Å)	1.00	1.05
Observed reflections	128362	83741
Unique reflections	31292	24703
Whole resolution range:		
Completeness (%)	96.7	94.5
<i>R</i> _{merge}	5.5	6.9
I/σ(I)	20.0	15.9
Last resolution shell		
Resolution range (Å)	1.9-2.0	1.9-2.0
Completeness (%)	85.6	85.1
<i>R</i> _{merge}	19.5	22.3
I/σ(I)	7.03	6.9
Refinement		
No. of reflections	30129	23584
Resolution (Å)	25-1.9	25-1.8
R-factor (%)	19.6	20.5
R _{free} (%)	25.7	24.2
Average B (Å ²)	17.0	14.9
R.m.s bond length (Å)	0.01	0.008
R.m.s. angles (°)	1.35	1.24
Content of asymmetric unit		
RMSD of monomers (Å)	0.35	0.31
No. of complexes	4	2
No. of protein residues/atoms	394/3151	196/1537
No. of solvent atoms	430	220

4.1.3.3.2 Structural properties of the p53 binding pocket of human Mdmx

The structures of human and zebrafish Mdmx show that although the principle features of the Mdm2-p53 interaction are preserved in the Mdmx-p53 structures the central hydrophobic cleft of Mdmx on which the p53 peptide binds is smaller and differently shaped than that of Mdm2. This is because the sidechains of Met53 and Tyr96 Tyr99 in human Mdmx (and Met50 and Tyr96 in the zebrafish variant) protrude into the binding pocket thus blocking a part of the cleft on its opposite sides. The Met50 sidechain is in the same orientation as the corresponding Leu46 of human Mdm2, but the larger Met50 sidechain makes the p53-binding cleft smaller (Figures. 4.11 A and 4.12).

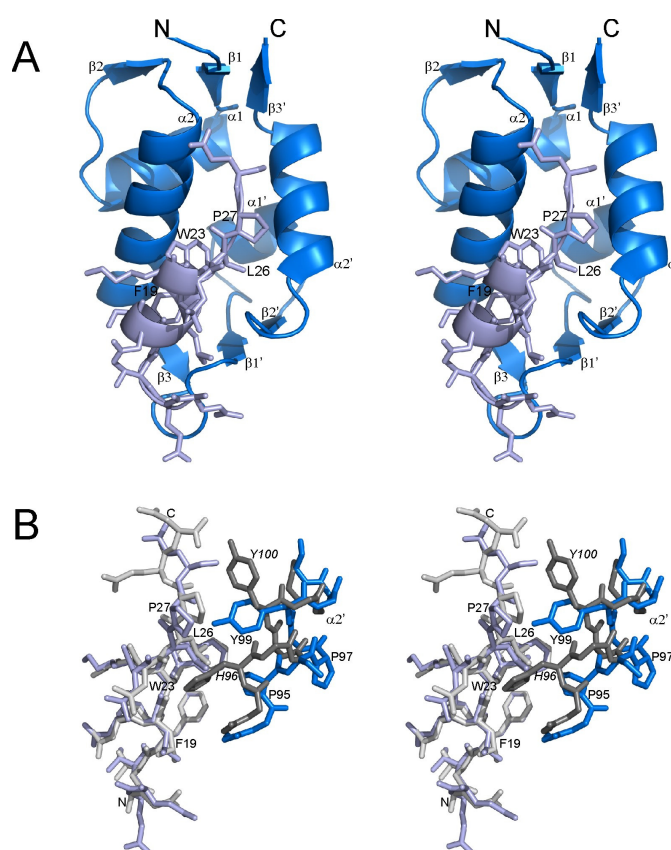


Figure 4.11. Structure of the Mdmx/p53 complex. (A) Stereoview of the complex of human Mdmx (dark-blue) and human p53 (light-blue). The p53 peptide is shown additionally as a stick-plot. p53 residues important for binding are labeled. (B) Stereoplot of differences in binding mode between p53 peptides (stick plot, light-blue for Mdmx, and light-gray for Mdm2) with part of helix $\alpha 2'$ of Mdmx (dark-blue) and Mdm2 (dark-grey).

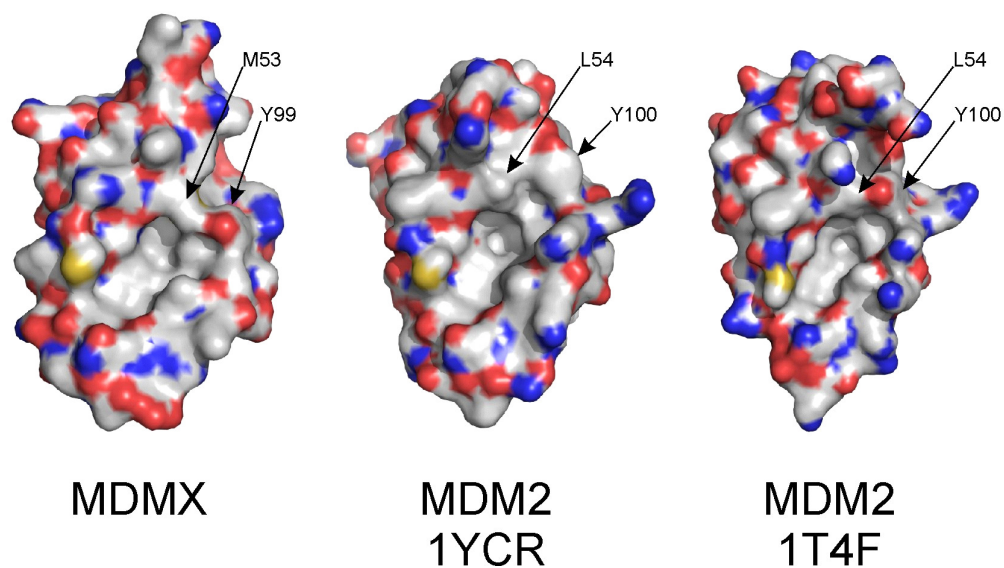


Figure 4.12. Surface representations of human Mdmx (the left side) and two human Mdm2 structures (the right side). Significant differences in the shape of p53 binding pocket are clearly visible. Residues responsible for differences in the binding groove are labeled.

For Tyr99 (Tyr96 in zebrafish variant), the position of the aromatic ring is nearly identical in all Mdmx molecules present in our structures ($\chi_1 = -72.3 \pm 2.5$) (Figure 4.13).

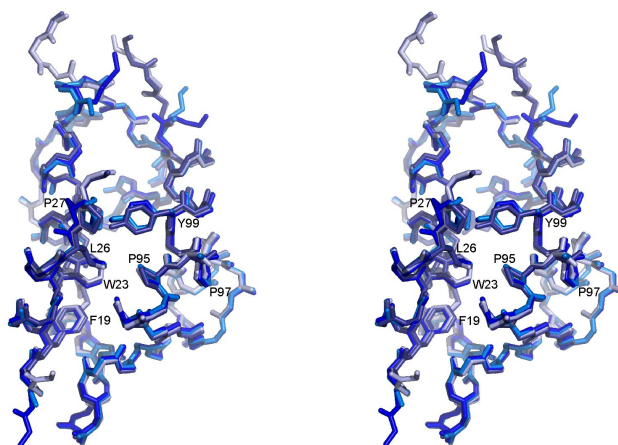


Figure 4.13. Structural alignment of all four p53-Mdmx complexes (wild-type zebrafish Mdmx, humanized zebrafish Mdmx and human Mdmx with p53 peptide P1, and humanized zebrafish Mdmx and peptide P3) present in an asymmetric unit. Despite of different crystal contacts, principal features of the p53 binding site are nearly identical.

We designate this configuration as the “closed conformation” of Tyr99 (Tyr96). This conformation is different to that of the corresponding Mdm2 Tyr100 in the structure of wt-p53/Mdm2 ($\chi_1 = +197.7$) (Kussie et al., 1996). In this Mdm2 structure the Tyr100 sidechain is flipped away from the p53 binding pocket (the “open” conformation of the Tyr) (Grasberger et al., 2005). The PDB Data Bank contains five additional structures of complexes of Mdm2 with short peptidic analogues: 1T4F (Bixby et al., 2008), 2GV2 (Sakurai et al., 2006), 2AXI (Fasan et al., 2006) and two small molecular weight compounds: nutlin 1RV1 (Kussie et al., 1996) and a benzodiazepinedione derivative (1T4E) (Grasberger et al., 2005). In all these cases the Tyr100 ring collapses into the p53 pocket assuming “the closed conformation” ($\chi_1 = -83.3 \pm 3.2$), thus filling the empty space that was occupied by the p53 residue Pro27. However, Tyr100 in human Mdm2’s never fully acquire the conformation seen in Mdmx structures.

Our present zebrafish variant of Mdmx includes a C-terminally extended p53 peptide to check whether such an extension could flip the tyrosine into the “open” conformation. This has not happened, and therefore we believe that the “closed” Tyr99 arrangement is the intrinsic property of Mdmxs that most probably arises from the differences between Mdmx and Mdm2 that are located in helix $\alpha 2'$ (Figure 4.11). This helix is moved by 3.0 Å at Pro95 and 1.5 Å at Lys104 in Mdmx towards its C-terminus and to the center of the molecule compared to human Mdm2. It also starts later, all because of the Pro95-Ser96-Pro97 sequence unique to Mdmx (although with the $\Phi\Psi$ angles still in the α -helical range). Significant changes in $\alpha 2'$ start already at the Lys93 (human Mdm2, Lys94) and the $\alpha 2'$ helices of Mdmx and Mdm2 get successively out of the register to each other until Asn105 (human Mdm2: Asn106), without large single differences in $\Phi\Psi$ angles. Different position of helix $\alpha 2'$ additionally changes the shape of the p53 binding pocket.

The primary contacts of the α -helical p53 peptide to Mdmx are made by its hydrophobic Phe19, Trp23, and Leu26 that form together an interface that is complementary to and fills up a hydrophobic pocket of Mdmx (Figure 4.11). When compared to previously solved structure of zebrafish Mdmx complexed to the human p53 peptide, the structures are similar with rmsd of 0.66 Å, however human Mdmx surrounds peptide much tighter and overall fit of these two molecules is much better. The surface area occupied by amino acids 17-27 of the p53 peptide has 440 Å² for human Mdmx and 407 Å² for zebrafish Mdmx. This trend is in agreement with the strength of the binding of the p53 peptide to these proteins; the K_D 's of the p53-Mdmx binding are $2.20 \pm 0.30 \mu\text{M}$ and $0.21 \pm 0.05 \mu\text{M}$, for zebrafish and human Mdmx, respectively (Shangary et al., 2008).

The structures presented here show clearly that Mdmx must be targeted independently from Mdm2 for drug development. Thus, structure of human Mdmx should provide a base for rational anticancer drug design against the p53-Mdmx interaction.

4.1.3.4 Structural base for nanomolar simultaneous inhibitors of Mdmx and Mdm2 interactions with p53

Both Mdm2 and Mdmx proteins share significant homology in the primary structure of their N-terminal p53 binding domains (Figure 4.14 and Introduction).

Mdm2 Human	M C N T N M S V P T D G A V T T S Q I P A S E Q E T L V R P K P L L L K L L K S	40
Mdmx human	- M T S F S T S A Q C S T S D S A C R I S P G Q I N Q V R P K L P L L K I L H A	39
Mdm2 Human	V G A Q K D T Y T M K E V L F Y L G Q Y I M T K R L Y D E K Q Q H I V Y C S N D	80
Mdmx human	A G A Q G E M F T V K E V M H Y L G Q Y I M V K Q L Y D Q Q E Q H M V Y C G G D	79
Mdm2 Human	L L G D L F G V E S F S V K E H R K I Y T M I Y R N L V V N Q Q E S S D S G T	120
Mdmx human	L L G E L L G R Q S E S V K D E S S I Y D M L R K N L V T L A T A T T D A A Q T	119

Figure 4.14: Structure-based sequence alignment between the p53 binding region of human Mdm2 and Mdmx. Identical residues are highlighted in gray; the similar residues are in light gray and the red-highlighted residues form directly the p53-binding site.

It was shown that the high-affinity Mdm2 inhibitors developed so far, e.g. Nutlins (Chene 2003, Vasilev 2008; Shangary and Wang 2008; Doemling 2008; Wade and Wahl 2009; Lehman et al., 2008, Vassilev et al., 2004) or Mi219 (reviewed by Bixby et al., 2008; Cheok et al., 2008; Shangary et al., 2008) are only weakly binding to Mdmx. Recently, however, Kallen et al. (2009) developed two p53 peptidomimetics which showed high affinity to both Mdmx and Mdm2, and in addition Hu et al. (2006) reported on a p53 mutant sequence that also had high affinity to these both proteins in a variety of cell lines. As the design of efficient dual Mdm2/Mdmx inhibitors requires the determination of pharmacophoric entities that share common features between these two proteins, we have decided to analyze the structural and functional properties of the p53 peptide sequence reported by Hu et al. (2006), further referred as the P4 peptide (Table 4.5).

In this part of my thesis I describe structural mechanism of the P4-Mdm2 and P4-Mdmx interactions. P4 does not disturb the native folds of Mdm2 or Mdmx and it thus should be possible to determine a simple pharmacophoric model for the mutual Mdm2-Mdmx inhibitors. This model indicates features necessary for the improvement of the binding constant from a submicromolar range, as is the case for native p53, to a low nanomolar range. We can confirm earlier assumptions (Zondlo et al., 2006; Dastidar et al., 2008) that the extension of the helical structure of the p53 peptide greatly improves its binding

properties to Mdm2 or Mdmx. It is thus possible to develop a peptide build up only from natural amino acids that is the strongest nM binder simultaneously to Mdm2 and Mdmx.

4.1.3.4.1 Crystallization and data collection

The P4-Mdmx crystals belong to the space group C2 and the P4-Mdm2 ones to P212121 and contained four complexes per an asymmetric unit for a human protein and two of human mimic zebrafish. High quality datasets up to 1.8 Å (Mdm2) and 1.4 Å (Mdmx) were collected on the SLS beamline PXII at Paul Scherrer Institut, Villigen, Switzerland. The final R crystallographic factor was 0.18 and Rfree 0.24 for the Mdmx complex and 21.2 and 26.8 for Mdm2. Relatively high R factors arise from significant radiation damage during measurement. Most of the Mdm2 complexes had a clear interpretable electron density between Glu25 and Asn111 for one Mdm2 molecule, and Thr26 and Val108 for the second. The Mdmx density was interpretable from Gln23 to Thr111 with one Ile residue at the N-terminus additionally visible - this residue originates from the His-tag after its cleavage. Several solvent exposed side-chains, without clear electron density, were omitted in the model. Data collection and refinement statistics are summarized in Table 4.8.

Table 4.8. Data collection and refinement summary

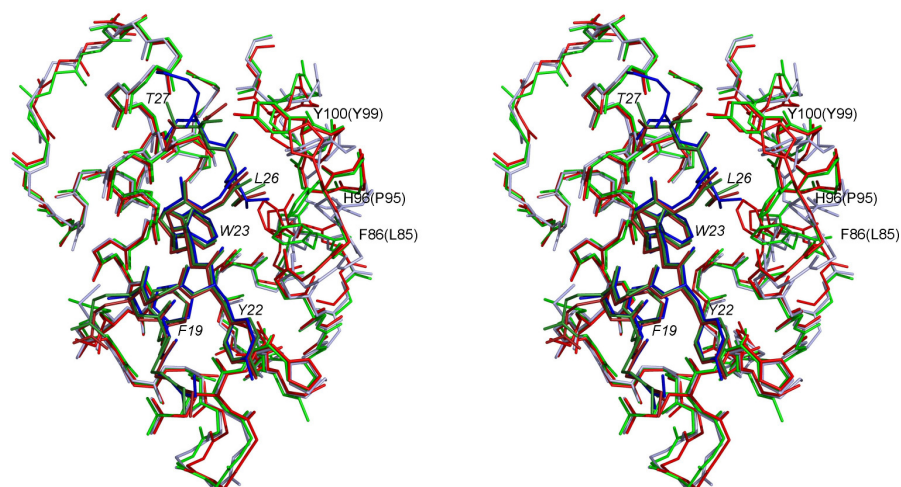
Data collection	Mdmx-P4	Mdm2-P4
Space group	C2	P2 ₁ 2 ₁ 2 ₁
Cell constants (Å)	a=69.23	a=44.36
	b=30.95	b=60.17
	c=50.42	c=71.02
	β=124.4	
Resolution range (Å)	40-1.4	30-1.8
Wavelength (Å)	1.00	1.00
Observed reflections	55334	122346
Unique reflections	14843	16226
Whole resolution range:		
Completeness (%)	84.1	89.0
R_{merge}	3.0	4.2
$I/\sigma(I)$	25.2	18.9
Last resolution shell		
Resolution range (Å)	1.4 – 1.5	1.8 – 1.9
Completeness (%)	46.2	32.5
R_{merge}	11.1	13.5
$I/\sigma(I)$	9.4	7.18
Refinement		
No. of reflections	12042	15382
Resolution (Å)	20 – 1.4	20 – 1.8
R-factor (%)	18	21
R_{free} (%)	22	26
Average B (Å ²)	19.1	26.6
R.m.s bond length (Å)	0.008	0.011
R.m.s. angles (°)	1.30	1.47
Content of asymmetric unit		
RMSD of monomers (Å)	NA	0.68
No. of complexes	1	2
No. of protein residues/atoms	102/825	192/1610
No. of solvent atoms	181	174

4.1.3.4.2 Structure of the complex between the N-terminal domain of Mdmx and the P4 peptide

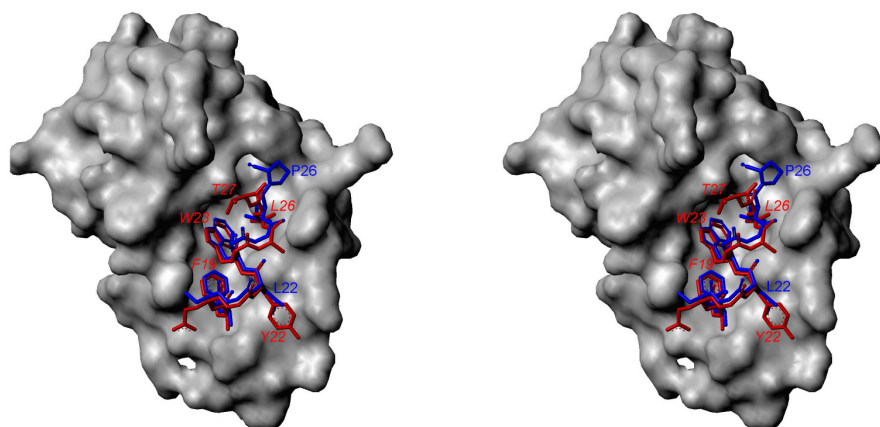
The general fold of the Mdmx protein in complex with the P4 peptide remains almost identical to that of the previously solved structure of the wt-p53/Mdmx complex (Figure 4.15 A) (RMSD of non-hydrogen atoms equals 0.57 Å). There are only two distinct structural differences caused by the binding of the non-native P4 peptide. The first difference occurs at Tyr99 whose aromatic plane is rotated by 90° relative to the orientation of Tyr99 found in the wt-53/Mdmx structure, but remains in the “closed” conformation as defined by Popowicz et al. (2007). The second is the conformation of the side chain of Met61, which folds over the P4 peptide instead of pointing away from peptide like in the native p53-Mdmx complex (Popowicz et al., 2007). This change is caused by the substitution of a short hydrophilic Ser20 with Glu20, whose C β and C γ form a locally hydrophobic environment suitable for Met61 interaction.

The P4 peptide shares Phe19, Trp23, Leu26 with the native p53 sequence (numbering of the P4 residues is as in the native p53 sequence). These are the key p53 residues that define the Mdm2/x binding (Kussie et al., 1996). The bound peptide forms a short α -helix, similarly to the native one. While spatial orientation and the position of the Phe19-Trp23-Leu26 triad remains identical to the native peptide, the P4 peptide shows a number of additional interactions that improve its binding affinity towards Mdmx. The most pronounced additional interaction is formed by Tyr22 (Leu22 in the native sequence). Its side-chain fills a large space with strong hydrophobic properties formed by aliphatic fragments of Gln71, His72 and Lys93. This space remains solvent-accessible in the native complex, as a much smaller side chain of Leu22 is not able to completely fill the cleft. Further, Pro27 of the native p53 sequence (which breaks the α -helical secondary structure of the native peptide) is substituted for Thr27 in P4. Despite of the fact that Thr27's ϕ and ψ angles fall in the β -region, Thr27 participates in a distorted turn that follows a helical pattern. Additionally, the hydrophobic part of Thr27 of P4 covers the exposed Met53 sidechain of Mdmx, extending the overall area of the hydrophobic interaction. This is in contrast to Pro27 present in the native sequence, which introduces its polar carbonyl atom into the vicinity of Met53 of Mdm2.

A



B



C

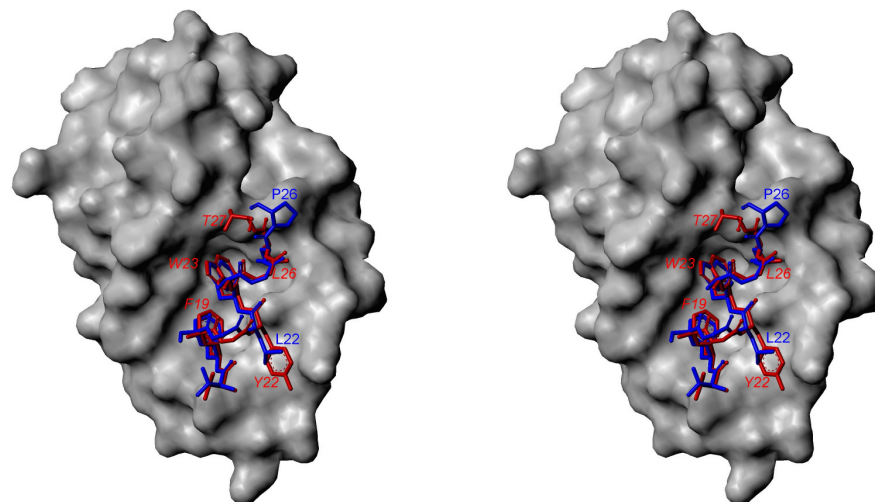


Figure 4.15. Structures of the P4-Mdm2 and P4-Mdmx complexes. A: The two P4-Mdm2 complexes present in the asymmetric unit are colored red and green, while the corresponding P4 chains are shown in dark red and dark green, respectively; Mdmx is colored light blue and its P4 peptide dark

blue. Sidechains of only most important residues are shown. The P4 residues are labeled in italics; the most important Mdm2 and Mdmx (in parentheses) residues are also labeled. Despite of significant differences between Mdm2/Mdmx chains the P4 peptide retains virtually an identical conformation. B: Structure of the wt-p53 peptide (blue) and the P4 peptide (red) shown on the surface of the Mdm2 protein. P4 residues and the wt-p53 residues common to both peptides are labelled in red, the wt-p53 residues different from P4 are labeled in blue. The P4 peptide is significantly more helical; thanks to the absence of Pro27 that “breaks” the helical character of wt-p53 sequence. Additionally, the interactions formed by the sidechain of Tyr22 are visible. C: Structure of the wt-p53 peptide (blue) and the P4 peptide (red) shown on the surface of Mdmx. P4 residues and the wt-p53 residues common to both peptides are labeled in red, the wt-p53 residues different from P4 are labelled in blue. P4 acquires a more helical structure than the wt-p53 sequence. Tyr22 fills the same area of the protein as in the Mdm2 structure.

4.1.3.4.3 Structure of the complex between the N-terminal domain of Mdm2 and the P4 peptide and comparison to the Mdmx-P4 structure

The structure of the N-terminal domain of Mdm2 in complex with the P4 peptide is similar to the structures of Mdm2 with the native p53 peptide (Kussie et al., 1996). Interestingly, however, the two molecules of Mdm2 present in an asymmetric unit contain small but distinct differences in their structures which are due to crystal contacts. The most prominent difference is seen in the region between Gly83 and Ser90, which is shifted towards its C-terminus in one Mdm2 molecule relative to the other Mdm2 chain. This difference is most prominent at Phe86, which forms the bottom of the p53 binding cleft (C α shifted by 1.25 Å and the phenyl ring's plane rotated by 90°). The region between Thr101 and Leu107 is also altered between the two Mdm2 molecules, with a main chain shift of 1.0 Å at Ile103, and with the Met102 sidechain acquiring a different conformation due to the proximity of the altered Phe86 sidechain. Despite these differences, the structure of the bound P4 peptide remains perfectly identical in the two P4/Mdm2 complexes of the asymmetric unit. This indicates that while Mdm2 can undergo considerable structural alterations, the binding conformation of the p53-like peptide remains invariant in such cases.

The structure of Mdm2 bound to P4 shows no significant difference to other known structures of Mdm2 in complex with p53 peptides. The RMSD between the Mdm2-P4 (of one of the two molecules in the asymmetric unit closest to the structures compared to) and the “native p53/ Mdm2” complex structure is 0.53 Å (1YCR) (Kussie et al., 1996) and with the structure with a so-called optimized p53 peptide is 0.68 Å (1T4F) (Grasberger et al., 2005). The Phe19-Trp23-Leu26 triad of all these peptides remains in virtually identical positions. Similarly to the Mdmx-P4 structure, Tyr22 of p53 forms extensive hydrophobic contacts with His73 and Lys94. It is worth noting that both the optimized peptide published by Grassberger

et al. (2005) (1T4F) and our structure share similar position of the p53 Tyr22 present in both peptides' sequences. The presence of this residue most probably is the key factor in increasing affinity of the mutant peptides towards Mdm2 and Mdmx. This data is in agreement with the ELISA assays published by Böttger et al. (1997). Met62 of Mdm2 shows different sidechain conformations when compared to the native p53-Mdm2 complex; however, both conformers are located close to the peptide, which is different from that seen in the Mdmx-p53 structures where the corresponding M61 sidechain points away from the p53 peptide. Tyr100 of Mdm2 assumes in our structure a more closed conformation when compared to the 1YCR structure (the "native-p53/Mdm2") this is very similar to the orientation seen in the optimized peptide structure 1T4F.

The next crucial difference between P4 and the native p53 peptide is formed by Thr27, which substitutes Pro27 in the native p53 sequence. Similarly to the Mdmx structure, while Pro27 breaks the helical organization of the peptide, Thr27 continues a loosely helical turn and H-bonding pattern. Additionally some solvent-exposed residues show divergence of conformations between P4 and the native p53 structures; these changes however are unlikely to influence the binding mechanism.

4.1.3.4.4 Conclusions

According to our data the structures of both the Mdmx-P4 and Mdm2-P4 complexes are very similar, with RMSD of 0.85 Å. The mayor difference is located at the Pro95-Ser96-Pro97 region of Mdmx where the helices of both proteins are out of register causing side chain of Tyr99 of Mdmx to penetrate deeper into the p53 binding interface. This is the so-called "closed" conformation of Tyr99 described earlier (Popowicz et al., 2007; Popowicz et al., 2008). Met53 of Mdmx (which corresponds to Leu54 of Mdm2) is the second major difference between the structures of Mdmx and Mdm2. Together those changes create a different shape of the p53-binding region in the Leu26 subpocket for these two proteins. Importantly, the conformation of the bound P4 peptide is not influenced by these differences in protein structures. The spatial organization of the p53 Phe19-Trp23-Leu26 triad, as well as additional Mdm2-interacting residues Tyr22 and Glu20, remain identical despite the alterations in the structures of Mdm2 and Mdmx.

4.1.4 Functional studies of the interaction between Mdm2/Mdmx proteins and p53

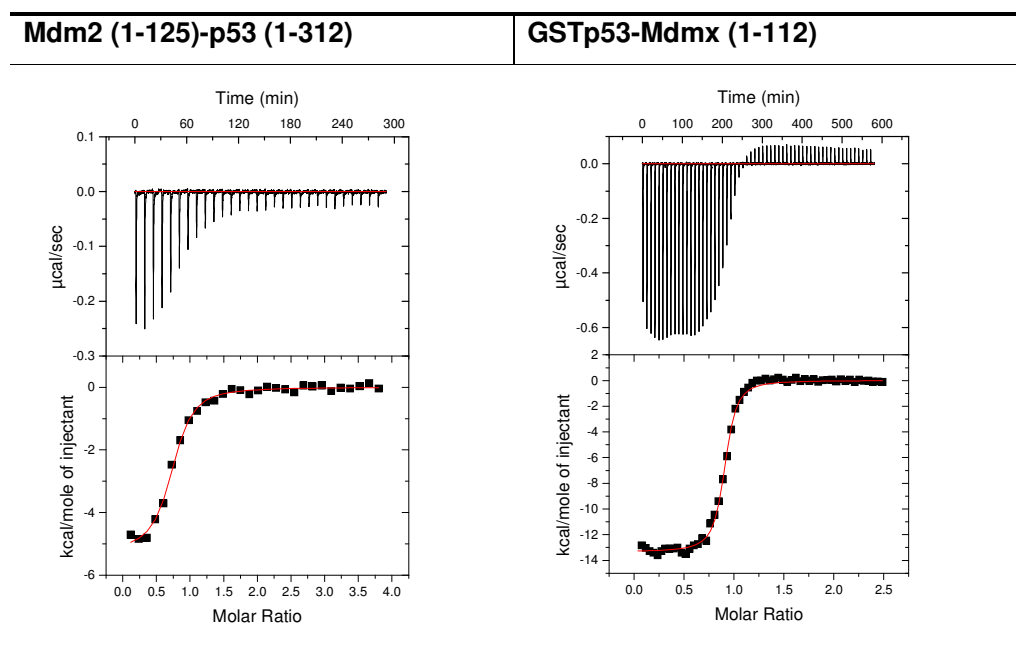
In this part of my thesis I document the results of the interactions of Mdm2 and Mdmx with p53. Furthermore, I will describe the binding of the p53 derived peptides and specific inhibitors designed for Mdm2. The crystal structures presented in chapter 4.1.3 revealed the structural details of the mechanism of binding p53 to Mdm2 and Mdmx.

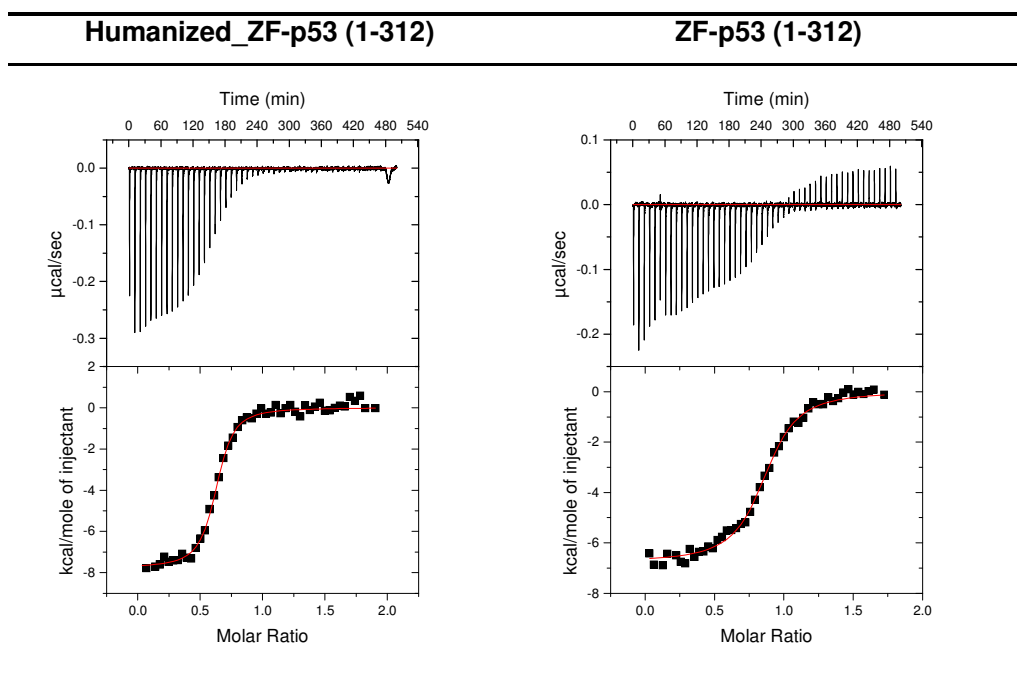
4.1.4.1 Binding of various p53 peptides, small molecule-binding partners to Mdm2, human Mdmx and zebrafish Mdmx

4.1.4.1.1 ITC

The binding of different p53 constructs to human Mdm2 (residues 1-118), human Mdmx (residues 1-134), and zebrafish Mdmx (residues 15-129) was measured by the isothermal titration calorimetry using a VP-ITC MicroCalorimeter (MicroCal, Northampton, MA). The protein concentration in the reservoir solution was around 0.02-0.035 mM, the concentration of the titrant was around 0.2-0.4 mM. Measurements were carried out in PBS, 2 mM TCEP, pH 7.4. All steps of the data analysis were performed using ORIGIN (V5.0) software provided by the manufacturer.

Table 4.1.1 Examples of ITC titration curves for Mdm2 and Mdmx and different p53 constructs.





The raw data (upper part) of ITC experiments were performed at 25°C. The integrated heat changes corrected for the heat of dilution as well as fitted curves based on a single model.

Published crystal structures of the complexes between Mdmx/2-p53 and wildtype p53 peptide together with biochemical and biophysical assays suggested that several mutant peptides and peptidomimetic compounds could serve promising pharmacophore models of the Mdm2/x-p53. I have shown the tight binding between Mdm2/Mdmx and peptide P1, P2, and P4. The Mdm2/x protein samples were titrated in 3 steps and shown the slow exchange for several resonances upon addition of these peptides. The affected cross peaks were mostly localized at 9.2-7.6 ppm ω_1 ^1H and 114-105 ppm ω_1 ^1N for all recorded spectra, indicating that the peptide binds on the same site for both Mdmx and Mdm2. Additionally Nutlin-3, as the strongest documented inhibitor for Mdm2-p53 was used for the positive control experiment. Its weak influence on the NMR Mdmx spectrum confirms lack of inhibitory interaction for Mdmx. Figure 4.1.1 shows 2D spectra recorded for these particular peptides.

The affinity of the P4 peptide in our FP assay was 3.6 ± 0.3 nM towards Mdm2 and 6.1 ± 0.5 nM for Mdmx (Figure 4.1.1 and Chapter 4.1.4.1.3). Additionally, we have found that labeling the P4 peptide with fluorescein allowed its use for a robust fluorescence anisotropy assay suitable for HTS screening for Mdm2/Mdmx inhibitors. The fluorescein/P4-based assay does not require expensive non-native amino acids, and allows measurements of the interaction to both Mdm2 and Mdmx in virtually identical conditions, without any modification of experimental conditions or setup between the two proteins.

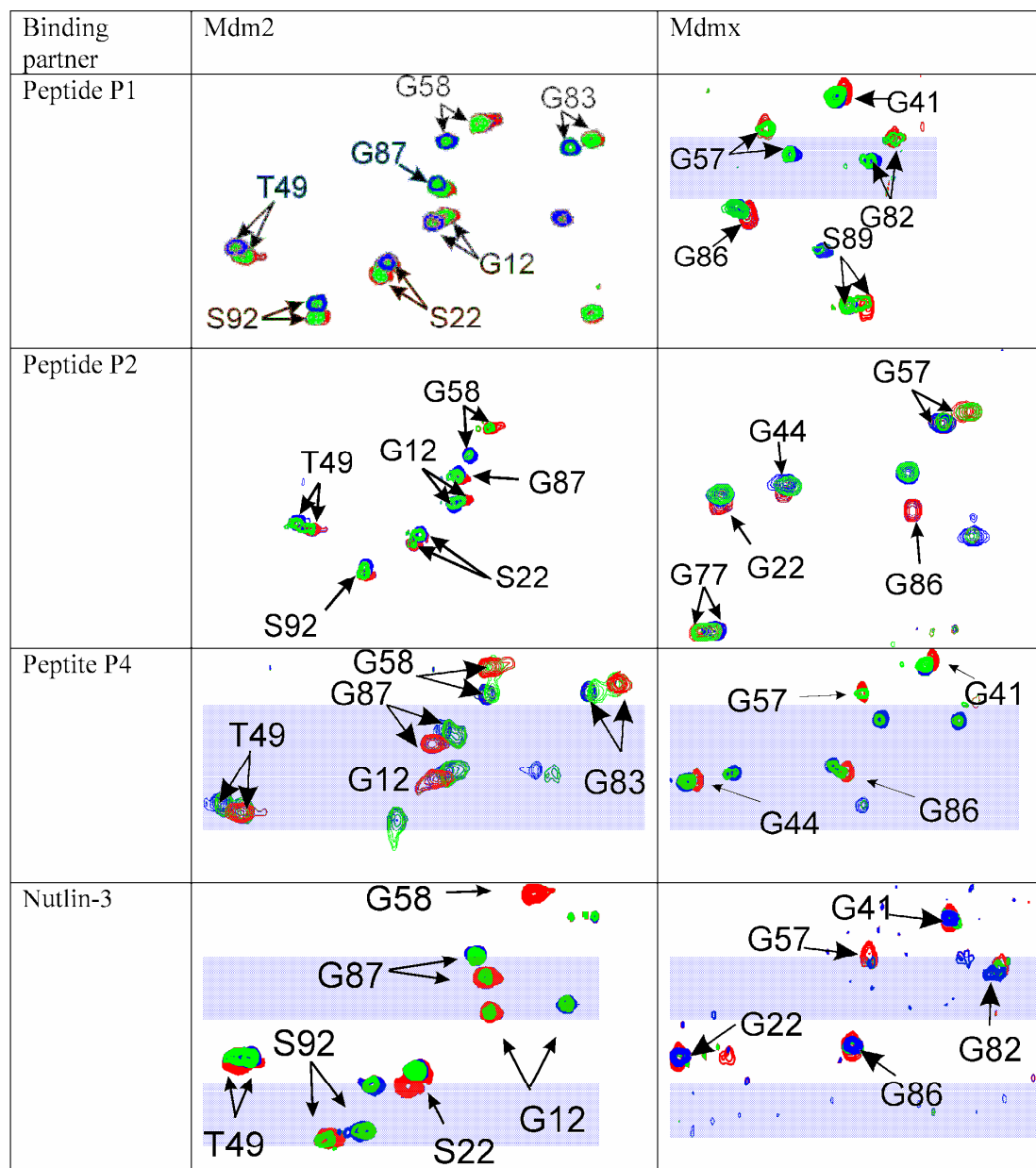
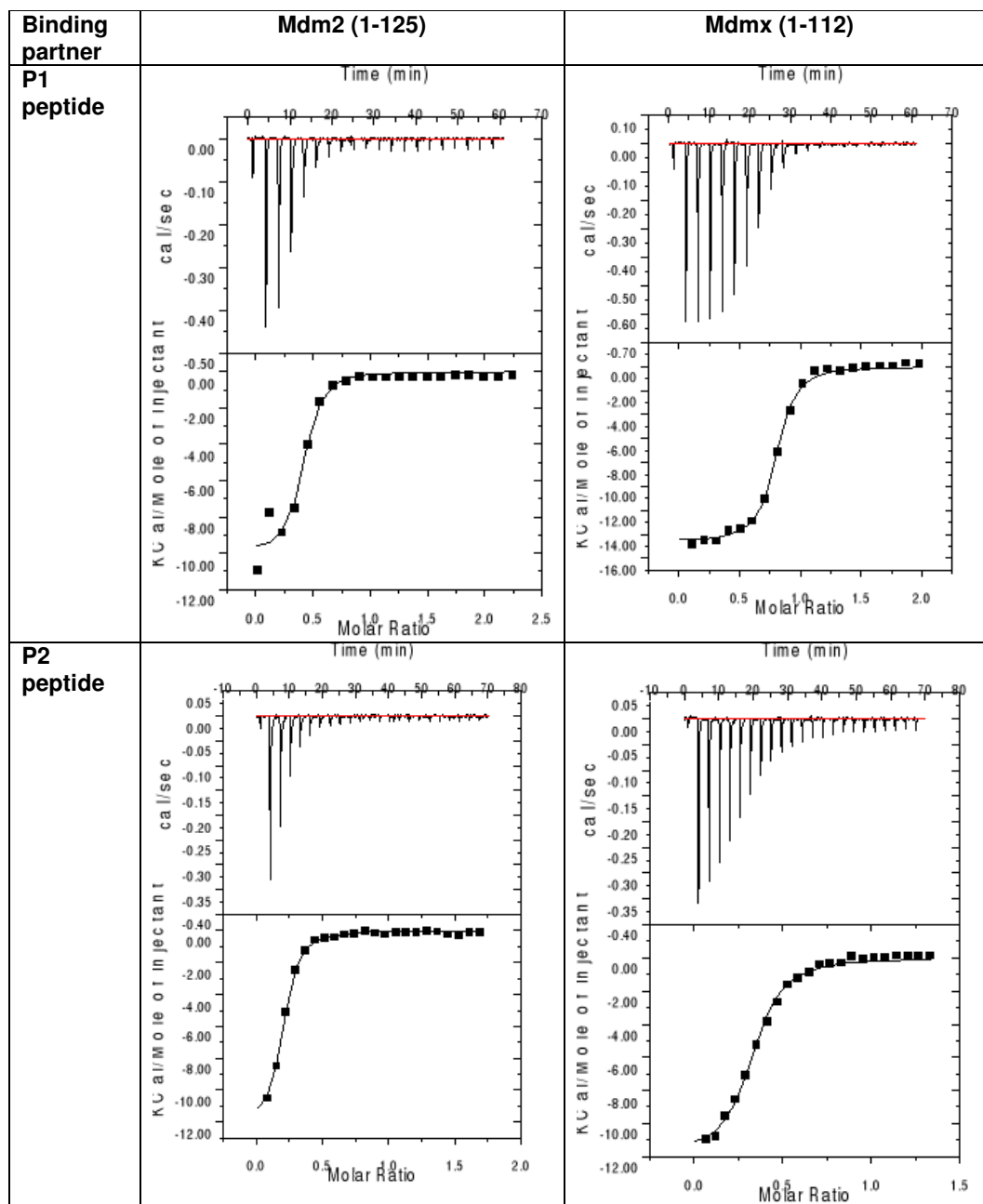


Figure 4.1.1. The Gly/Ser region of ^1H - ^{15}N HSQC spectra. Mdm2 (construct: 1-125) and Mdmx (construct: 1-112) were titrated with p53 peptides: wildtype peptide (P1), mutant peptides P2 (Grasberger et al., 2004) and P4 (reported by Hu et al., 2007), and Nutlin-3. The cross-peaks of on the reference spectrum are coloured in red, the 1:1 molar ratio of the peptide: protein complex is in green, the overtitrated (2:1) complex is presented in blue.

The K_D values were mostly calculated using ITC technique, and for fast exchange binding, observed for Nutli-3 and Mdmx, we used the NMR binary-titration data. The results are summarized in Zable 4.1.2.

Table 4.1.2. ITC titration curves for Mdm2 and Mdmx and different p53 peptides.



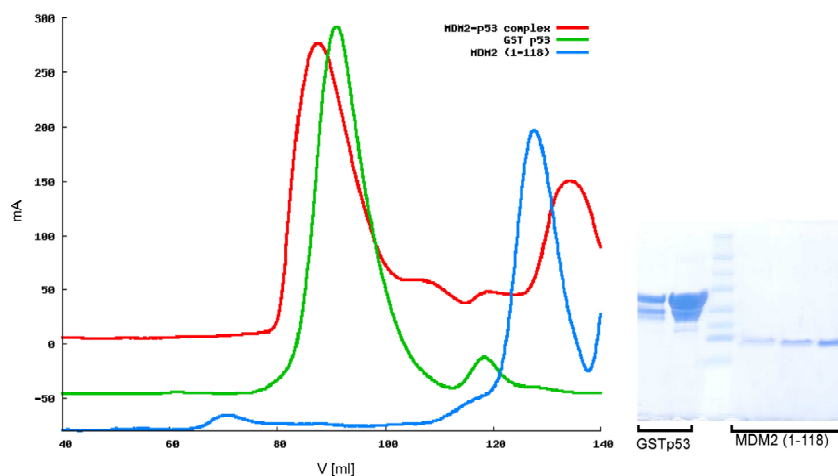
ITC experiments were performed at 25°C, upper part shows the raw data. The integrated heat changes corrected for the heat of dilution, as well as fitted curves based on a single model are shown in the lower panels.

The affinities of human Mdmx versus human Mdm2 for p53 are similar, in the range of 0.1 - 2 μM for the p53 protein fragments and the p53 peptide 1 (P1) (Figure 4.1.1, Table 4.1.1, Table 4.1.2) and are in agreement with results of Laurie et al. (2006) for the wildtype p53 peptide/Mdmx and close to the K_D obtained for the N-terminal domain of Mdm2/peptide 1 ($K_D=0.6 \mu\text{M}$, (Kussie et al., 1996)). The same experiments performed for a 9mer of the “optimized” p53 peptide (Böttger et al., 1996; Böttger et al., 1997; Böttger et al., 1997b), used for crystallization of Mdm2 by Grasberger et al. (2005) showed also strong binding in ITC and in NMR slow exchange between bound and unbound states of Mdmx (Figure 4.1.1, Table 4.1.1 and Table 4.1.2). Our K_D data is broadly in agreement with the results of Böttger et al. (1999), who tested a number of p53 peptides for binding to Mdmx and Mdm2.

4.1.4.1.2 The inhibitory activity of known Mdm2-p53 inhibitors on the Mdmx-p53 binding as studied by NMR techniques

For the AIDA method (Materials and Methods) the following complexes have been prepared as shown in Figure 4.1.2 A, B.

A



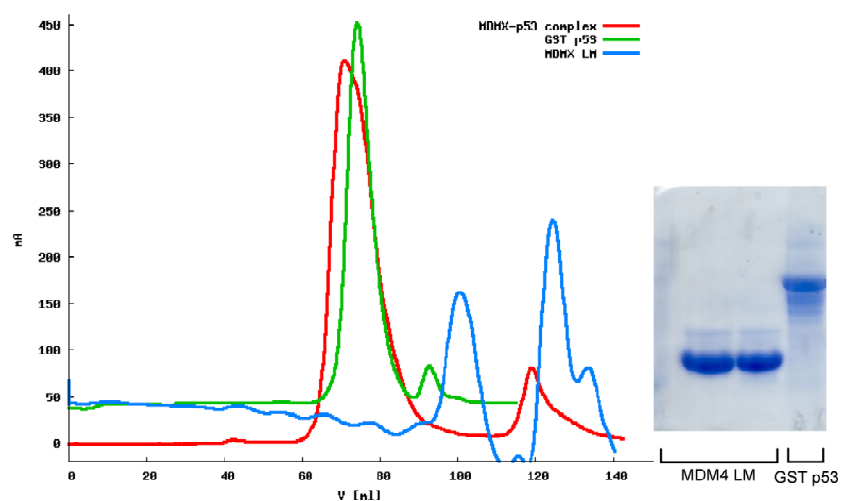
B

Figure 4.1.2. Monitoring the formation of the protein-protein complex by gel filtration chromatography. A: Complex formation between Mdm2 and GST-p53 and corresponding SDS-PAGE of purified proteins used for the experiment. B: the complex of Mdmx and p53 using purified proteins. Both: Mdm2 and Mdmx proteins were mixed with GST-p53 with molar ratio 3:1. The last 3 fractions from the final peak were not collected.

To check whether nutlin-3 is capable to compete with p53 for binding to Mdmx, we monitored the influence of nutlin-3 on NMR spectra of a complex of the N-terminal domain of Mdmx and GST-p53 (residues 1-73) and compared these results with the corresponding Mdm2/p53 spectra. Top traces in Figure 4.1.3 show 1D proton NMR spectra of the NH side chains of Trp residues of the free, Mdm2/Mdmx unbound p53.

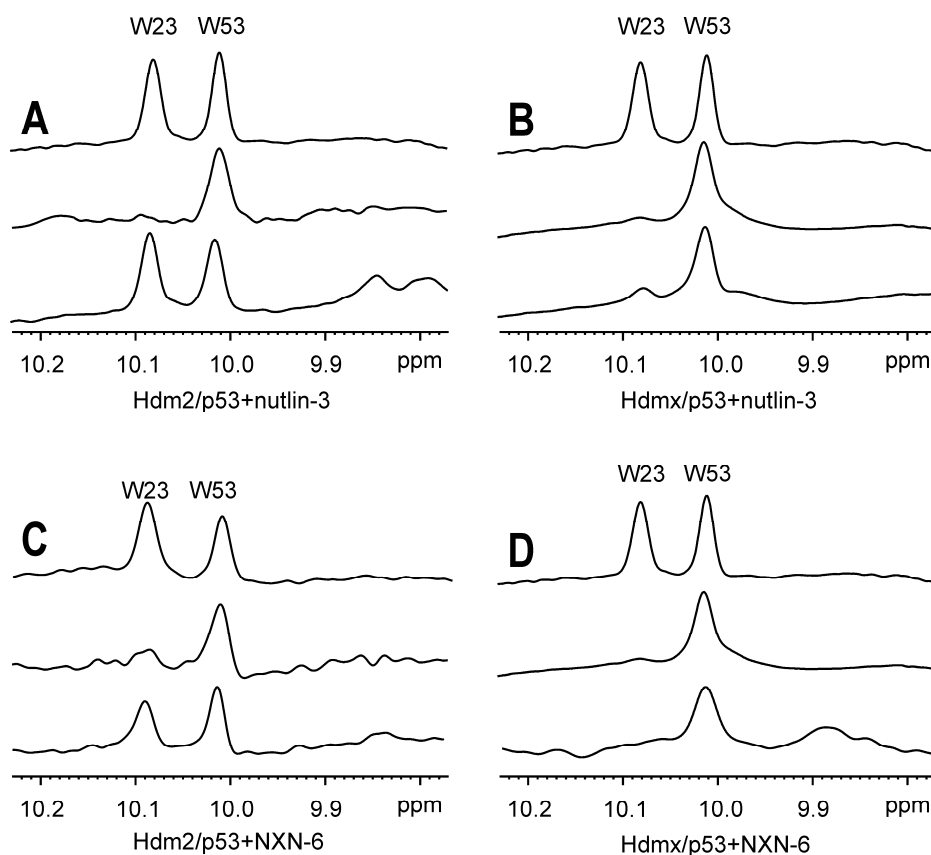


Figure 4.1.3. NMR competition binding experiments. Top spectra: 1D proton spectra of the side chains of tryptophans (W) of free p53 (residues 1-73), showing W23, W53. Middle spectra: on forming a complex with Mdm2 or Mdmx, the signal of the sidechain of W23 disappears. Bottom spectra: when we added nutlin-3, the signal of W23 recovered as a result of a complete (**A**, complex Mdm2/p53) or partial dissociation of the complexes. **B**: the recovery of the W23 signal is about 15% for the Mdmx/p53 complex. **C**: when we added NXN-6, the signal of W23 in spectrum recovered as a result of a 70% dissociation of the Mdm2/p53 complex. **D**: there is a 10% recovery of the W23 signal for the Mdmx/p53 complex. The molar ratio of the compound to protein was 6 : 1 in all four cases.

Because of a highly flexible nature of the N-terminal domain of p53, the side chains of Trp23 and Trp53 give rise to sharp lines (Schon et al., 2002; D'Silva et al., 2005; Dawsom et al., 2003; Schon et al., 2006). On forming a complex with Mdm2 or Mdmx, the signal of Trp23 disappears (Figure 4:1.3, middle traces). This is because Trp23, together with the p53 residues 17 to 26, comprise the primary binding site for Mdm2 and Mdmx. Upon binding, these residues participate in well-defined structures of large p53-Mdm2, p53-Mdmx complexes, whereas Trp53 is still not structured when p53 is bound to Mdm2 or Mdmx (D'Silva et al., 2005). The observed $1/T_2$ transverse relaxation rate of the bound Trp23 in the complexes increases thus significantly and broadening of NMR resonances results in the

disappearance of this signal in the spectra. Nutlin-3 was then added to the Mdm2/p53 and Mdmx/p53 complexes. For Mdm2, the Trp23 peak reappears on addition of nutlin-3, indicating that p53 has been released (Figure 4.1.3 A, lower trace). The NMR spectrum additionally showed that the freed p53 is folded, that the Mdm2/nutlin-3 complex is soluble, and that nutlin-3 did not induce precipitation of Mdm2. Nutlin-3 was however not able to efficiently disrupt the Mdmx-p53 binding, even at the molar ratio of the compound to protein 6 : 1 (Figure 4.1.3 B); even at the molar ratio 50 : 1 only 20% of p53 is released. Similar results were obtained for small molecular weight antagonists of Mdm2/p53 compounds called NXN-6 and NXN-7 (Figure 4.1.3 C, D and Figure 4.1.3*; Weber, International Patent, 2006).

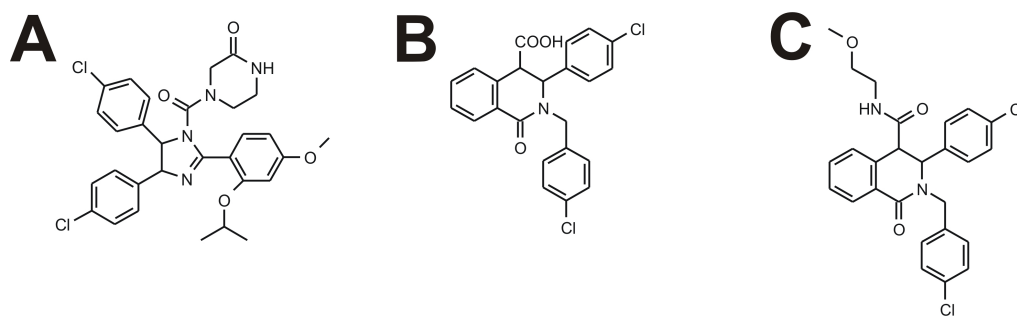


Figure 4.1.3*. Chemical formulas for: A: nutlin-3, B: NXN-6, and C: NXN-7.

Our NMR and ITC binding data clearly show that Mdm2/p53 antagonists are not effective in the inhibition of the Mdmx/p53 interaction. The retinoblastoma tumor cell killing effect of nutlin-3 observed by Laurie et al (2006) could only be explained by their use of extremely high, "rancid" concentrations of nutlin-3 to block the Mdmx-p53 interaction. Nutlin-3 might also exert its action indirectly, effecting Mdmx protein levels⁵ or by activating E2F1 (Ambrosini et al., 2007; Wunderlich et al., 2004).

The structures of Mdmx show that, compared to Mdm2, a part of the p53 binding cleft is blocked by sidechains of Met and Tyr of Mdmx. Since these differences are relevant for nutlin binding, we have mutated these residues in Mdmx to those with smaller sidechains (mutants Met53Val and Tyr99Thr) and determined their binding to nutlin and p53 (Figure 4.1.5 A, B and Table 4.1.4). The Figure 4.1.4 shows the complex formation between one of the mutants with GST-p53 protein via gel filtration. The complex was prepared as described in section 4.1.4.1.2. After purification the complex was identified by SDS-PAGE.

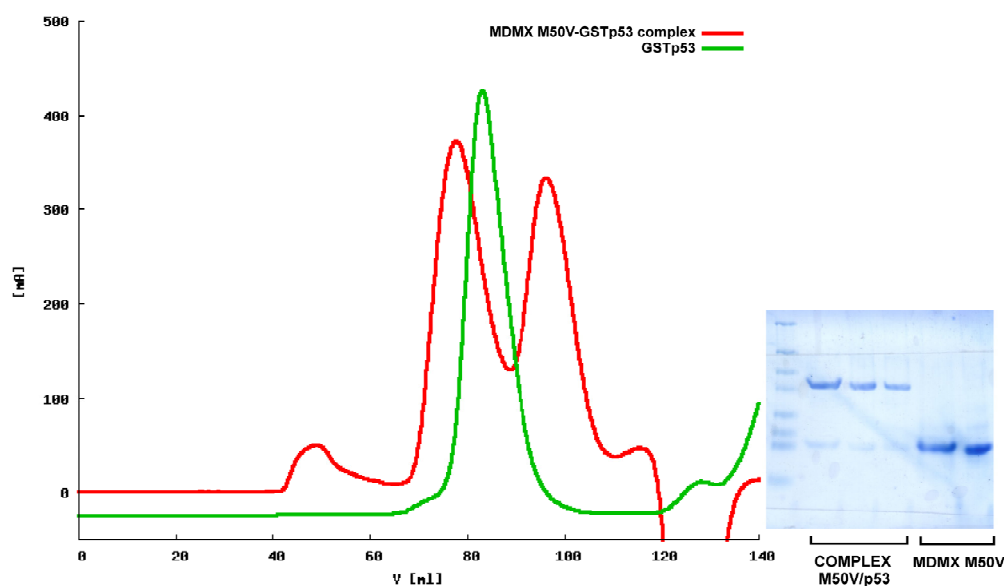


Figure 4.1.4. Monitoring of the complex formation via gel filtration chromatography (S200 Superdex pg column) between mutated Mdmx and GST-p53 construct.

Mutation of Met53Val had a pronounced effect on dissociation capability of nutlin-3: about 40% of p53 is released; for the Tyr99Thr mutant the difference to the wt-Mdmx was not significant. This trend is in agreement with the K_D data for the direct interactions of these Mdmx mutants with p53 or nutlin-3 (Table 4.1.4). For example, the binding of nutlin-3 to mutant Met53Val is 25-fold stronger (K_D , 6 μ M) than to the Tyr99Thr mutant (K_D , 150 μ M) and 5-fold stronger than to wt-Mdmx (K_D , 25 μ M).

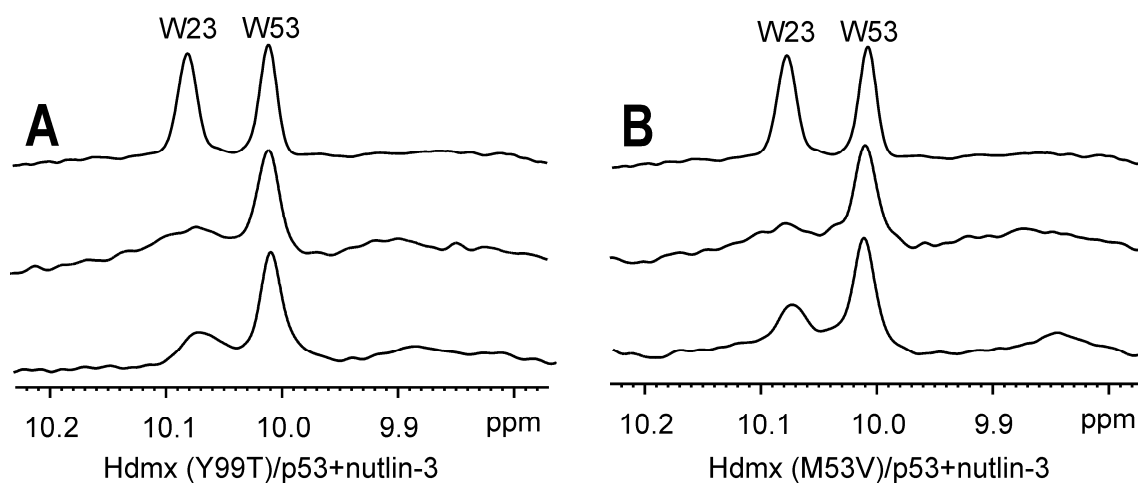
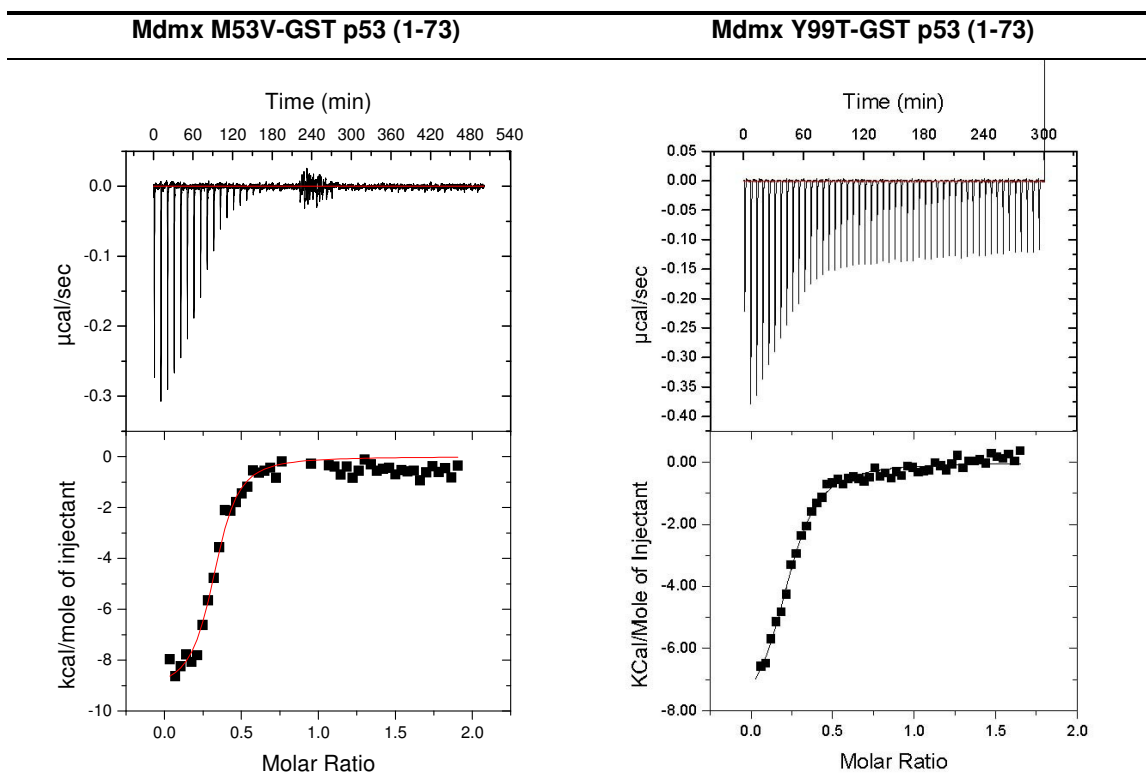


Figure 4.1.5. NMR competition binding experiments. Top spectra: 1D proton spectra of the side chains of tryptophans (W) of free p53 (residues 1-73), showing W23, W53. Middle spectra: on forming a complex with Mdm2 or Mdmx, the signal of the sidechain of W23 disappears. Bottom spectra: when we added nutlin-3, the signal of W23 recovered as a result of a dissociation of the complexes. A: the recovery of the W23 signal is about 20% for the human Mdmx(Y99T)/p53 complex. B: the recovery is around 40% for human Mdmx(M53V)/p53. The molar ratio of the compound to protein was 6:1 in both cases.

Table 4.1.3 ITC titration curves for Mdmx M50V and Y99T mutants with GSTp53 construct comprising residues 1-73.



The raw data (upper part) of ITC experiments were performed at 25°C. The integrated heat changes corrected for the heat of dilution as well as fitted curves based on a single model.

The structural observation of the Mdm2/Nutlin-3 complex and the role of Tyr 100 in forming the crucial interaction has been used for studying Mdmx-Nutlin3 binding. Our competition experiments for mutant Mdmx's beautifully support this conclusion (Figure 4.1.5): Mutation of the human Mdmx-corresponding Tyr99 to Thr in Mmdx does not help the Nutlin -3in its effectiveness to dissociate the Mdmx-p53 complex (Figure 4.1.3 B and Figure 4.1.5 A). However, mutation of Met53 to Val, e.g. mutating to a smaller sidechain amino acid with

however uncompromised hydrophobicity, increased 2-fold the dissociating power of nutlin-3 compared to that of human wt-Mdmx (Figure 4.1.3 B and Figure 4.1.5 B).

Table 4.1.4. ITC and NMR titration data for various peptide/small-molecule binding partners of Mdm2, Hdmx and zebrafish Mdmx.

Binding partner	Mdm2	Hdmx	Zebrafish	Human-mimic
			Mdmx	Mdmx
p53 (res. 1-312)	0.77 ± 0.07	0.48 ± 0.05	0.35 ± 0.03	0.45 ± 0.04
p53 (res. 1-312)	0.39 ± 0.20 ^a			
GST-p53 (res. 1-73)	0.50 ± 0.05	0.13 ± 0.03	0.40 ± 0.06	
GST-p53 (res. 1-73)		0.10 ± 0.01 ^b		
GST-p53 (res. 1-73)		0.29 ± 0.05 ^c		
GST-p53 (res. 1-73)		1.51 ± 0.3 ^d		
p53 peptide 1	0.60 ± 0.07	0.21 ± 0.05	2.20 ± 0.30	2.40 ± 0.40
p53 peptide 2	0.45 ± 0.05	6.9±0.18 ^b	0.83±0.20	-
p53 peptide Z	1.22 ± 0.2	3.6 ± 0.4	0.67 ± 0.05	1.33 ± 0.2
Nutlin-3	0.70 ± 0.08	25 ± 18	28 ± 20	25 ± 20
Nutlin-3		5 ± 2 ^c		
Nutlin-3		150 ± 20 ^d		
NXN-6	2 ± 1	600 ± 120	-	-
NXN-7	4 ± 2	-	-	-

K_D values in μ M were determined by NMR in case of fast exchange/weak binders. Peptides sequence Table X. Entries: - not measured, ^aMdm2 (residues 1-125), ^bHdmx (residues 1-112), ^cHdmx (M53V), ^dHdmx (Y99T).

4.1.4.1.3 Fluorescence polarization (FP) assay.

Strong binding properties of the P4 peptide suggested its use as a fluorescently labeled reporter molecule in the fluorescence polarization (FP) assay. This kind of the assay is commonly regarded as an industry standard in high throughput screening (Xinyj, 2003). The FP assay for the p53-Mdm2 interaction has been established by Zondlo at al. (2006) with the

use of their mutant peptide (different from P4) and by Shangary et al. (2008), who used the peptide which contains non-native amino acids. So far there were no FP assays published that would be suitable for Mdmx or the both proteins. It is worth mentioning that Zondlo et al. (2006) reported a single-site mutation Pro27Ser in the p53 sequence that improved the binding constant of p53-Mdm2 to 4.7 nM. Dastidar et al. (2008) proposed on the basis of molecular dynamics simulation that the increase of this affinity is due to a higher helicity of the mutant peptide. This is in excellent agreement with our structural data. Surprisingly, however, the Pro27Ser substituted peptide used by Zondlo et al. (2006) showed very weak binding to Mdmx in our assay (Figure 4.1.6).

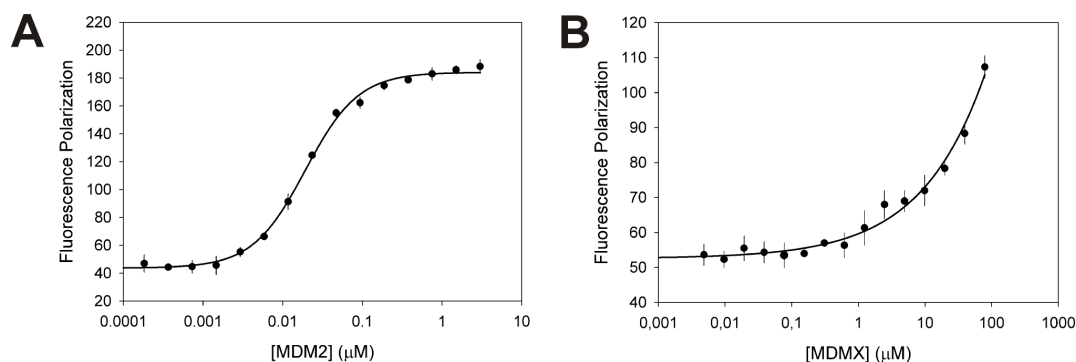


Figure 4.1.6. FP binding curves of Mdm2 and Mdmx titrated with the mutated peptide described by Zondlo et al. (2006). **A:** Mdm2, **B:** Mdmx.

The range of the resolvable inhibitor potency measured in FP is determined by the solubility of an inhibitor and the affinity constant of the reporter molecule (peptide) (Xinyj et al., 2003) To measure accurate values of the affinity constant of the fluorescent labeled P4 peptide, we have performed the binary titration of a constant amount of the peptide with the increasing amounts of Mdm2 and separately with Mdmx. Our experiments show that the binding of the labeled P4 peptide towards Mdm2 has $K_D = 5.6$ nM and for Mdmx the K_D of 40.8 nM. Values are for the 10% DMSO solutions, the maximal concentration of DMSO used in subsequent measurements with small molecule ligands (see below). The titration curves are shown in Figure 4.1.7 A and B for the conditions optimized for our assay. We have also tested the binding of the peptide used by Zondlo et al. (2006). The K_D value obtained for Mdm2 was 15 nM and is in agreement with published data of the same author (as mentioned above this peptide binds extremely weakly to Mdmx, with the K_D weaker than 100 μM (Figure 4.1.6).

Table 4.1.5. Influence of NaCl concentration on the equilibrium dissociation constants of Mdm2 and Mdmx towards FAM-P4 peptide

Salt concentration	Mdm2 towards FAM-P4, K_D (nM)	Mdmx towards FAM-P4, K_D (nM)
50 mM NaCl	5.4 ± 0.3	40.8 ± 2.0
100 mM NaCl	6.0 ± 0.3	33.9 ± 3.1
200 mM NaCl	5.1 ± 0.3	38.4 ± 2.5

To determine the optimal experimental buffer conditions, we have tested the dependency of the binding constant on salt concentration. Our experiment indicated that there is virtually no influence of salt on binding properties of the P4 peptide for Mdm2 and slight decrease of K_D with increasing salt concentration for Mdmx. (Figures 4.1.8 A and B; Table 4.1.5). The results are in agreement with our expectations from the structural data above, as the P4-Mdm2/x binding is mostly based on hydrophobic interactions. Temporal stability of the assay was analyzed to assess its suitability for long experiments. The measurements were repeated at 4, 8 and 24 h after mixing all components and showed absolute stability of the assay in a given time period (Figures 4.1.9 A and B, Table 4.1.6).

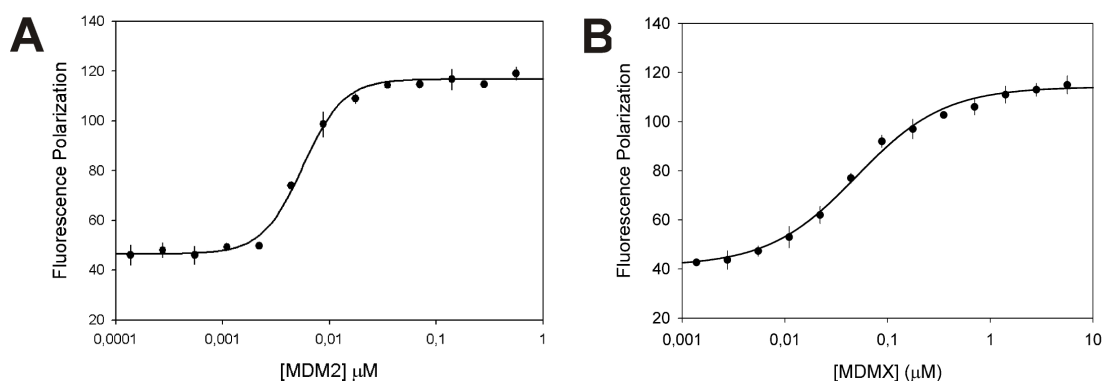


Figure 4.1.7. FP binding curves of Mdm2 and Mdmx titrated with the 5-carboxyfluorescein-LTFEHYWAQLTS (the FAM-P4 peptide). **A:** Mdm2, **B:** Mdmx.

Table 4.1.6. Influence of time on the equilibrium dissociation constants of Mdm2 and Mdmx towards FAM-P4 peptide

Time	Mdm2 towards FAM-P4, K_D (nM)	Mdmx towards FAM-P4, K_D (nM)
0 h	5.4 ± 0.3	35.8 ± 3.8
4 h	5.6 ± 0.3	36.9 ± 2.4
8 h	5.3 ± 0.3	36.9 ± 3.2
24 h	5.7 ± 0.3	38.5 ± 3.7

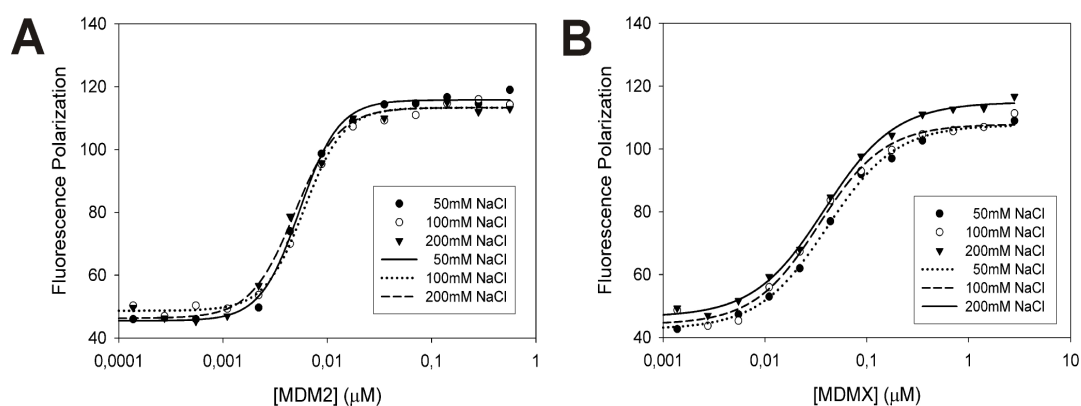


Figure 4.1.8. Effect of salt concentration on the interactions between FAM-P4 and Mdm2/x. A: Mdm2, B: Mdmx.

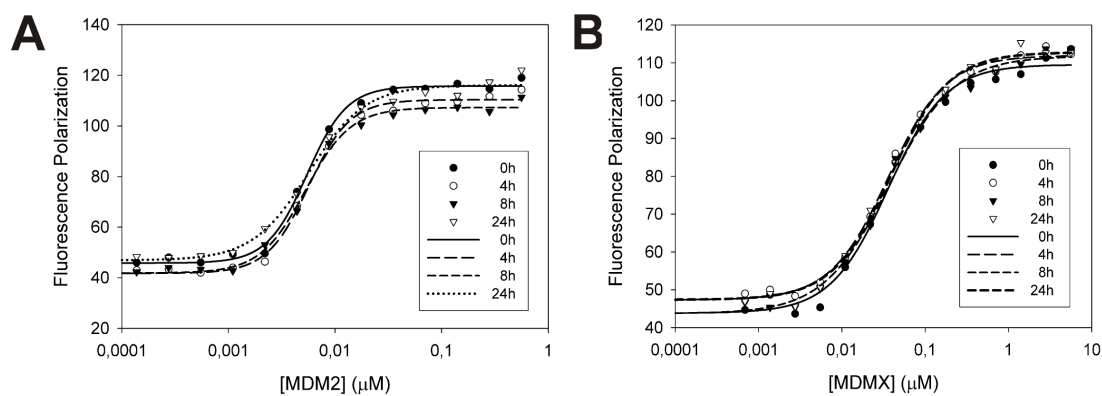


Figure 4.1.9. Temporal stability of the binding FP assay. A: Mdm2, B: Mdmx.

Since most of the compounds tested in drug discovery processes are dissolved in DMSO, we have analyzed the influence of DMSO on binding properties of P4 to Mdm2 and Mdmx (Figures 4.1.10 A and B; Table 4.1.7). Increasing the DMSO concentration has a weakening effect on the peptide binding, especially for Mdmx. For the FPs with small molecules, we have chosen to use 10% of DMSO; this concentration ensures good solubility of tested compounds and still high affinity of the reporter peptide. We further carried out ternary competition experiments (Fig 4.1.11 A and B), using the unlabeled P4 peptide, a peptide derived from the wild type p53 (designated as the P1 peptide), and a high potency small molecule Mdm2 inhibitor Mi219 (Shangary et al., 2008). The measured inhibition constant (K_i) values were in agreement with the published results and are summarized in Table 4.1.8.

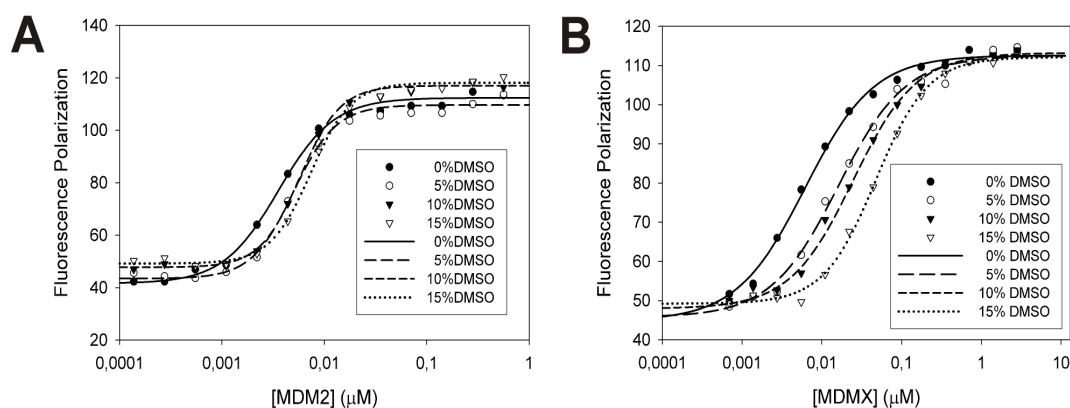


Figure 4.1.10. Effect of DMSO concentration on binding of the FAM-P4 peptide to Mdm2/x. **A:** Mdm2, **B:** Mdmx; a clear weakening effect on the peptide binding for Mdmx is visible upon an increase in the DMSO concentration.

Table 4.1.7. Influence of DMSO concentration on the equilibrium dissociation constants of Mdm2 and Mdmx towards FAM-P4 peptide.

DMSO concentration	Mdm2 towards FAM-P4, K_D (nM)	Mdmx towards FAM-P4, K_D (nM)
0 %	3.6 ± 0.3	6.1 ± 0.5
5 %	5.0 ± 0.3	15.9 ± 1.7
10%	5.8 ± 0.3	27.5 ± 2.6
15%	7.3 ± 0.4	47.4 ± 2.4

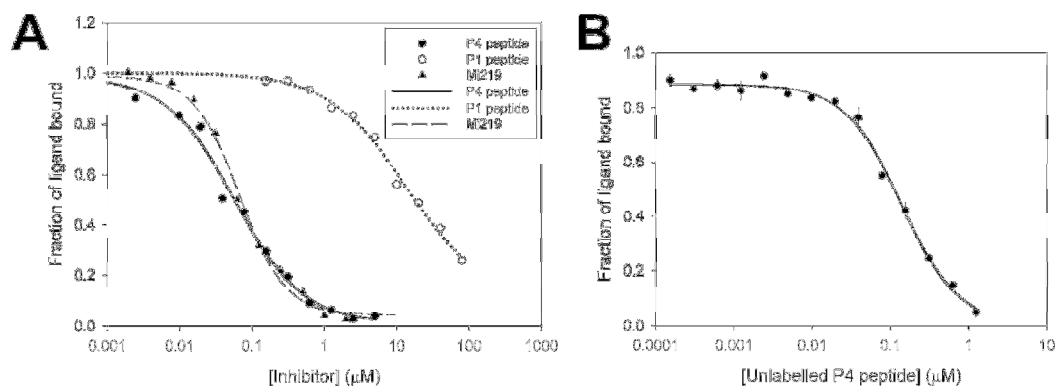


Figure 4.1.11. Competitive displacement of the FAM-P4 peptide by different inhibitors. **A:** Mdm2, **B:** Mdmx.

Table 4.1.8. Results of inhibitory activity against FAM-P4 peptide with Mdm2/Mdmx receptor protein

Inhibitor	Mdm2 towards FAM-P4,		Mdmx towards FAM-P4,	
	IC ₅₀ (nM)	K _i (nM)	IC ₅₀ (nM)	K _i (nM)
LTFEHYWAQLTS (P4)	61.9	4	112.3	7.59
SQETFSDLWKLLPEN (P1)	1600	890	--	--
Mi 219	120	15	--	--

Suitability of the FP assay for HTS experiments is determined by the value of the Z'-factor (Zhang et al., 1999) which corresponds to the variations in well-to-well fluorescence polarization signals between the free and bound fluorescently labelled peptide. We have analysed data from 96 wells containing either bound or released P4 peptide. The Z'-factor values for Mdm2 and Mdmx were 0.58 and 0.70, respectively, which indicates that the assay is suitable for high-throughput screening for both receptor proteins.

4.1.1.1 Conclusions

In conclusion, the structures of p53/Mdmx indicate that although Mdmx and Mdm2 utilize the same p53-binding motif and many of the same residues for binding to p53, their binding details differ significantly and thus the development of specific Mdmx inhibitors will have to take into account the unique structural properties of Mdmx. The data further suggests that there is high probability that a good binder to Mdmx would bind even stronger to Mdm2, whereas the reverse would not be true. Nutlin-3 shows this trend and we have tested several

other compounds for Mdm2, all showing the same characteristics. For example, recently developed inhibitors of the Hdm2-p53 interaction, compounds called NXN-6 and NXN-7, bind to Mdm2 with K_D 's of ca. 2-5 μ M, are moderately potent in dissociating the Mdm2-p53 complex, but marginally effective in antagonizing the Mdmx-p53 interaction (Figures 4.1.3 C, D). Thus, the development of new therapeutic antagonists for the Mdm2/Mdmx system should start with the screening of Mdmx first. It appears therefore that possible anti-cancer therapy based on releasing native p53 from Mdm2/Mdmx will require either mutual use of selective Mdmx and Mdm2 inhibitors or potent Mdmx antagonists, which, based on our data, are expected to also be effective in the interactions with Mdm2. Recently several high resolution crystal structures of the "relative" of Mdm2 and Mdmx in complex with p53 peptides have been published and allowed insight into the details of this interaction. Surprisingly all current highly potent binder e.g. Nutlin-3 and Mi-219 do not show appreciable affinity to Mdmx despite the very similar binding sites (Shangary et al., 2008). Thus there is no small molecular weight Mdmx antagonist up to date. However several groups discovered peptides showing similar and potent nm affinity to both Mdm2 and Mdmx (Kallen et al., 2009; Hu et al., 2007; Harker et al., 2009). The fluorescence assay described in our study is suitable for HTS to discover antagonists for both proteins in the same assay. Thus, new and highly improved tools are provided for the discovery of new Mdm2, Mdmx and dual action Mdm2/Mdmx antagonists.

4.2 Multiple Small Molecular Weight Scaffolds Inhibiting the Protein-Protein Interaction p53-Mdm2

Protein-protein interactions (PPIs) recently have been recognized as a major class of drug targets. Despite the importance of protein protein interactions (PPIs) for understanding basic questions of biology and intervening in disease etiology and progression, the discovery of small molecular weight antagonists remains one of the most challenging areas in drug discovery. For certain target classes, however, HTS often yields very low number of hits (Spencer 1998). For example, protein-protein interactions (PPIs) are notoriously difficult to hit with small drug-like molecules (Wells and McClendon, 2007). Antagonizing a PPI by a chemical agent constitutes a temporal reversible process and could thus have therapeutic advantages over covalent irreversible inhibition processes. The structure, topology and flexibility of protein-protein interfaces are very divers and consequently there is currently no general approach to discover antagonists of a wide range of interactions (Nooren and Thornton, 2003). Some PPIs comprise an extended surface and lack structured and deep binding sites. In other interactions only a spatially confined small number of amino acid side

chains play an important role for binding energetic and these interactions have been termed “hot spots” and were first described in the complex between human-growth hormone and the human-growth hormone-binding protein (Clackson and Wells, 1995).

In this part of my thesis I would like to describe a complementary process that led to the parallel discovery of several compounds belonging to 9 different scaffold classes amenable by efficient chemistry in just one step, antagonizing the PPI between p53 and Mdm2. The p53/Mdm2 axis has been recognized as an important anticancer target and several compounds are in preclinical development or entered recently early clinical trials (Dömling, 2008). The best-documented drug-like compounds developed are cis-imidazoline derivatives called nutlins (Vassilev et al., 2004). For example, Nutlin-3 is a selective and potent inhibitor of the p53-Mdm2 interaction, which induces apoptosis in p53 wildtype cells and shows in vivo efficacy in mice xenograft models. In the following I am going to describe a process for the parallel discovery of multiple scaffolds to antagonize the PPI p53/Mdm2.

4.2.1 Results and discussion

Protein-protein interactions are often mediated by only a few key amino acid side chains and the term “hot spot” has been introduced for such locally constrained areas on the surface of interaction proteins (Clackson and Wells, 1995; Bogan and Thorn, 1998). In a first approximation the burriedness of a specific amino acid side chain of the donor protein in the acceptor protein is indicative for its energetically importance. We reasoned that this “hot spot” amino acid side chain might serve as reasonable starting point for the design of (ant)agonists of the PPI. Thus, we introduce this particular amino acid side chain as an initial “anchor” into virtual libraries of small molecular weight scaffolds. Anchor side chain-containing incorporating virtual compounds are selected for synthesis and screening based on docking into the protein-protein interaction interface. The starting pose for the docking procedure is forced in such a way that an overlap between the anchor and the template amino acid side chain is ensured. In order to rapidly test our antagonist ideas, we chose an efficient, fast, but versatile chemistry, the so-called multicomponent reaction chemistry (MCR) (Figure 4.2.1) (Dömling, 2006). MCR allows the assembly of many different complex scaffolds in a one-step one-pot manner thus saving time and resources. The NMR based K_D data for more than 200 of the initial compounds are shown in Chapter 7.2.

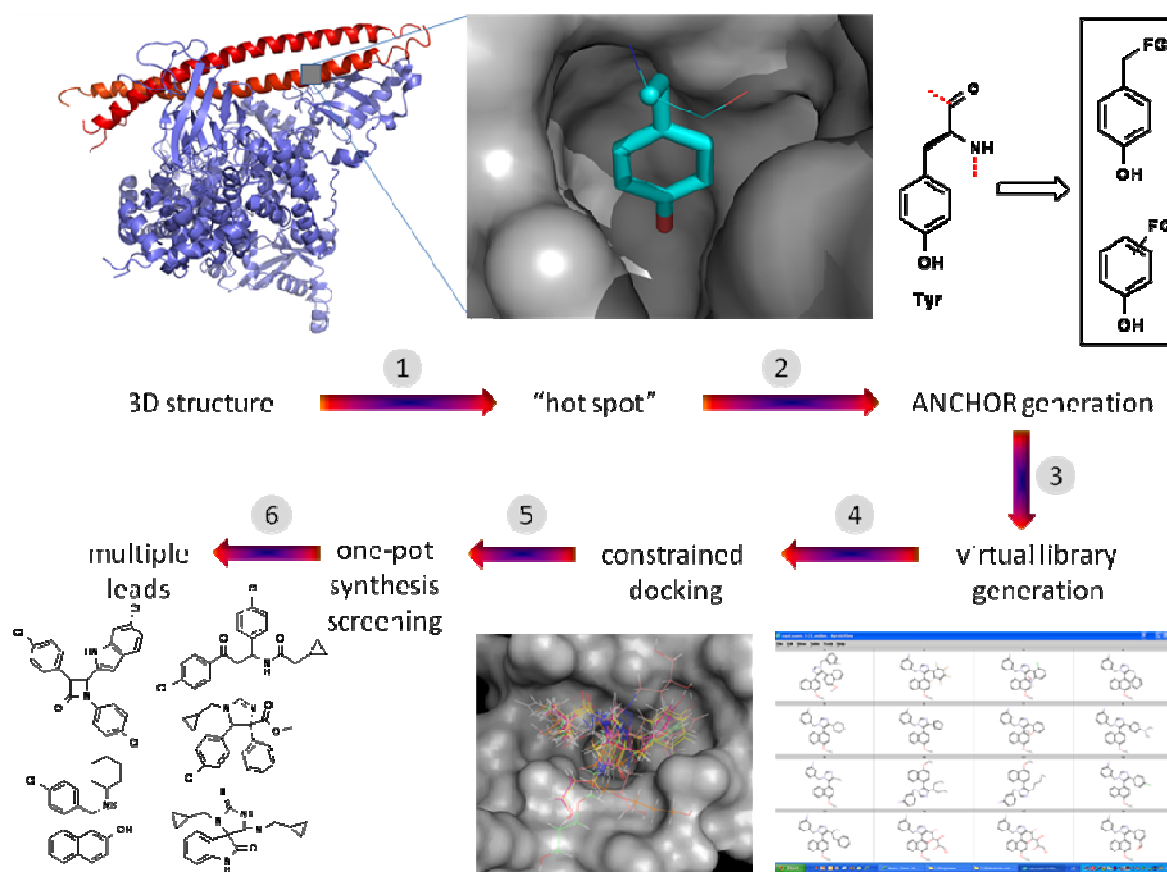


Figure 4.2.1. Graphical representation of the workflow of the discovery procedure for the rapid generation of small molecular weight (ant)agonists of protein-protein interactions. The process relies on high resolution structural target data (1), the presence and identification of a "hot spot" (2), a fragmentation/anchor generation step (3), virtual chemistry employing the anchor and based on multicomponent reactions (4), constrained docking forcing the anchor fragment into the binding site (5), synthesis and screening (6). (FG = functional group)

4.2.1.1 Anchor generation, docking and MCR chemistry

The PPI interface of p53/Mdm2 is characterized in molecular detail by X-ray structure analysis. It relies on the steric complementarity between the Mdm2 cleft and the hydrophobic face of the p53 α -helix and, in particular, on a triad of p53 amino acids Phe19, Trp23, and Leu26, which insert deep into the Mdm2 cleft (Figure 4.2.2) (Kussie et al., 1996).

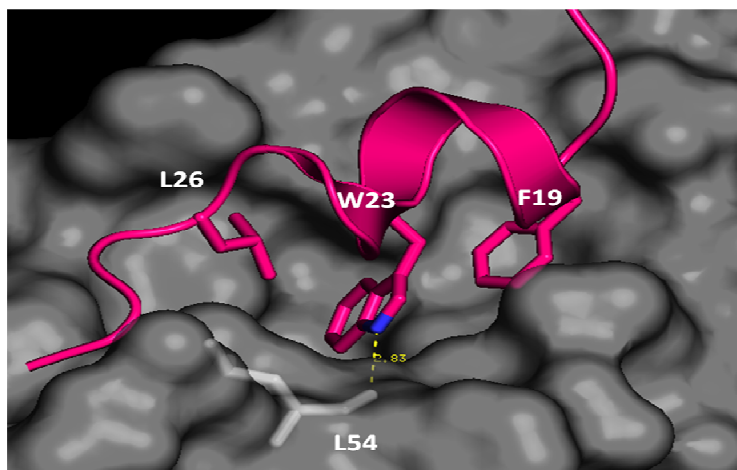


Figure 4.2.2. Architecture of the “hot spot” of the p53/Mdm2 interface (PDB Identifier: 1YCR). The three amino acid side chains of the interacting p53 α -helix Phe19, Trp23 and Leu26 make strong van der Waals contacts. Trp23 in addition forms a hydrogen bond to Mdm2 Leu54 backbone amide. The Mdm2 surface is shown in grey. The hot spot amino acid side chains of p53 are shown as pink sticks and the p53 α -helix as cartoon.

In agreement with these structural features, site-directed mutagenesis studies also showed the importance of the key residues Phe19, Trp23, and Leu26 (Lin et al., 1994). Thus the p53 amino acid triad comprise the “hot spot” of the p53/Mdm2 interaction. Noteworthy is the cross section dimension of the p53 binding site in Mdm2 of 18 Å (from C α -Tyr67 to C α -Tyr100), which is the size of small organic molecules thus indicating the possibility of small molecule interference. We chose the indole side chain of Trp23 as the “anchor” residue for our approach for three reasons: it is the central amino acid of the triad, it is deeply buried in Mdm2 and it features, in addition to strong van der Waals contacts, a hydrogen bond to the Leu54 backbone carbonyl of Mdm2 (Figure 4.2.2). In fact, calculation of the solvent-accessible surface areas of all amino acid in the p53/Mdm2 ranks Trp23>Phe19>Leu26 the highest (Meireles et al., 2004). Next, from the database of several hundred MCR scaffolds, 40 MCR scaffolds was selected to create virtual compound libraries. By design each of the compounds of the different scaffolds incorporates the anchor. As anchors we used indole and 4-chloro phenyl derivatives endowed with the corresponding functional groups to act as starting materials for the MCRs (Figure 4.2.3); e.g. we used unsubstituted indole and oxindole to perform a Friedel-Crafts type alkylation and an Ugi-four component condensation, respectively (Table 4.2.1). The virtual library of compounds comprising all stereochemically possible isomers was generated using the REACTOR software (Pirok et al., 2006). Different

aliphatic and aromatic starting materials to represent different shape and electrostatic features were chosen for the MCR starting material classes.

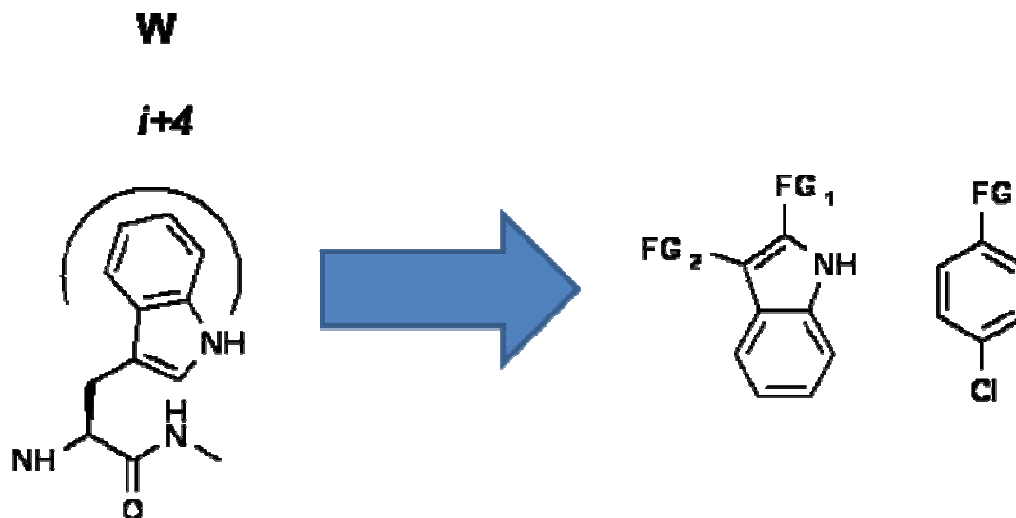


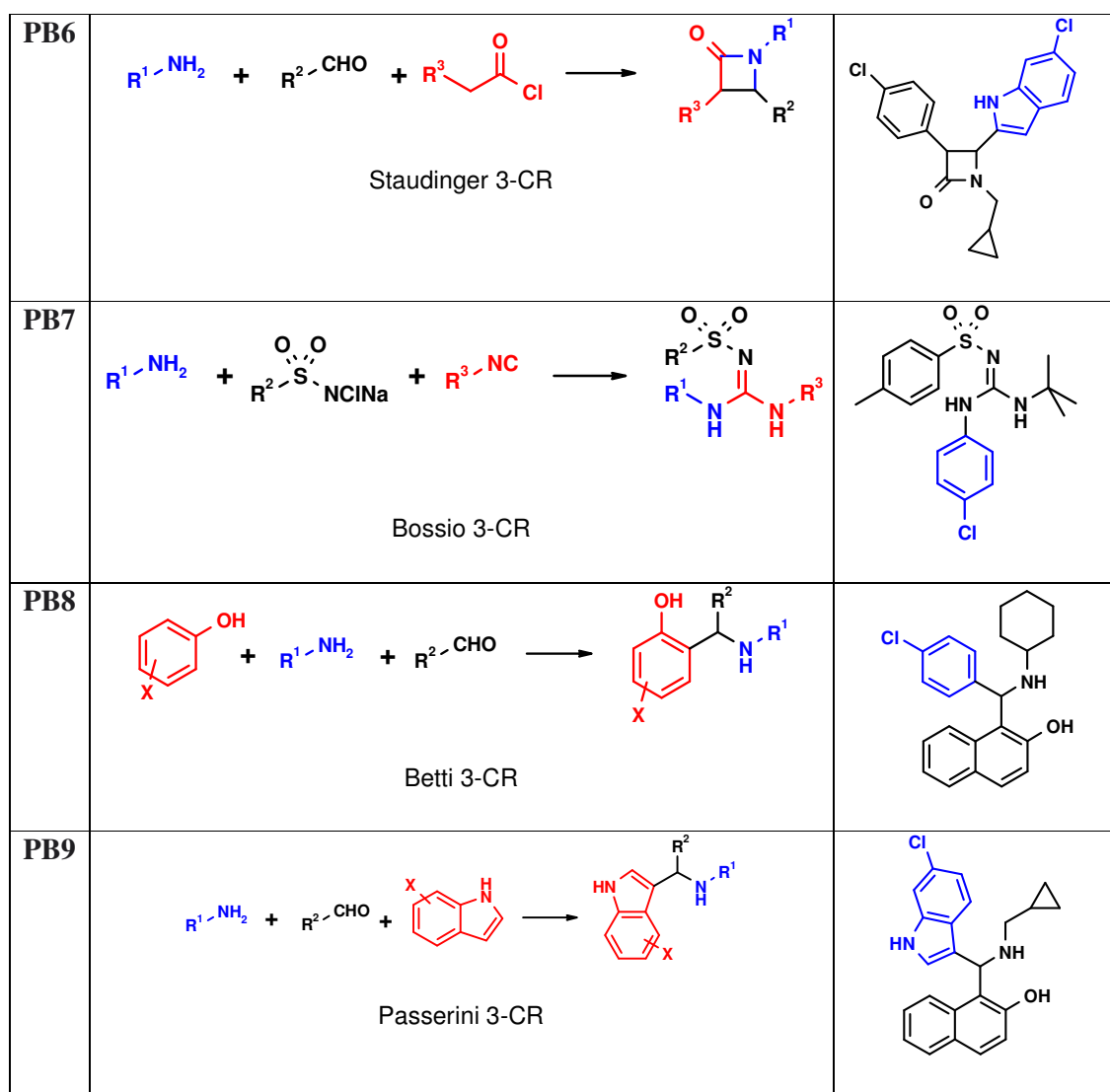
Figure 4.2.3. Schematic representation of the anchor-generation from the p53 hot spot template amino acid W23. The backbone of W23 is cut and the resulting indole or the bioisosteric 4-chlorophenyl moiety is attached to different functional groups (FG), e.g. -COOH, -NH₂, -CHO, -CN according to the requirements of the MCR chemistry.

The virtual compound libraries incorporating the anchor side chain were docked into the rigid p53 binding site in the Mdm2 receptor (PDB identifier 1YCR) using the modelling/docking software package Moloc (Gerber and Müller, 1995; Gerber, 1998). Assuming that the anchor residue predefines the binding site of the molecules and in order to avoid non productive docking poses, we forced the anchor part (indole or 4-chlorophenyl) of the compounds to overlap with the respective Trp23 anchor as a starting point for energy minimisation. From the highest ranking compounds, which addressed all three binding sites of p53 Phe19, Trp23, and Leu26, we chose several compounds for synthesis and screening based on different features. First, the compounds were chosen to belong to different types of scaffolds to ensure variation in backbones. Second, we chose reactions where the corresponding starting materials are commercially available or synthetically easily to access. As a third criterion, we preferentially chose MCRs for which we had previous synthetic experience in the laboratory. Products were synthesized according to two different Ugi reaction variations (PB3, PB5) (Ugi, 1971; Kalinski et al., 2006), van Leusen reaction (PB1) (VanLeusen, 2001), Orru reaction. (PB2, PB10) (Bon et al., 2003), Passerini reaction (PB9) (Passerini and

bonciani, 1933), Betti reaction (PB8, PB12) (Betti, 1900), Staudinger (PB6, PB13) (Staudinger, 1907), amidinosulfone amide (PB7) (Bossio et al., 1995), and other MCRs (PB4, PB11). Of 12 different MCR scaffolds predicted to be p53/Mdm2 antagonists 9 were subsequently shown to be active and are shown in Table 4.2.1 (see also Appendix 7.1 for the synthesis).

Table 4.2.1. MCRs used to produce representative p53/Mdm2 antagonists. The different classes of starting materials are color coded and represent the variation of the MCR. The anchor moiety in column three is marked in blue.

no	reaction scheme	representative antagonist
PB1	$R^1-NH_2 + R^2-CHO + \text{Tos-}CH(R^3)-NC \rightarrow$ <p>Van Leusen 3-CR</p>	
PB2	$R^1-NH_2 + R^2-CHO + \text{MeOOC-}CH(R^3)-NC \rightarrow$ <p>Orru 3-CR</p>	
PB3	$R^1-NH_2 + R^2-C(=O)-R^3 + HSCN + R^4-NC \rightarrow$ <p>Ugi 4-CR ()</p>	
PB4	$R^1-C(=O)-R^2 + R^3-CHO + R^4-CN \rightarrow$ <p>α-amido-alkylation 3-CR</p>	
PB5	$R^1-NH_2 + R^2-CHO + HN_3 + \text{C}_6\text{H}_4(\text{F})(\text{NC}) \rightarrow$ <p>Ugi 4-CR</p>	



PB = Pittsburgh.

Representative docking poses of the predicted p53/Mdm2 antagonist compounds are shown in Figure 4.2.4. Several compounds representing each of the scaffolds were efficiently synthesized using one-pot MCR chemistry (Appendix, 7.1). Next, these compounds were screened for their ability to bind to Mdm2 and to antagonize the protein complex p53/Mdm2.

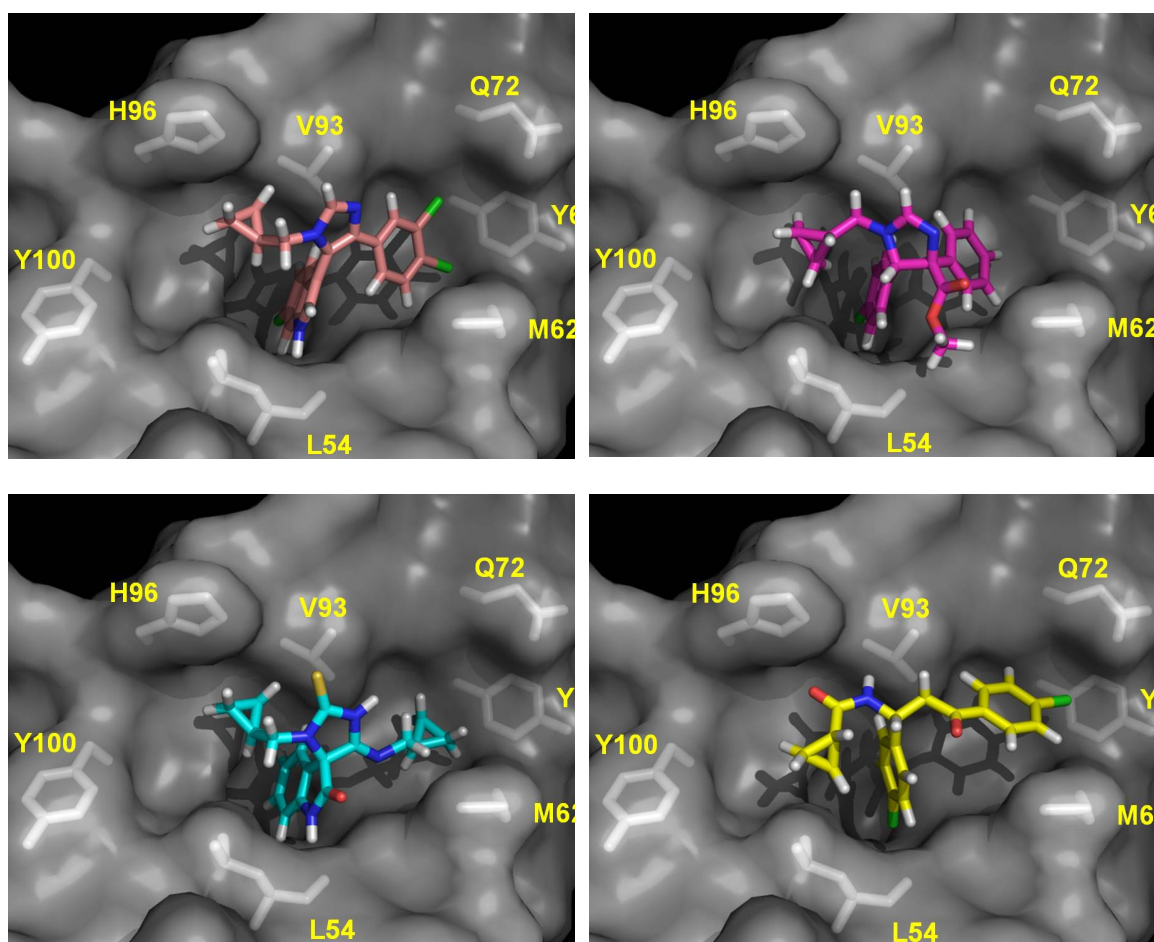
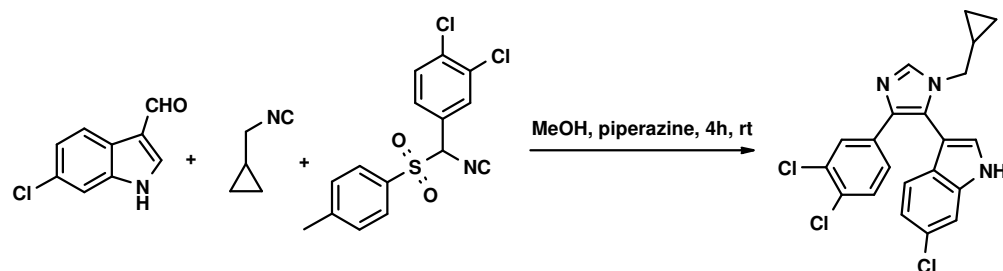


Figure 4.2.4. Docking poses of four different p53/Mdm2 antagonists based on four different scaffolds as obtained through constrained docking into PDB 1YCR. Clockwise: 5-indolo-imidazole PB1, imidazoline PB2, thiohydantoin-imide PB3, and α -ketoamide PB4. Several key amino acids of the receptor Mdm2 are shown as grey sticks and numbered. The docking poses are in accordance with the observed Mdm2 HSQC-NMR shifts obtained from the compound titrations. All poses show the receptor in the same orientation similar to the Figure 4.2.2.

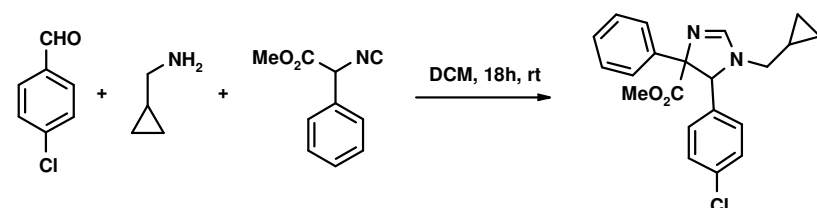
4.2.1.2 Exemplary reactions of the antagonist synthesis

The complete chemical synthesis and characterization of the compounds is summarized in Chapter 7.1. Below I show the compounds that are representative for the different scaffolds discovered. These were then efficiently synthesized using one-pot MCR chemistry.

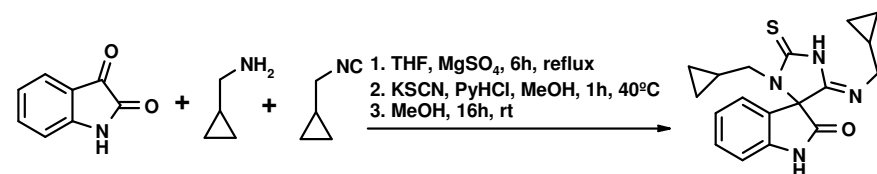
PB1: 6-Chloro-3-[3-cyclopropylmethyl-5-(3,4-dichloro-phenyl)-3H-imidazol-4-yl]-1H-indole



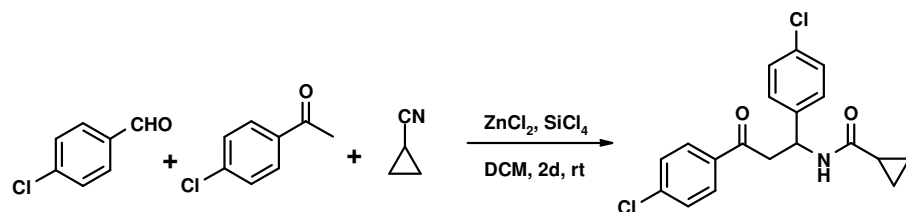
PB2: 5-(4-Chloro-phenyl)-1-cyclopropylmethyl-4-phenyl-4,5-dihydro-1H-imidazole-4-carboxylic acid methyl ester



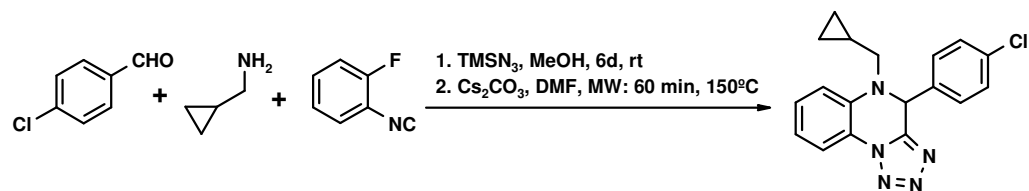
PB3: (Z)-3-(cyclopropylmethyl)-5-(cyclopropylmethylimino)-2-thioxospiro[imidazolidine-4,3'-indolin]-2'-one



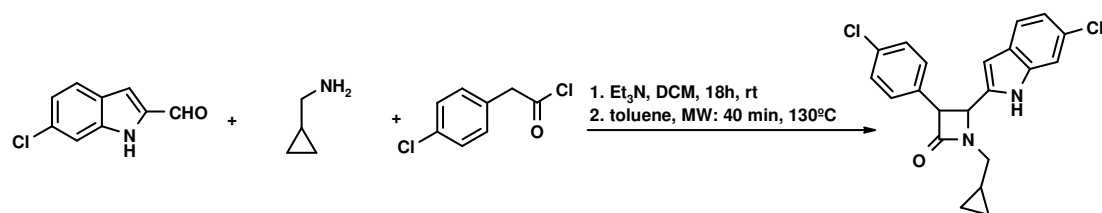
PB4: Cyclopropanecarboxylic acid [1,3-bis-(4-chloro-phenyl)-3-oxo-propyl]-amide



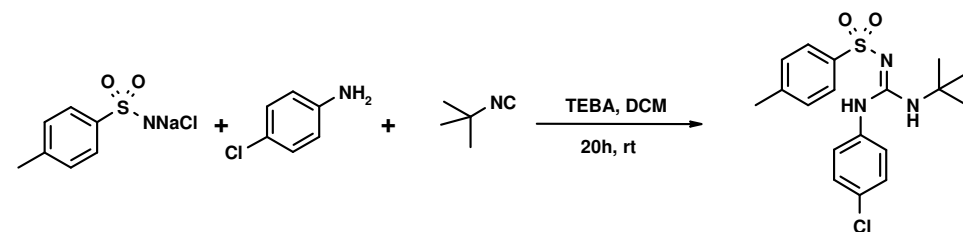
PB5: 4-(4-Chloro-phenyl)-5-cyclopropylmethyl-4,5-dihydro-1,2,3,5,9b-pentaazacyclopenta[a]-naphthalene



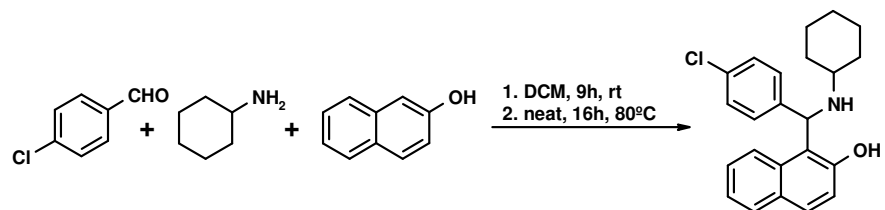
PB6: 4-(6-Chloro-1H-indol-2-yl)-3-(4-chloro-phenyl)-1-cyclopropylmethyl-azetidin-2-one



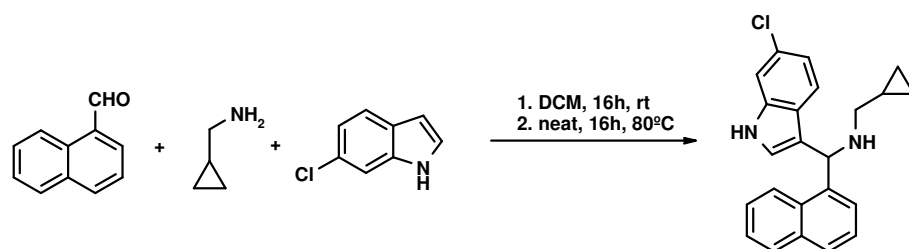
PB7: N-[1-tert-Butylamino-1-(4-chloro-phenylamino)-meth-(Z)-ylidene]-4-methyl-benzene-sulfon amide



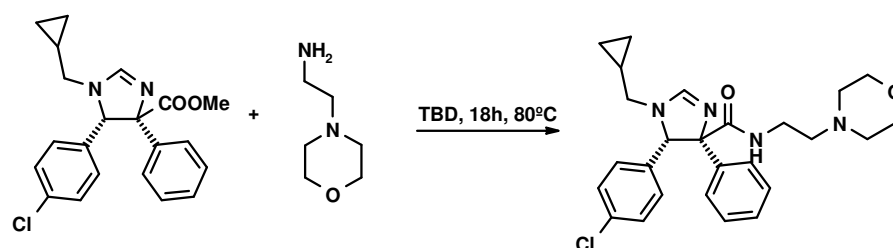
PB8: 1-((4-chlorophenyl)(cyclohexylamino)methyl)naphthalen-2-ol



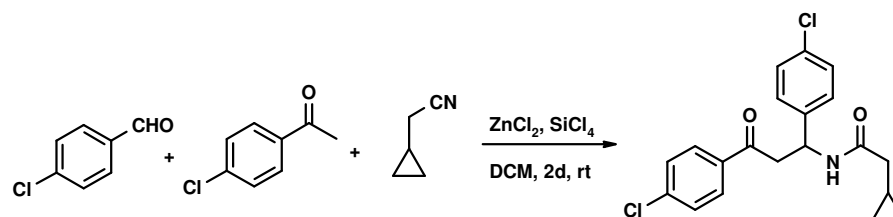
PB9: [(6-Chloro-1H-indol-3-yl)-naphthalen-1-yl-methyl]-cyclopropylmethyl-amine



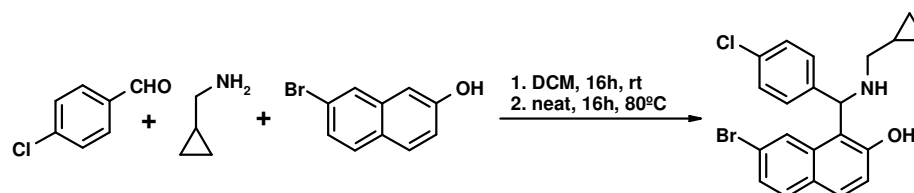
PB10: 5-(4-Chloro-phenyl)-1-cyclopropylmethyl-4-phenyl-4,5-dihydro-1H-imidazole-4-carboxylic acid (2-morpholin-4-yl-ethyl)-amide



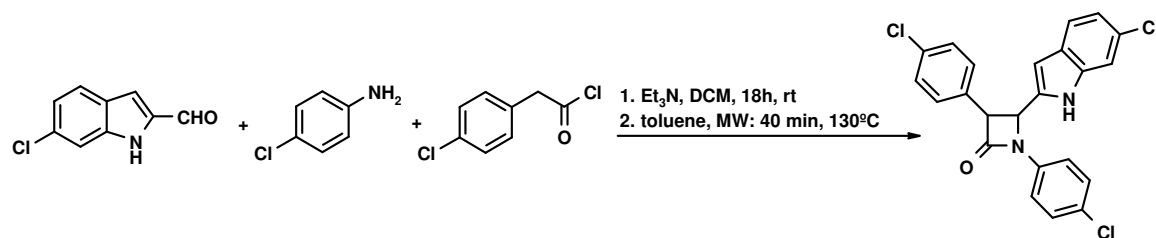
PB11: N-[1,3-Bis-(4-chloro-phenyl)-3-oxo-propyl]-2-cyclopropyl-acetamide



PB12: 7-Bromo-1-[(4-chloro-phenyl)-(cyclopropylmethyl-amino)-methyl]-naphthalen-2-ol



PB13: 4-(6-Chloro-1H-indol-2-yl)-1,3-bis-(4-chloro-phenyl)-azetidin-2-one



4.2.1.3 High content NMR-based affinity screening

All NMR spectra were acquired as described in Materials and Methods. The NMR ligand binding experiments carried out in an analogous way to those previously described (Popowicz et al., 2007; D'Silva et al., 2005). As an additional assay, the Trp101 Mdm2 mutant was used for K_D estimation. The NMR sample was prepared in a standard way. The protein concentration was measured and fixed with accordance to the expectable range of the K_D value.

The inhibitor was added stepwise to the protein solution and a 1D ^1H proton spectrum was recorded for each step. Figure 4.2.5 shows the plot of the chemical shift of the tryptophan 101 (101W) versus the inhibitor concentration for compound PB10. The calculated K_D for PB 10 is around $1\mu\text{M}$ (see also Table 4.2.2)

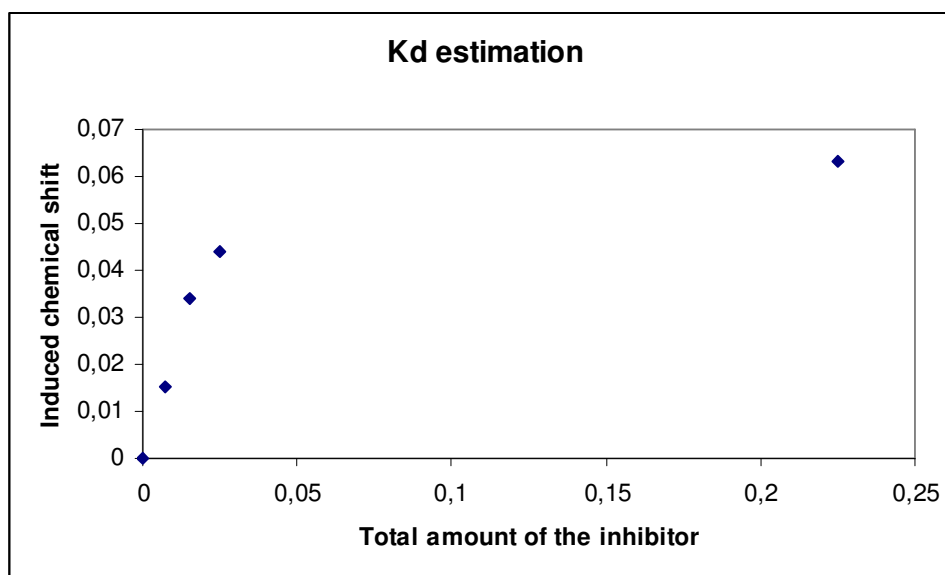
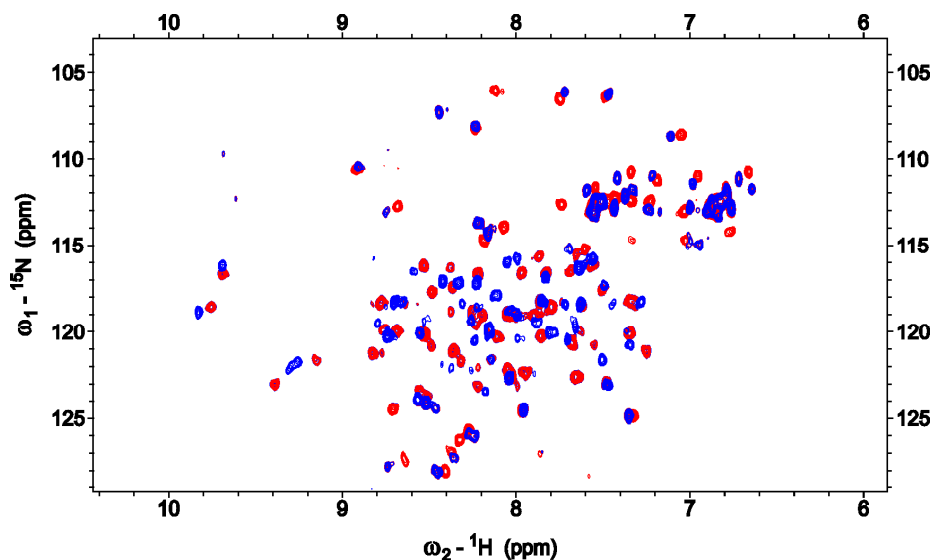


Figure 4.2.5. K_D estimation curve for PB10 by stepwise titration of the Mdm2 T101W at low protein concentration ($0.03\mu\text{M}$). The K_D was calculated using following the equation: $K_D = \frac{[P] \cdot [I]}{[PI]}$, P- protein, I – inhibitor. $K_D = \text{IC}_{50} - [P]/2$.

To test the compounds ability to antagonize the p53/Mdm2 complex, we have chosen NMR spectroscopy as it can provide a wealth of information, which otherwise cannot be assessed in high-throughput assays. Importantly, the compounds affinity to Mdm2 and their ability to dissociate preformed p53/Mdm2 protein complex can be obtained. Other important questions about the compound properties can also be answered: Is the compound sufficiently water soluble? Does the compound bind to Mdm2 or p53? Does the compound cause precipitation of any of the proteins? Does the compound lead to major conformational changes in the binding protein? Where on the protein surface does the compound bind? This information is instrumental in order to optimize a compound series not only for potency and selectivity but also for e.g. water solubility and protein binding. To find an inhibitor for the Mdm2 p53 interaction, the different compounds were tested for binding to Mdm2 by performing a series of NMR titrations with isotopically enriched ^{15}N -Mdm2 (Shuker et al., 1996; Stoll et al., 2001, Pellecchia et al., 2008). Strong binding of a compound to its target is indicated by appearance of splitting of the peaks in a HSQC spectrum, whereas a shift of peaks indicated weaker binding. Figure 4.2.6 shows ^{15}N -HSQC spectra of Mdm2 titrated with two diastereomers of PB2.

A

B

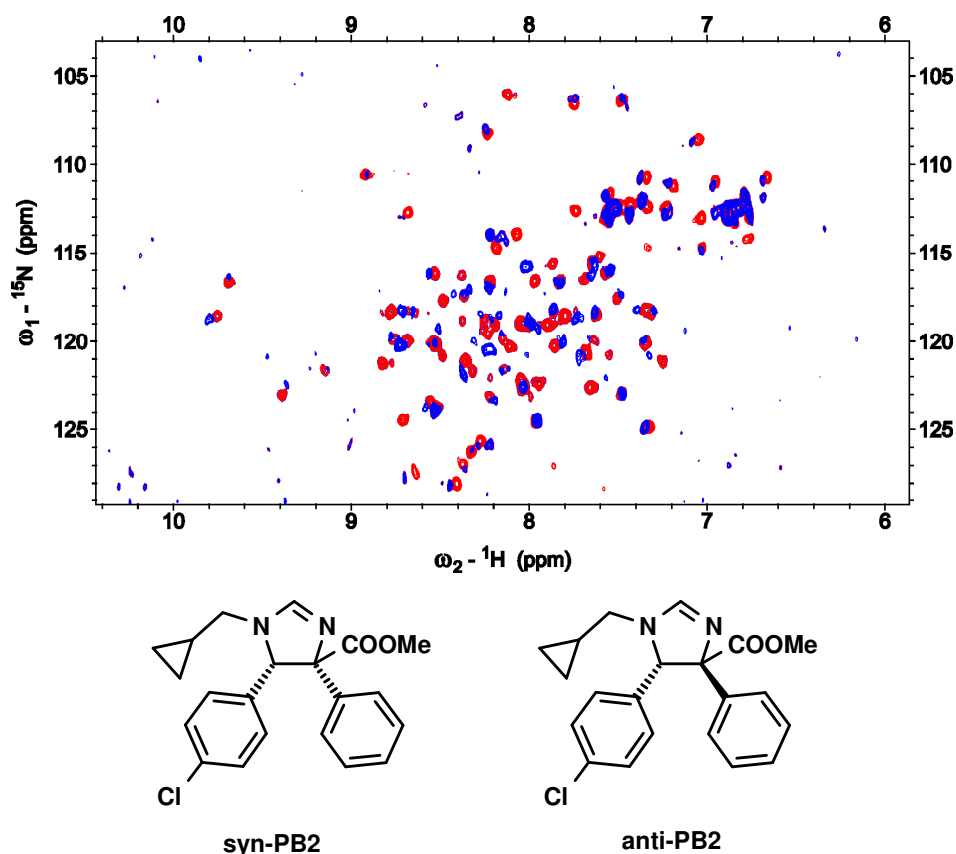


Figure 4.2.6. The HSQC perturbation spectra of Mdm2. A: The spectrum of free Mdm2 (red), and Mdm2 plus syn-PB2 (blue): final ratio Mdm2: syn-PB2 1:5; B: anti-PB2, the spectrum of free Mdm2 (red), and Mdm2 plus anti-PB2 (blue): final ratio Mdm2: anti-PB2 1:2, C: The chemical formula of syn-PB2 and anti-PB2.

Almost all residues of Mdm2 are affected upon binding to syn-PB2. The spectra show a shift of peaks rather than a splitting, which indicates that syn-PB2 binds to Mdm2 in fast exchange (Wüthrich, 1996; D'Silva et al., 2005). The pattern of interaction of anti-PB2 to Mdm2 is similar to that of syn-PB2, however, anti-PB2 causes precipitation of the protein (seen in Figure 4.2.6 B) already at lower ligand concentrations compared to syn-PB2 (5: 1 compound to protein for syn-PB2 and 2: 1 for anti-PB2). From the ^{15}N -HSQC spectra, we calculated a K_D^{NMR} for syn-PB2 and anti-PB2 to be $3 \pm 1 \mu\text{M}$ and ca. $40 \mu\text{M}$, respectively (Table 4.2.2). Table 4.2.2 shows selection of other Mdm2-binding compounds with their K_D s, ranking from $60 \mu\text{M}$ down to the best compound showing $1 \mu\text{M}$. (The complete data for all measured K_i 's during my study is summarized in Chapter 7.2)

Table 4.2.2. K_i as measured by HSQC-NMR based compound titration (μM) for selected compounds.

No	Name	Binding to Mdm2	Molecular Weight [g/mol]	Method of the K_D calculation*
1	PB1	40 μM	416.74	bin. titr
2	<i>syn</i> -PB2	3 μM	368.87	bin. titr.
3	<i>anti</i> -PB2	40 μM	368.87	bin. titr.
4	PB3	20 μM	324.38	bin. titr.
5	PB4	30 μM	362.25	bin. titr.
6	PB5	30 μM	337.81	AIDA
7	PB6	precipitation	385.30	bin.titr
8	PB7	>100 μM	379.91	bin.titr
9	PB8	60 μM	365.91	bin.titr, AIDA
10	PB9	60 μM	360.89	bin.titr
11	PB10	1 μM	467.02	bin.titr, AIDA T101W
12	PB11	30 μM	376.27	bin.titr AIDA
13	PB12	precipitation	416.75	bin.titr
14	PB13	60 μM	440.02	bin.titr

*bin. titr: the binary titration of a ligand with the apo- ^{15}N -Mdm2 protein using ^{15}N -HSQC
AIDA: the competition NMR experiment between ligand and the p53-Mdm2 complex.

Figure 4.2.7 shows examples of the NMR shift perturbation patterns together with the graphical representation of the shifts mapped on the structure of Mdm2 for *syn*-PB2 and *anti*-PB2, PB2, and PB10. Analysis of ligand-induced 1HN and the ^{15}N shifts was performed as described in the supplementary material (Stoll et al., 2001). Generally, the largest ligand-induced NMR shifts lined the three binding subpockets of p53 on Mdm2 (Figure 4.2.2). The detailed NMR shift perturbation pattern, however, is different between *syn*-PB2 and *anti*-PB2. *syn*-PB2 shows interactions for Met50, Lys51, Ile61, Leu82 and Val109 of Mdm2, the sites that are missing for the Mdm2 interactions in *anti*-PB2. Thus *syn*-PB2 reaches residues of Mdm2 which constitute all three p53 leucine-, tryptophan-, and phenylalanine-binding sites, whereas *anti*-PB2 lacks contacts to the p53 leucine subpocket (Figure 4.2.7).

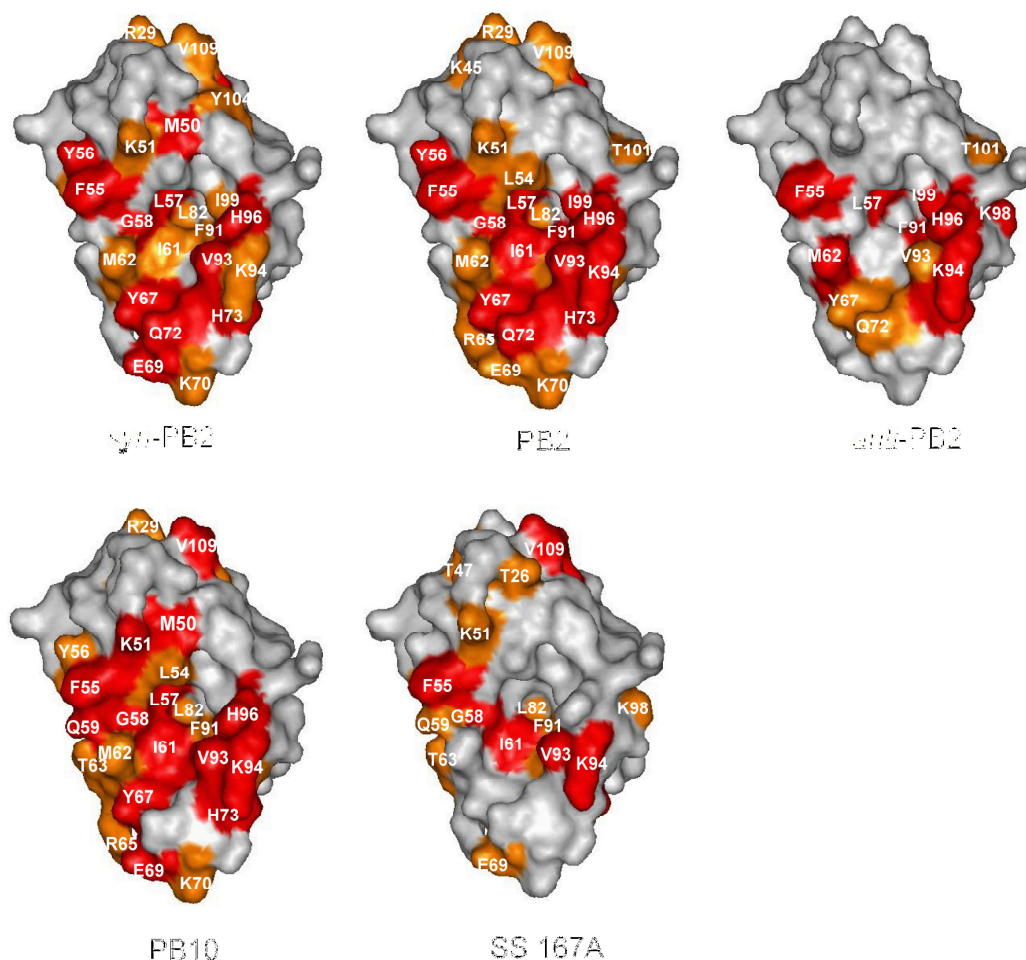
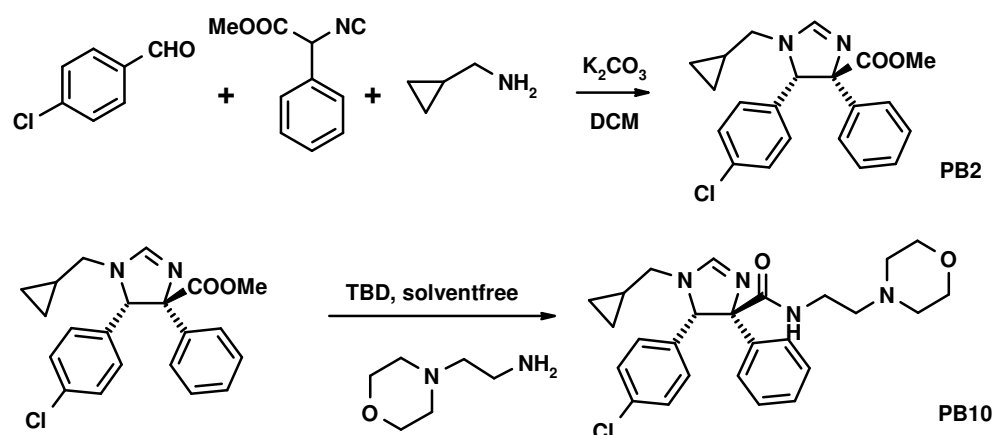


Figure 4.2.7. Contact surfaces of Mdm2 for ligands: syn-PB2, PB2, anti-PB2 and PB10. Residues that show significant induced NMR chemical shifts upon complexation with compounds are highlighted in orange and red for observed NMR vectorial shifts of 0.09-0.15 and greater than 0.15 ppm, respectively.

Due to the inherent requirements of the Mdm2 binding pocket the PB compounds are highly hydrophobic (Table 4.2.3) and show low water solubility, often an unfavorable quality of compounds aiming to become drugs. According to our binding model of PB2 the carboxymethyl group is not involved in the binding site but rather sticks into the solvent (Figure 4.2.4 B). Therefore, we reasoned that derivatisation of the ester bond by amidation could potentially improve water solubility and binding affinity. Indeed by derivatizing the carboxymethyl group of compound PB10 with amide side chains, we could improve the potency of the imidazoline scaffold as well as its water solubility (Scheme 4.2.1, Table 4.2.2).



Scheme 4.2.1. One-pot isocyanide-based MCR synthesis of imidazoline and optimization by amidation yielding derivative PB10 with improved affinity and water solubility. (TBD = 1,5,7-triazabicyclo[4.4.0]dec-5-ene)

Table 4.2.3. Drug like characteristics of **PB** compounds according to the Pfizer rules. Violations of the rules are indicated in red. (MW molecular weight; TPSA total polar surface area; HBD HPA hydrogen bond donor, -acceptor; clogP calculated logarithm of the partition octanol water; north number or rotatable bonds).

No	MW [g/mol]	TPSA	HBD	HBA	clogP	nrotb	Pfizer rules
PB1	416.74	28.155	1	1	6.298	4	yes
PB2	368.87	41.907	0	3	4.701	6	yes
PB3	324.38	73.798	3	2	2.162	4	yes
PB4	362.25	46.169	2	1	3.743	6	yes
PB5	337.81	46.848	0	4	3.925	3	yes
PB6	385.30	36.1	1	1	5.838	4	yes
PB7	379.91	70.56	2	3	4.711	6	yes
PB8	365.91	32.255	2	2	6.957	4	yes
PB9	376.89	48.046	3	2	6.048	5	yes
PB10	467.01	57.172	1	4	3.821	8	yes
Nutlin-3	581.50	83.477	1	5	5.492	6	no

4.2.1.4 Antagonist induced dissociation assay (AIDA)

To determine the inhibitory strength of the compounds for the interaction between Mdm2 and p53, we performed the AIDA-NMR assay (D'Silva et al., 2005; Krajewski et al., 2005; Krajewski et al., 2007) on the preformed Mdm2 (res. 1-118)/p53 (res. 1-321) complex. Top traces in all panels in Figure 4.2.9 show 1D proton NMR spectra of the NH side chains of Trp residues of the free, Mdm2 unbound p53. Because of a highly flexible nature of the N terminal domain of p53, the side chains of Trp23 and Trp53 give rise to sharp lines. This is in contrast to the broad linewidth of Trp91, which is located in the rigid fragment of p53 that encompasses the DNA binding domain (Lee et al., 2000; Ayed et al., 2001; Schon et al., 2002; Dawson et al., 2003; D'Silva et al., 2005; Wells et al., 2008; Joerger et al., 2008).

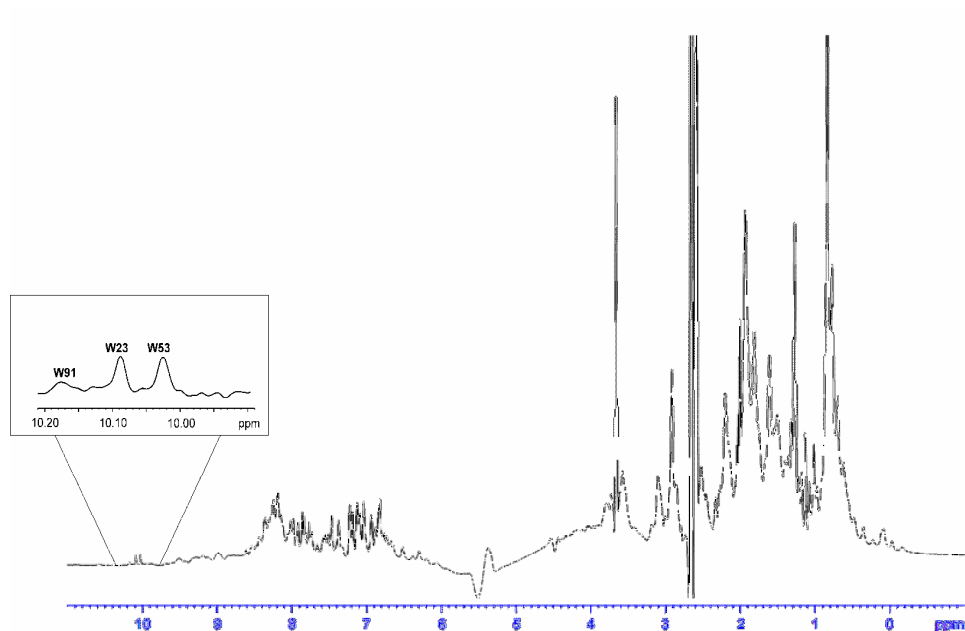


Figure 4.2.8. The 1D ¹H proton spectrum of p53 (residues 1-321) with signals of 3 Trp in aromatic region corresponding to Trp 91, Trp23 and Trp53. The Trp23 is involved in binding to Mdm2 and during that binding gets structured and the signal broadens what is observed in 1D spectrum of complex.

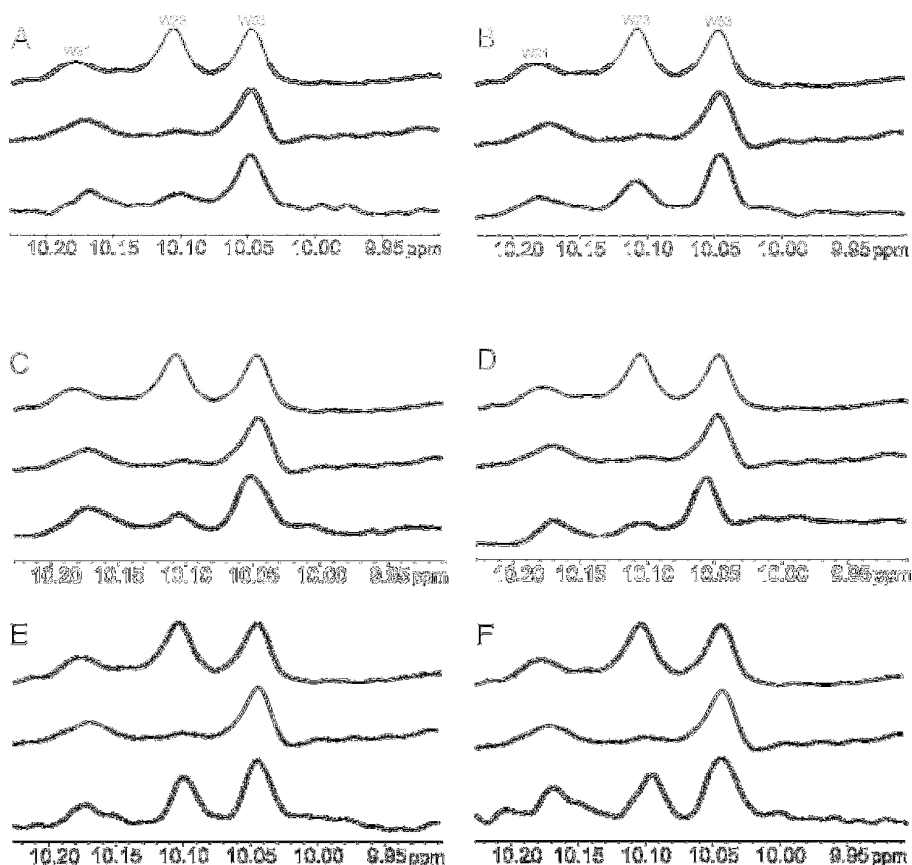
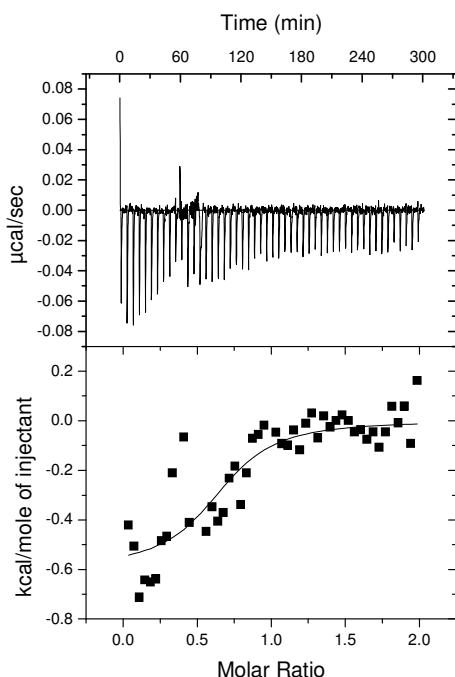


Figure 4.2.9. 1D AIDA with PB compounds. Upper trace: spectrum of p53 (res. 1-321). The three peaks are tryptophans of p53: Trp91, Trp23, and Trp53. Middle trace: the spectrum of the complex of p53 (res. 1-321) + Mdm2 (res. 1-125). Tryptophans 53 and 91 are not sensitive to the binding to Mdm2. Trp23 is in the binding site and therefore disappears on binding to Mdm2. Lower trace: Addition of PB compounds to the complex releases p53 as seen by the reappearance of the tryptophan Trp23. (A: anti-PB2, B: syn-PB2, C: PB3, D: PB5 and E: PB10 (F: SS167A).

On forming the complex with Mdm2, the signal of Trp23 disappears (Figure 7, middle traces in all panels). This is because Trp23, together with the p53 residues 17 to 26, comprise the primary binding site for Mdm2. Upon binding, these residues participate in well defined structures of a large p53 Mdm2 complex, whereas Trp53 is still not structured when p53 is bound to Mdm2. The observed $1/T_2$ transverse relaxation rate of the bound Trp23 in the complexes increases thus significantly and broadening of NMR resonances results in the disappearance of this signal in the spectra (D'Silva et al., 2005). PB compounds were then added to the Mdm2/p53 complexes and the NMR signal of $^1H^{\epsilon}$ of Trp-23 of p53 was used for the estimation of the fraction of the freed p53 from the complex. With the concentration of freed p53 known, we can obtain PB ligand-Mdm2 K_D s (Krajewski et al., 2007). The strongest inhibitory activity for the Mdm2/p53 is shown by ligand PB10 (Figures 4.2.9 E, 4.2.7; Table

4.2.1). Figures 4.2.9 A, 4.2.9 B clearly show that different inhibitory strengths are seen for syn-PB2 and anti-PB2 ligands, and PB10. For our best ligand compound PB10 we also performed isothermal titration calorimetry (ITC) as an alternative assessment of the K_D . The ITC based K_D ($2.9 \pm 1.7 \mu\text{M}$) as shown in Figure 4.2.10, nicely fits with the NMR based K_D of $1 \mu\text{M}$ (Table 4.2.2).



4.2.10. Isothermal Calorimetry titration assay of PB10. The Mdm2 concentration was established around 0.025mM , the titrant (PB10) was 0.28mM dissolved in DMSO. The same molarity of DMSO was added to Mdm2 solution keep the environment homogenous for both reagents.

4.2.1.5 Cell based studies

In order to learn more about the cellular activity of our predicted p53/Mdm2 antagonists, we performed cell based studies, assessing proliferation, apoptosis and protein analysis of p53 dependant proteins. Thus we screened the compounds in the cell lines HCT116, and an modified p53(-- knock out HCT116 (Vogelstein 1997), the ovarian cancer derived A2780 and cis platinum resistant CP70. (The complete cell based assay is described in section Materials and Methods). All compounds showed μM potency to induce apoptotic phenotypes in these cell lines and thus compare well with Nutlin-3 (Table 4.2.4)

Table 4.2.4. Selected GI50 of PB compounds in cancer cell lines with different p53 status.

Test agent	HCT116 p53 ⁽⁺⁺⁾	HCT116 p53 ⁽⁻⁾	A2780	CP70
PB1	6	18	4.5	20
PB4	>25	>25	1	15
PB8	19	22	1	25
PB9	11	10	1	7
PB10			4	25
PB12	24	>25	1	25
Nutlin-3	2	38	1	7

All GIs in μM .

p21 and Mdm2 are translationally regulated by p53. To assess the cellular mode-of-action of the compounds, we performed Western blot analysis of the p53 dependent proteins Mdm2, p21 and p53 for several compounds (Figure 4.2.11) (Thomas 2008). Clearly all assessed compounds show the mechanism based cell based activity.

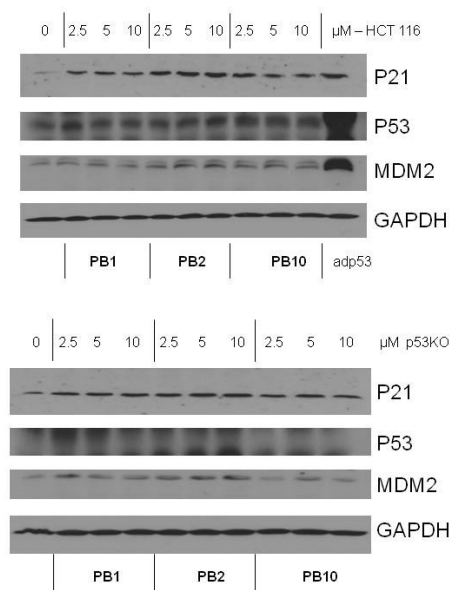


Figure 4.2.11. Western blot analysis of PB 1, 2, and 10 to determine of the mechanism based cellular activity. P53 translational products Mdm2 and p21 are upregulated upon the addition of compounds. Differential behavior of the compounds in p53⁽⁻⁾ and p53⁽⁺⁺⁾ cell lines HCT116 indicate that the compounds are acting in cells by antagonizing p53/Mdm2. Protein control GAPDH and compound control p53.

4.2.2 Conclusions

We have introduced a new process for predicting antagonists of PPIs and predicted several new small molecular weight scaffolds able to interrupt the PPI p53/Mdm2 based on MCR scaffolds. The technique is substantially different from currently used techniques including high throughput screening, fragment-based approaches, structure-based design or computational screening of compound libraries. Although our approach incorporates elements of most aforementioned techniques it involves a tight interplay of several techniques from different disciplines, including structural biology, NMR-based screening, virtual computational chemistry, organic chemistry, docking and cell biology. Out of 12 predicted compound classes 9 compounds based on 9 different scaffolds showed double or single digit μM affinity to Mdm2. The compounds are based on small heterocyclic scaffolds or linear acyclic structures based on convergent and fast MCR chemistry. All the compounds are small molecular weight compounds with advantageous drug like properties (e.g. molecular weight, water solubility, ClogD, number of H-bond donors and acceptors, PSA, see Table 4.2.3) and can form starting points for optimization by medicinal chemistry.

A metric for lead selection is the so-called ligand efficiency defined as the ratio of the free energy of binding over the number of heavy atoms in a molecule (Abad-Zapatero and Metz 2005; Lipinski, 2004; Andrews et al. 1984). A plot of our PB compounds together with the currently best Mdm2 binders nutlin-3 and MI-219 (Shangary et al., 2008) is shown in Figure 4.2.12. This plot suggests that the PB compounds are useful starting points to obtain potent Mdm2 binder. As shown in Figure 4.2.12, the relationship between pK_D and MW is expected to be almost perfectly linear for optimized inhibitors of the Mdm2/x interactions. Thus the binding efficiency index, BEI, defined as the pK_D divided by the MW in kDa, should remain constant at a value of ca. 11-12 when moving from optimized fragments to optimized drug lead (nutlin-3 for Mdm2). These data gives us a quantitative measure of the efficiency of fragment elaboration. For example, as the size of the fragment is increased through synthetic means, a drop in the BEI of more than 10% is likely an indication that either the site or the nature of the modification is not ideal.

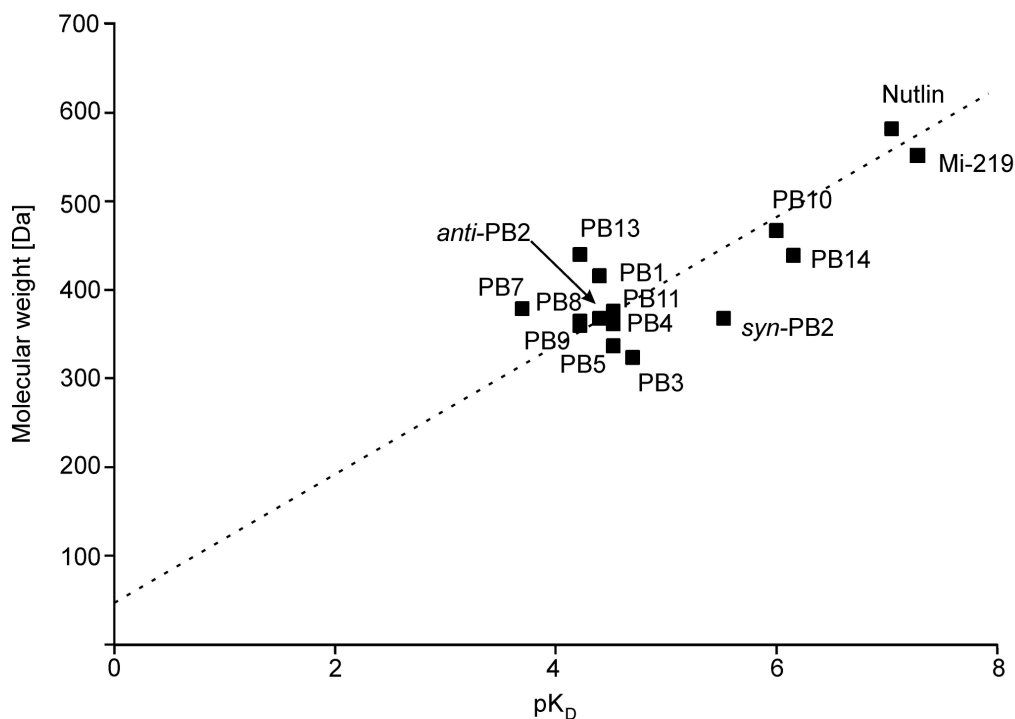


Figure 4.2.12. Plot of pK_D values (defined as the negative base-10 logarithm of the K_D value expressed in molar units) vs. MW for the compounds depicted in Table 1. The dashed line shows the plot expected for the best, minimal leads of Mdm2. Known p53/Mdm2 antagonists nutlin-3 and MI-219 are included for reference.

Optimization of initial leads for affinity, selectivity and ADMET parameters is a key undertaking in drug discovery and development. Thus, scaffolds are preferable which allow for easy derivatization and thus property optimization. For example, syn-PB2 and PB9 show poor water solubility and PB6 and PB12 lead to Mdm2 precipitation at a concentration of 0.5 mM. Exemplary, we showed the optimization of the water solubility and affinity to Mdm2 of the parent compound PB2 by preparing the amide derivative PB10 involving only one additional chemical transformation (amidation). By design, the MCR chemistry allows for a straight-forward “build-in” optimization strategy, simply by variation of the starting materials. The importance of a high content screening in the early phases of drug discovery cannot be overemphasized. NMR spectroscopy is such a high content screening since in addition to affinity it delivers information about the binding site, the water solubility of the compounds and its ability to precipitate the target protein. Other high throughput methods are often not able to give this wealth of information which can result in false positive compounds especially

when used isolated (Galatin and Abraham, 2004; D'Silva et al., 2005; Issaeva et. al., 2004; Krajewski et al., 2005; Shuker et al., 1996).

All of the compounds exhibit μM binding to the Mdm2 p53 groove as shown by NMR-based assays. However, binding of a compound to Mdm2 might not be sufficient to excerpt biological activity since p53/Mdm2 complex is mostly present in the cell nucleus in cells. Biological activity might require the compounds ability to disrupt preformed p53/Mdm2 complex. By using AIDA NMR we showed that several PB compounds (2, 3, 5) are able to disrupt preformed p53/Mdm2 complex as well as optimized compound PB10 with low μM affinity and 75% p53 recovery. Growth inhibitory activity was observed for all compounds in several differentially p53 expressing cell lines. Some activities are comparable to a well known p53/Mdm2 antagonist nutlin-3 and mechanism based action was shown by concentration dependant upregulation of different p53 gene products. Additionally, we could show that the type of cell death of cells treated with PB compounds (1, 2, 10) is apoptosis. Based on the number of predicted and active found compounds the rate of active compounds (hit rate) is $>75\%$ and is thus much higher than in usual HTS or other described drug discovery techniques. For example HTS campaigns are described to be particularly unsuccessful in delivering reproducible hits and hit rates less than 1% have been described. Another benefit of the above described process is that several scaffolds are discovered in parallel. Often during preclinical drug discovery and development compound leads have to be abandoned due to adverse properties, e.g. high protein binding, fast metabolism, toxicity or lacking oral bioavailability.

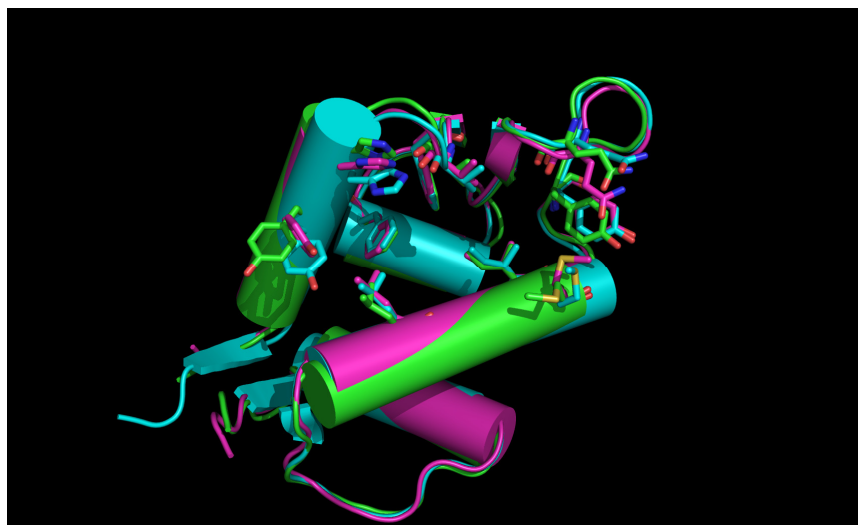


Figure 4.2.13. Adaptability of the Hdm2 receptor to different molecules: Overlap of several available high resolution Hdm2 structures reveals a small RMSD, particularly in the p53 binding site (shown).

Hdm2 in complex with p53 peptide (1YCR, green), with a benzodiazepine inhibitor (1T4E, blue) and with a nutlin inhibitor (1RV1, pink), however omitting the ligands. Cartoon representations, key amino acid side chains (Y100, L54, H96, F86, F91, V93, Y67, M62, Q72, I61) of the p53 binding side in Hdm2 are shown as sticks (2, 3, 4).

Thus optimizing several unrelated compound series based on different scaffolds greatly enhances the chance of bringing a specific lead into humans. All of the newly discovered scaffolds incorporate chemistry which allows for easy derivatization. An important part of the process is also the fast and efficient one-pot multicomponent reaction chemistry (MCR) which allows rapidly testing the computationally generated binding idea by synthesizing several compounds based on multiple scaffolds in a short time. This is in contrast to most other chemistries where a target test molecule is synthesized by a sequential lengthy process. Our new approach for the discovery of antagonists of protein-protein interactions will be useful in cases where there are no major structural adoptions of the acceptor protein upon donor protein binding or antagonist binding. In the case of p53/Mdm2 there is plenty of high resolution structural information available and the RMS deviation of the p53 binding sites is very small and no major induced fit occurs (Figure 4.2.13). Therefore, our rigid docking approach not accounting for protein flexibility turned out to be successful. Certainly this new approach successful in one example demands for further validation with different types of PPIs.

5 Summary

The work presented in this thesis was carried out in the Department of Structural Research at the Max Planck Institute in Martinsried. The first part of this thesis focused on the structural and functional characterization of the interaction between Mdm2/Mdmx and p53. The second part concerned the identification of small molecular weight inhibitors for those interactions. The Mdm2 and Mdmx proteins are the principal negative regulators of the p53 tumour suppressor. Reactivation of p53 activity by disrupting the Mdm2/Mdmx interactions offers new possibilities for anticancer therapeutics.

The structures of complexes of wild-type p53 peptides with the p53 binding domains of Mdmx and Mdm2 revealed that although the principle features of the Mdm2-p53 interaction are preserved in Mdmx-p53 complexes, the Mdmx hydrophobic cleft on which the p53 peptide binds is significantly altered: a part of the cleft is blocked by side chains of Met and Tyr of Mdmx. Thus, specific inhibitors of Mdm2-p53 would not be optimal for binding to Mdmx. Our binding assays showed indeed that nutlins, the most potent antagonists of the Mdm2-p53 interaction do not efficiently disrupt the Mdmx-p53 interaction. To achieve full activation of p53 in tumour cells, compounds that are specific for Mdmx are necessary to complement the Mdm2 specific binders.

I also describe the crystal structures of two complexes of a p53-like mutant peptide with the N-terminal domains of Mdm2 and Mdmx. The structures revealed that the p53 mutant peptide (amino acid sequence LTFEHYWAQLTS) assumes virtually identical conformations in both complexes despite the different shapes of the p53 pockets in these two proteins, has a more extended helical nature compared to Mdm2 bound wild-type p53 peptide, and does not disturb the native folds of Mdm2 or Mdmx. The extension of the helical structure in the mutant p53 peptide greatly improves its binding to both Mdm2 and Mdmx. The fluorescence polarization assay that we have developed using this peptide indicates the affinities of the mutant peptide towards Mdm2 of 3.6 nM and for Mdmx of 6.1 nM, compared to the low micromolar binding of a similar length wild-type p53 peptide to Mdm2/Mdmx. These structures, coupled with the robust fluorescence polarization assay, should enable development of a simple pharmacophore model of cross-selective Mdm2-Mdmx/p53 inhibitors. Finally, I have carried out the NMR screening of small molecule weight compounds and their fragments against human Mdmx and Mdm2.

Despite the importance of protein-protein interactions (PPIs) for understanding basic questions of biology and intervention in disease, the discovery of small molecular weight antagonists for PPIs remains one of the most challenging areas in drug discovery. In the second part of the thesis I describe a complementary approach for the rational design of PPI antagonists. This method is based on a tight interplay of structural biology information, the “anchor” concept, virtual and real multicomponent reactions (MCRs) and high content

screening. Applying the method, more of different scaffolds for the PPI p53/Mdm2 were found than previously described. Eight different scaffolds with initial μM affinity to Mdm2 were discovered that can serve as starting point for medicinal chemistry optimization. The compounds were selected from more than 200 scaffolds. The affinity for each of them was estimated via NMR and FP assays. Advantages of our approach include high hit rates and less attrition based on the parallel discovery of multiple scaffolds, built-in optimization pathways using efficient MCRs, and fast testing of computationally generated hypotheses.

6 Zusammenfassung

Die in dieser Doktorarbeit vorgestellten Ergebnisse wurden in der Abteilung für Strukturforschung am Max Planck Institut für Biochemie in Martinsried erarbeitet.

Der erste Abschnitt der Arbeit beschäftigt sich vorranglich mit der strukturellen und funktionalen Charakterisierung der Interaktion zwischen Mdm2/Mdmx und p53. Der zweite Abschnitt beinhaltet die Identifikation von kleinen niedermolekularen Inhibitoren für diese Interaktion. Die Proteine Mdm2 und Mdmx sind die bedeutendsten negativen Regulatoren des Tumorsuppressors p53. Die Wiederherstellung der p53 Aktivität durch die Zerrstörung der Mdm2/Mdmx Interaktion öffnet somit neue Wege in der Krebstherapie.

Die Kristallstrukturen der Komplexe zwischen wildtyp p53 Peptid und der p53-Bindungsdomäne von Mdm2 bzw. Mdmx zeigen, dass trotz der Tatsache, dass die prinzipiellen Eigenschaften der Mdm2-p53 Interaktion im Mdmx-p53 Komplex erhalten bleiben, die hydrophobe Bindungstasche, in der das p53 Peptid bindet signifikant verändert ist: Ein Teil der Bindungstasche ist durch die Seitenreste der Aminosäuren Met und Tyr blockiert. Daher sind die spezifischen Inhibitoren für Mdm2 nicht zwangsläufig optimal für die Bindung an Mdmx. Unsere Bindungsassays zeigen in der Tat, dass die potentesten Antagonisten der Mdm2-p53 Interaktion nicht in der Lage sind die Mdmx-p53 Interaktion effektiv zu unterbrechen. Um in Tumorzellen die volle Aktivität von p53 zu erreichen sind daher spezifische Antagonisten für Mdmx nötig, um die Mdm2 spezifischen Inhibitoren zu ergänzen.

In der Arbeit werden von mir zusätzlich die Kristallstrukturen von zwei Komplexen zwischen einem p53 ähnlichen mutierten Peptiden und der N-terminalen p53-Bindungsdomäne von Mdm2 bzw. Mdmx beschrieben.

Die Strukturen zeigen, dass erstens das mutierte p53-Peptid (Aminosäuresequenz: LTFEHYWAQLTS) in beiden Komplexen fast identische Konformationen annimmt (trotz der unterschiedlichen Struktur der p53 Bindungstasche in diesen zwei Proteinen), dass zweitens das Peptid eine erweiterte helicale Struktur hat im Vergleich zum Mdm2 gebunden wildtyp p53-Peptid, und dass es drittens nicht die native Faltung von Mdm2 oder Mdmx stört.

Die Erweiterung der helicalen Struktur in dem mutierten p53-Peptid verbessert die Bindung sowohl an Mdm2 als auch an Mdmx. Ein von uns entwickelter Fluorescence Polarisations Assay mit diesem Peptid zeigt dass die Bindungskonstante des mutierten Peptids zu Mdm2 bei 3,6 nM und für Mdmx bei 6,1 nM liegt. Im Vergleich dazu liegt die Bindungskonstante für die Bindung an Mdm2/Mdmx für das wildtyp Peptid mit ähnlicher Länge im unteren micromolaren Bereich.

Diese Strukturen zusammen mit dem robusten Fluorescence Polarisation Assay, sollten die Entwicklung eines einfachen Pharmakophor Modells für Inhibitoren mit einer Kreuzselektivität für Mdm2-Mdmx/p53 ermöglichen.

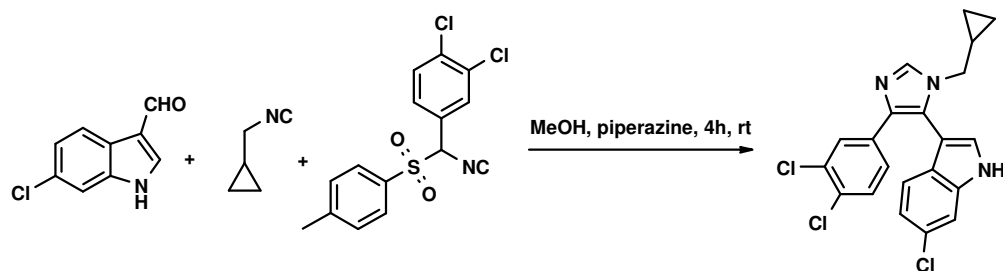
Der zweite Abschnitt der Arbeit beinhaltet ein NMR Screening mit niedermolekularen Verbindungen und deren Fragmenten für die Bindung an Mdm2 und Mdmx. Trotz der Bedeutung von Protein-Protein Interaktionen (PPI) für das Verständnis von elementaren Fragen für die Biologie von Krankheiten, der Intervention in deren Ursachen bzw. in deren Verlauf, bleibt die Suche und Entdeckung von niedermolekularen Verbindungen von PPI Antagonisten eines der herausforderndsten Felder der Medikamentenentwicklung. Ich beschreibe einen komplementären Ansatz für ein rationales Design von PPI Antagonisten. Diese Methode basiert auf dem engen Zusammenspiel von struktureller Information, als dem „Anker“ Konzept, virtueller und reeller multikomponenten Reaktionen (MCRs) und einem „High Content Screening“.

Durch die Anwendung dieser Methode wurden mehr verschiedene Grundstrukturen für die p53/Mdm2 Interaktion gefunden als jemals vorher beschrieben wurden. Acht verschiedene Grundstrukturen mit einer anfänglichen μM Affinität für Mdm2 wurden gefunden, die als Ausgangspunkt für die medizinisch chemische Optimierung dienen können. Diese Verbindungen wurden aus über 200 Grundstrukturen ausgewählt. Die Affinität jeder dieser Verbindungen wurde mittels NMR und FP Assays abgeschätzt. Der Vorteil unserer Methode beinhaltet eine hohe Trefferquote und geringere Einbußen durch parallele Entdeckungen von multiplen Grundstrukturen, eingebaute Optimierungswege durch die Verwendung effizienter MCRs und dem schnellen Testen von computergenerierten Hypothesen.

7 Appendix

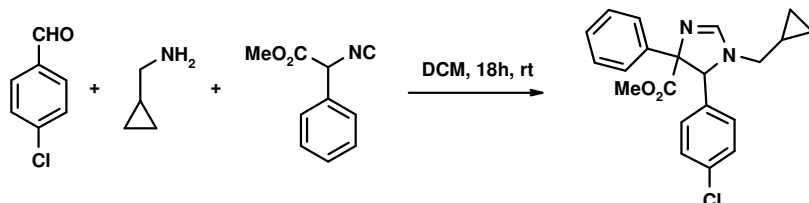
7.1 Synthesis of the small molecular weight compounds with different scaffolds.

PB1: 6-Chloro-3-[3-cyclopropylmethyl-5-(3,4-dichloro-phenyl)-3H-imidazol-4-yl]-1H-indole



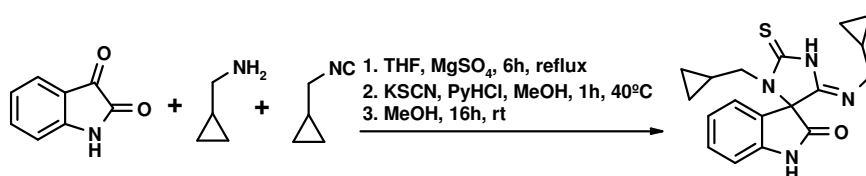
180 mg (1 mmol) 6-Chloro-1H-indole-3-carbaldehyde is solubilized in 2 mL MeOH and 85.6 μL (1 mmol) cyclopropylmethyl amine are added dropwise. The reaction mixture is stirred for 4 h at room temperature and 340 mg (1 mmol) 1,2-dichloro-4-[(isocyanomethyl)phenyl]benzene-4-sulfonamide and 86 mg (1 mmol) piperazine are added and stirred over night at room temperature. The solvent is evaporated and the crude product is purified by chromatography on silica with a gradient of heptane/ethyl acetate 3:1 to 1:2 to yield 6-chloro-3-[3-cyclopropylmethyl-5-(3,4-dichloro-phenyl)-3H-imidazol-4-yl]-1H-indole (PB1) 356 mg (86%); $^1\text{H-NMR}$ (CDCl_3 , 600 MHz): δ = 0.17 (d, J = 4.80 Hz, 2H), 0.54 (d, J = 7.86 Hz, 2H), 0.99-1.03 (m, 1H), 3.59 (d, J = 6.90 Hz, 2H), 7.07-7.12 (m, 2H), 7.17-7.21 (m, 2H), 7.25-7.26 (m, 1H), 7.46 (m, 1H), 7.74-7.75 (m, 1H), 7.86 (s, 1H), 9.63 (s, 1H); $^{13}\text{C-NMR}$ (CDCl_3 , 150 MHz): δ = 4.0, 11.2, 49.8, 104.5, 111.4, 120.0, 131.2, 131.6, 124.8, 125.4, 125.6, 127.5, 128.5, 129.5, 129.7, 131.8, 134.5, 136.3, 136.6, 137.1; HPLC-MS (ESI-TOF): r_t = 9.53 min m/z = 416 $[\text{M}+\text{H}]^+$; HRMS (ESI-TOF) m/z calcd for $\text{C}_{21}\text{H}_{16}\text{Cl}_3\text{N}_3$ $[\text{M}+\text{H}]^+$ 416.0488, found 416.0498.

PB2: 5-(4-Chloro-phenyl)-1-cyclopropylmethyl-4-phenyl-4,5-dihydro-1H-imidazole-4-carboxylic acid methyl ester



422 mg (3 mmol) p-Chlorobenzaldehyde is solubilized in 20 ml dry dichloromethane 257 μ l (3mmol) cyclopropylmethyl amine and 525 mg (3mmol) isocyano-phenyl-acetic acid methyl ester are added and the mixture is allowed to stir over night at room temperature. Isolation of the mixture of the two diastereomers by column chromatography on silica gel with petroleum ether/ethyl acetate gradient from 3/1 to 1/5 yields 893 mg (81%) 5-(4-chloro-phenyl)-1-cyclopropylmethyl-4-phenyl-4,5-dihydro-1*H*-imidazole-4-carboxylic acid methyl ester (PB2) as a yellow oil as a mixture of diastereomers (66:34). 760 mg of the mixture of two diastereomers are separated by column chromatography on neutral alumina with ethylacetate to give 260 mg pure major diastereomer and 374 mg of the mixture of two diastereomers. $^1\text{H-NMR}$ for the major diastereomer (CDCl_3 , 600 MHz): δ = 0.05-0.06 (m, 2H), 0.47-0.51 (m, 1H), 0.59-0.62 (m, 1H), 0.88-0.91 (m, 1H), 2.55-2.59 (m, 1H), 3.09-3.12 (m, 1H), 3.79 (s, 3H), 5.64 (s, 1H), 6.90-6.91 (m, 4H), 7.04-7.06 (m, 5H), 7.44 (s, 1H); $^{13}\text{C-NMR}$ for the major diastereomer (CDCl_3 , 150 MHz): δ = 2.4, 4.5, 9.1, 50.0, 52.7, 68.7, 84.1, 126.2, 126.8, 127.3, 127.5, 132.7, 134.1, 136.9, 156.3, 173.8; $^1\text{H-NMR}$ for the minor diastereomer (CDCl_3 , 600 MHz): δ = 0.02-0.04 (m, 2H), 0.44-0.46 (m, 1H), 0.54-0.56 (m, 1H), 0.82-0.84 (m, 1H), 2.61-2.65 (m, 1H), 3.09-3.13 (m, 1H), 3.29 (s, 3H), 5.09 (s, 1H), 7.31-7.43 (m, 8H), 7.76-7.77 (m, 2H); $^{13}\text{C-NMR}$ for the minor diastereomer (CDCl_3 , 150 MHz): δ = 2.5, 4.3, 9.3, 49.7, 51.7, 72.8, 85.0, 126.3, 127.4, 128.0, 128.3, 129.0, 133.8, 135.3, 143.2, 155.1, 170.7; HPLC-MS (ESI-TOF): t_r = 12.13 min m/z = 369 $[\text{M}+\text{H}]^+$; HRMS (ESI-TOF) m/z calcd for $\text{C}_{21}\text{H}_{22}\text{ClN}_2\text{O}_2$ $[\text{M}+\text{H}]^+$ 369.1370, found 369.1365.

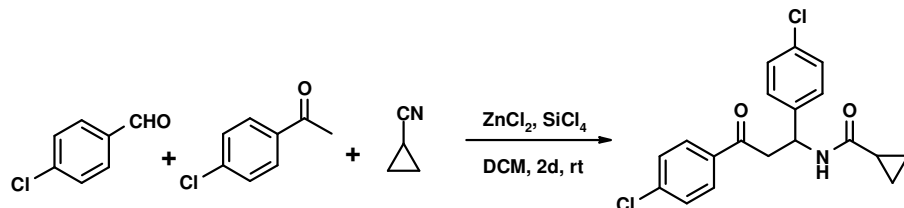
PB3: (Z)-3-(cyclopropylmethyl)-5-(cyclopropylmethylimino)-2-thioxospiro[imidazolidine-4,3'-indolin]-2'-one



908 mg (5 mmol) Isatin and 431 μ L (5 mmol) cyclopropylmethylamine are dissolved in THF. A small amount MgSO_4 is added and the reaction mixture is refluxed for 6h, filtrated and evaporated to give the precondensed Schiff base. A solution of 485 (5 mmol) KSCN and 528 mg (5 mmol) pyridium hydrochloride in 15 mL MeOH is heated at 40 $^\circ\text{C}$ for 1h, then cooled with ice-water and filtrered. 1.0g (5mmol) Schiff base is added to the solution and 405mg (5 mmol) isocyanomethyl-cyclopropane is added drop wise. The reaction mixture is stirred at room temperature overnight. The solvent is evaporated and the residue is purified by column chromatography to yield (Z)-3-(cyclopropylmethyl)-5-(cyclopropylmethylimino)-2-thioxospiro[imidazolidine-4,3'-indolin]-2'-one (PB3) 70 mg (4%); $^1\text{H-NMR}$ for the major diastereomer (MeOD, 600 MHz): δ = -0.10 (m, 1H), -0.01 (m, 1H), 0.22 (m, 2H), 0.27 (m,

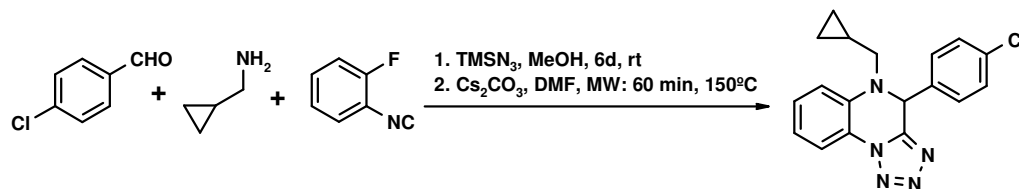
1H), 0.35 (m, 1H), 0.46 (m, 2H), 0.81 (m, 1H), 1.03 (m, 1H), 3.18 (dd, $J = 7.2, 14.4$ Hz, 1H), 3.23 (dd, $J = 1.2, 6.6$ Hz, 2H), 3.70 (dd, $J = 6.6, 14.4$ Hz, 1H), 7.07 (d, $J = 7.8$ Hz, 1H), 7.14 (m, 2H), 7.45 (m, 1H); $^{13}\text{C-NMR}$ (MeOD, 150 MHz): $\delta = 2.3, 2.4, 3.2, 4.2, 9.5, 9.6, 49.4, 76.9, 111.3, 123.2, 123.3, 124.9, 131.4, 143.3, 171.3, 173.4, 197.7$; ; HPLC-MS (ESI-TOF): $r_t = 8.25$ min $m/z = 341$ $[\text{M}+\text{H}]^+$; HRMS (ESI-TOF) m/z calcd for $\text{C}_{18}\text{H}_{20}\text{N}_4\text{OS}$ $[\text{M}]^+$ 340.1357, found 340.1366.

PB4: Cyclopropanecarboxylic acid [1,3-bis-(4-chloro-phenyl)-3-oxo-propyl]-amide



141 mg (1 mmol) 4-Chlorobenzaldehyde, 132.6 μL (1 mmol) 1-(4-chloro-phenyl)-ethanone and 75.6 μL (1 mmol) cyclopropanecarbonitrile are combined in dry DCM. 273 mg (2eq, 2 mmol) zinc chloride and 458.3 μL (4eq, 4 mmol) silicon tetrachloride are added and the reaction mixture is allowed to stir for 2d at room temperature. The reaction mixture is purified by chromatography on silica gel with heptane/ethyl acetate 4:1 to yield cyclopropanecarboxylic acid [1,3-bis-(4-chloro-phenyl)-3-oxo-propyl]-amide (PB4) 43 mg (12%); $^1\text{H-NMR}$ (CDCl_3 , 600 MHz): $\delta = 0.77\text{-}0.79$ (m, 2H), 0.98-1.00 (m, 2H), 1.40-1.45 (m, 1H), 3.39-3.43 (m, 1H), 3.73-3.77 (m, 1H), 5.53-5.56 (m, 1H), 6.80 (d, 1H), 7.28-7.33 (m, 4H), 7.44-7.47 (m, 2H), 7.86 (d, 2H); $^{13}\text{C-NMR}$ (CDCl_3 , 150 MHz): $\delta = 7.4, 7.5, 14.9, 43.1, 49.5, 127.9, 128.8, 129.1, 129.5, 133.3, 134.8, 139.4, 140.2, 173.1, 197.2$; HPLC-MS (ESI-TOF): $r_t = 11.30$ min $m/z = 362$ $[\text{M}+\text{H}]^+$; HRMS (ESI-TOF) m/z calcd for $\text{C}_{19}\text{H}_{17}\text{Cl}_2\text{NO}_2$ $[\text{M}+\text{Na}]^+$ 384.0534, found 384.0550.

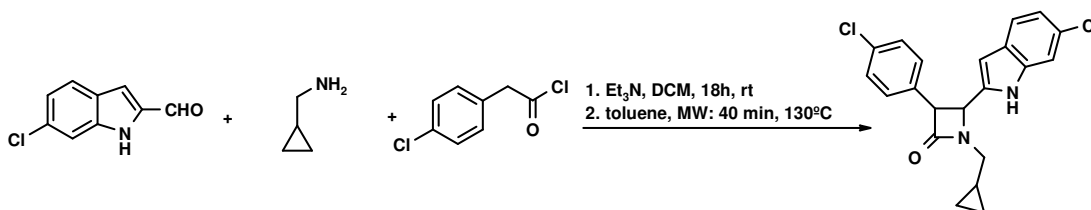
PB5:4-(4-Chloro-phenyl)-5-cyclopropylmethyl-4,5-dihydro-1,2,3,5,9b-pentaazacyclopenta[a]- naphthalene



422 mg (3 mmol) 4-Chlorobenzaldehyde and 262.6 μL (3mmol) cyclopropyl-methylamine are dissolved in 3 ml MeOH and stirred for 5 h at room temperature. 472 mg (1.3 eq, 3.9 mmol) 1-Fluoro-2-isocyanobenzene are added and the reaction mixture is allowed to stir for 6 days at room temperature. The solvent is evaporated and the residue is dissolved in ethyl acetate and washed with water and brine. The organic layer is dried over MgSO_4 and concentrated.

The crude product is purified by chromatography on silica gel with a gradient of heptane/ethyl acetate 9:1 to 4:1 to yield 1074 mg {(4-chloro-phenyl)-[1-(2-fluoro-phenyl)-1H-tetrazol-5-yl]-methyl}-cyclopropylmethylamine. 100mg (0.28 mmol) {(4-Chloro-phenyl)-[1-(2-fluoro-phenyl)-1H-tetrazol-5-yl]-methyl}-cyclopropylmethylamine are dissolved in 4ml dry DMF and 182 mg (2eq, 0.56 mmol) baked Cs_2CO_3 are added and the reaction mixture is heated in the microwave for 60 min at 150 °C. The solvent is evaporated and the residue is dissolved in ethyl acetate and extracted with water and brine. The organic layer is dried over MgSO_4 and evaporated. The crude product is purified by chromatography on silica gel with heptane/ethyl acetate 4:1 to yield 4-(4-chloro-phenyl)-5-cyclopropylmethyl-4,5-dihydro-1,2,3,5,9b-pentaaza-cyclopenta[a]naphthalene (PB5) 19 mg (20%); $^1\text{H-NMR}$ (CDCl_3 , 600 MHz): $\delta = 0.15-0.23$ (m, 2H), 0.53-0.57 (m, 1H), 0.65-0.68 (m, 1H), 1.04-1.06 (m, 1H), 3.01-3.05 (m, 1H), 3.57-3.60 (m, 1H), 6.50 (s, 1), 7.00-7.05 (m, 2H), 7.22-7.31 (m, 4H), 7.37-7.40 (m, 1H), 7.99-7.00 (d, 1H). ; HPLC-MS (ESI-TOF): $r_t = 12.29$ min $m/z = 336$ $[\text{M}+\text{H}]^+$; HRMS (ESI-TOF) m/z calcd for $\text{C}_{18}\text{H}_{16}\text{ClN}_5$ 337.1094, found 337.1093.

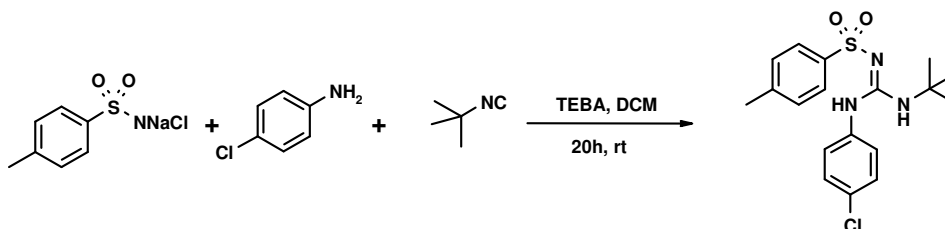
PB6: 4-(6-Chloro-1H-indol-2-yl)-3-(4-chloro-phenyl)-1-cyclopropylmethyl-azetidin-2-one



180 mg (1 mmol) 6-Chloro-1H-indole-2-carbaldehyde and 85.6 mL (1 mmol) cyclopropylmethylamine are dissolved in DCM and a small amount MgSO_4 is added and stirred over night. The salt is filtered off and the filtrate is concentrated under reduced pressure. The residue is dissolved in toluene and 669 μL (4.8 mmol) triethylamine and 251.6 μL (1.72 mmol) (4-chlorophenyl)-acetylchloride are added simultaneously. The reaction mixture is heated in the microwave for 40 min at 130 °C. After the mixture cooled to room temperature the solid is filtered off and the filtrate is evaporated. The residue is dissolved in ethyl acetate and extracted with water and brine. The organic layer is dried over MgSO_4 and evaporated. The crude product is purified by chromatography on silica gel with heptane/ethyl acetate 4:1 to yield 4-(6-chloro-1H-indol-2-yl)-3-(4-chloro-phenyl)-1-cyclopropylmethyl-azetidin-2-one (PB6) 33 mg (9%); $^1\text{H-NMR}$ (CDCl_3 , 600 MHz): $\delta = 0.43-0.45$ (m, 2H), 0.51-0.52 (m, 2H) 0.92-0.95 (m, 1H), 2.65-2.69 (m, 1H), 3.52-3.56 (m, 1H), 4.43 (s, 1H), 4.79 (s, 1H), 6.52 (s, 1H), 7.07-7.08 (m, 1H), 7.24-7.48 (m, 6H), 9.98 (s, 1H); $^{13}\text{C-NMR}$ (CDCl_3 , 150 MHz): $\delta = 3.0, 4.2, 9.3, 45.9, 58.2, 62.2, 103.5, 111.3, 120.8, 121.3, 126.3, 128.5, 128.6,$

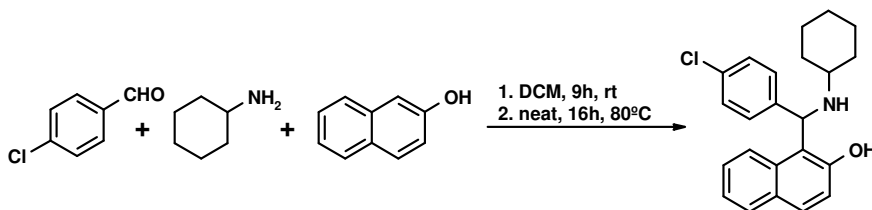
129.3, 133.0, 133.9, 134.6, 137.5, 168.1; HPLC-MS (ESI-TOF): $t_r = 12.54$ min $m/z = 384$ [M]⁺; HRMS (ESI-TOF) m/z calcd for C₂₁H₁₈Cl₂N₂O 384.0796, found 384.07977.

PB7: N-[1-tert-Butylamino-1-(4-chloro-phenylamino)-meth-(Z)-ylidene]-4-methyl-benzenesulfon amide



To a solution of 228 mg (1 mmol) Chloramine T, 128 mg (1 mmol) 4-chlorophenylamine and 83 mg (1 mmol) *tert*-butylisocyanide in 5 ml dry DCM are added 5 mg benzyltriethyl ammoniumchloride and stirred for 20h at room temperature. The reaction is quenched with water and the organic layer is separated, dried over Na₂SO₄ and evaporated. The crude product is purified by chromatography on silica with petroleum ether/ethyl acetate 2:1 to yield N-[1-*tert*-butylamino-1-(4-chloro-phenylamino)-meth-(Z)-ylidene]-4-methyl-benzenesulfonamide (PB7) 47 mg (12%); ¹H-NMR (CDCl₃, 600 MHz): $\delta = 1.32$ (s, 9H), 2.43 (s, 3H), 6.62 (d, 1H), 7.07-7.10 (m, 2H), 7.28 (d, 2H), 7.38 (d, 2H), 7.84 (d, 2H), 8.81 (bs, 1H); ¹³C-NMR (CDCl₃, 150 MHz): $\delta = 21.5, 29.2, 52.8, 116.3, 125.9, 126.4, 127.0, 129.1, 129.3, 130.3, 134.4, 140.7, 142.1, 145.1, 152.7$; HPLC-MS (ESI-TOF): $t_r = 11.75$ min $m/z = 380$ [M+H]⁺; HRMS (ESI-TOF) m/z calcd for C₁₈H₂₂ClN₃O₂S [M+H]⁺ 380.1200, found 380.1189.

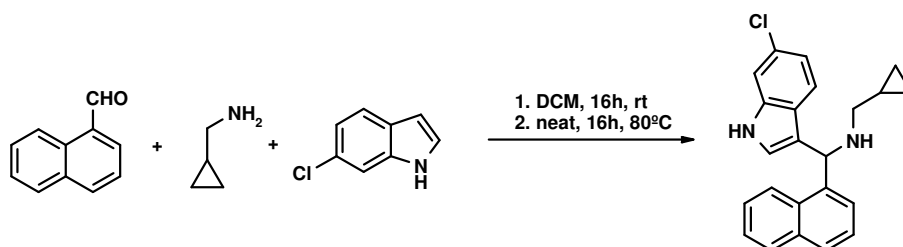
PB8: 1-((4-chlorophenyl)(cyclohexylamino)methyl)naphthalen-2-ol



337 mg (1.2 eq, 2.4 mmol) 4-Chlorobenzaldehyde and 239.9 μ L (1.05 eq, 2.1 mmol) cyclohexylamine are diluted in DCM and stirred for 9h at room temperature. The solvent is evaporated and the precondensed Schiff base is combined with 288 mg (1 eq, 2 mmol) naphthalen-2-ol and heated to 80 °C for 15h. The reaction mixture is purified by chromatography on silica gel with heptane/ethyl acetate 4:1 to yield 1-[(4-chloro-phenyl)-cyclohexylamino-methyl]-naphthalen-2-ol (PB8) 343 mg (47%); ¹H-NMR (CDCl₃, 600 MHz): $\delta = 0.71$ -0.82 (m, 2H), 1.06-1.22 (m, 3H), 1.50-1.51 (m, 1H), 1.51-1.53 (m, 1H), 1.58-1.61 (m, 1H), 1.86-1.88 (m, 1H), 2.15-2.17 (m, 1H), 2.61(bs, 1H), 5.76 (s, 1H), 7.06-7.07 (d, 1H), 7.15-

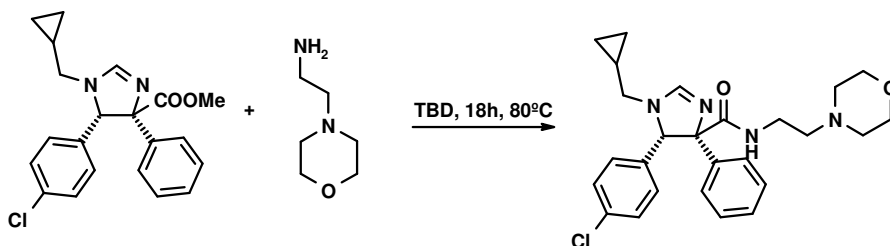
7.19 (m, 3H), 7.25-7.28 (m, 3H), 7.56-7.58 (d, 1H), 7.64-7.66 (m, 2H), 13.88 (bs, 1H); ^{13}C -NMR (CDCl_3 , 150 MHz): δ = 24.6, 24.7, 25.5, 32.4, 33.2, 55.5, 59.6, 113.2, 120.1, 120.6, 122.2, 126.3, 128.3, 128.7, 129.5, 131.9, 133.5, 140.4, 157.2; HPLC-MS (ESI-TOF): r_t = 10.43 min m/z = 366 $[\text{M}+\text{H}]^+$; HRMS (ESI-TOF) m/z calcd for $\text{C}_{23}\text{H}_{24}\text{ClNO}$ 365.1546, found 365.1549.

PB9: [(6-Chloro-1H-indol-3-yl)-naphthalen-1-yl-methyl]-cyclopropylmethyl-amine



327 μL (1.2 eq, 2.4 mmol) Naphthalene-1-carbaldehyde and 180 μL (1.05 eq, 2.1 mmol) cyclopropylmethylamine are diluted in DCM and stirred over night at room temperature. The solvent is evaporated and the precondensed Schiff base is combined with 303 mg (1 eq, 2 mmol) 6-Chloro-1H-indole and heated to 80 $^{\circ}\text{C}$ for 15h. The reaction mixture is purified by chromatography on silica gel with heptane/ethyl acetate 4:1 to yield [(6-chloro-1H-indol-3-yl)-naphthalen-1-yl-methyl]-cyclopropylmethyl-amine (PB9) 270 mg (37%); ^1H -NMR (CDCl_3 , 600 MHz): δ = 0.08 (m, 2H), 0.45 (m, 2H), 1.03-1.05 (m, 1H), 2.44 (bs, 1H), 2.57-2.64 (m, 2H), 5.95 (s, 1H), 6.66 (s, 1H), 7.03 (d, 1H), 7.16 (s, 1H), 7.37-7.45 (m, 3H), 7.55 (d, 1H), 7.74-7.75 (m, 2H), 7.76 (d, 1H), 7.85 (d, 1H), 8.06 (s, 1H); ^{13}C -NMR (CDCl_3 , 150 MHz): δ = 3.5, 3.7, 11.4, 53.7, 55.1, 111.3, 118.9, 119.9, 120.3, 123.3, 123.9, 124.4, 125.1, 125.5, 125.6, 126.0, 127.9, 128.9, 131.5, 134.1, 136.8, 138.3; HPLC-MS (ESI-TOF): r_t = 9.34 min m/z = 359 $[\text{M}]$; HRMS (ESI-TOF) m/z calcd for $\text{C}_{23}\text{H}_{21}\text{ClN}_2$ 360.1393, found 360.1401.

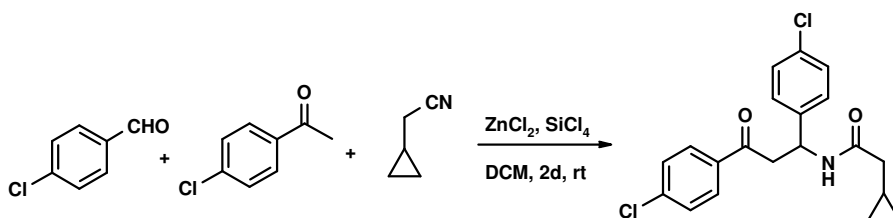
PB10: 5-(4-Chloro-phenyl)-1-cyclopropylmethyl-4-phenyl-4,5-dihydro-1H-imidazole-4-carboxylic acid (2-morpholin-4-yl-ethyl)-amide



50 mg (0.14 mmol) major diastereomer 5-(4-chloro-phenyl)-1-cyclopropylmethyl-4-phenyl-4,5-dihydro-1H-imidazole-4-carboxylic acid methyl ester (PB2) and 9.6 mg (0.07 mmol, 30%) TBD are combined with 36 μL (0.27 mmol, 2 eq) 2-morpholin-4-yl-ethylamine. The reaction mixture is heated to 80 $^{\circ}\text{C}$ over night and purified on column chromatography on silica gel

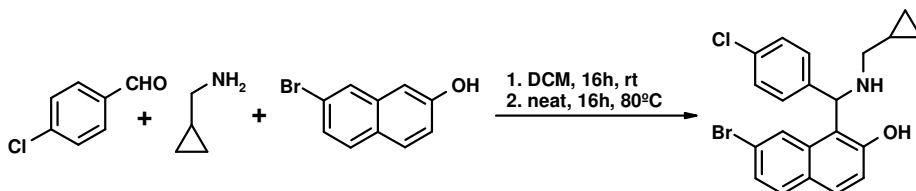
with dichloromethane/methanol as gradient from 0-5% MeOH to yield 5-(4-chloro-phenyl)-1-cyclopropylmethyl-4-phenyl-4,5-dihydro-1H-imidazole-4-carboxylic acid (2-morpholin-4-yl-ethyl)-amide (PB10) 50 mg (79%); $^1\text{H-NMR}$ (CDCl_3 , 600 MHz): δ 0.01-0.04 (2H, m), 0.44-0.49 (1H, m), 0.56-0.61 (1H, m), 0.85-0.91 (1H, m), 2.27-2.46 (6H, m), 2.60 (1H, dd, $J=14.22$ Hz & 7.68 Hz), 3.09 (1H, dd, $J=14.22$ Hz & 6.24 Hz), 3.30-3.35 (1H, m), 3.39-3.44 (1H, m), 3.53-3.61 (4H, m), 5.54 (1H, s), 6.98-7.07 (8H, m), 7.10-7.11 (2H, m), 7.38 (1H, s); $^{13}\text{C-NMR}$ (CDCl_3 , 150 MHz): δ 2.81, 4.77, 9.56, 36.20, 50.33, 53.26, 56.85, 66.84, 68.63, 83.96, 126.76, 126.92, 127.43, 127.78, 132.84, 135.04, 138.42, 155.35, 174.60. HPLC-MS (ESI-TOF): $r_t = 8.22$ min $m/z = 467$ $[\text{M}+\text{H}]^+$; HRMS (ESI-TOF) m/z calcd for $\text{C}_{26}\text{H}_{31}\text{ClN}_4\text{O}_2$ $[\text{M}+\text{H}]^+$ 467.2214, found 467.2198.

PB11: N-[1,3-Bis-(4-chloro-phenyl)-3-oxo-propyl]-2-cyclopropyl-acetamide



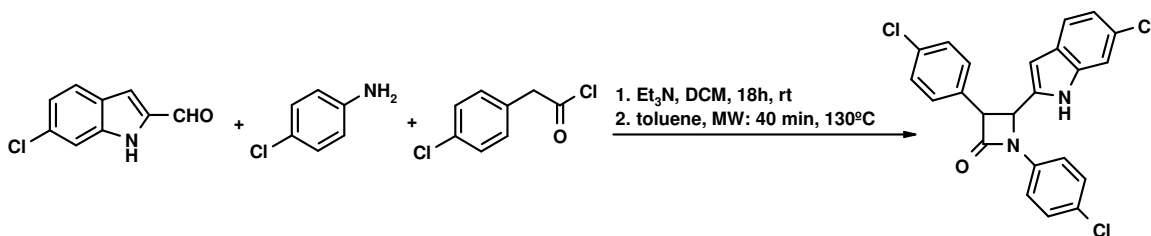
141 mg (1 mmol) 4-Chlorobenzaldehyde, 132.6 μL (1 mmol) 1-(4-chloro-phenyl)-ethanone and 93.9 μL (1 mmol) cyclopropyl acetonitrile are combined in dry DCM. 273 mg (2eq, 2 mmol) zinc chloride and 458.3 μL (4eq, 4 mmol) silicon tetrachloride are added and the reaction mixture is allowed to stir for 2d at room temperature. The reaction mixture is purified by chromatography on silica gel with heptane/ethyl acetate 4:1 to yield N-[1,3-bis-(4-chloro-phenyl)-3-oxo-propyl]-2-cyclopropyl-acetamide (PB11) yield 71 mg (19%); $^1\text{H-NMR}$ (CDCl_3 , 600 MHz): $\delta = 0.22$ -0.25 (m, 2H), 0.66-0.69 (m, 2H), 0.97-1.05 (m, 1H), 2.21 (d, 2H), 3.39-3.43 (m, 1H), 3.73-3.77 (m, 1H), 5.55-5.59 (m, 1H), 7.22 (d, 1H), 7.28-7.31 (m, 4H), 7.44-7.46 (m, 2H), 7.85-7.87 (m, 2H); $^{13}\text{C-NMR}$ (CDCl_3 , 150 MHz): $\delta = 4.4$, 4.6, 7.1, 41.6, 42.9, 49.1, 125.5, 127.1, 127.9, 128.5, 128.7, 128.8, 129.1, 129.5, 133.3, 134.8, 139.5, 140.2, 172.0, 197.3; HPLC-MS (ESI-TOF): $r_t = 11.49$ min $m/z = 376$ $[\text{M}+\text{H}]^+$; HRMS (ESI-TOF) m/z calcd for $\text{C}_{20}\text{H}_{19}\text{Cl}_2\text{NO}_2$ $[\text{M}+\text{Na}]^+$ 398.0691, found 398.0678.

PB12: 7-Bromo-1-[(4-chloro-phenyl)-(cyclopropylmethyl-amino)-methyl]-naphthalen-2-ol



337 mg (1.2 eq, 2.4 mmol) 4-Chlorobenzaldehyde and 180.1 μ L (1.05 eq, 2.1 mmol) cyclopropylmethyl amine are diluted in DCM and stirred over night at room temperature. The solvent is evaporated and the precondensed Schiff base is combined with 444 mg (1eq, 2mmol) 7-bromo-naphthalen-2-ol and heated to 80 $^{\circ}$ C for 15h. The reaction mixture is purified by chromatography on silica gel with heptane/ethyl acetate 4:1 to yield 7-bromo-1-[(4-chloro-phenyl)-(cyclopropylmethyl-amino)-methyl]-naphthalen-2-ol (PB12) 320 mg (38%); 1 H-NMR (CDCl_3 , 600 MHz): δ = 0.13-0.19 (m, 1H), 0.19-0.21 (m, 1H), 0.51-0.56 (m, 2H), 1.02-1.05 (m, 1H), 2.55-2.58 (m, 1H), 2.71-2.74 (m, 1H), 5.58 (s, 1H), 7.13 (d, 1H), 7.25-7.7.31 (m, 3H), 7.37-7.39 (m, 2H), 7.57 (d, 1H), 7.65 (d, 1H), 7.79 (s, 1H); 13 C-NMR (CDCl_3 , 150 MHz): δ = 3.3, 4.0, 10.6, 53.8, 62.9, 11.3, 120.7, 121.2, 123.3, 125.8, 127.0, 129.1, 129.4, 129.8, 130.5, 133.8, 134.1, 139.7, 157.8; HPLC-MS (ESI-TOF): r_t = 9.86 min m/z = 417 $[\text{M}+\text{H}]^+$; HRMS (ESI-TOF) m/z calcd for $\text{C}_{21}\text{H}_{19}\text{BrClNO}$ 415.0339, found 415.0338.

PB13: 4-(6-Chloro-1H-indol-2-yl)-1,3-bis-(4-chloro-phenyl)-azetidin-2-one



90 mg (0.5 mmol) 6-Chloro-1H-indole-2-carbaldehyde and 65 mg (0.5 mmol) 4-chlorophenylamine are dissolved in DCM and a small amount MgSO_4 is added and stirred over night. The salt is filtered off and the filtrate is concentrated under reduced pressure. The residue is dissolved in toluene and 335 μ L (4.8 eq, 2.4 mmol) triethylamine and 125.8 μ L (1.72 eq, 0.86 mmol) (4-chlorophenyl)-acetylchloride are added simultaneously. The reaction mixture is heated in the microwave for 40 min at 130 $^{\circ}$ C. After the mixture cooled to room temperature the solid is filtered off and the filtrate is evaporated. The residue is dissolved in ethyl acetate and extracted with water and brine. The organic layer is dried over MgSO_4 and evaporated. The crude product is purified by chromatography on silica gel with heptane/ethyl acetate 4:1 to yield 4-(6-chloro-1H-indol-2-yl)-1,3-bis-(4-chloro-phenyl)-azetidin-2-one (PB13) 54 mg (25%); 1 H-NMR (CDCl_3 , 600 MHz): δ = 4.58 (s, 1H), 5.12 (s, 1H), 6.61-6.65 (m, 1H), 6.69 (m, 1H), 7.10-7.16 (m, 3H), 7.24-7.32 (m, 4H), 7.37-7.38 (m, 2H), 7.54 (d, 1H), 9.69 (s, 1H); 13 C-NMR (CDCl_3 , 150 MHz): δ = 58.6, 62.6, 103.7, 111.4, 116.3, 118.2, 121.2, 121.6, 126.4, 128.6, 128.9, 129.1, 129.4, 129.5, 130.1, 130.2, 132.1, 133.7, 134.4, 135.7, 137.5, 165.7; HPLC-MS (ESI-TOF): r_t = 13.16 min m/z = 441 $[\text{M}]$; HRMS (ESI-TOF) m/z calcd for $\text{C}_{23}\text{H}_{15}\text{Cl}_3\text{N}_2\text{O}$ 440.0249, found 440.0254.

7.2 K_i of the small molecular weight inhibitors for Mdm2 as measured by HSQC-NMR based compound titration (μM).

Compound No.	MW [Da]	Kd [μM]	Kd [M]	pKd (-Log K_D)	BEI (pKd/MW [kDa])
BEB 55	347,84	60,0	6,00E-05	4,221849	12,13733
BEB 59	361,87	60,0	6,00E-05	4,221849	11,66676
BEB 62	343	60,0	6,00E-05	4,221849	12,3086
BEB 64	382,29	80,0	8,00E-05	4,09691	10,71676
BEB 65	382,29	60,0	6,00E-05	4,221849	11,04358
BEB 68	466,79	60,0	6,00E-05	4,221849	9,044428
BEB 96	466,8	precipitation			
BEB 97	466,8	60,0	6,00E-05	4,221849	9,044235
BEB 98	482,41	no interaction			
BEB 110	368,87	15,0	1,50E-05	4,823909	13,07753
BEB 110 major	368,87	3,0	3,00E-06	5,522879	14,97243
BEB 110 minor	368,87	40,0	4,00E-05	4,39794	11,92274
BEB 111	407,9	30,0	3,00E-05	4,522879	11,0882
BEB 112	391,86	200,0	2,00E-04	3,69897	9,439519
BEB 113	416,74	30,0	3,00E-05	4,522879	10,853
BEB 116	403,31	60,0	6,00E-05	4,221849	10,468
BEB 116 major	403,31	1,5	1,50E-06	5,823909	14,44028
BEB 116 major f20-30	403,31	1,5	1,50E-06	5,823909	14,44028
BEB 116 minor	403,31	precipitation			
BEB 117A	444,36	60,0	6,00E-05	4,221849	9,500965
BEB 117C	444,36	60,0	6,00E-05	4,221849	9,500965
BEB 119	397,28	30,0	3,00E-05	4,522879	11,38461
BEB 120	379,91	150,0	1,50E-04	3,823909	10,0653
BEB 124	386,86	5,0	5,00E-06	5,30103	13,70271
BEB 124_II dia mix	386,86	5,0	5,00E-06	5,30103	13,70271
BEB 125	361,25	60,0	6,00E-05	4,221849	11,68678
BEB 126_II	386,87	15,0	1,50E-05	4,823909	12,46907
BEB 130	419,91	30,0	3,00E-05	4,522879	10,77107
BEB 134	425,31	5,0	5,00E-06	5,30103	12,46392
BEB 141 dia mix	405,89	6,0	6,00E-06	5,221849	12,86518
BEB 142	453,37	15,0	1,50E-05	4,823909	10,64011
BEB 162	422,86	5,0	5,00E-06	5,30103	12,53613
BEB 165	387,91	15,0	1,50E-05	4,823909	12,43564
BEB 171	354,8	10,0	1,00E-05	5	14,09245
BEB 180A	306,8	60,0	6,00E-05	4,221849	13,76092
BEB 180B	306,8	10,0	1,00E-05	5	16,29726
BEB 181 dia mix	334,85	30,0	3,00E-05	4,522879	13,50718

BEB 182A	348,88	1,5	1,50E-06	5,823909	16,69316
BEB 182B	348,88	4,0	4,00E-06	5,39794	15,4722
BEB 190 diaA	373,46	not determined			
BEB 190 diaB	373,46	30,0	3,00E-05	4,522879	12,11074
BEB 191 dia B	311,39	60,0	6,00E-05	4,221849	13,55807
BEB 191 dia mix	311,39	60,0	6,00E-05	4,221849	13,55807
BEB 191 dia A	311,39	60,0	6,00E-05	4,221849	13,55807
BEB 192 f30-44BII	345,83	30,0	3,00E-05	4,522879	13,07833
Bv040	447,9	60,0	6,00E-05	4,221849	9,425874
Bv070	400,35	80,0	8,00E-05	4,09691	10,23332
Cp231	151,59	30,0	3,00E-05	4,522879	29,83626
Cpd01	511,44	80,0	8,00E-05	4,09691	8,010539
Cpd02	439,33	80,0	8,00E-05	4,09691	9,325359
Cpd03	469,36	80,0	8,00E-05	4,09691	8,728716
Cpd04	481,41	80,0	8,00E-05	4,09691	8,51023
SS 35A	343,25	60,0	6,00E-05	4,221849	12,29963
SS 43D	440,02	60,0	6,00E-05	4,221849	9,594675
SS 45D	440,02	60,0	6,00E-05	4,221849	9,594675
SS 78C	337,81	60,0	6,00E-05	4,221849	12,4977
SS 85A	365,91	60,0	6,00E-05	4,221849	11,53794
SS 87B-1	385,3	precipitation			
SS 92C-1	416,75	precipitation			
SS 95E	360,89	60,0	6,00E-05	4,221849	11,69844
SS 96C-1	340,4	60,0	6,00E-05	4,221849	12,40261
SS 100A-1	468,96	60,0	6,00E-05	4,221849	9,002578
SS 104A	388,73	100,0	1,00E-04	4	10,28992
SS 115	399,9	80,0	8,00E-05	4,09691	10,24484
SS 125H	362,25	30,0	3,00E-05	4,522879	12,48552
SS 127A	419,9	10,0	1,00E-05	5	11,9076
SS 127B	419,9	10,0	1,00E-05	5	11,9076
SS 128E	411,94	30,0	3,00E-05	4,522879	10,97946
SS 130D	376,27	30,0	3,00E-05	4,522879	12,0203
SS 132A	413,32	6,0	6,00E-06	5,221849	12,63391
SS 132B	413,32	7,0	7,00E-06	5,154902	12,47194
SS 136A	366,91	10,0	1,00E-05	5	13,62732
SS 137B	411,36	15,0	1,50E-05	4,823909	11,72673
SS 138 major	386,86	5,0	5,00E-06	5,30103	13,70271
SS 138A-3	386,86	5,0	5,00E-06	5,30103	13,70271
SS 138A pure diaA	386,86	5,0	5,00E-06	5,30103	13,70271
SS 147A	467,02	5,0	5,00E-06	5,30103	11,35076
SS 148A	481,04	5,0	5,00E-06	5,30103	11,01994
LHX 14b	340,44	30,0	3,00E-05	4,522879	13,28539
SS150Adia1	419,9	10,0	1,00E-05	5	11,9076
SS152Adia2	419,9	15,0	1,50E-05	4,823909	11,48823
SS 127AB	419,9	15,0	1,50E-05	4,823909	11,48823

BEB 135	396,92	precipitation				
BEB 137	370,88	precipitation				
LHX 05	350,37	80,0	8,00E-05	4,09691	11,6931	
LHX 08	412,87	80,0	8,00E-05	4,09691	9,923002	
KH 12cis	522,42	precipitation				
KH 14 cis	553,39	precipitation				
KH 14 trans	553,39	precipitation				
LHX 09 b2	324,38	20,0	2,00E-05	4,69897	14,486	
SS 154 A	444,97	2,5	2,50E-06	5,60206	12,58975	
SS 155 A	459	not soluble				
SS 156 A	425,9627	10,0	1,00E-05	5	11,73812	
SS 159	425,96	not soluble				
SS 157 A	439,99	5,0	5,00E-06	5,30103	12,04807	
SS 158 A	411,94	1,0	1,00E-06	6	14,56523	
SS 160 A	397,1	5,0	5,00E-06	5,30103	13,34936	
SS 164 A	447,03	7,5	7,50E-06	5,124939	11,46442	
SS 165 A	461,05	7,5	7,50E-06	5,124939	11,1158	
cpdo05	394,66	compound not soluble				
cpd09	432,97	60,0	6,00E-05	4,221849	9,750904	
cpd011	497,02	22,0	2,20E-05	4,657577	9,371006	
cpd012	501,44	5,0	5,00E-06	5,30103	10,57161	
SS 142 major E1	368,87	35,0	3,50E-05	4,455932	12,07995	
SS 142 major E2	368,87	7,5	7,50E-06	5,124939	13,89362	
SS 150A	419,9148	35,0	3,50E-05	4,455932	10,61151	
SS 167 A1/BEB232	439,01	0,8	7,50E-07	6,124939	13,95171	
SS 168 A1	405,97	1,0	1,00E-06	6	14,77942	
SS 169 f2	420	1,0	1,00E-06	6	14,28571	
SS183	630,2	no interaction				
BEB 217A	414,138	prec				
BEB 217B	414,138	prec				
BEB 218A	434,1067	>100				
BEB 218B	434,1067	degradation				
BEB 219C	432,0944	degradation				
WKI_011	421,93	15,0	1,50E-05	4,823909	11,43296	
WKI-011-2	421,93	7,0	7,00E-06	5,154902	12,21743	
WKI_020	506	60,0	6,00E-05	4,221849	8,343575	
WKI-020-2	506	35,0	3,50E-05	4,455932	8,80619	
SJ-14-2	356,442	100,0	1,00E-04	4	11,22202	
SJ-12-1	315,3901	100,0	1,00E-04	4	12,68271	
WK1-026-A	429,3439	degradation				
WK1036-2	376,9084	40,0	4,00E-05	4,39794	11,66846	
WK1-038-1	488,0095	7,0	7,00E-06	5,154902	10,56312	
SS 161-1	382,89	25,0	2,50E-05	4,60206	12,01927	
SS 161-4	382,89	80,0	8,00E-05	4,09691	10,69997	
SS 170 A	391,98	20,0	2,00E-05	4,69897	11,98778	

SS 166B	424,98	15,0	1,50E-05	4,823909	11,35091
SS 171 A	377,92	8,0	8,00E-06	5,09691	13,48674
SS175 A	481,04	1,0 or precipitation			
SS 176 A	495,07	3,5	3,50E-06	5,455932	11,02053
SS172 A	405,97	7,0	7,00E-06	5,154902	12,69774
SS173 A	454,02	4,0	4,00E-06	5,39794	11,88921
SS 179 A	439,99	25,0	2,50E-05	4,60206	10,45946
SS 177A	459	done			
SS178 A	473,02	10,0	1,00E-05	5	10,57038
SS181 A	411,94	7,0	7,00E-06	5,154902	12,51372
SS180A	425,96	0,8	7,50E-07	6,124939	14,37914
SS 182A	439,99	30,0	3,00E-05	4,522879	10,2795
BEB 210 (f21-30)	448,97	75,0	7,50E-05	4,124939	9,18756
BEB 210 (f13-16)	449,97	75,0	7,50E-05	4,124939	9,167142
BEB 214f10	547,12	23,0	2,30E-05	4,638272	8,477614
WK1-066-1	531,07	80,0	8,00E-05	4,09691	7,714444
WKI-056-1	423,94	20,0	2,00E-05	4,69897	11,08404
WK1-056-2	423,94	>100			
WK1-065-1	533,08	80,0	8,00E-05	4,09691	7,685357
WK1-067-1	478,01	100,0	1,00E-04	4	8,368026
WKI075-1	483,0023	3,0	3,00E-06	5,522879	11,43448
WKI075-2	483,0023	1,0	1,00E-06	6	12,4223
WK1-075	483,0023	10,0	1,00E-05	5	10,35192
SS 153-2	348,867	100,0	1,00E-04	4	11,46569
SS 153-1	348.867	>100			
SS-147-2	467,0029	1,0	1,00E-06	6	12,84789
SS 147-1	467,0029	15,0	1,50E-05	4,823909	10,3295
KN009f110-129	368,87	7,0	7,00E-06	5,154902	13,97485
KN009f170-220	368,87	5,0	5,00E-06	5,30103	14,371
SS148	481,0143	1,0	1,00E-06	6	12,47364
WK1-058-2	578,09	8,0	8,00E-06	5,09691	8,816811
WKI-041	506,999	6,0	6,00E-06	5,221849	10,29952
WK1-038-2	488,01	5,0	5,00E-06	5,30103	10,86254
m-CIPhOH	128,55	90,0	9,00E-05	4,045757	31,47225
CH020 f35-43	398,89	80,0	8,00E-05	4,09691	10,27078
CH020 f1-6	398,89	15,0	1,50E-05	4,823909	12,09333
WK1-049(??)	464,9623	precipitation			
WK1 072	464,9996	10,0	1,00E-05	5	10,7527
WW 114	458,9825	prec			
WK1- 053_1	479,94	>100			
WK1-053-2	479,94	>100			
WK1-080	555,1007	60,0	6,00E-05	4,221849	7,605555
WW 104	411,9244	2,0	2,00E-06	5,69897	13,83499
WW 103-1	444,9559	2,0	2,00E-06	5,69897	12,80794
WK1-056-10	384,8661	>100			

WK1-069	427,935	7,0	7,00E-06	5,154902	12,04599
WK1-074	520,0796	not soluble			
WK1-076	512,0595	30,0	3,00E-05	4,522879	8,832721
WK1-078	508,0408	>60			
WK1-077	525,0742	40,0	4,00E-05	4,39794	8,375845
WK1-104-2	355,4406	>200			
WW 145-1	398,9368	50,0	5,00E-05	4,30103	10,78123
WK1-146	384,856	80,0	8,00E-05	4,09691	10,64531
WK1-106-1	497,0421	30,0	3,00E-05	4,522879	9,099589
WK1-106-3	398,8826	5,0	5,00E-06	5,30103	13,2897
WK1-134-2	441,9504	25,0	2,50E-05	4,60206	10,41307
WW 126-1	483,4405	0,7	7,00E-07	6,154902	12,73146
WW 127-1	446,3806	0,8	8,00E-07	6,09691	13,65855
WW 128-1	350,8922	50,0	5,00E-05	4,30103	12,25741
WK1-134-1	444,0427	80,0	8,00E-05	4,09691	9,226387
WK1-073-2	380,0826	60,0	6,00E-05	4,221849	11,10771
WK1-079	563,1208	80,0	8,00E-05	4,09691	7,275366
CH020	398,8826	>100			
WK1-084-2	492,0414	4,0	4,00E-06	5,39794	10,9705
WK1-086	474,9819	4,0	4,00E-06	5,39794	11,36452
WK1-089	563,1101	2,5	2,50E-06	5,60206	9,948427
WK1-082-1	496,0047	>100			
WK1-092	533,0826	5,0	5,00E-06	5,30103	9,944106
WK1-102	479,0676	40,0	4,00E-05	4,39794	9,180208
WK1-094	440,9308	20,0	2,00E-05	4,69897	10,65693
WK1-117-1	346,8096	35,0	3,50E-05	4,455932	12,84835
WK1-095	550,1089	1,0	1,00E-06	6	10,90693
WW 132-2	449,0411	45,0	4,50E-05	4,346787	9,680155
WW133-1	393,9611	50,0	5,00E-05	4,30103	10,9174
WW 139-1	364,9193	60,0	6,00E-05	4,221849	11,56927
WK1-058-1	578,09	150,0	1,50E-04	3,823909	6,614729
WK1-071	415,9426	65,0	6,50E-05	4,187087	10,0665
WW 144-2	786,3315	50,0	5,00E-05	4,30103	5,469741
WW 165-2	440,2343	10,0	1,00E-05	5	11,35759

BEI: binding efficiency index

8 Abbreviations

• 1D	one-dimensional
• 2D	two-dimensional
• Å	Ångström (10^{-10} m)
• aa	amino acid
• ADME	absorption, distribution, metabolism and excretion
• APS	ammonium peroxydisulphate
• BEI	binding efficiency index
• bp	base pair
• brd	broad doublet
• brs	broad singlet
• BSA	bovine serum albumine
• cDNA	complementary DNA
• clogP	calculated logarithm of the 1-octanol-waterpartition coefficient
• COSY	correlation spectroscopy
• CP	carboxypeptidase
• d	doublet
• Da	Dalton (g mol^{-1})
• DMSO	dimethylsulfoxide
• EDTA	ethylenediamine tetraacetic acid
• g	gravity (9.81 m s^{-2})
• GH	growth hormone
• GuHCl	guanidine hydrochlorid
• GST	glutathione S-transferase
• HBA	hydrogen bond acceptor
• HBD	hydrogen bond donor
• Hdm2	Murine DoubleMinute-2 (human equivalent)
• Hdmx	Murine DoubleMinute-4 (human equivalent)
• HPLC	High performance liquid chromatography
• HSQC	heteronuclear single quantum coherence
• hs	Homo sapiens
• HTS	high-throughput screening
• Hz	Hertz
• IB	inclusion bodies
• IMAC	immobilized metal affinity chromatography
• IPTG	isopropyl- β -thiogalactopyranoside
• ITC	isothermal titration calorimetry

• K_D	dissociation constant
• LB	Luria-Broth medium
• m	multiplet
• MCR	multicomponent reaction
• Mdm2	Murine DoubleMinute-2
• Mdmx/Mdm4	Murine DoubleMinute-4
• MES	2-(N-Morpholino)ethanesulfonic acid sodium salt
• MIR	multiple isomorphous replacement
• MM	minimal medium
• MS	mass spectrometry
• MW	molecular weight
• NMR	nuclear magnetic resonance
• NOE	nuclear Overhauser effect
• NOESY	nuclear Overhauser enhancement spectroscopy
• nrotb	number of rotatable bonds
• OD	optical density
• PAGE	polyacrylamide gel electrophoresis
• PB	Pittsburgh
• PBS	phosphate-buffered saline
• PDB	Protein Data Bank
• PEG	polyethylene glycol
• PPI	protein-protein interaction
• ppm	parts per million
• s	singlet
• RMSD	root mean square deviation
• SAD	single anomalous dispersion
• SDS	sodium dodecyl sulfate
• spl	serine protease like
• TEMED	N,N,N',N'-tetramethylethylenediamine
• TCEP	(tris(2-carboxyethyl)phosphine)
• TOCSY	total correlation spectroscopy
• TPSA	total polar surface area
• ZF	zebrafish (<i>Danio rerio</i>)

Amino acids and nucleotides are abbreviated according to either one or three letter IUPAC code.

9 Literature references

- Abad-Zapatero, C., Metz, J.T. (2005). Ligand efficiency indices as guideposts for drug discovery. *Drug Discovery Today* 10, 464-469.
- Ambrosini, G., Sambol, E.B., Carvajal D., Vassilev, L.T., Singer, S. and Schwartz, G.K. (2007). Mouse double minute antagonist Nutlin-3a enhances chemotherapy-induced apoptosis in cancer cells with mutant p53 by activating E2F1. *Oncogene* 26, 3473-3481
- Andrews, P.R., Craik, D.J., Martin, J.L. (1984). Functional group contributions to drug-receptor interactions. *J. Med. Chem.* 27, 1648-1657.
- Ayed, A., Mulder, A.A.F., Gwan-Su, Y., Lu, Kay, L.E., Arrowsmith, C. (2001). Latent and active p53 are identical in conformation. *Nat. Struct. Biol.* 8, 756-760.
- Babaoglu, K. and Shoichet, B.K. (2006). Deconstructing fragment-based inhibitor discovery. *Nature Chem. Biol.* 2, 720-723.
- Barak, Y., Oren, M.(1992). Enhanced binding of a 95 kDa protein to p53 in cells undergoing p53-mediated growth arrest. *EMBO J.* 11, 2115-2121.
- Berg, T. (2008). Small-molecule inhibitors of protein-protein interactions. *Curr Opin Drug Disc Dev* 11, 666-674.
- Betti, M. (1900). Reazione generale di condensazione fra β -naftolo, aldeidi e amine. *Gazz. Chim. Ital.* 30, 306-316.
- Bista, M., Kowalska, K., Janczyk, W., Dömling, A., Holak, T.A. (2009). Robust NMR screening for lead compounds using tryptophan-containing proteins. *J. Am. Chem. Soc.* 131, 7500-7501.
- Bixby D, Lisa Kujawski L, Shaomeng Wang S, Sami N. Malek SN. (2008). The pre-clinical development of MDM2 inhibitors in chronic lymphocytic leukemia uncovers a central role for p53 status in sensitivity to MDM2 inhibitor-mediated apoptosis. *Cell Cycle* 7, 971-9.
- Bon, R.S., Hong, C., Bouma, M.J., Schmitz, R.F., de Kanter, F.J.J., Lutz, m., Spek, A.L., Orru, R.V.A. (2003). Novel multicomponent reaction for the combinatorial synthesis of 2-imidazolines. *Org. Lett.* 5, 3759-3762.
- Bossio, R., Marcaccini, S., Pepino, R. (1995). Studies on isocyanides. Synthesis of N-tosylguanidines. *Tetrahedron Lett.* 36, 2325-2326.
- Böttger A, Böttger V, Garcia Echeverria C, Chene P, Hochkeppel HK, Sampson W, Ang K, Howard SF, Picksley SM, Lane DP. (1997). Molecular characterization of the hdm2–p53 interaction. *J Mol Biol* 269, 744–756.
- Böttger V, Böttger A, Howard, SF, Picksley SM, Chene P, Garcia Echeverria C, HK Hochkeppel HK, Lane DP. (1996). Identification of novel Mdm2 binding peptides by phage display. *Oncogene* 13, 2141–2147.

- Böttger, A., Böttger, V., Sparks, A., Liu, W.L., Howard, S.F., Lane, D.P. (1997). Design of a synthetic Mdm2-binding mini protein that activates the p53 response in vivo. *Curr Biol* 7, 860-869.
- Böttger, V., Böttger, A., Garcia-Echeverria, C., Ramos, Y.F., van der Eb, A.J., Jochemsen, A.G., Lane, D.P. (1999). Comparative study of the p53-mdm2 and p53-MDMX interfaces. *Oncogene* 18, 189-199.
- Cañadillas, J.M., Tidow, H., Freund, S.M., Rutherford, T.J., Ang, H.C., Fersht, A.R. (2006). Solution structure of p53 core domain: structural basis for its instability. *Proc Natl Acad Sci U S A* 103, 2109-2114.
- Cahilly-Snyder, L., Yang-Feng, T., Francke, U., George, D.L. (1987). Molecular analysis and chromosomal mapping of amplified genes isolated from a transformed mouse 3T3 cell line. *Somat Cell Mol Genet* 13, 235-244.
- CCP4, Collaborative computational project, Number 4. *Acta Crystallogr Sect D* 1994; 50, 760-763.
- Chene, P. (2003). Inhibiting the p53-MDM2 interaction: an important target for cancer therapy *Nature Rev. Cancer* 3, 102-109.
- Cheok, C.F., Lane, D.P. New developments in small molecules targeting p53 pathways in anticancer therapy. *Drug Develop. Res.* 69, 289-296 (2008).
- Clackson, T., Wells, J.A. (1995). A hot spot of binding energy in a hormone-receptor interface. *Science* 267, 383-386.
- Czarna, A., Popowicz, G.M., Holak T.A., Doemling A. (2009). Novel small molecular weight inhibitors of the Hdm2-p53 protein-protein interaction obtained from rapid multicomponent chemistry. *Proc. Natl. Acad. Sci. USA* submitted.
- Czarna, A., Popowicz, G.M., Pecak, A., Wolf, S., Dubin, G., and Holak, T.A. (2009). High affinity interaction of the p53 peptide-analogue with human Mdm2 and Mdmx. *Cell Cycle* 8, 1174-1183.
- Coles, M., Heller, M. and Kessler, H. (2003). NMR-based screening technologies. *Drug Discov. Today* 8, 803-810.
- Dastidar, S.G., Lane, D.P., Verma, C.V. (2008). Multiple peptide conformations give rise to similar binding affinities: molecular simulations of p53-MDM2. *J Am Chem Soc* 130, 13514-15.
- Dawson, R., Mueller, L., Dehner, A., Klein, C., Kessler, H. and Buchner, J. (2003). The N-terminal domain of p53 is natively unfolded. *J. Mol. Biol.* 332, 1131-1141.
- DeLeo, A.B., Jay, G., Apella, E., Dubois, G.C., Law, L., W., Old, L., J. (1979). Detection of a transformation-related antigen in chemically-induced sarcomas and other transformed cells of the mouse. *Proc Natl Acad Sci U S A* 76, 2420-2424.

- Diercks, T., Coles, M. and Kessler, H. (2001). Applications of NMR in drug discovery. *Curr. Opin. Chem. Biol.* 5, 285-291.
- Dömling, A. Small molecular weight protein-protein interaction antagonists - an insurmountable challenge? *Curr. Opin. Chem. Biol.* 12, 281-291 (2008).
- D'Silva, L., Ozdowy, P., Krajewski, M., Rothweiler, U., Singh, M. and Holak, T.A. (2005). Monitoring the effects of antagonists on protein-protein interactions with NMR spectroscopy. *J. Amer. Chem. Soc.* 127, 13220-13226.
- Eliyahu, D., Michalovitz, D., Eliyahu, S., Pinhasi-Kimhi, O., Oren, M. (1989). Wild-type p53 can inhibit oncogene-mediated focus formation. *Proc Natl Acad Sci U S A* 86, 8763-8767.
- Erlanson, D.A. (2006). T. Fragment-based lead discovery: a chemical update. *Curr. Opin. Biotech.* 17, 643-652.
- Fasan, R., Dias, R.L., Moehle, K., Zerbe, O., Obrecht, D., Mittl, P.R., Robinson, J.A. (2006). Structure-activity studies in a family of beta-hairpin protein epitope mimetic inhibitors of the p53-HDM2 protein-protein interaction. *Chembiochem* 7, 515-526.
- Finlay, C.A., Hinds, P.W., Eliyahu, d., Oren, M., Levine, A.J., (1988). Activating mutations for transformation by p53 produce a gene product that forms an hsc70-p53 complex with an altered half-life. *Molecular and cellular Biology* 8, 531-539.
- Finlay, C.A., Hinds, P.W., Levine, A.J. (1989). The p53 proto-oncogene can act as a suppressor of transformation. *Cell* 57, 1083-1093
- Francoz, S., Froment, P., Bogaerts, S., De Clercq, S., Maetens, M., Doumont, G., Bellefroid, E., Marine, J.C. (2006). Mdm4 and Mdm2 cooperate to inhibit p53 activity in proliferating and quiescent cells in vivo. *Proc Natl Acad Sci USA* 103, 3232-3237.
- Galatin, P.S., Abraham, D.J. (2004). A nonpeptidic sulfonamide inhibits the p53-mdm2 interaction and activates p53-dependent transcription in mdm2-overexpressing cells. *J. Med. Chem.* 47, 4163-4165.
- Gerber, P.R., Müller, K. (1995). MAB, a generally applicable molecular force field for structure modelling in medicinal chemistry. *J. Comp.-Aided Mol. Des.* 9, 251-268.
- Gerber, P.R. (1998). Charge distribution from a simple molecular orbital type calculation and non-bonding interaction terms in the force field MAB. *J. Comp.-Aided Mol. Des.* 12, 37-51.
- Ghosh, M., Weghorst, K., Berberich, S.J. (2005). MdmX inhibits ARF mediated Mdm2 sumoylation. *Cell Cycle* 4, 604-608.
- Gilkes, D.M., Chen, J. (2007). Distinct roles of MDMX in the regulation of p53 response to ribosomal stress. *Cell Cycle* 6, 151-155.
- Grasberger, B.L., Lu, T., Schubert, C., Parks, D.J., Carver, T.E., Koblisch, H.K., Cummings, M.D., LaFrance, L.V., Milkiewicz, K.L., Calvo, R.R., Maguire, D., Lattanze, J., Franks,

- C.F., Zhao, S., Ramachandren, K., Bylebyl, G.R., Zhang, M., Manthey, C.L., Petrella, E.C., Pantoliano, M.W., Deckman, I.C., Spurlino, J.C., Maroney, A.C., Tomczuk, B.E., Molloy, C.J. and Bone, R.F. (2005). Discovery and cocrystal structure of benzodiazepinedione HDM2 antagonists that activate p53 in cells. *J. Med. Chem.* 48, 909-912.
- Hajduk, P.J. (2006). Fragment-Based Drug Design: How Big Is Too Big? *J. Med. Chem.* 49, 6972-6976.
- Hajduk, P.J. and Greer, J. (2007). A decade of fragment-based drug design: strategic advances and lessons learned. *Nature Rev. Drug Discov.* 6, 211-219.
- S.L. Harris and A.J. Levine, The p53 pathway: positive and negative feedback loops, *Oncogene* 24 (2005), pp. 2899–2908.
- Haupt, Y., Maya, R., Kazaz, A. and Oren, M. (1997). Mdm2 promotes the rapid degradation of p53. *Nature* 387, 296-299.
- Haupt, Y. (2004). p53 Regulation: a family affair. *Cell Cycle* 3, 884-885.
- Hu, C.Q., Hu, Y.Z. (2008). Small molecule inhibitors of the p53-MDM2. *Curr Med Chem* 15, 1720-1730.
- Hu, B., Gilkes, D.M., Farooqi, B., Sebt, S.M. and Chen, J. (2006). MDMX overexpression prevents p53 activation by the MDM2 inhibitor Nutlin. *J Biol Chem.* 281, 33030-33035.
- Hu, B., Gilkes, D.M., Chen, J. (2006). Efficient p53 activation and apoptosis by simultaneous disruption of binding to MDM2 and MDMX. *Cancer Res* 67, 8810-8817.
- Hubbard, R.E., Chen, I. and Davis B. (2007). Informatics and modeling challenges in fragment-based drug discovery. *Curr. Opin. Drug Discov. Dev.* 10, 289-297.
- Irwin, J.J. and Shoichet, B.K. (2005). ZINC-a free database of commercially available compounds for virtual screening. *J. Chem. Inf. Model.* 4, 177-182.
- Issaeva, N., Bozko, P., Enge, M., Protopopova, M., Verhoef, L.G., Masucci M., Pramanik, A., Selivanova, G. (2004). Small molecule RITA binds to p53, blocks p53–mdm2 interaction and activates p53 function in tumors. *Nat. Med.* 10, 1321-1328.
- Jahnke, W. and Erlanson, D.A. (Eds) (2006): Fragment-based approaches in drug discovery. Vol 34 in series *Methods and Principles in Medicinal Chemistry* (Series Eds: R Mannhold, H Kubinyi, G Folkers). Weinheim, Germany: Wiley-VCH.
- Jahnke, W. and Widmer H. (2004). Protein NMR in biomedical research. *Cell. Mol. Life Sci.* 61, 580-599.
- Joerger, A.C., Fersht, A.R. Structural biology of the tumor suppressor p53. *Ann. Rev. Biochem.* 77, 557-582 (2008).
- Kabsch, W. (1993). Automatic processing of rotation diffraction data from crystals of initially unknown symmetry and cell constants. *J Appl Cryst* 26, 795-800.

- Kalinski, C., Umkehrer, M., Gonnard, S., Jäger, N., Ross, G., Hiller, W. (2006). A new and versatile Ugi/SNAr synthesis of fused 4,5-dihydro-tetrazolo[1,5-a]quinoxalines. *Tetrahedron Lett.* 47, 2041-2044.
- Kallen, J., Goepfert, A., Blechschmidt, A., Izaac, A., Geiser, M., Tavares, G., Ramage, P., Furet, P., Masuya, K., Lisztwan, J. (2009). Crystal Structures of Human MdmX (HdmX) in Complex with p53 Peptide-Analogues reveal Surprising Conformational Changes. *J. Biol. Chem.* In press 10.1074/jbc.M809096200.
- Klages, J., Coles, M. and Kessler, H. (2007). NMR-based screening: a powerful tool in fragment-based drug discovery. *Analyst* 7, 693-705.
- Koblish, H.K., Zhao, S.Y., Franks, C.F., Donatelli, R.R., Tominovich, R.M., LaFrance, L.V., Leonard, K.A., Gushue, J.M., Parks, D.J., Calvo, R.R., Milkiewicz, K.L., Marugan, J.J., Raboisson, P., Cummings, M.D., Grasberger, B.L., Johnson, D.L., Lu, T.B., Molloy, C.J. and Maroney, A.C. (2006). Benzodiazepinedione inhibitors of the Hdm2 : p53 complex suppress human tumor cell proliferation in vitro and sensitize tumors to doxorubicin in vivo. *Mol. Cancer Therap.* 5, 160-169.
- Krajewski, M., Ozdowy, P., D'Silva, L., Rothweiler, U. and Holak T.A. (2005). NMR indicates that the small molecule RITA does not block the p53-MDM2 binding in vitro. *Nature Med.* 11, 1135-1136.
- Krajewski, M., Rothweiler, U., D'Silva, L., Majumdar, S., Klein, C., and Holak T.A. (2007). An NMR-based antagonist induced dissociation assay for targeting the ligand-protein and protein-protein interactions in competition binding experiments. *J. Med. Chem.* 50, 4382-4387.
- Kubbutat, M.H., Jones, S.N. and Vousden, K.H. (1997). Regulation of p53 stability by Mdm2. *Nature* 387, 299-303.
- Kussie, P.H., Gorina, S., Marechal, V., Elenbaas, B., Moreau, J., Levine, A.J. and Pavletich, N.P. (1996). Structure of the MDM2 oncoprotein bound to the p53 tumor suppressor transactivation domain. *Science* 274, 948-953.
- Lamzin VS, Wilson KS. (1993). Automated refinement of protein models. *Acta Crystallogr Sect D* 49, 129-49.
- Lane DP, Crawford LV. (1979). T antigen is bound to a host protein in SV40-transformed cells. *Nature* 15, 261-263.
- Laurie, N.A., Donovan, S.L., Shih, C.S., Zhang, J., Mills, N., Fuller, C., Teunisse, A., Lam, S., Ramos, Y., Mohan, A., Johnson, D., Wilson, M., Rodriguez-Galindo, C., Quarto, M., Francoz, S., Mendrysa, S.M., Guy, R.K., Marine, J.C., Jochemsen, A.G. and Dyer, M.A. (2006). Inactivation of the p53 pathway in retinoblastoma. *Nature* 444, 61-66.

- Lavigueur, A., Maltby, V., Mock, D., Rossant, J., Pawson, T., Bernstein, A. (1989). High Incidence of Lung, Bone, and Lymphoid Tumors in Transgenic Mice Overexpressing Mutant Alleles of the p53 Oncogene. *Molecular and Cellular Biology* 3982-3991.
- Lee, H., Mok, K.,H., Muhandiram, R., Park, K., Suk, J., Kim, D., Chang, J., Sung, Y.C., Choi, K.Y., Han, K. (2000). Local structural elements in the mostly unstructured transcriptional activation domain of human p53. *J. Biol. Chem.* 275, 29426-29432.
- Lehman, J.A., Eitel, J.A., Batuello, C.N. et al. (2008). Therapeutic considerations for Mdm2: not just a one trick pony. *Expert Opin on Drug Discov* 3, 1309-1321
- Lepre, C.A., Moore, J.M. and Peng, J.W. (2004). Theory and applications of NMR-based screening in pharmaceutical research. *Chem. Rev.* 104, 3641-3675.
- Levine, A. J. (1997). p53, the cellular gatekeeper for growth and division, *Cell* 88, 323–331.
- Lin, J., Chen, J., Elenbaas, B., Levine, A.J. (1994). Several hydrophobic amino acids in the p53 amino-terminal domain are required for transcriptional activation, binding to mdm-2 and the adenovirus 5 E1B 55-kD protein. *Genes Dev.* 8, 1235-1246.
- Linke, K, Mace P.H, smith, C.A. Vaux D.L., Silke, J., Day, C.L. (2008). Structure of the MDM2/MDMX RING domain heterodimer reveals dimerization is required for their ubiquitilation in trans. *Cell Death Differ* 15, 841-848.
- Linzer, D.I, Levine, A.J. (1979). Characterization of a 54K dalton cellular SV40 tumor antigen present in SV40-transformed cells and uninfected embryonal carcinoma cells. *Cell* 17, 43-52.
- Lipinski, C.A. (2004). Lead- and drug-like compounds: the rule-of-five revolution. *Drug Discovery Today Technol.* 1, 337-341.
- Lorber, D.M. and Shoichet. B.K. (2005). Hierarchical docking of databases of multiple ligand conformations. *Curr. Top. Med. Chem.* 5, 739-749.
- Marine, J.C.W., Dyer, M.A. and Jochemsen, A.G. (2007). MDMX: from bench to bedside. *J. Cell. Sci.* 120, 371-378.
- Marine JC, Francoz S, Maetens M, Wahl G, Toledo F, Lozano G. (2006). Keeping p53 in check: essential and synergistic functions of Mdm2 and Mdm4. *Cell Death Differ* 13, 927-934.
- Martins, C.P, Brown-Swigart, L. and Evan, G.I. (2006). Modeling the therapeutic efficacy of p53 restoration in tumors. *Cell* 127, 1323-1334.
- Marx, J. (2007). Recruiting the cell's own guardian for cancer therapy. *Science* 315, 1211-1213.
- Meulmeester, E., Pereg, Y., Shiloh, Y., Jochemsen, A.G. (2005). ATM-mediated phosphorylations inhibit Mdmx/Mdm2 stabilization by HAUSP in favor of p53 activation. *Cell Cycle* 4, 1166-1170.

- Meireles, L., Dömling, A., Camacho, C.J. ANCHOR database: A PDB-wide screening tool of protein-protein interactions for small molecule intervention. submitted.
- McFadyen, I., Walker, G., Alvarez, J. Enhancing hit quality and diversity within assay throughput constraints. *Methods and Principles in Medicinal Chemistry: Chemoinformatics in Drug Discovery Vol 23*, ed. Oprea TI (Wiley-VCH, Weinheim, 2004).
- McRee DE. (1999). XtalView/Xfit - A versatile program for manipulating atomic coordinates and electron density. *J Struc Biol* 125, 156-65.
- Meulmeester, E., Jochemsen, A.G. (2008). p53: A guide to apoptosis. *Curr Cancer Drug Targets* 8, 87-97.
- Meyer, B. and Peters, T. (2003). NMR spectroscopy techniques for screening and identifying ligand binding to protein receptors. *Angew. Chem. Int. Ed.* 42, 864-890.
- Moll, U.M., Wolff, S., Speidel, D., Deppert, W. (2005). Transcription-independent pro-apoptotic functions of p53, *Curr. Opin. Cell Biol.* 17, 631–636
- Momand, J., Zambetti, G.P., Olson, D.C., George, D. and Levine, A.J. (1992). The mdm-2 oncogene product forms a complex with the p53 protein and inhibits p53-mediated transactivation. *Cell* 69, 1237-1245.
- Murray, J.K., Gellman, S.H. (2007). Targeting protein-protein interactions: Lessons from p53/MDM2. *Biopolymers* 88, 657-86.
- Murshudov, G.N., Vagin, A.A., and Dodsonm, E.J. (1997). *Acta Crystallogr D Biol Crystallogr* 53, 240-255.
- Nolan, G.P. (2007). What's wrong with drug screening today. *Nature Chem. Biol.* 3, 187-191.
- Nooren, I.M.A., Thornton, J.M. (2003). Diversity of protein-protein interactions. *EMBO J.* 22, 3466-3492.
- Oliner, J.D., Kinzler, K.W., Meltzer, P.S., George, D.L., Vogelstein, B. (1992). Amplification of a gene encoding a p53-associated protein in human sarcomas.. *Nature* 358, 80-83.
- Oren, M., Levine, A.J., (1983). Molecular cloning of a cDNA specific for the murine p53 cellular tumor antigen. *Proc Natl Acad Sci U S A* 80, 56-59.
- Passerini, M., Bonciani, T. (1933). Reazione fra indoli e basi de Schiff. *Gazz. Chim. Ital.* 63, 138-144.
- Patton, J.T., Mayo, L.D., Singhi, A.D., Gudkov, A.V., Stark, G.R., Jackson, M.W. (2006). Levels of HdmX expression dictate the sensitivity of normal and transformed cells to Nutlin-3. *Cancer Res* 66, 3169-76.
- Pearlman, D.A., Case, D.A., Caldwell, J.W., Ross, W.S., Cheatham, T.E., III., DeBolt, S., Ferguson, D., Seibel, G. and Kollman P. (1995). AMBER, a package of computer programs for applying molecular mechanics, normal mode analysis, molecular

- dynamics and free energy calculations to simulate the structural and energetic properties of molecules. *Comp. Phys. Commun.* 91, 1-41.
- Pellecchia, M., Bertini, I., Cowburn, d., Dalvit, C., Giralt, E., Jahnke, W., James, T.L., Homans, S.W., Kessler, H., Luchinat, C., Meyer, B., Oschkinat, H., Peng, J., Schwalbe, H., Siegal, G. (2008) Perspectives on NMR in drug discovery: a technique comes of age. *Nat. Rev. Drug Disc.* 7, 738-745 (2008).
- Peng, J.,W., Moore, J. and Abdul-Manan, N. (2004). NMR experiments for lead generation in drug discovery. *Prog. NMR Spectr.* 44, 225-256.
- Picksley, S.M., Vojtesek, B., Sparks, A., Lane, D.P. (1994). Immunochemical analysis of the interaction of p53 with MDM2;--fine mapping of the MDM2 binding site on p53 using synthetic peptides. *Oncogene* 9, 2523-2529.
- Pirok, G., Mate, N., Varga, J., Vargyas, M., Dorent, S., Csizmadia, F. (2006). Making "real" molecules in virtual space. *J. Chem. Inf. Model* 46, 563-568.
- Popowicz, G.M., Czarna, A., Rothweiler, U., Szwagierczak, A., Krajewski, M., Weber, L. and Holak, T.A. (2007). Molecular basis for the inhibition of p53 by Mdmx. *Cell Cycle*, 6, 2386-2392.
- Popowicz, G.M., Czarna, A., and Holak T.A. (2008). Structure of the human Mdmx protein bound to the p53 tumor suppressor transactivation domain. (2007). *Cell Cycle* 7, 2441 – 2443.
- Rago, C., Vogelstein, B., Bunz, F. (2007). Genetic knockouts and knockins in human somatic cells. *Nat. Prot.* 2, 2732-2746.
- Rees, D.C., Congreve, M., Murray, C.W. and Carr, R. (2004). Fragment-based lead discovery. *Nat. Rev. Drug Discov.* 3, 660-672.
- Rehm, T., Huber, R. and Holak, T.A. (2002a) Application of NMR in Structural Proteomics: Screening for Proteins Amenable to Structural Analysis. *Structure* 10, 1613-1618.
- Ringshausen, I., O'Shea, C.C., Finch, A.J., Swigart, L.B. and Evan, G.I. (2006). Mdm2 is critically and continuously required to suppress lethal p53 activity in vivo. *Cancer Cell* 10, 501-514.
- Rothweiler, U., Czarna, A., Krajewski, M., Ciombor, J. Kalinski, C., Khazak, V. Ross, G., Skobeleva, N., Weber, L. and Holak, T.A. (2008a). Isoquinolin-1-one inhibitors of the MDM2-p53 interaction. *ChemMedChem* 3, 1118-1128.
- Rothweiler, U., Czarna, A., Weber, L., Popowicz, G.M., Brongel, K., Kowalska, K., Orth, M., Stemmann, O., and Holak, T.A. (2008b). NMR screening for lead compounds using tryptophan-mutated proteins. *J. Med. Chem.* 51, 5035-5042.
- Sakurai K, Schubert C, Kahne D. (2006). Crystallographic analysis of an 8-mer p53 peptide analogue complexed with MDM2. *J Am Chem Soc* 128, 11000-11001

- Schade, M. and Oschkinat H. (2005). NMR fragment screening: Tackling protein-protein interaction targets. *Curr. Opin. Drug Discov. Dev.* 8, 365-373.
- Schon O, Friedler A, Bycroft M, Freund SMV, Fersht AR. (2002). Molecular mechanism of the interaction between MDM2 and p53. *J Mol Biol* 323, 491-501.
- Shangary, S., Qin, D., McEachern, D., Liu, M., Miller, R.S., Qiu, S., Nikolovska-Coleska, Z., Ding, K., Wang, G., Chen, J., Bernard, D., Zhang, J., Lu, Y., Gu, Q., Shah, R.B., Pienta, K.J., Ling, X., Kang, S., Guo, M., Sun, Y., Yang, D. and Wang, S. (2008). Temporal activation of p53 by a specific MDM2 inhibitor is selectively toxic to tumors and leads to complete tumor growth inhibition. *Proc. Natl. Acad. Sci. USA*, 105, 3933-3938.
- Shangary S, Wang SM. (2008). Targeting the MDM2-p53 interaction for cancer therapy. *Clin Cancer Res* 14, 5318-5324.
- Shuker, S.B., Hajduk, P. J., Meadows, R.P. and Fesik, S.W. (1996). Discovering high-affinity ligands for proteins: SAR by NMR. *Science*, 274, 1531-1534.
- Shvarts A, Steegenga WT, Riteco N, van Laar T, Dekker P, Bazuine M, van Ham RC, van der Houven van Oordt W, Hateboer G, van der Eb AJ, Jochemsen AG. (1996). MDMX: a novel p53-binding protein with some functional properties of MDM2. *EMBO J* 15, 5349-5357.
- Spencer, R.W. (1998). High-throughput screening of historic collections: Observations on file size, biological targets, and file diversity. *Biotech. Bioeng. Comb. Chem.* 61, 61-67.
- Srivastava, S., Beck, B., Wang, W., Czarna, A., Holak, T.A., Dömling, A. (2009). Rapid and efficient hydrophilicity tuning of p53/mdm2 antagonists. *J. Comb. Chem.* 11, 631-639.
- Staudinger, H. (1907). Zur Kenntniss der Ketene. Diphenylketen. *Liebigs Ann. Chem.* 356, 51-123.
- Stockman, B.J. and Dalvit, C. (2002). NMR screening techniques in drug discovery and drug design. *Prog. NMR Spectr.* 41, 187-231.
- Stoll, R., Renner, C., Hansen, S., Palme, S., Klein, C., Belling, A., Zeslawski, W., Kamionka, M., Rehm, T., Mühlhahn, P., Schumacher, R., Hesse, F., Kaluza, B., Voelter, W., Engh, R.A. and Holak, T.A. (2001). Chalcone derivatives antagonize interactions between the human oncoprotein MDM2 and p53. *Biochemistry* 40, 336-344.
- Stommel, J.M., Wahl, G.M. (2005). A new twist in the feedback loop: stress-activated MDM2 destabilization is required for p53 activation. *Cell Cycle* 4, 411-417.
- Thanos, C.D., DeLano, W.L., Wells, J.A. (2006). Hot-spot mimicry of a cytokine receptor by a small molecule. *Proc. Natl. Acad. Sci. USA* 103, 15422-15427.
- Thomas, C.A., Grant, S.G., Pflug, B.R., Getzenberg, R.H., Day, B.W. (2008). (Z)-1,1-Dichloro-2-(4-methoxyphenyl)-3-phenylcyclopropane induces concentration-dependent

- growth inhibition, apoptosis, and coordinates regulation of apoptotic genes in TRAMP cells. *Urol. Oncol.* 26, 378-383.
- Toledo, F. and Wahl, G.M. (2006). Regulating the p53 pathway: in vitro hypotheses, in vivo veritas. *Nature Rev. Cancer* 6, 909–923.
- Toledo, F., Krummel, K.A., Lee, C.J., Liu, C.W., Rodewald, L.W., Tang, M. and Wahl, G.M. (2006). A mouse p53 mutant lacking the proline-rich domain rescues Mdm4 deficiency and provides insight into the Mdm2-Mdm4-p53 regulatory network. *Cancer Cell* 9, 273-285.
- Tse, C., et al. ABT-263: a potent and orally bioavailable Bcl-2 family inhibitor. *Cancer Res.* 68, 3421-3428 (2008).
- Ugi, I. (1971). *Isonitrile Chemistry*, Academic Press, New York, 149-155.
- Vassilev, L.T. (2007). MDM2 inhibitors for cancer therapy. *Trends Mol. Med.* 13, 23-31.
- Vassilev, L.T., Vu, B.T., Graves, B., Carvajal, D., Podlaski, F., Filipovic, Z., Kong, N., Kammlott, U., Lukacs, C., Klein, C., Fotouhi, N. and Liu, E.A. (2004). In vivo activation of the p53 pathway by small-molecular antagonists of Mdm2. *Science* 303, 844-848.
- van Leusen, D. (2001). Synthetic uses of tosylmethyl isocyanide (TosMIC). *Org. React.* 57, 417-666.
- Vazquez A, Bond EE, Levine AJ, Bond GL. (2008). The genetics of the p53 pathway, apoptosis and cancer therapy. *Nat Rev Drug Discov* 7, 979-987.
- Ventura, A., Kirsch, D.G., McLaughlin, M.E., Tuveson, D.A., Grimm, J., Lintault, L., Newman, J., Reczek, E.E., Weissleder, R. and Jacks, T. (2007). Restoration of p53 function leads to tumour regression in vivo. *Nature* 445, 661-665.
- Vogelstein, B., Lane, D. and Levine, A.J. (2000). Surfing the p53 network. *Nature* 408, 307-310.
- Vousden, K.H. and Lane, D.P. (2007). p53 in health and disease. *Nature Rev. Mol. Cell Biol.* 8, 275-283.
- Vousden, K.H., and X. Lu, X. (2002). Live or let die: the cell's response to p53, *Nat. Rev. Cancer* 2, 594–604.
- Wade, M., Wahl, G.M. (2009). Targeting Mdm2 and Mdmx in cancer therapy: better living through medicinal chemistry? *Mol Cancer Res* 7, 1-11
- Wade, M., Wong, E.T., Tang, M., Stommel, J.M. and Wahl, G.M. (2006). Hdmx modulates the outcome of p53 activation in human tumor cells. *J. Biol. Chem.* 281, 33036-33044.
- Weber, L. Tetrahydro-isoquinolin-1-ones for the treatment of cancer, International patent 2006; PCT/EP2006/002471.
- Wells, J.A., McClendon, C.L. (2007). Reaching for high-hanging fruit in drug discovery at protein–protein interfaces. *Nature* 450, 1001-1009.

- Wunderlich, M., Ghosh, M., Weghorst, K., Berberich, S.J. (2004). MdmX represses E2F1 trans-activation. *Cell Cycle*, 3, 472-8.
- Wüthrich, K. (1986). *NMR of Proteins and Nucleic Acids* (Wiley, New York).
- Xia, M.X., Knezevic, D., Tovar, C., Huang, B.Y., Heimbrook, D.C., Vassilev, L.T. (2008). Elevated MDM2 boosts the apoptotic activity of p53-MDM2 binding inhibitors by facilitating MDMX degradation. *Cell Cycle* 7, 1604-12.
- Huang, X. (2003). Fluorescence polarization competition assay: the range of resolvable inhibitor potency is limited by the affinity of the fluorescent ligand. *J Biomol Screen* 8, 34-8.
- Xue, W., Zender, L., Miething, C., Dickins, R.A., Hernando, E., Krizhanovskiy, V., Cordon-Cardo, C. and Lowe, S.W. (2007). Senescence and tumour clearance is triggered by p53 restoration in murine liver carcinomas. *Nature* 44, 656-660.
- Yu, G.W., Rudiger, S., Veprintsev, D., Freund, S., Fernandez-Fernandez, M.R. and Fersht, A.R. (2006). The central region of HDM2 provides a second binding site for p53. *Proc. Natl. Acad. Sci. USA* 103, 1227-1232.
- Zaugg, H.E., Martin, W.B. (1965). α Amidoalkylations at carbon. *Org. React.* 14, 52-269.
- Zhang, J.H., Chung, T.D.Y., Oldenburg, K.R. (1999). A simple statistical parameter for use in evaluation and validation of high throughput screening assays. *J. Biomol Screen* 4, 67-73.
- Zobel, K., et al. (2006). Design, synthesis, and biological activity of a potent Smac mimetic that sensitizes cancer cells to apoptosis by antagonizing IAPs. *ACS Chem. Biol.* 1, 525-533
- Zondlo, S.C., Lee, A.E., Zondlo, N.J. (2006). Determinants of specificity of MDM2 for the activation domains of p53 and p65: proline27 disrupts the MDM2-binding motif of p53. *Biochemistry* 45, 11945-11957.
- Zuckerman, V., Lenos, K., Popowicz, G.M., Silberman, I., Grossman, T., Marine, J.C., Holak T.A., Jochemsen, A.G., and Haupt, Y. (2009). c-Abl phosphorylates Hdmx and regulates its interaction with p53. *J. Biol. Chem.* 284, 4031-4039.